Pharmaciana
Vol.14, No.3, Nov 2024, Page. 267-275
ISSN: 2088 4559; e-ISSN: 2477 0256
DOI: 10.12928/pharmaciana.v14i3.28432

Enterobacter hormaechei: an endophytic bacterium found in Avocado Peel (*Persea americana* Mill.) with antioxidant properties

Rustini Rustini[1*], Khalila Rahmi[1], Purnawan Pontana Putra[1], Regina Andayani[1], Khiky Dwinatrana[2]
[1]Faculty of Pharmacy, Universitas of Andalas, Limau Manis, Padang, West Sumatera, Indonesia
[2]Department of Pharmacy, University of Dharma Andalas, Limau Manis, Padang, West Sumatera, Indonesia

Submitted: 17-02-2024 ***Reviewed: 17-03-2024*** ***Accepted: 02-08-2024***

ABSTRACT

Avocado peels (AVP) are renowned for their potent antioxidant properties, making them highly effective in preventing oxidation and free radical formation. Endophytes, microorganisms residing within plant tissues, have demonstrated the ability to produce novel compounds with remarkable biological activities. These bioactive compounds are sometimes even more potent than those found in their host plants. This study explores the potential of endophytes from avocado peels as rich sources of antioxidant compounds. AVP samples are collected, surface-sterilized, and segmented before being cultured in growth media. The bacteria are then isolated, purified, and subjected to ethyl acetate extraction to evaluate their antioxidant activity using the 2,2-diphenyl-1-picrylhydrazyl (DPPH) microassay. Samples demonstrating favorable antioxidant properties undergo molecular identification through 16S rRNA gene sequencing. Four bacterial strains are successfully isolated, with only the APK4 strain exhibiting significant antioxidant activity with an IC_{50} value of 302.3 μg/mL. Molecular analysis and phylogenetic tree construction reveal that APK4 is closely related to the *Enterobacter hormaechei* species, with a percent identity value of 99.93%. These findings highlight the potential of active metabolites from endophytic bacteria in AVP extracts as promising lead compounds for the development of novel drugs, nutraceuticals, and cosmetic ingredients.

Keywords: Avocado peel (AVP), Endophytic bacteria, *Enterobacter hormachei*, antioxidant activity

Corresponding author:
Rustini Rustini
Faculty of Pharmacy, Universitas of Andalas
Limau Manis, Padang, West Sumatera, Indonesia
Email: rustini@phar.unand.ac.id

INTRODUCTION

Free radicals are unstable molecules that harm cells, leading to aging, cancer, and cardiovascular diseases. Antioxidants neutralize these molecules, protecting cells. Natural antioxidants from fruits and vegetables are safe and beneficial, while synthetic ones in supplements and processed foods can be harmful. Excessive synthetic antioxidants may disrupt the body's balance, causing toxicity and increasing disease risk. Thus, obtaining antioxidants from natural sources is essential (Rautiainen et al., 2016).

Avocado peels (AVP) are known for their potent antioxidant properties, containing over phenolic compounds including hydroxycinnamic acids, flavonols, and flavan-3-ols (Akan, 2021). Quercetin derivatives, the main flavonols in avocado peels, are known for their antioxidative (Feng et al., 2019). Endophytes, microorganisms residing within plant tissues, are emerging as a promising source of natural products for oxidative stress and bioactive agents. These endophytes influence plant metabolite production through microbial-host interactions, potentially enhancing antioxidant compound production. They produce bioactive compounds, sometimes the derivates are more potent than those in their host plants and have shown the ability to generate both plant-associated and novel compounds with remarkable biological activities. For example, phenazine-1-carboxylic acid from *Pseudomonas aeruginosa* effectively scavenges free radicals and inhibits oxidative processes (Denning et al., 2003). *Methylobacterium radiotolerans*, from *Combretum erythrophyllum* seeds, showed an IC_{50} of 5.65 µg/mL in the 2,2-Diphenyl-1-picrylhydrazyl (DPPH) assay (Photolo et al., 2020). Endophytes, which can be cultivated rapidly under controlled conditions and in a short time, are a viable source of natural bioactive molecules.

This study is interested in the potential of endophytes of avocado peel to be an abundant source of antioxidant compounds. It focuses on the development of more potent and sustainable antioxidant agents that can replace synthetic alternatives in the food and nutraceutical industry. This is the first study that will explore endophytes from avocado peels as a source of antioxidant, hence not yet explored.

MATERIALS AND METHOD

Sample preparation and surface sterilization

Avocados (*Persea americana* Mill.) were harvested In January 2023 from Kuranji in Padang City, West Sumatra. These plants were verified at Universitas Andalas Herbarium. The avocados were then prepared by peeling and sterilizing them through a process involving soaking in 1% NaOCl for two minutes followed by treating with 70% alcohol for two minutes and rinsing five times with water. To ensure sterilization a sample of the avocado skin rinse was cultured on agar (NA) media. After two days of incubation, at 37°C the NA medium was examined to confirm if any microbial growth had taken place (Anjum & Chandra, 2015; Rustini et al., 2023).

Isolation and fermentation of endophytic bacteria

Sterile AVP was cut into 1x1 cm lengths and then cultured on Nutrient Agar (NA) media. It was purifying the bacteria that grew around the avocado skin involved picking each colony that grew and inoculating it on fresh NA media until a pure isolate was obtained. The colour and surface texture of the colonies were observed. Fermentation of endophytic bacteria in AVP skin was carried out using Nutrient Broth (NB). The substrate was separated by pipetting during 24, 48, 72, and 96 hours of fermentation in a shaker incubator set at 37°C and 120 rpm. Next, the mixture was centrifuged for 15 minutes at 5000 rpm, and then the filtrate and residue were separated (Beal et al., 2020; Yati et al., 2018).

Extraction and antioxidant assay

Endophytic bacterial fermentation products were extracted with ethyl acetate solvent in 1:1 v/v, then macerate for 3 days. The product was then pumped into a seperatory funnel, stirred, and allowed to settle until two separate layers were formed. After distillation, the organic extract was separated and finally was evaporated to give widely-used and easily transferable concentrated organic extract for more

fractionation and isolation. In this experiment, the antioxidant activity of this extract was tested using DPPH assay at the concentration of 24mg/100 mL of methanol. The stock solution was further filtered using methanol and further diluted to get a concentration approximately yielding a mixture with an absorbance of 0.1713 at 517 nm. Eighty microliters of the DPPH solution was mixed with 50 µL of the extract at different concentrations in test tubes; triplicate extractions of each concentration were made for the assay A standard solution of DPPH at 12.5 mg dissolved in 100 mL methanol was prepared with ascorbic acid as a positive control. Incubation in the dark lasted for 30 min. Subsequently, absorbance was read at 517 nm using a microplate reader to get the IC_{50} value. The percentage of antioxidant activity was calculated using the following equation (Mohamed et al., 2013).

$$\% \text{ of antioxidant activity= = } [(Ac-As) \div Ac] \times 100 \quad \text{.....(1)}$$

where:
Ac=Control reaction absorbance;
As=Testing sampel absorbance

Molecular identification

A 35-cycle PCR protocol was used with denaturation at 95°C for 45 s, annealing at 56°C for 45 s, and extension at 72 °C for 1 min. The PCR protocol included an initial 2-minute denaturation step at 95°C, and the last extension step was at 72°C for 5 minutes. After the PCR cycles, the samples were assessed using electrophoresis on a 1% agarose gel. Loading the 1 kb marker in the leftmost well (2 µL) and the remaining wells containing 5 µL each of PCR reaction mixture. Sanger Sequencing of the 16S rRNA Gene PCR Products of Bacteria. The following primers for sequencing: 16SrRNA_27F (5' AGA GTT TGA TCM TGG CTC AG 3') and 16SrRNA_1525R (5' AAG GAG GTG WTC CAR CC 3') had the product was a 1,498 bp long sequence. Then, it aligned children sequences derived from applying forward and reverse primers using the SeqMan (Kumar et al., 2018).

Phylogenetic analysis

The base sequence of the 16S rRNA was aligned using the BLAST program from the NCBI Gene Bank to identify similarities with closely related organisms. Based on the BLAST results, bacterial sample sequences were chosen from the Gene Bank for further analysis. These sequences were aligned, and a phylogenetic tree was constructed. Genetic distances were determined using the MEGA software with the Kimura 2-Parameter method. The reliability of the phylogenetic tree was validated with a bootstrap value of 1,000. Finally, genetic distances were analyzed using the Pairwise Distances Method (Saitou & Nei, 1987; Tamura et al., 2011).

RESULT AND DISCUSSION

In this study, four isolates of endophytic bacteria APK1, APK2, APK3, and APK4 were successfully obtained from the avocado peel (*Persea americana* Mill.) with different shapes, colors, and textures (Figure 1). APK1 colony is almost clear white, with a ratty surface and edges, whereas APK2 is structurally and morphologically similar to APK1 but has a milky white colony color. In contrast, APK3 has a yellowish colony color with a slimy and ratty surface while the APK4 colony is yellowish, with a raised surface, wavy edges, and a slightly dull/cloudy appearance.

The optimum growth time of isolates is revealed by fermentation. The Optical Density (OD) calculation is used to calculate the fermentation time. Fermentation occurs at the beginning of the stationary phase, as indicated by the bacterial growth curve because secondary metabolites are produced during this phase. Metabolite synthesis occurs as a result of a lack of available nutrients, which causes an accumulation of metabolite enzyme inducers and the release of genes that can trigger metabolite synthesis. The induction of enzymes that can be obtained from the cell's metabolism is linked to biosynthesis. APK1 bacteria reach their optimum time in the fermentation process close to 24 hours, then significantly decrease entering the death phase, which is similar to APK2, which enters the

stationary phase after 24 hours, with isolates reaching their optimum time approaching 40 hours. APK3 discovered that the optimum growth time was close to 40 hours, which was relatively similar to the APK4 isolate (Figure 2).

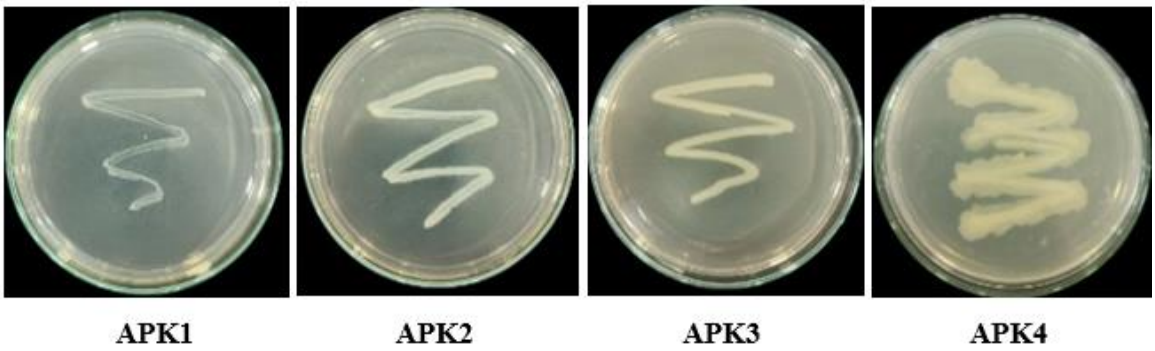

Figure 1. Endophityc bacteria colony isolated from Avocado peel *Persea americana* Mill.

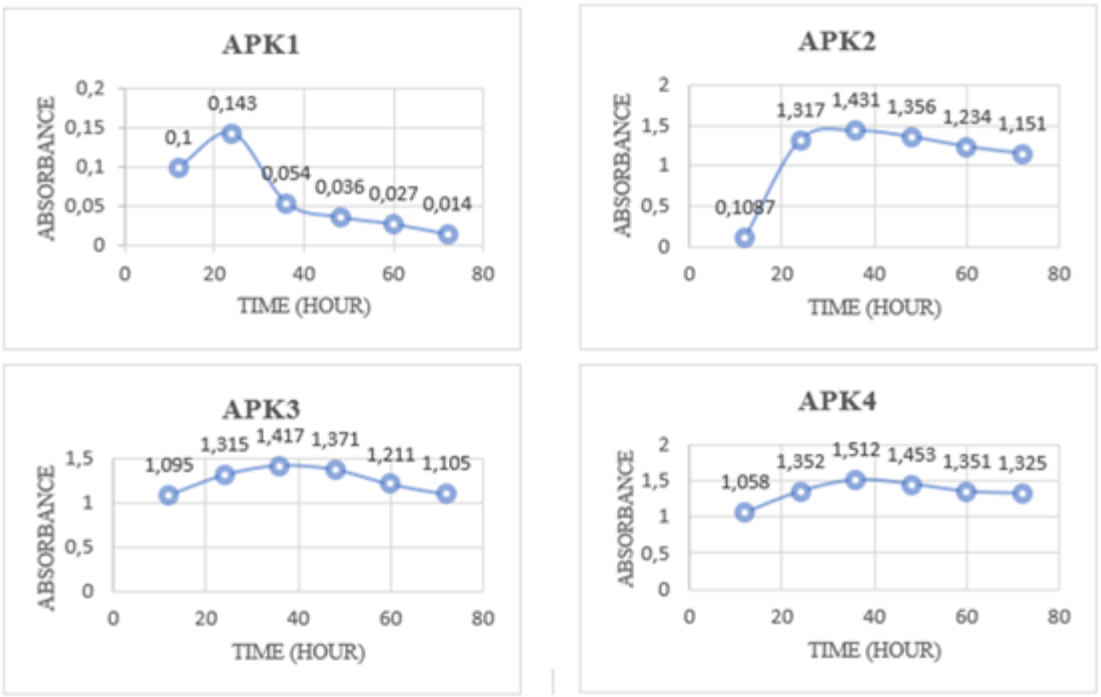

Figure 2. Optical density measurements of bacterial isolates' growth curves

The antioxidant testing results of the APK4 bacterial isolate extract demonstrated the highest antioxidant activity, evidenced by the lowest IC_{50} value of 302.3 µg/mL. This activity was significantly high when compared to the other isolates, APK1, APK2, and APK3, which exhibited IC_{50} values of 19.737 µg/mL, 18.972µg/mL, and 31.217 µg/mL, respectively (Table. 1).

Table 1. DPPH assay results for antioxidant activity of bacterial isolate extracts

Isolate (extract)	Standard Concentration (µg/mL)	Average Absorbance ± SD	Sample Absorbance	Inhibition (%)	IC_{50} (µg/mL)
APK1	1000	0.1033 ± 0.047	0.0636	35.906	19.737
	500	0.1476 ± 0.009	0.1080	-8.724	
	250	0.1513 ± 0.009	0.1116	-12.416	
	125	0.1510 ± 0.021	0.1113	-12.080	
	62.5	0.1546 ± 0.002	0.1150	-15.771	
	31.25	0.1553 ± 0.005	0.1156	-16.443	
APK2	1000	0.1596 ± 0.003	0.1180	12.807	18.972
	500	0.1636 ± 0.005	0.1220	9.852	
	250	0.2006 ± 0.010	0.1590	-17.487	
	125	0.2103 ± 0.004	0.1686	-24.630	
	62.5	0.2140 ± 0.001	0.1723	-27.339	
	31.25	0.2153 ± 0.003	0.1736	-28.325	
APK3	1000	0.1610 ± 0.004	0.0996	37.184	31.217
	500	0.1703 ± 0.004	0.1090	31.302	
	250	0.1680 ± 0.008	0.1066	32.773	
	125	0.1786 ± 0.006	0.1173	26.050	
	62.5	0.1806 ± 0.003	0.1193	24.789	
	31.25	0.1836 ± 0.002	0.1223	22.899	
APK4	1000	0.1010 ± 0.008	0.0393	75.105	302.3
	500	0.1260 ± 0.002	0.0643	59.282	
	250	0.1606 ± 0.003	0.0990	37.341	
	125	0.1656 ± 0.003	0.1040	34.177	
	62.5	0.1863 ± 0.003	0.1246	21.097	
	31.25	0.1843 ± 0.004	0.1226	22.362	
Ascorbic acid	1000	0.0397 ± 0.000	0.000	100	3.54
	10	0.0496 ± 0.000	0.0100	86.238	
	5	0.0616 ± 0.002	0.0220	69.724	
	2.5	0.0850 ± 0.002	0.0453	37.614	
	1.25	0.0930 ± 0.003	0.0533	26.605	
	0.625	0.0963 ± 0.004	0.0566	22.018	

The bacterial isolates containing antioxidant properties in APK4 were subsequently identified molecularly. The genomic DNA of the bacterial isolate APK4 was confirmed by the presence of a single band on the gel (Figure 3). A λ DNA marker with a concentration of 100 µg/mL was used as a reference. The clear, singular DNA band indicates that there are no contaminating substances, such as RNA or proteins, in the sample. This result demonstrates the purity and integrity of the extracted DNA, which is crucial for accurate downstream molecular analyses.

DNA concentration is measured in µg/mL, while purity is assessed using absorbance ratios at 260/230 nm and 260/280 nm. A pure DNA sample has a 260/230 ratio between 2.0 and 2.2. The bacterial isolate APK4 has a 260/230 ratio of 2.197, indicating minimal contamination. Similarly, a pure DNA sample should have a 260/280 ratio between 1.7 and 2.0. The APK4 sample has a 260/280 ratio of 2.000, confirming high purity. Thus, the DNA from the bacterial isolate APK4 is very pure and suitable for further analysis. The estimated size of the amplified 16S rRNA gene product is 1,498 bp. For bacterial isolate APK4, the target band, indicated by a red arrow, matches this estimated size (Figure 3). Additionally, several faint bands of various sizes were observed. These faint bands likely result from the

presence of multiple copies of the 16S rRNA gene in the bacterial genome, causing the primers to anneal to other regions of the genome.

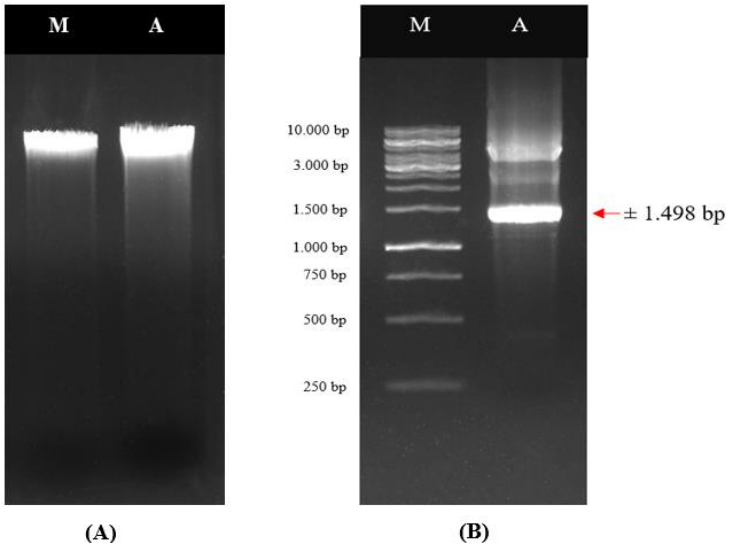

Figure 3. (A) Visualization of genomic DNA and (B) 16S rRNA gene amplification results for bacterial isolate APK4, M (Marker), A (DNA sample genome)

The PCR product of the 16S rRNA gene from the bacterial sample was sequenced in both directions. The electropherogram of the 16S rRNA gene from bacterial isolate APK4 was analyzed. The amplicon, amplified using primers 16SrRNA_27F and 16SrRNA_1525R, was 1,498 bp long. The forward primer (16SrRNA_27F) produced a 757 bp read, while the reverse primer (16SrRNA_1525R) produced a 1,197 bp read. The 5' and 3' ends of both electropherograms had overlapping, unclear, and low-quality peaks, which required trimming. Specifically, the forward primer read was trimmed by 40 bp at the 5' end and 39 bp at the 3' end, and the reverse primer read was trimmed by 38 bp at the 5' end and 94 bp at the 3' end. After editing, the final sequence length of the 16S rRNA gene fragment for isolate APK4 was 1,389 bp Figure 4).

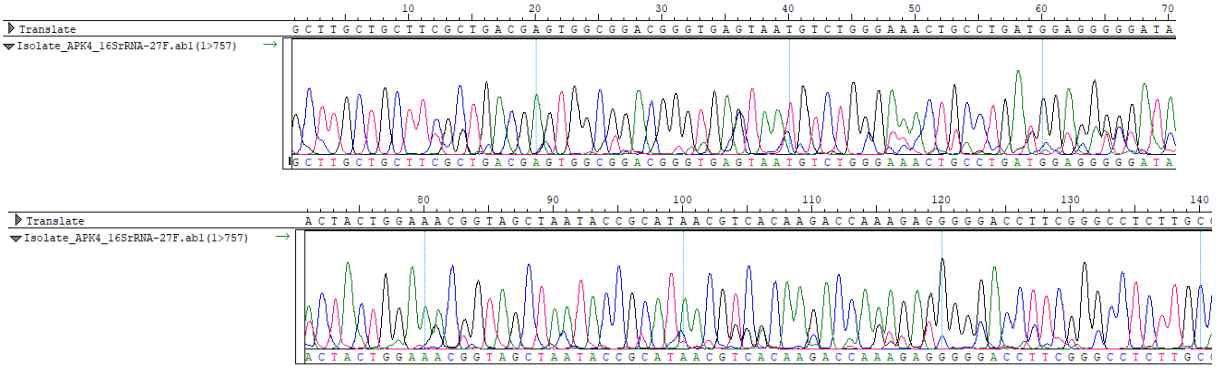

Figure 4. Electropherogram of 16S rRNA gne sequencing for bacterial isolate APK4

Based on the phylogenetic tree construction, two main branches are dividing the bacteria into two clusters. Cluster A comprises 12 bacteria, while Cluster B consists of 4 bacteria. Bacterial isolate APK4,

highlighted by a red box, is located in Cluster B. The closest branch to isolate APK4 includes *Enterobacter hormaechei* subsp. *xiangfangensis* strain FJAT-30604, followed by *Enterobacter hormaechei* isolate EC-TO80 and *Enterobacter hormaechei* strain A1. According to BLAST results, alignment, genetic distance calculations, and phylogenetic tree construction, it is concluded that bacterial isolate APK4 belongs to the species *Enterobacter hormaechei* with percentage of similarity value of 99.93% with 100% query cover (Figure 5).

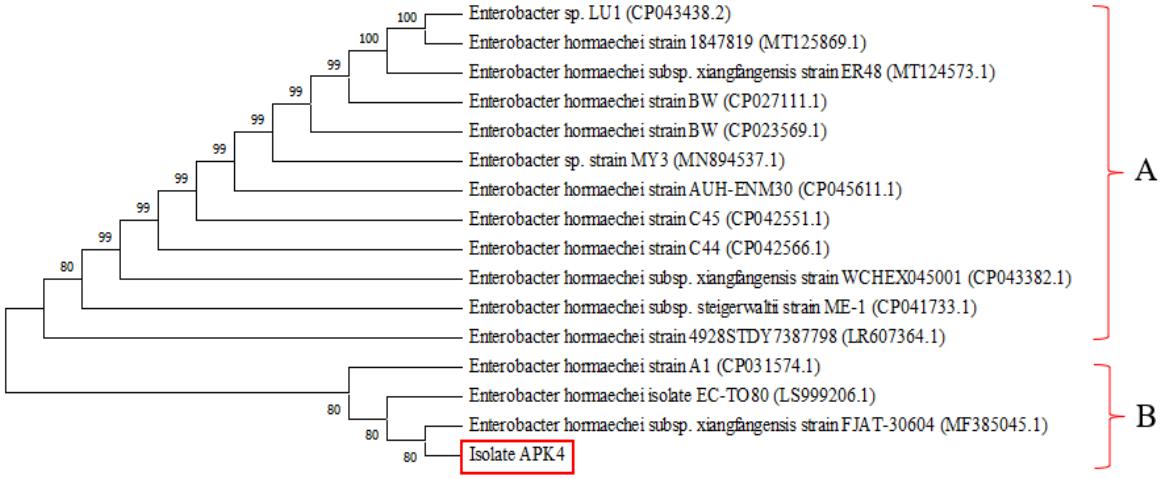

Figure 5. Phylogenetic tree analysis of the isolate APK4-comparison bacteria relationship

The name of the endophyc bacteria in this study is *Enterobacter hormaechei*. It is a Gram-negative bacterium within the enterobacter cloacae complex (ECC), was first identified and described in 1989 (O'Hara et al., 1989). Like other Enterobacter species, *E. hormaechei* has been found in diverse natural settings, including plants, water, soil, and the digestive tracts of insects and animals (Rizwan et al., 2023) (Martins et al., 2020). Previous research has shown that this bacterial isolate extract has strong anti-larvicidal, antimicrobial, and fungicidal properties. However, there are still no specific reports on its antioxidant potential (Wang et al., 2019).

This study highlights an interesting link to the natural habitat of avocados (*Persea americana* Mill.). It suggests that avocados and their endophytes, including *E. hormaechei*, may have developed increased antioxidant activity to survive in tough conditions. This idea fits with the broader understanding that endophytic bacteria play a crucial role in helping plants adapt to and thrive in difficult environments. The ability of *E. hormaechei* to handle and reduce oxidative stress in avocados emphasizes the importance of these bacteria in the plant's resilience. Investigating the antioxidant properties of *E. hormaechei* further, particularly in relation to avocados, could shed light on the complex relationship between endophytes and their host plants in challenging habitats.

CONCLUSION

This research successfully identified four distinct endophytic bacteria from avocado peel, each with unique characteristics. Four isolates were obtained, namely APK1, APK2, APK3, and APK4. Through fermentation analysis, we determined that APK1 and APK2 have optimal growth times of 24 hours, while APK3 and APK4 peak at around 40 hours. Only APK4 exhibited antioxidant properties. We conclusively identified APK4 as a member of the *Enterobacter hormaechei* species using molecular identification with percentage of similarity of 99,93%.

ACKNOWLEDGEMENT

We are grateful to the Dean of the Universitas Andalas Faculty of Pharmacy for his We are grateful to the Dean of the Universitas Andalas Faculty of Pharmacy for his encouragement, funding, support, encouragement, and funding.

REFERENCES

Akan, S. (2021). Phytochemicals in avocado peel and their potential uses. *Food and Health*, *7*(2), 138–149. https://doi.org/10.3153/fh21015

Anjum, N., & Chandra, R. (2015). Endophytic bacteria: optimizaton of isolation procedure from various medicinal plants and their preliminary characterization. *Asian Journal of Pharmaceutical and Clinical Research*, *8*(4), 233–238

Beal, J., Farny, N. G., Haddock-Angelli, T., Selvarajah, V., Baldwin, G. S., Buckley-Taylor, R., Gershater, M., Kiga, D., Marken, J., Sanchania, V., Sison, A., Workman, C. T., Pehlivan, M., Roige, B. B., Aarnio, T., Kivisto, S., Koski, J., Lehtonen, L., Pezzutto, D., … Zhou, J. (2020). Robust estimation of bacterial cell count from optical density. *Communications Biology*, *3*(1). https://doi.org/10.1038/s42003-020-01127-5

Denning, G. M., Iyer, S. S., Reszka, K. J., O'Malley, Y., Rasmussen, G. T., & Britigan, B. E. (2003). Phenazine-1-carboxylic acid, a secondary metabolite of Pseudomonas aeruginosa, alters expression of immunomodulatory proteins by human airway epithelial cells. *American Journal of Physiology - Lung Cellular and Molecular Physiology*, *285*(3 29-3). https://doi.org/10.1152/ajplung.00086.2003

Feng, X., Tao, A., & Song, Z. (2019). Extraction of quercetin from Avocado meal and its antioxidant activity. *IOP Conference Series: Earth and Environmental Science*, *330*(4). https://doi.org/10.1088/1755-1315/330/4/042057

Kumar, S., Stecher, G., Li, M., Knyaz, C., & Tamura, K. (2018). MEGA X: Molecular evolutionary genetics analysis across computing platforms. *Molecular Biology and Evolution*, *35*(6), 1547–1549. https://doi.org/10.1093/molbev/msy096

Martins, E. R., Bueno, M. F. C., Francisco, G. R., Casella, T., de Oliveira Garcia, D., Cerdeira, L. T., Gerber, A. L., de Almeida, L. G. P., Lincopan, N., de Vasconcelos, A. T. R., Nogueira, M. C. L., & Estofolete, C. F. (2020). Genome and plasmid context of two rmtG-carrying Enterobacter hormaechei isolated from urinary tract infections in Brazil. *Journal of Global Antimicrobial Resistance*, *20*, 36–40. https://doi.org/10.1016/j.jgar.2019.06.020

Mohamed, A. A., Ali, S. I., & El-Baz, F. K. (2013). Antioxidant and antibacterial activities of Crude extracts and essential oils of Syzygium cumini leaves. *PLoS ONE*, *8*(4). https://doi.org/10.1371/journal.pone.0060269

O'Hara, C. M., Steigerwalt, A. G., Hill, B. C., Farmer, J. J., Fanning, G. R., & Brenner, D. J. (1989). Enterobacter hormaechei, a new species of the family Enterobacteriaceae formerly known as enteric Group 75. *Journal of Clinical Microbiology*, *27*(9), 2046–2049. https://doi.org/10.1128/jcm.27.9.2046-2049.1989

Photolo, M. M., Mavumengwana, V., Sitole, L., & Tlou, M. G. (2020). Antimicrobial and antioxidant properties of a bacterial endophyte, methylobacterium radiotolerans MAMP 4754, isolated from Combretum erythrophyllum Seeds. *International Journal of Microbiology*, *2020*. https://doi.org/10.1155/2020/9483670

Rautiainen, S., Manson, J. E., Lichtenstein, A. H., & Sesso, H. D. (2016). Dietary supplements and disease prevention-a global overview. *Nature Reviews Endocrinology*, *12*(7), 407–420. https://doi.org/10.1038/nrendo.2016.54

Rizwan, M., Faisal, S., Tariq, M. H., Zafar, S., Khan, A., & Ahmad, F. (2023). Enterobacter hormaechei-driven novel biosynthesis of tin oxide nanoparticles and evaluation of their anti-aging, cytotoxic, and enzyme inhibition potential. *ACS Omega*, *8*(30), 27439–27449. https://doi.org/10.1021/acsomega.3c02932

Rustini, R., Aisy, D. R., Putra, P. P., Andayani, R., & Dwinatrana, K. (2023). Antibacterial activity of

endophytic Bacterial extracts isolated from Pineapple Peel (Ananas comosus L.). *Tropical Journal of Natural Product Research*, *7*(7), 3320–3324. https://doi.org/10.26538/tjnpr/v7i7.8

Saitou, N., & Nei, M. (1987). The neighbor-joining method: a new method for reconstructing phylogenetic trees. *Molecular Biology and Evolution*, *4*(4), 406–425. https://doi.org/10.1093/oxfordjournals.molbev.a040454

Tamura, K., Peterson, D., Peterson, N., Stecher, G., Nei, M., & Kumar, S. (2011). MEGA5: molecular evolutionary genetics analysis using maximum likelihood, evolutionary distance, and maximum parsimony methods. *Molecular Biology and Evolution*, *28*(10), 2731–2739. https://doi.org/10.1093/molbev/msr121

Wang, Y., Ji, D., Chen, T., Li, B., Zhang, Z., Qin, G., & Tian, S. (2019). Production, signaling, and scavenging mechanisms of reactive oxygen species in fruit–pathogen interactions. *International Journal of Molecular Sciences*, *20*(12). https://doi.org/10.3390/ijms20122994

Yati, S. J., Sumpono, S., & Candra, I. N. (2018). Potential antioxidant activity of secondary metabolites from endophyte bacteria on Moringa oleifera L leaf. *Alotrop*, *2*(1), 82–87. https://doi.org/10.33369/atp.v2i1.4744

Pharmaciana
Vol.14, No.2, Nov 2024, Page. 276-288
ISSN: 2088 4559; e-ISSN: 2477 0256
DOI: 10.12928/pharmaciana.v14i3.28638

The redox titration of Fe (II) ions with $K_2Cr_2O_7$ using a potentiometry method the effect of EDTA and SCN^- ligands

Herlina*[1], Muhammad Razali[2]
[1]Institut Kesehatan Medistra Lubuk Pakam,
Jl. Sudirman No.38 Lubuk Pakam, Deli Serdang, Sumatera Utara, Indonesia
[2]Universitas Pembinaan Masyarakat Indonesia,
Jl. Teladan No.15, Teladan Bar., Kec. Medan Kota, Kota Medan, Sumatera Utara, Indonesia

Submitted: 28-03-2024 ***Reviewed: 13-03-2024*** ***Accepted: 02-09-2024***

ABSTRACT

Complexometric titration is often used for determining the metal content, either through direct titration or back titration. This study aimed to investigate redox titration between Mohr salt solutions and potassium dichromate in an acidic atmosphere in the pH range 2. The results showed that the reaction proceeded effectively at pH 2, with Mohr's salt solution acting as titrant. Furthermore, experiments were conducted to compare the effectiveness of EDTA ligands and SCN^- ligands in improving the sharpness of the Fe^{2+}/ $Cr_2O_7^{2-}$ redox titration curve at pH 2. Results show that EDTA ligands are more effective than SCN- ligands in improving the sharpness of the titration curve. However, it should be noted that the addition of EDTA ligands can shift the equivalent point volume earlier, so adjustments need to be made in redox titration analysis. The use of EDTA and SCN^- ligands in the redox titration of Fe(II) ions with $K_2Cr_2O_7$ using a potentiometric method help in forming stable and detectable complexes with Fe(II), leading to clear and reliable potentiometric measurements. Research has also shown that adding excess moles of EDTA to total Fe (II) ions can decrease redox potential in Fe^{2+}/ $Cr_2O_7^{2-}$ systems. Based on the volume at the equivalence point, the Fe^{2+} ion in Mohr salt is 14.30%. with an average titration error of less than 0.30%. These results highlight the role of EDTA ligands in redox titration analysis and their impact on redox potential changes. The use of EDTA and SCN- ligands in the redox titration of Fe(II) ions with K2Cr2O7 using a potentiometric method help in forming stable and detectable complexes with Fe(II), leading to clear and reliable potentiometric measurements.

Keywords: complexation, EDTA, ligands, redox potential, pH

Corresponding author:
Herlina
Institut Kesehatan Medistra Lubuk Pakam
Jl. Sudirman No.38 Lubuk Pakam, Deli Serdang, Sumatera Utara, Indonesia
Email: herlina@medistra.ac.id

INTRODUCTION

Redox titration serves as a fundamental analytical technique in chemistry, allowing precise determination of the target concentration of analytes by measuring the titrant volume required to reach a specific endpoint. In the context of quantitative analysis, redox titration of Fe^{2+} ions using potassium dichromate ($K_2Cr_2O_7$) as a titrant has been widely used. This classical titration, often used to quantify iron content in various samples, is essential in educational and industrial laboratories (Barrera-Díaz et al., 2012; El Jamal, 2008). The Fe^{2+}/Fe^{3+} redox pair is known for its sensitivity to various environmental factors, especially pH and the presence of ligands. These variables can significantly impact the accuracy and precision of titration results, so it is essential to understand their effects. In this study, we explored the effect of pH and the role of ligands in redox titration of Fe^{2+} ions in Mohr salts ($FeSO_4(NH_4)_2SO_4 \cdot 6H_2O$) with $K_2Cr_2O_7$ (Kabdaşlı & Tünay, 2023).

The redox system Fe^{2+}/ $Cr_2O_7^{2-}$ is the research focus due to its significant impact on chemical analysis and waste treatment. This reaction can only occur in an acidic environment due to modification of the redox potential by the pH of the solution. However, an increased pH can result in an unspontaneous reaction, so further research is needed to understand and address the problem (Kang et al., 2022). Using ligands, such as Tiron, 1,10–phenanthroline, and EDTA, became a strategy to increase the spontaneity of redox reactions by modifying the reduction potential. This is important because of the complexity of interactions between ligands and metal ions in forming complex compounds, which is also affected by the pH of the solution (Bashir et al., 2018).

The determination of metal ion concentrations is often conducted using UV/Vis absorption spectrometric titration with special ligands. Electrochemical measurements using selective electrodes to measure metal ion concentrations also require specific treatment to prepare the membrane to be active, and any defects can affect their response. Anodic stripping voltammetry and cyclic voltammetry have been widely utilized for the determination of various metals, as has amperometric titration using a dropping mercury electrode, though it requires special treatment. In this study, we propose a method that is relatively easy to use and does not require special preparation before use (El Jamal & Hammud, 2007).

Potentiometric titration techniques are relevant in this context because they are simple, easy, inexpensive, and environmentally friendly. However, special attention is needed to the pH range when performing redox titration of Fe^{2+}/ $Cr_2O_7^{2-}$ with ligands because it can affect the formation of deposits and the stability of complex compounds (Sukekava et al., 2024). Many studies in analytical chemistry have highlighted the significance of pH in redox titrations, as changes in pH levels can substantially upset the balance between Fe^{2+} and $K_2Cr_2O_7$. In addition, the presence of ligands in the sample matrix can lead to the formation of complex ions with Fe^{2+}, potentially complicating the stoichiometry of redox reactions. Therefore, this study aims to uncover the nuances of these critical factors and their collective influence on accuracy and reliability in Fe^{2+} determination via $K_2Cr_2O_7$ titration (Das et al., 2014).

Understanding how changes in pH levels affect the titration process is essential because it can significantly affect the redox balance between Fe^{2+} and $K_2Cr_2O_7$. In addition, ligands in the sample can form complex ions with Fe^{2+}, altering the stoichiometry of redox reactions. As a result, this study aims to provide a deeper understanding of these influential factors to improve accuracy and reliability in Fe^{2+} determination through $K_2Cr_2O_7$ titration. Potentiometric titration is a suitable electroanalytical technique for applying ligand influence concepts in redox systems due to its simplicity, ease of use, cost-effectiveness, and environmental friendliness. While this method is less commonly employed, it is crucial for evaluating samples in industries, pharmaceuticals, and environmental settings. The method has been used in iron speciation in drug samples and lake water, utilizing the concept of redox potential modification by the ligand 1,10-phenanthroline in Fe(II)-Co(II) redox systems (Rizvi et al., 2016).

EDTA and SCN^- are recognized for their ability to form stable complexes with metal ions such as Fe(II). In our study, these ligands interact with Fe(II) ions during the redox titration process. EDTA acts as a strong chelating agent, binding tightly to metal ions and preventing their precipitation, which is essential for achieving accurate titration results. The presence of EDTA and SCN^- influences the redox chemistry of Fe(II) ions. EDTA stabilizes Fe(II) ions in solution, thereby preventing premature oxidation

or reduction during titration. SCN^-, on the other hand, forms complexes with Fe(II) that can modify the redox potential, thereby impacting the titration endpoint.

The determination of metal ion concentrations is often conducted using UV/Vis absorption spectrometric titration with special ligands. Electrochemical measurements using selective electrodes to measure metal ion concentrations also require specific treatment to prepare the membrane to be active, and any defects can affect their response. Anodic stripping voltammetry and cyclic voltammetry have been widely utilized for the determination of various metals, as has amperometric titration using a dropping mercury electrode, though it requires special treatment. In this study, we propose a method that is relatively easy to use and does not require special preparation before use.

By investigating the interaction between pH, ligands, and Fe^{2+} ion redox titration, we hope to develop a more comprehensive understanding of this analytical technique, which can ultimately lead to more precise and reproducible results in various practical applications.

MATERIALS AND METHOD

This research was conducted on the potentiometric titration method for the Redox reaction Fe^{2+}/ $Cr_2O_7^{2-}$. This redox reaction involves Fe^{2+} ions of Mohr Salt as a reducing agent (titrate) with potassium dichromate as an oxidizing agent (titrant). The cell potential measurement results are used to create a titration curve to determine the effect of ligands and pH on Fe^{2+}/ $Cr_2O_7^{2-}$ redox titration. Compounds used as ligands for this study include EDTA and SCN^- ligands.

Manufacture and characterization of Ag/AgCl comparator electrodes

The Ag/AgCl reference electrode is made by electrodeposition of AgCl on Ag wire in 0.1 M NaCl solution for 1 minute with a current source of 2.20 V until a blackish-gray AgCl precipitate is formed that coats the Ag wire. The Ag/AgCl electrode was placed into the electrode body filled with a 3.0 M NaCl saturated solution. The Ag/AgCl reference electrode that had been made was then characterized voltammetrically in a solution of $K_3[Fe(CN)_6]$ 0.01 M and $K_4[Fe(CN)_6]$ 0.01 M in a solution of 0.1 M NaCl supporting electrolyte using cyclic voltammetry techniques in the potential range of -200 mV to 800 mV with a scan rate of 100 mV/s. Cyclic voltammogram measurement results from artificial Ag/AgCl reference electrodes compared to commercial Ag/AgCl (BAS) electrodes. In addition, the artificial Ag/AgCl electrode is also potentiometrically characterized using Ag/AgCl as a working electrode. Measurement of electrode potentials in NaCl solutions of various concentrations is carried out in stages from low concentration to high concentration, respectively are 5×10^{-5}; 10^{-4}; 5×10^{-4}; 10^{-3}; 5×10^{-3}; $10^{-2;}$ 5×10^{-2} and 10^{-1} M.

Potentiometric titration in redox reactions Fe^{2+}/ $Cr_2O_7^{2-}$

Potentiometric titration uses a Pt wire working electrode as the cathode and an artificial Ag/AgCl reference electrode as the anode, and both are connected to the potentiometer. Cell potential measurements are carried out at room temperature.

Titration of 0.1 M Mohr salt solution by $K_2Cr_2O_7$ 0.0277 M with variation in H_2SO_4 concentration

A solution of 0.1 M Mohr salt in 0.05 M sulfuric acid, as much as 10 mL, is pipetted and put into a beaker, and 25 mL of 1 M sulfuric acid solution is added. The analyte solution is then titrated with 0.028 M potassium dichromate solution and stirred slowly until the solution is homogeneous. The cell potential in the solution is measured and recorded with every addition of 1 mL of titrant. The same procedure is repeated for variations of sulfuric acid with a concentration of 0.30; 0.08; and 0.02 M each. The repetition of each titration is carried out three times.

Titration of 0.01 M Fe(II) and Fe(III) mixed solution by 0.5 M NaOH with EDTA variation

A mixed solution of Mohr salt and $FeCl_3.6H_2O$ 0.01 M in 0.5 M sulfuric acid, as much as 5 mL, was put into a beaker and added with 2 mL of 0.03 M EDTA solution. Next, the solution was diluted with

aqua DM to 50 mL and titrated slowly with 0.5 M NaOH. pH and cell potential measurements were carried out after adding NaOH solution. The same working procedure is repeated with variations in the volume of EDTA solution by 4 and 6 mL. In addition, titration of mixed solutions of Fe(II) and Fe(III) without adding EDTA ligands is carried out with the same working procedure. Each titration is carried out triplo.

Titration of 0.02 M Mohr salt solution by $K_2Cr_2O_7$ 0.007 M with EDTA concentration variation

A 0.02 M Mohr salt solution in 0.02 M sulfuric acid of 10 mL is put into a beaker, added with 25 mL of EDTA solution, and titrated with 0.007 M potassium dichromate solution slowly and stirred until the solution is homogeneous. Cell potential measurements were recorded with every addition of 1 mL of potassium dichromate solution. The work procedure was repeated for adding different EDTA concentrations, namely 0.008 M, 0.009 M, and 0.01 M. The redox titration curve Fe^{2+}/ $Cr_2O_7^{2-}$ with variations in EDTA concentration is then compared with the titration curve without EDTA ligands. Redox titration of Mohr salt solution with potassium dichromate without EDTA ligands was performed by replacing EDTA solution with aqua DM as much as 25 mL. Each of these redox titrations is performed triplo.

Titration of 0.02 M Mohr salt solution by $K_2Cr_2O_7$ 0.007 M with the addition of SCN- ligands

A 0.02 M Mohr salt solution in 0.02 M sulfuric acid, as much as 10 mL, was pipetted and put into a beaker, then added with a 25 mL SCN- solution and titrated slowly with 0.007 M potassium dichromate solution. Triple cell potential measurements are performed per mL titrant, and the results are recorded. The results of the possible measurement of the cell are then compared with the redox titration curve Fe^{2+}/ $Cr_2O_7^{2-}$ with the addition of EDTA ligands that have been performed.

RESULT AND DISCUSSION

Characterization of Ag/AgCl reference electrode

The reference electrode is essential in monitoring the working electrode in potentiometric titration. The characterization of Ag/AgCl reference electrodes is carried out by two methods, namely voltammetry and potentiometry. Voltammetry involves the ratio of artificial to commercial Ag/AgCl (BAS) electrodes in a mixed solution of $K_3[Fe(CN)_6]$ and $K_4[Fe(CN)_6]$. This solution was chosen because of its rapid and electrochemically reversible electron transfer reaction. NaCl solution acts as a supporting electrolyte to minimize the rate of ion migration from the analyte. Furthermore, the Cyclic Voltammetry method characterized the Ag/AgCl reference electrode in the potential range of -200 to +800 mV with a scan rate of 100 mV/s. The results show voltammogram similarity between the artificial Ag/AgCl electrode and BAS, as seen in Figure 1. The voltammogram profile allows the measurement of cathodic and anodic peak potentials and currents from mixed solutions of $K_3[Fe(CN)_6]$ and $K_4[Fe(CN)_6]$ 0.01 M. The ratio of anodic peak (Ip_a) and cathodic (Ip_c) currents is close to 1, indicating a reversible redox process. The peak potential difference (ΔEp) between the anodic and cathodic peaks for artificial Ag/AgCl and BAS electrodes is 0.112 V, while the theoretical value is 0.059 V. The higher ΔEp in the experiment showed uncompensated electrical resistance, leading to slower electron transfer rates and higher separation between anodic and cathodic peaks (Brownson & Banks, 2014).

A paired t-test determines the difference between an artificial Ag/AgCl voltammogram and a BAS. The results of the t-test obtained a calculated t value (1.359) < t table (2.78), which means that there is no significant difference between the voltammogram of artificial Ag/AgCl electrodes and BAS. In addition, the voltammogram difference between the two electrodes can also be observed from the formal potential values. The formal potential of the two electrodes has the same value of 0.210 V, so there is no difference between them. These parameters indicate that the artificial Ag/AgCl electrode performs well with BAS.

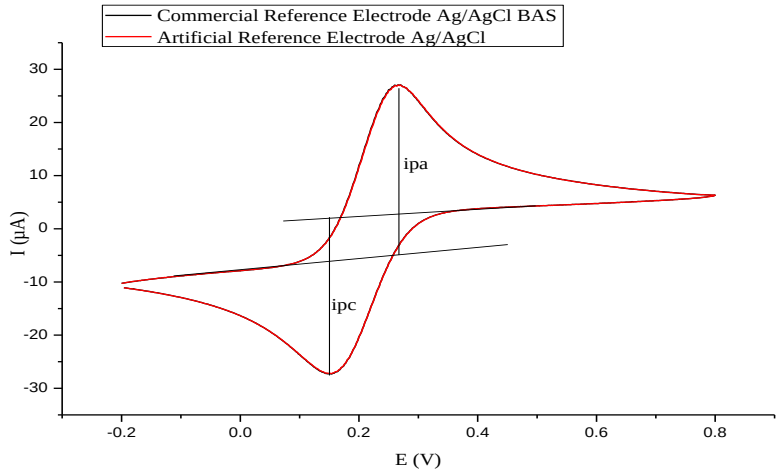

Figure 1. Cyclic voltammogram of commercial Ag/AgCl reference electrode (BAS) with artificial in a mixed solution of $K_3[Fe(CN)_6]$ and $K_4[Fe(CN)_6]$ 0.01 M in 0.1 M NaCl solution

Potentiometric characterization of electrodes is carried out by measuring NaCl solutions in the concentration range of 5 x 10^{-5} - 10^{-1} M using Ag/AgCl wire as the working electrode. A deficient concentration of NaCl solution can dissolve the AgCl layer (K_{sp} = 1.8 x $10^{-10)}$ on the working electrode so that the lowest limit for measuring NaCl solution is 5 x 10^{-5} M. The results of measuring electrode potential in NaCl solution have theoretical compatibility; namely, the cell potential is directly proportional to pCl (-log Cl- ion concentration).

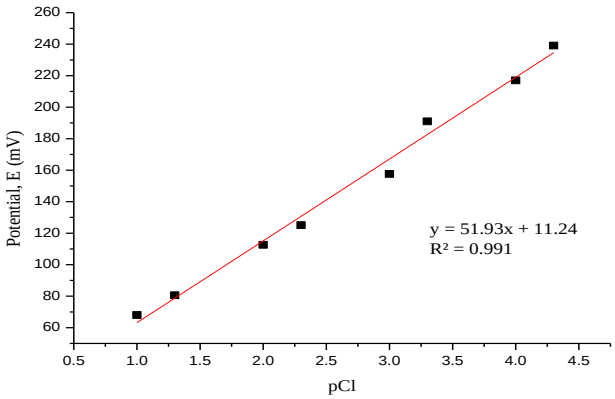

Figure 2. Cell potential curve to pCl of a homemade Ag/AgCl reference electrode with an Ag/AgCl wire working electrode

The Nernst factor is a commonly used parameter to determine electrode performance through the slope value of the relationship curve between potential to –-log analyte concentration. The test results of the artificial Ag / AgCl reference electrode in Figure 2 obtained a straight-line equation of E = 11.24 – 51.93 log[Cl^-], which is subject to the Nernst equation. The experimental Nernst factor value of 51.93 mV/decade is *Under-Nerstian* smaller than the theoretical value of 59.2 mV/decade at 25 °C. The difference in the value of the experimental Nernst factor with the theoretical value is influenced by temperature, the character of the AgCl precipitate on the Ag wire (purity and homogeneity), ion activity in the solution, the purity of the analyte solution, the solution in the reference, the connecting fluid

potential, the cleanliness of the electrodes, and the membrane composition of the electrodes. However, the correlation factor value of 0.991, close to one, indicates that the system of working and comparator electrodes responded well to a slight increase in chloride ion concentration.

The results of overall electrode characterization by voltammetry and potentiometry methods show that the artificial Ag/AgCl reference electrode has good performance, so it is suitable for further potentiometric titration measurements. The things that need to be considered in making Ag / AgCl electrodes are the potential used during the electrolysis process and the selection of solutions in the reference electrode. The potential applied for the electrolysis process must be greater than the standard potential of the Ag/AgCl electrode due to the reduction of the potential by the *Ohmic potential*.

Effect of H_2SO_4 concentration on redox titration of mohr salt solution with $K_2Cr_2O_7$

Variations in sulfuric acid concentration were carried out to determine the effect of H^+ ion concentration on redox titration between Mohr salt solution and potassium dichromate. This can be known through the titration curve by channeling the relationship between the cell potential of the measurement results and the titrant volume. The cell potential measurement is carried out by potentiometric titration method using Pt wire as the working electrode and an artificial Ag/AgCl reference electrode that has been characterized. Mohr salts are a source of Fe^{2+} ions acting as analytes in titration. The use of sulfuric acid in making Fe (II) solution is to give an acidic atmosphere to the solution to slow down the rate of oxidation of Fe^{2+} ions to Fe^{3+} by dissolved oxygen (dissolve oxygen*) and prevent the formation of* hydrolyzed Fe^{2+} ion species that are easily oxidized. In addition, sulfuric acid is also used to vary the concentration of H^+ ions in redox titration of Mohr salt solution with potassium dichromate. Sulfuric acid is one of the appropriate acids used for titration because sulfate ions are not involved in the reaction and can meet the needs of H^+ ions for the redox reaction (Rizvi et al., 2016). Potentiometric titration between Mohr salt solution and potassium dichromate was performed in the acidic pH range to prevent the transformation of dichromate ions to chromate at pH > 6 and prevent an increase in the oxidation rate of Fe^{2+} ions by dissolved oxygen at pH > 4. Theoretically, the redox reaction between Mohr salt solution and potassium dichromate can be spontaneous up to pH 4. However, titration between 0.1 M Mohr salt solution and 0.03 M potassium dichromate was experimentally stopped to a pH of less than three due to the formation of brownish-yellow deposits derived from $Fe(OH)_3$ (Tian et al., 2024). The chemical reaction between a solution of Mohr salt and potassium dichromate in an acidic atmosphere is shown in Equation 3.

Anode: $6Fe^{2+}_{(aq)} \rightleftharpoons 6Fe^{3+}_{(aq)} + 6e^-$ .....(1)

Cathode: $Cr_2O_7^{2-}{}_{(aq)} + 14H^+_{(aq)} + 6e^- \rightleftharpoons 2Cr^{3+}_{(aq)} + 7H_2O_{(l)}$ ..... (2)

Hence the equation of the chemical reaction that occurs:

$Cr_2O_7^{2-}{}_{(aq)} + 6Fe^{2+}_{(aq)} + 14H^+_{(aq)} \rightleftharpoons 2Cr^{3+}_{(aq)} + 6Fe^{3+}_{(aq)} + 7H_2O(l)$ ..... (3)

The standard reduction potential () of the redox system Cr(VI)/Cr(III) is greater than that of the redox system Fe(III)/Fe(II) so that dichromate ions tend to be reduced while Fe^{2+} ions undergo oxidation. The redox titration curve between Mohr salt solution and potassium dichromate with variations in H^+ ion concentration is shown in Figure 3. The cell potential in the state before titration yields a positive value. This shows that there is already a Fe species^{3+} derived from the oxidation of Fe^{2+} by dissolved oxygen. The cell potential in the pre-titration state approaches the theoretical value for the Fe(III)/Fe(II) redox system in H_2SO_4 1.0 M is 0.460 V against the Ag/AgCl reference electrode so that the number of Fe^{3+} species that is present in solution in tiny amounts and can be ignored. states that redox potential without titrant addition cannot be calculated since the exact sum of Fe^{3+} ion concentrations, which is present in the solution, cannot be determined. If Fe^{3+} ions are not in solution or Fe^{3+} ion concentration is zero, the resulting redox potential becomes infinite.

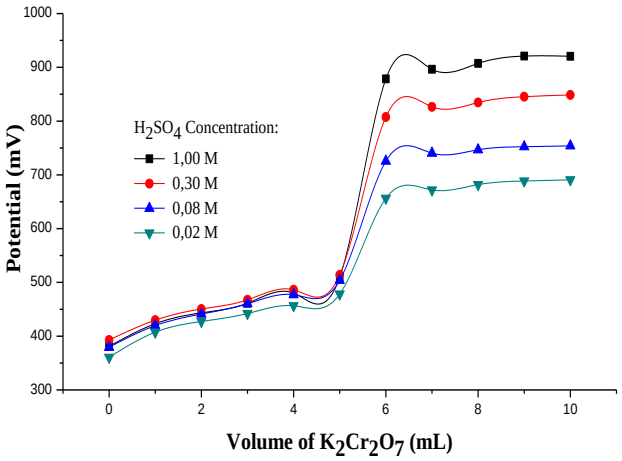

Figure 3a. Redox titration curve of 10 mL Mohr salt solution 0.1 M with $K_2Cr_2O_7$ 0.03 M with concentration variation H_2SO_4

Figure 3a. shows that a decrease in sulfuric acid concentration can decrease redox potential values in regions after the equivalence point. In that state, the redox potential value depends on the half-reaction Cr(VI)/Cr(III) in Equation (3) (El Jamal, 2008). H^+ ions as electroactive species are involved in the Cr(VI)/Cr(III) reduction reaction, so the sulfuric acid concentration directly affects the redox potential (Gao & Liu, 2017; Kabdaşlı & Tünay, 2023). The results of measuring cell potential in redox titration Fe^{2+}/ $Cr_2O_7^{2-}$ with variations in sulfuric acid concentration at that state are in theory that cell potential is directly proportional to the concentration of H^+ ions and inversely proportional to the pH of the solution. The relationship of cell potential to solution pH for Cr(VI)/Cr(III) reduction systems can be proved by the Nernst equation in Equation 4.

$$E = E^0_{Cr^{6+}/Cr^{3+}} - \frac{RT}{nF} \ln - 0.138\ pH\ \frac{[Cr^{3+}]^2}{[Cr_2O_7^{2-}]} \quad \text{.....(4)}$$

The sulfuric acid concentration does not affect the redox potential found in the area before the equivalence point. In this situation, the amount of analyte in reduced and oxidized form is present in significant quantities in solution so that the cell potential value is influenced by half the reaction of the Fe(III)/Fe(II) system in Equation (1). Fe(III)/Fe(II) reduction reactions do not involve H ions$^+$, so the sulfuric acid concentration does not directly affect redox potential. However, the pH of a solution plays a role in determining the rate of oxidation of Fe ions^{2+} by dissolved oxygen. The oxidation rate of Fe ions^{2+} becomes Fe^{3+} by dissolved oxygen in the acidic state (pH <4) proceeds very slowly while in the alkaline state (pH 4-8) proceeds very quickly (El Jamal & Hammud, 2007). Redox potential at the state before the equivalence point for $Fe^{2+}/Cr_2O_7^{2-}$ redox can be determined by Equation (5).

$$E = E^0_{Fe^{3+}/Fe^{2+}} - \frac{RT}{nF} \text{Log}\ \frac{[Fe^{2+}]}{[Fe^{3+}]} \quad \text{.....(5)}$$

Redox titration between Mohr salt solution and potassium dichromate does not use visual indicators so that the volume of the titration endpoint cannot be determined through colour changes in solution. The analyte solution changes colour to greenish-yellow as the volume of titrant increases. The volume of the equivalence point of such redox titration is determined based on the first derived curve in Figure 4. In the redox titration curve $Fe^{2+}/Cr_2O_7^{2-}$ it is seen that variations in sulfuric acid concentration do not shift the volume of the equivalent point. However, the variation in sulfuric acid concentration causes a

change in the cell potential in the equivalence point region and can be calculated theoretically through Equation (6). Based on the volume of the equivalent point, it can be calculated that the Fe^{2+} ion content in Mohr salt is 14.30 %. The potentiometric titration method in the redox reaction $Fe^{2+}/Cr_2O_7^{2-}$ has a fairly good accuracy with an average titration error percentage of less than 0.30%.

$$E = -0.0591\ V \log \frac{m\ x\ E^0_{Fe^{3+}/Fe^{2+}} + n\ x\ E^0_{Cr^{6+}/Cr^{3+}}}{m[Fe^{3+}]/[Fe^{2+}] + n\,[Cr^{6+}]/[Cr^{3+}]} \frac{2.[Cr^{3+}]}{[H^+]^{14}} \quad \text{..... (6)}$$

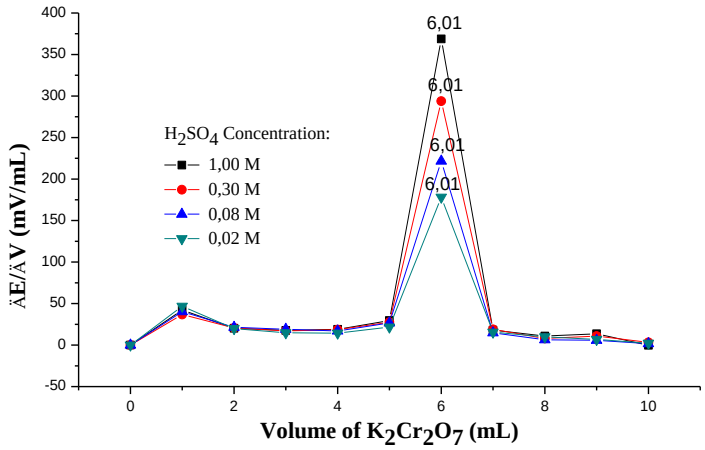

Figure 3b. First derived curve of redox titration of Mohr salt 0.1 M with $K_2Cr_2O_7$ 0.03 M with concentration variation H_2SO_4

The increase in sulfuric acid concentration in Figure 3b increases the equivalence point potential so that the resulting curve is sharper. The sharper the redox titration curve, the easier it is to determine the equivalent point volume on redox titration $Fe^{2+}/ Cr_2O_7^{2-}$. Based on Figure 3, the potential fracture is very large on the redox titration curve $Fe^{2+}/ Cr_2O_7^{2-}$ found at a very acidic pH i.e. at the addition of sulfuric acid 1 M. The potential fault on the titration curve shows a difference *E* between analytes and titrants. The greater the difference *E*, then the greater the equilibrium constant produced so that the equilibrium reaction progresses in the direction of the product. Therefore, redox titration $Fe^{2+}/ Cr_2O_7^{2-}$ in highly acidic atmospheres is preferred. Based on the results of the experiment as a whole, it can be concluded that the concentration of sulfuric acid can modify the cell potential of the redox system $Fe^{2+}/ Cr_2O_7^{2-}$ (Gao et al., 2022; Kang et al., 2022).

Effect of ligands on redox titration $Fe^{2+}/ Cr_2O_7^{2-}$

The effect of ligands on redox titration between Mohr salt solution and potassium dichromate was carried out at an initial pH of 2. The pH range of the solution is determined based on the results of previous studies that redox titration $Fe^{2+}/ Cr_2O_7^{2-}$ can last up to pH 2 without precipitate formation. However, potential jumps in the $Fe^{2+}/ Cr_2O_7^{2-}$ redox titration curve at that pH were found to be very low. The higher the cell potential jump produced by the titration curve, the easier it is to determine the equivalent point volume. The addition of appropriate ligands is expected to increase the sharpness of the $Fe^{2+}/ Cr_2O_7^{2-}$ redox titration curve at pH 2. Compounds used as ligands for such redox systems include EDTA and SCN- (Bashir et al., 2020; Rizvi et al., 2016; Sukekava et al., 2024). $Fe^{2+}/ Cr_2O_7^{2-}$ titration with variations in EDTA ligand concentration at pH 2 is performed to determine the optimum conditions for redox titration in the presence of ligands. An E-pH diagram for the Fe(III)/Fe(II) system with EDTA ligands was experimentally created to determine the effect of pH on the stability of the $[Fe\text{-}EDTA]^-/[Fe\text{-}EDTA]^{2-}$ complex. In redox systems Cr(VI)/Cr(III), E-pH diagrams in the presence of EDTA ligands

are not investigated because the rate of complex formation of Cr(III) with ligands is so slow that measurement results are inaccurate. The results of cell potential measurements for Fe(III)/Fe(II) systems with variations in EDTA ligand volume can be seen in the E-pH diagram for the redox system is shown in Figure 5.

Figure 4 shows that the E-pH diagram of the Fe(III)/Fe(II) system without the presence of EDTA ligands is close to theoretical values and is not affected by the pH of the solution. The standard reduction potential Fe(III)/Fe(II) in H_2SO_4 1 M is theoretically 460 mV against the Ag/AgCl reference electrode due to the formation of the $[FeSO_4]^+$/[FeSO4] complex. At the addition of 2 mL EDTA to 0.03 M, the cell potential decreases compared to the absence of ligands and is constant to changes in the pH of the solution. The decrease in cell potential occurs due to the formation of complexes between EDTA ligands and the redox system Fe(III)/Fe(II) in Equation 7. At pH below 3, the EDTA (Y4-) species that predominate in solution are in the form of H_3Y-. Thus, the most likely reaction formed between Fe(III)/Fe(II) ions and EDTA ligands at pH is shown by Equation 7.

$$[FeH_3Y]^{2+}(aq) + e^- \rightleftharpoons [FeH_3Y]^{+}(aq) \ldots\ldots\ldots\ldots\ldots\ldots (7)$$

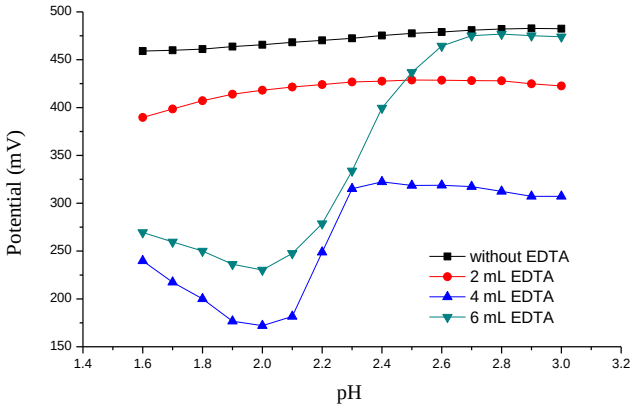

Figure 4. E-pH diagram of 5 mL mixture of Fe(III) and Fe(II) 0.01 M with EDTA mole variation of 0.03 M

A significant decrease in cell potential due to complexation occurs in the addition of 4 and 6 mL EDTA 0.03 M. At solution pH below 3, the cell potential value changes significantly with changes in solution pH. The inconstant cell potential value indicates that the formation of complex compounds between EDTA ligands and Fe(III)/Fe(II) ions is influenced by the pH of the solution. The complex [Fe-EDTA]^2- is unstable at very low pH due to the low value of the conditional constant, but the complex formation constant [Fe-EDTA]- is so large that it causes a decrease in the reduction potential of its free ionic state (Bashir et al., 2020). The experimental results of the E-pH diagram for the Fe(III)/Fe(II) system with the presence of EDTA ligands as a whole can be concluded that Fe(II) ions do not complex completely with ligands in very acidic atmospheres. In addition, the number of moles of EDTA also affects the formation of complexes $[FeH_3Y]^{2+}$/$[FeH_3Y]^+$. A comparable number of moles of EDTA and an excess of the total metal ions can significantly lower the cell potential. The lower the reduction potential, the greater the amount of $[FeH_3Y_]^{2+}$/$[FeH_3Y]^+$ formed. Next, the determination of the complex formula of the EDTA ligand in the redox system Fe^{2+}/ $Cr_2O_7^{2-}$ at pH 2. The effect of EDTA ligand concentration on the redox system can be observed in Figure 5.

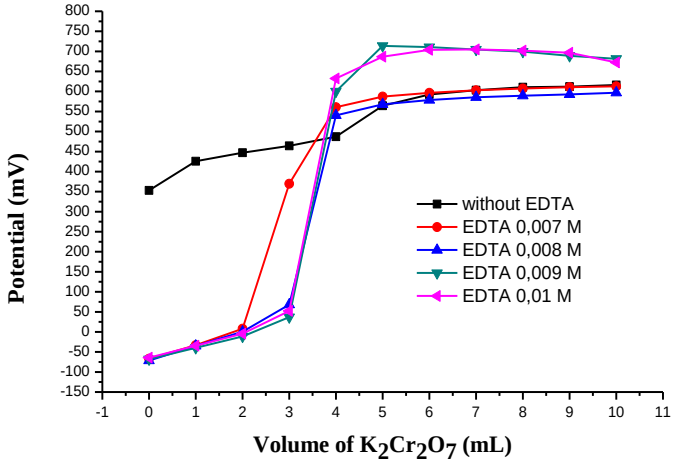

Figure 5. Redox titration curve of 10 mL 0.02 M Mohr salt solution with $K_2Cr_2O_7$ 0.0067 M with 25 mL EDTA at pH 2

Figure 6 shows a significant decrease in redox potential in the region before the equivalence point compared to without the presence of ligands. The decrease in redox potential occurs due to the formation of complexes $[FeH_{3Y}]^{2+}$/$[FeH_3Y]^{+}$ which is reinforced by the results of the E-pH diagram in Figure 5. The experimental results are in accordance with the theory that the complex formation constant between EDTA ligands and Fe(III) ($\beta=10^{25,1}$) greater than Fe(II) ($\beta=10^{25,1}$) so that the reduction potential decreases from the state of the free metal ion. In the state after the equivalence point, the addition of EDTA ligands does not significantly change the redox potential compared to the absence of EDTA ligands. Although metal ions are Cr(VI)/Cr(III) in significant quantities, the kinetics of complex formation with EDTA ligands are very slow at room temperature. In this situation, the redox potential value is influenced by the pH of the solution. The addition of EDTA ligands can maintain the pH of the solution in redox titrations Fe^{2+}/ $Cr_2O_7^{2-}$ compared to the absence of ligands. Therefore, the redox potential with the addition of excess EDTA ligands is higher than without the presence of ligands in the state after the equivalence point (Bashir et al., 2018; El Jamal & Hammud, 2007; Morgan & Lahav, 2007; Rizvi et al., 2013).

The equivalent point volume in the redox system Fe^{2+}/ $Cr_2O_7^{2-}$ at pH 2 with variations in EDTA concentration can be determined by the first derived curve in Figure 7. The volume of the equivalent point shows the ratio of moles between the total complex Fe(II) ions and EDTA ligands to the dichromate ions. The volume of the equivalent point in the presence of the EDTA ligand experimentally shifts earlier than the theoretical equivalent point volume. This happens because there is a small part of Fe(II) species that do not complex completely with EDTA ligands, resulting in a decrease in total moles of complex between Fe(II) ions and EDTA ligands. This condition is caused by the pH of the solution which affects the stability of complex formation. Furthermore, the effect of EDTA ligand concentration on equivalence point cell potential in the Fe^{2+}/ $Cr_2O_7^{2-}$ redox system can also be observed in Figure 7. In the state of excess EDTA ligands of metal ions, the equivalence point cell potential increases. Thus, it can be concluded that in excess EDTA conditions it is effective to increase the equivalence point potential in redox titration Fe^{2+}/ $Cr_2O_7^{2-}$(Bashir et al., 2020; Rizvi et al., 2013, 2016; Sukekava et al., 2024).

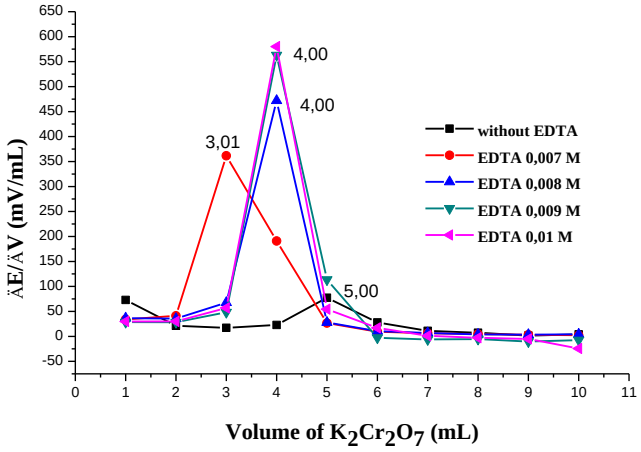

Figure 6. First derived curve of redox titration of Mohr salt solutions 0.02 M to $K_2Cr_2O_7$ 0.0067 M with variations in EDTA concentration at pH 2

The effect of EDTA and SCN- ligands on Fe^{2+}/ $Cr_2O_7^{2-}$ redox titration at pH 2 can be compared in Figure 8 which shows that EDTA ligands are effective enough to improve the sharpness of the Fe^{2+}/ $Cr_2O_7^{2-}$ redox titration curve compared to the presence of SCN^- ligands. The reaction that mention Equation 8

$$Cr_2O_7^{2-} + 6Fe^{2+} + 14H^+ \rightarrow 6Fe^{3+} + 2Cr^{3+} + 7H_2O \quad \text{.....(8)}$$

The reaction between (Fe^{2+}) and EDTA forms a stable complex, typically written as $Fe(EDTA)^{2-}$. When titrated with $K_2Cr_2O_7$, the $Cr_2O_7^{2-}$ ion acts as an oxidizing agent, converting Fe^{2+} to Fe^{3+} while itself being reduced to Cr^{3+}.

Fe reacts with SCN^- to form the reddish complex ion $Fe(SCN)^{2+}$, which is often used as an indicator for the presence of Fe^{3+}. $Fe^{3+} + SCN^- \rightleftharpoons Fe(SCN)^{2+}$. When titrated with $K_2Cr_2O_7$, Fe^{2+} is oxidized to Fe^{3+} by the $Cr_2O_7^{2}$ which is reduced to Cr^{3+} similarly to the above reaction (El Jamal & Hammud, 2007; Najib & Hayder, 2011).

The complex formation constant between SCN^- ligands and Fe(II) ions is so small that the possibility of forming complex compounds is very low. Therefore, the addition of SCN^- ligands does not affect the redox potential Fe^{2+}/ $Cr_2O_7^{2-}$ at the state before the equivalence point.

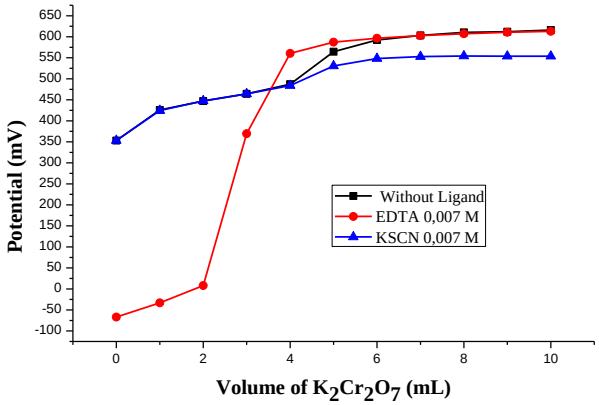

Figure 7. Reference of redox titration curve of 10 mL Mohr 0.02 M salt solution to $K_2Cr_2O_7$ 0.0067 M with 25 mL of EDTA ligand or SCN- at pH 2

CONCLUSION

Redox titration between Mohr salt solution and potassium dichromate can take place well in acidic atmospheres up to pH 2. EDTA ligands are quite effectively used to improve the sharpness of the Fe^{2+}/ $Cr_2O_7^{2-}$ redox titration curve at pH 2 compared to SCN- ligands. However, the addition of EDTA ligands can shift the volume of the equivalent point earlier. Adding excess moles of EDTA to total Fe(II) ions can decrease the redox potential Fe^{2+}/ $Cr_2O_7^{2-}$. Based on the volume at the equivalence point, the Fe^{2+} ion in Mohr salt is 14.30%. with an average titration error of less than 0.30%. Potentiometric titration is a suitable electroanalytical technique for applying ligand influence concepts in redox systems due to its simplicity, ease of use, cost-effectiveness, environmental friendliness and their impact on redox potential changes.

ACKNOWLEDGEMENT

The author would like to thank the Chairman of the Foundation and the Analytical Chemistry Laboratory for funding this research.

REFERENCES

Barrera-Díaz, C. E., Lugo-Lugo, V., & Bilyeu, B. (2012). A review of chemical, electrochemical and biological methods for aqueous Cr(VI) reduction. *Journal of Hazardous Materials*, *223–224*, 1–12. https://doi.org/10.1016/j.jhazmat.2012.04.054

Bashir, S., Banday, S. M., Mustafa, M., & Rizvi, M. A. (2020). Complexation modulated Iron redox systems for waste water treatment: a natural attenuation model. *ChemistrySelect*, *5*(35), 10945–10952. https://doi.org/10.1002/slct.202002241

Bashir, S., Mustafa, M., Safvi, S. W., Farhad, N. A., & Rizvi, M. A. (2018). Iron reduces iron: A spectroelectrochemical insight of ligand effect on iron redox potential. *Chiang Mai Journal of Science*, *45*(2), 1087–1098.

Brownson, D. A. C., & Banks, C. E. (2014). *The Handbook of Graphene Electrochemistry | Dale A. C. Brownson | Springer*.

Das, S., Mishra, J., Das, S. K., Pandey, S., Rao, D. S., Chakraborty, A., Sudarshan, M., Das, N., & Thatoi, H. (2014). Investigation on mechanism of Cr(VI) reduction and removal by Bacillus amyloliquefaciens, a novel chromate tolerant bacterium isolated from chromite mine soil. *Chemosphere*, *96*, 112–121. https://doi.org/10.1016/j.chemosphere.2013.08.080

El Jamal, M. M. (2008). Experimental E-pH diagrams of Fe(III)/Fe(II) system in presence of variable concentration of different ligands. *Journal of the University of Chemical Technology and Metallurgy*, *43*(Iii), 129–138.

El Jamal, M. M., & Hammud, H. H. (2007). Quantitative Determination Of Metals Ions Using Fe (III)/ Fe (II) redox titration system with a platinum electrode. *Journal of the University of Chemical Technology and Metallurgy*, *42*(Iii), 97–104.

Gao, Yanjiao, & Liu, R. (2017). Removal of Cr(VI) from groundwater by Fe(0). *Applied Water Science*, *7*(7), 3625–3631. https://doi.org/10.1007/s13201-016-0506-0

Gao, Ying, Wang, H., Xu, R., Wang, Y. nan, Sun, Y., Bian, R., & Li, W. (2022). Remediation of Cr(VI)-contaminated soil by combined chemical reduction and microbial stabilization: The role of biogas solid residue (BSR). *Ecotoxicology and Environmental Safety*, *231*, 113198. https://doi.org/10.1016/j.ecoenv.2022.113198

Kabdaşlı, I., & Tünay, O. (2023). Hexavalent chromium removal from water and wastewaters by electrochemical processes: review. *Molecules*, *28*(5). https://doi.org/10.3390/molecules28052411

Kang, H., Liu, Y., Li, D., & Xu, L. (2022). Study on the removal of iron and manganese from groundwater using modified manganese sand based on response surface methodology. *Applied Sciences (Switzerland)*, *12*(22). https://doi.org/10.3390/app122211798

Morgan, B., & Lahav, O. (2007). The effect of pH on the kinetics of spontaneous Fe(II) oxidation by

O2 in aqueous solution - basic principles and a simple heuristic description. *Chemosphere*, *68*(11), 2080–2084. https://doi.org/10.1016/j.chemosphere.2007.02.015

Najib, F. M., & Hayder, O. I. (2011). *Study of stoichiometry of ferric thiocyanate complex for analytical*. *Iii*, 135–155.

Rizvi, M. A., Dangat, Y., Shams, T., & Khan, K. Z. (2016). Complexation Key to a pH Locked Redox Reaction. *Journal of Chemical Education*, *93*(2), 355–361. https://doi.org/10.1021/acs.jchemed.5b00499

Rizvi, M. A., Teshima, N., & Peerzada, G. M. (2013). Utilizing Fe(III)/(II)-EDTA couple for estimation of transition metal ion mixture over platinum electrode. *Asian Journal of Chemistry*, *25*(9), 4776–4778. https://doi.org/10.14233/ajchem.2013.14099

Sukekava, C. F., Downes, J., Filella, M., Vilanova, B., & Laglera, L. M. (2024). Ligand exchange provides new insight into the role of humic substances in the marine iron cycle. *Geochimica et Cosmochimica Acta*, *366*(December 2023), 17–30. https://doi.org/10.1016/j.gca.2023.12.007

Tian, N., Giannakis, S., Oji-Okoro, O. C., Farinelli, G., Garcia-Muñoz, P., & Pulgarin, C. (2024). Photo-Fenton inactivation of MS2 bacteriophage at alkaline pH by Fe salts or nm to μm-sized oxides, and the Janus-faced effects of natural organic matter in surface waters. *Catalysis Today*, *430*(November 2023). https://doi.org/10.1016/j.cattod.2024.114536

Pharmaciana
Vol.14, No.3, Nov 2024, Page. 289-298
ISSN: 2088 4559; e-ISSN: 2477 0256
DOI: 10.12928/pharmaciana.v14i3.28263

In vitro and *in vivo* anti-hyperglycemia effects of extract of Faloak (*Sterculia quadrifida* R.Br.) leaves

Velia Andrestia Dias[1], Laurenza Celine Dinanda[1], Charles Conrad Rambung[2], Maria Dewi Puspitasari Tirtaningtyas Gunawan Puteri[3], Jeffry Julianus[1], Phebe Hendra[1*]

[1]Faculty of Pharmacy Sanata Dharma University, Yogyakarta,
Paingan, Maguwoharjo, Depok, Sleman, Indonesia
[2]BAPPELITBANGDA, Prov. Nusa Tenggara Timur
Jl. Polisi Militer No.2, Oebobo, Kec. Oebobo, Kota Kupang, Nusa Tenggara Timur, Indonesia
[3]Department of Food Technology, Faculty of Life Sciences and Technology, Swiss German University,
Jl. Jalur Sutera Bar. No.Kav 15, Panunggangan Tim., Kec. Pinang, Kota Tangerang, Banten, Indonesia

Submitted: 22-01-2024 ***Reviewed: 23-09-2024*** ***Accepted: 18 -11-2024***

ABSTRACT

Despite the availability of various conventional treatments, diabetes mellitus remains a serious global health concern with an increasing prevalence. This trend underscores the need to explore potential natural alternatives. Faloak, an indigenous plant of Indonesia, has been traditionally used for various health conditions, yet its potential as an anti-hyperglycemic agent has not been comprehensively investigated. This research focused on identifying the ingredients of Faloak leaves that could lower blood sugar levels and confirm these effects in laboratory and animal models. At various concentrations, the *in vitro* evaluation assessed the inhibitory effect of α-amylase and α-glucosidase enzymes. For *in vivo* evaluation, male mice were administered glucose, sucrose, and starch after being pretreated with Faloak leaf extract, and their blood glucose levels were monitored for 120 min. Faloak leaf extract demonstrated significant inhibitory activity against α-amylase and α-glucosidase enzymes. The IC_{50} values for sucrose and maltose inhibition were 30.37 and 65.36 mg/mL, respectively, while α-amylase inhibition showed an IC_{50} of 27.02 mg/mL. In the in vivo test, mice pretreated with the extract exhibited significantly decreased blood glucose levels at 120 min compared to the control group. These findings indicate that the ethanolic extract of Faloak leaves possesses promising anti-hyperglycemic activities, positioning it as a potential candidate for developing plant-based blood glucose management. Our results demonstrate that Faloak leaf extract exhibits substantial anti-hyperglycemic properties, inhibiting vital digestive enzymes and effectively reducing postprandial glucose levels. Identifying active ingredients paves the way for further research to elucidate specific bioactive compounds and their mechanisms of action.

.

Keywords: glucose; sugar; starch; glucosidase; amylase; *Sterculia quadrifida*

Corresponding author:
Phebe Hendra
Faculty of Pharmacy Sanata Dharma University
Paingan, Maguwoharjo, Depok, Sleman, Indonesia
Email: phebe_hendra@usd.ac.id

INTRODUCTION

High blood sugar, or hyperglycemia, can indicate diabetes and other health problems (Perkumpulan Endokrinologi Indonesia, 2021). Long-term hyperglycemia increases the risk of liver, kidney, and heart impairment in patients with diabetes mellitus (American Diabetes Association, 2022). The International Diabetes Federation estimates that the number of adults with diabetes is expected to rise from 643 million in 2030 to 783 million by 2045. Furthermore, because of impaired glucose tolerance, around 500 million people are more likely to acquire type 2 diabetes (International Diabetes Federation, 2021).

A "back to nature" lifestyle is currently popular in Indonesian society, where medicinal plants are used to preserve and improve health. The genus Sterculia includes the common medicinal plant Faloak (*Sterculia quadrifida* R. Br.) found in the East Nusa Tenggara area. According to a previous study, various types of Sterculia were historically employed to address various health issues such as microbial infections, diabetes, skin conditions, gastrointestinal disorders, inflammation, and more. The Sterculia plant has been used in many countries for diverse traditional and medicinal purposes, from roots to leaves. They have been utilized for the treatment of different conditions like skin problems, gastrointestinal disorders, diabetes, and respiratory ailments (El-Sherei et al., 2016; Rollando et al., 2020; Siswadi et al., 2014; Susanto, 2019).

Studies have shown that Faloak bark exhibits an in vivo anti-hyperglycemic activity (Fernandez & Edel, 2017; Julianus et al., 2023). This activity is made possible by the secondary metabolites found in Faloak bark, which include tannins, phenols, steroids, and flavonoids. The community's harvesting of Faloak bark often exceeds the plant's ability to regenerate bark. The continued exploitation of Faloak bark raises concerns about the potential depletion of Faloak plants. Therefore, research into the Faloak's other components, particularly its leaves, is crucial for practical use and conservation.

Radjah et al. (2021) discovered that both Faloak leaves and bark contain similar secondary metabolites, such as phenols, tannins, steroids, and flavonoids (Dillak et al., 2019; Siswadi & Saragih, 2021). Despite this, the anti-hyperglycemic effects of Faloak leaf extract have not been studied. The purpose of this study was to find out whether the extract could lower blood sugar levels. Furthermore, to determine the component (s) responsible for the pharmacological activity, the active ingredients of the Faloak leaf extracts were identified, and the anti-hyperglycemic effect was also assessed through in vivo and in vitro studies.

MATERIALS AND METHOD

Materials

Dried Faloak leaf Simplicia was collected from Kupang, East Nusa Tenggara, in March 2022 and identified by experts from the Biologic Department of Sanata Dharma University. The study utilized ethanol, glucose, sucrose, starch, p-nitrophenyl-α-D-glucopyranoside, phosphate buffer pH 7, DMSO, α-glucosidase, and sodium carbonate, all of which were procured from E-Merck.

Methods

Preparation of ethanol extract from Faloak leaves (EEF)

Dried Faloak leaf simplicia was powdered and macerated using 70% ethanol for 24 hours with a ratio of 1:10. The mixture was filtered, and then it was concentrated at 40°C in a rotary evaporator to extract the active components (Tzanova et al., 2020; Zhang et al., 2018). The crude extract was stored in a dark glass bottle at four °C.

Qualitative phytochemical screening

Standard assays were used to perform a phytochemical screening of the plant under study to determine the presence of active principles. Table 1 shows standard screening tests were carried out to determine whether secondary metabolites were present or absent.

Table 1. Tests for phytochemical screening of ethanol extract from Faloak leaves

Tests	Reagent	Color appearance	Inference	References
Flavonoid detection	Extract + magnesium + HCl	Pink color appears	Flavonoids present	(Katja, 2020)
Test for tannins	Extract + 2 mL $FeCl_3$	Blue and green colors appear	Tannins present	(Arrisujaya et al., 2019)
Test for alkaloids	Extract +HCl + Mayer reagent	White precipitate	Alkaloids present	(Endah, 2017)
Test for terpenoids	Extract + chloroform + H_2SO_4	Brownish color appears	Terpenoids present	(Bhernama, 2020)

In vitro sugar tolerance study

Sample preparation

The ethanol extract was dissolved in 50% DMSO to make a 100 mg/mL solution, which was then further diluted to concentrations of 50, 25, 12.5, and 6.25 mg/mL. These samples were evaluated for their α-glucosidase inhibition (AGI) and α-amylase inhibition (AAI) activities, with each sample being tested twice (Duplo). The AGI and AAI assay was carried out utilizing our previous protocol (Benedé-Ubieto et al., 2020; Puteri et al., 2020; Sornalakshmi et al., 2016).

Alpha-glucosidase inhibition

The AGI assay was conducted in 2 µL microtubes. 100 µL of sample solution was used for samples and sample blanks; for controls and control blanks, 100 µL of 50% DMSO was utilized. 600 µL of potassium phosphate buffer (0.1 M, pH 6.9) was added to the blanks. 200 µL of the substrate solution-56 mM sucrose in potassium phosphate buffer-was added to each tube. Rat intestinal glucosidase solution in 400 µL was added to the sample and control tubes. Tubes were mixed and then incubated for 55 min at 37°C. Following incubation, each tube received 750 µL of Tris-HCl solution (2M, pH 9). The liquids were run through a glass pipette containing a cotton column and one centimeter of aluminum oxide. The absorbance was then measured at 505 nm using a microplate reader to determine enzyme inhibition (Hendra et al., 2021).

The method utilized to assess the inhibition of sucrose hydrolysis was also applied to maltose hydrolysis, with a couple of modifications: maltose solution (3.5 mM) was substituted for the sucrose solution (56 mM), and the volume of enzyme solution was decreased from 0.4 mL to 0.2 mL.

Alpha-amylase inhibition

The AAI assay was conducted in a 1.5 mL sampling tube. The mixture for the reaction included 100 µL of sample and 350 µL of starch azure solution (4 mg/mL). After a 5-min pre-incubation, 50 µL of swine pancreatic α-amylase (0.5 unit/mL) was added, and the enzymatic reaction was then incubated at 37°C for 10 min in a water bath shaker. After stopping the process with a 50 µL solution of 50% acetic acid, the mixture was centrifuged for five minutes at 9000 rpm. A 96-well plate containing 200 µL of the supernatant was used for analysis, and the absorbance of the sample was measured at 595 nm (Hendra et al., 2021; Puteri et al., 2020).

The difference between the two absorbances was used to compute the AGI and AAI activity, which was then expressed as a percentage of inhibition, as presented in Equation 1. The results were expressed as the concentration at which the enzyme activity was reduced by 50% (IC_{50}), calculated using a statistical method called regression analysis.

$$\%\ Inhibition = \frac{(A_{control} - A_{control\ blank}) - (A_{sample} - A_{sample\ blank})}{(A_{control} - A_{control\ blank})} \quad \text{.....(1)}$$

A $_{sample}$ is the absorbance while EEF is present, whereas A $_{control}$ is the absorbance value for the control. Reaction blanks were prepared using sodium phosphate buffer rather than intestinal acetone powder (Hendra et al., 2021; Puteri et al., 2020).

In vivo study in normal mice

The investigation employed male Swiss mice, aged between 2 to 3 months and with a body weight of 20 to 30 g. They were allowed a two-week acclimatization period to the laboratory conditions. Ethical approval for this study was obtained from Gadjah Mada University, with the approval code KE/FK/0323/EC/2022.

Glucose tolerance test (GTT)

Prior to the trial, normal mice were subjected to an overnight fast and given unrestricted access to water. They were then orally given different treatments in five groups: 40 mg/kg Acarbose (positive control), 0.8, 1.67, and 3.3 g/kg EEF, and CMC-Na (negative control). After 30 minutes, the mice were administered 2 g/kg of oral glucose (Chaimum-am et al., 2017). Blood glucose levels (BGL) were measured using a glucometer at different intervals, as illustrated in Figure 1 (Fransisca et al., 2018; Benedé-Ubieto et al., 2020; Sato et al., 2023).

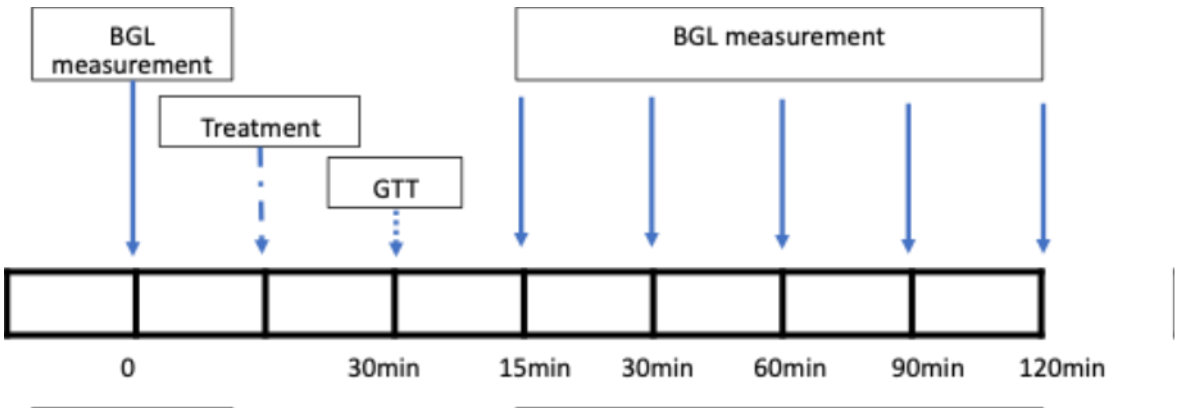

Figure 1. The timeline for the GTT

Note: BGL= blood glucose level; GTT = glucose test tolerance

Sucrose tolerance test

An identical protocol was used to determine glucose tolerance and conduct the sucrose tolerance test. However, sucrose was administered at 4 g/kg instead of glucose (Gunawan-Puteri et al., 2018; Luyen et al., 2018).

Starch tolerance test

The same method used to measure blood sugar levels after glucose injection was also used to measure blood sugar levels after starch intake, except that starch was given instead of glucose (Ogunyemi et al., 2022; Weng et al., 2021).

Data Analysis

We conducted data analysis using a one-way ANOVA, followed by a Bonferroni test, and considered a significant difference if the P-value < 0.05.

RESULT AND DISCUSSION

Phytochemical Screening

The Faloak leaves underwent phytochemical screening, identifying several secondary metabolites, as listed in Table 2. Analysis of an ethanol extract of Faloak leaves confirmed the presence of flavonoids, tannins, alkaloids, and terpenoids. Previous research has also documented the presence of these compounds in Faloak leaves (Dillak et al., 2019).

Table 2. Phytochemical constituents of ethanol extract from Faloak leaves

Metabolites	Results
Flavonoid	Positive
Tannins	Positive
Alkaloids	Positive
Terpenoids	Positive

Alpha-glucosidase inhibitors are a more valuable class of oral hypoglycemic treatments than other antidiabetic medications due to their effectiveness in treating postprandial hyperglycemia (Alssema et al., 2021). These inhibitors, like Acarbose, function by delaying the breakdown of carbohydrates, thereby prolonging the duration of the postprandial plasma glucose spike. This is crucial for preventing the absorption of carbs in the intestines and can be beneficial for treating diabetes mellitus and impaired glucose tolerance (Das et al., 2016). Consequently, an investigation was conducted to examine in vitro activity of α-glucosidase and α-amylase of the extract from Faloak leaves.

For the first time, the study shows that the ethanol extract from Faloak leaves significantly inhibits α-glucosidase and α-amylase in vitro. The IC_{50} values for the inhibition of maltose and sucrose were 65.36 and 30.37 mg/mL, respectively. Additionally, the IC_{50} for the inhibitory effect of α-amylase is 27.02 mg/mL. Based on the results, it is suggested that the ethanol extract of Faloak leaves may possess α-glucosidase inhibitory properties.

The impact of Faloak's ethanol extract on blood glucose levels was assessed using a sugar-loading test, as the inhibition of α-amylase and α-glucosidase can reduce postprandial glucose levels. The widely recognized oral sugar tolerance test was employed to screen hypoglycemic activity. Following the sugar challenge test, a significant increase in blood glucose levels was observed (Benedé-Ubieto et al., 2020). This phenomenon may be attributed to either a decrease in insulin secretion, an increase in hepatic glucose synthesis, or a reduction in tissue glucose utilization (Dilworth et al., 2021).

The graph in Figure 2 shows the blood glucose in normal mice at various time intervals (0–120 min) after they were orally given glucose, sucrose, and starch. The ethanol extract of Faloak considerably decreased the elevation of blood glucose following glucose loading, according to the findings of the glucose tolerance test (2 g/kg). All dosages of the Faloak ethanol extract significantly ($P<0.05$) lowered blood glucose levels in normal mice in a dose-dependent manner as compared to the glucose group (Table 3). The extract with the most significant percentage reduction in AUC (33.6%) was found at 3.3 g/kg. The mice that received glucose experienced a noticeable ($P<0.05$) reduction in their blood sugar levels when treated with Acarbose.

Normal mice administered sucrose showed that Acarbose and all the ethanol extract of Faloak reduced AUC significantly ($P<0.05$). The highest amount of blood glucose was lowered (36.6%) by the 3.3 g/kg ethanol extract of Faloak, which was followed by Acarbose, 1.67 g/kg of Faloak ethanol extract, and 0.8 g/kg (27.3, 25.0, and 20.9%) respectively. These data correlated with the ethanol extract from the Faloak dose.

The starch tolerance test findings demonstrated that Acarbose significantly decreased the AUC (34.6%) ($P<0.05$). Normal mice fed starch had considerably ($P<0.05$) lower blood sugar levels after being treated with ethanol extract from Faloak leaves. However, the ethanol extract of Faloak showed the greatest reduction in blood glucose at 3.3 g/kg, accounting for a 45.9% reduction. This was followed by 1.67 g/kg (42.3%) and 0.8 g/kg (33.6%).

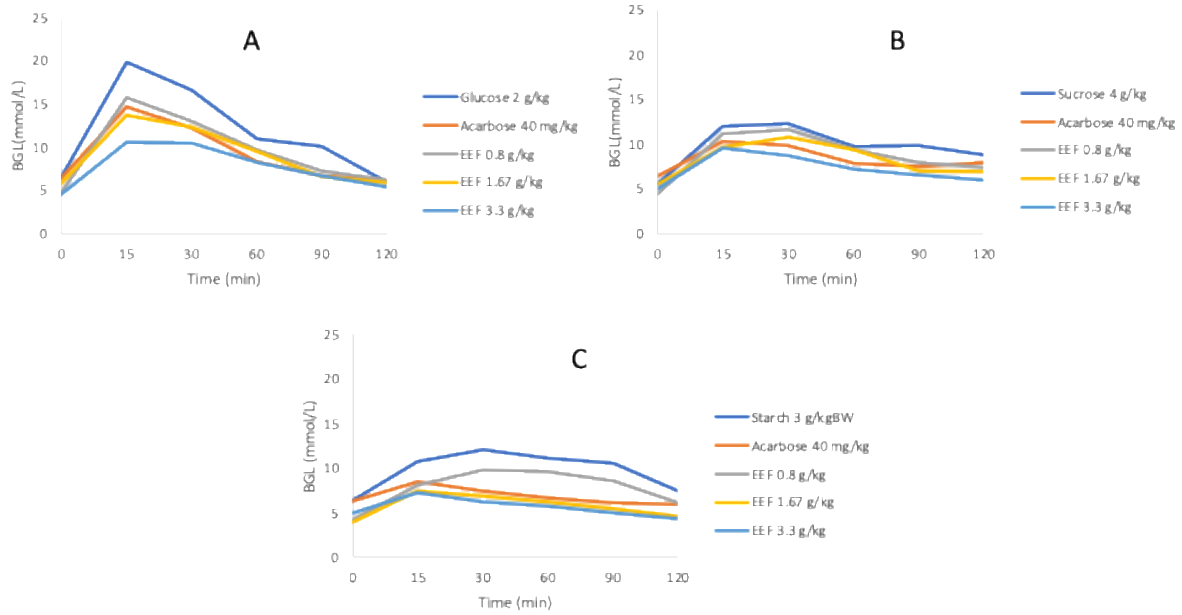

Figure 2. Effects of extract of Faloak on sugar tolerance test. A. Glucose tolerance test; B. Sucrose tolerance test; C. Starch tolerance test; EEF: ethanol extract of Faloak leaves

Table 3. Effect of extract of Faloak on sugar tolerance test in mice

Treatment	AUC (mg.min/dL)	% reduction AUC
Glucose 2 g/kg	1440.9 ± 43.2	-
Acarbose 40 mg/kg	1087.3 ± 48.8[a]	24.5
EEF 0.8 g/kg	1167.8 ± 73.2[a]	18.9
EEF 1.67 g/kg	1097.9 ± 60.4[a]	23.8
EEF 3.3 g/kg	956.2 ± 45.1[a]	33.6
Sucrose 4 g/kg	1384.8 ± 48.2	-
Acarbose 40 mg/kg	1006.2 ± 47.4[b]	27.3
EEF 0.8 g/kg	1094.9 ± 48.3[b]	20.9
EEF 1.67 g/kg	1024.8 ± 87.2[b]	25.9
EEF 3.3 g/kg	877.4 ± 50.4[b]	36.6
Starch 3 g/kg	1243.0 ± 30.3	-
Acarbose 40 mg/kg	813.1 ± 38.4[c]	34.6
EEF 0.8 g/kg	825.6 ± 26.9[c]	33.6
EEF 1.67 g/kg	717.0 ± 42.9[c]	42.3
EEF 3.3 g/kg	673.1 ± 46.8[c]	45.9

Note: All data is given as mean ±SD (n=5); [a] P<0,05 comparing treatment and glucose; [b] P<0,05 comparing treatment and sucrose (P<0,05); [c] P<0,05 comparing treatment and starch (P<0,05); EEF: ethanol extract of Faloak leaves; AUC: Area Under Curve

Our recent results revealed that the ethanol extract of Faloak could inhibit the alpha-glucosidase and alpha-amylase activity. Furthermore, after loading normal mice with glucose, sucrose, or starch, the ethanol extract of Faloak lowered the AUC and decreased the rise in blood glucose concentrations. The results demonstrated that after all sugar loading from the response for 120 min, the ethanol extract of Faloak at 3.3 g/kg had the greatest efficacy of lowering blood glucose when compared with Acarbose. The results align with previous studies by Julianus et al. (2023), indicating that a Faloak bark decoction reduces blood glucose by inhibiting alpha-glucosidase activity.

Several studies reported that flavonoids, tannins, and terpenoids are known to be bioactive antidiabetic principles. Their presence improves regulatory processes like insulin, possibly by enhancing peripheral glucose uptake or -cell glucose responsiveness. Their effectiveness may be further enhanced when they work together or separately (Darojati et al., 2022; Rahimi-Madiseh et al., 2016; Shamsudin et al., 2022; Sieniawska, 2015; Sornalakshmi et al., 2016). Ethanol as a solvent helps extract phytochemical components like flavonoids and tannins (Dias et al., 2021). Consequently, the effects of the Faloak leaf ethanol extract observed in this study might be attributed to their presence.

CONCLUSION

The present study elucidated the anti-hyperglycemic properties of the ethanolic extract of Faloak (*Sterculia quadrifida* R.Br.) leaves. Our findings demonstrate the extract's efficacy in lowering blood glucose levels through a dual mechanism: inhibiting key digestive enzymes (α-amylase and α-glucosidase) and reducing postprandial glucose levels. In vitro experiments revealed significant enzyme inhibition, while in vivo tests confirmed the extract's ability to mitigate glucose spikes. We have found several active ingredients that may be responsible for these pharmacological effects. However, more research is required to identify the specific compounds and understand their work. Our findings support the traditional uses of Faloak and provide scientific evidence for its potential in managing blood glucose levels. This comprehensive evaluation positions Faloak leaf extract as a promising candidate for developing natural anti-hyperglycemic interventions.

ACKNOWLEDGEMENT

The author acknowledges the funding for the research provided by Directorate of Academic Research and Community Service of Sanata Dharma University.

REFERENCES

Ali, R. B., Atangwho, I. J., Kuar, N., Ahmad, M., Mahmud, R., & Asmawi, M. Z. (2013). In vitro and in vivo effects of standardized extract and fractions of *Phaleria macrocarpa* fruits pericarp on lead carbohydrate digesting enzymes. *BMC Complementary and Alternative Medicine*, *13*(1), 39. https://doi.org/10.1186/1472-6882-13-39

Alssema, M., Ruijgrok, C., Blaak, E. E., Egli, L., Dussort, P., Vinoy, S., Dekker, J. M., & Denise Robertson, M. (2021). Effects of alpha-glucosidase-inhibiting drugs on acute postprandial glucose and insulin responses: A systematic review and meta-analysis. *Nutrition & Diabetes*, *11*(1), 11. https://doi.org/10.1038/s41387-021-00152-5

American Diabetes Association. (2022). Introduction: *Standards of Medical Care in Diabetes—2022*. *Diabetes Care*, *45*(Supplement_1), S1–S2. https://doi.org/10.2337/dc22-Sint

Arrisujaya, D., Susanty, D., & Kusumah, R. R. (2019). Skrining fitokimia dan kadar flavonoid total ekstrak aseton dan etil asetat biji buah bisbul (*Diospyros discolor* tumbuhan endemik Bogor. *Cendekia Journal of Pharmacy*, *3*(2), 130–136.

Benedé-Ubieto, R., Estévez-Vázquez, O., Ramadori, P., Cubero, F. J., & Nevzorova, Y. A. (2020). Guidelines and considerations for metabolic tolerance tests in mice. *Diabetes, Metabolic Syndrome and Obesity: Targets and Therapy*, *13*, 439–450. https://doi.org/10.2147/DMSO.S234665

Bhernama, B. G. (2020). Skrining fitokimia ekstrak etanol rumput laut *Gracilaria* sp asal Desa Neusu Kabupaten Aceh Besar. *AMINA*, *2*(1), 1–5.

Chaimum-aom, N., Chomko, S., & Talubmook, C. (2017). Toxicology and oral glucose tolerance test (OGTT) of Thai medicinal plant used for diabetes controls, *Phyllanthus acidus* L. (Euphorbiacea). *Pharmacognosy Journal*, *9*(1), 58–61. https://doi.org/10.5530/pj.2017.1.11

Darojati, U. A., Murwanti, R., & Hertiani, T. (2022). Sterculia quadrifid R.Br: A comprehensive review of ethnobotany, phytochemistry, pharmacology, and toxicology. *JPSCR: Journal of Pharmaceutical Science and Clinical Research*, *7*(1), 1–14. https://doi.org/10.20961/jpscr.v7i1.52244

Das, S. K., Samanta, L., & Thatoi, H. (2016). In vitro antidiabetic and antioxidant potentials of leaf and stem bark extracts of a mangrove plant, *Xylocarpus granatum*. *Journal of Herbs, Spices & Medicinal Plants*, *22*(2), 105–117. https://doi.org/10.1080/10496475.2015.1057352

Dias, M. C., Pinto, D. C. G. A., & Silva, A. M. S. (2021). Plant flavonoids: Chemical characteristics and biological activity. *Molecules*, *26*(5377), 1–16. https://doi.org/10.3390/molecules26175377

Dillak, H. I., Kristiani, E. B. E., & Kasmiyati, S. (2019). Secondary metabolites and antioxidant activity of ethanolic extract of Faloak (*Sterculia quadrifida*). *Biosaintifika*, *11*(3), 296–303

Dilworth, L., Facey, A., & Omoruyi, F. (2021). Diabetes mellitus and its metabolic complications: The role of adipose tissues. *International Journal of Molecular Sciences*, *22*(7644), 1–18. https://doi.org/10.3390/ijms22147644

El-Sherei, M. M., Ragheb, A. Y., Kassem, M. E. S., Marzouk, M. M., Mosharrafa, S. A., & Saleh, N. A. M. (2016). Phytochemistry, biological activities and economical uses of the genus Sterculia and the related genera: A reveiw. *Asian Pacific Journal of Tropical Disease*, *6*(6), 492–501. https://doi.org/10.1016/S2222-1808(16)61075-7

Endah, S. R. N. (2017). Pembuatan ekstrak etanol dan penapisan fitokimia ekstrak etanol kulit batang sintok (*Cinnamomun sintoc* Bl.). *Jurnal Hexagro*, *1*(2), 29–35. https://doi.org/10.36423/hexagro.v1i2.95

Fernandez, S., & Edel, E. (2017). Effect of extract ethanol leather Faloak rubber (*Sterculia* sp.) to decrease of blood glucoasa content in glucose induction. *Jurnal Info Kesehatan*, *15*(1), 129–136.

Fransisca, F., Kalangi, G. E., Candrasari, D. S., & Hendra, P. (2018). The effect of Pasak Bumi roots towards blood glucose level in glucose-loaded mice. *Jurnal Farmasi Sains Dan Komunitas (Journal of Pharmaceutical Sciences and Community)*, *15*(1), Article 1. https://doi.org/10.24071/jpsc.00965

Gunawan-Puteri, M. D. P. T., Rustandi, F., & Hendra, P. (2018). Spray dried aqueous extract of lemongrass (*Cymbopogon citratus*) exhibits in vitro dan in vivo anti hyperglycemic activities. *Journal of Pharmaceutical Sciences and Community*, *15*(2), 55–61. https://doi.org/10.24071/jpsc.1521531

Hendra, P., Rizki, N., & Safitri, E. (2021). Antihyperglycemic activities of uli banana leaves on oral sugar tolerance. *Journal of Functional Food and Nutraceutical*, *2*(2), 75–79. https://doi.org/10.33555/jffn.v2i2.59

International Diabetes Federation. (2021). *IDF diabetes atlas* (10th edition). International Diabetes Federation.

Julianus, J., Gunawan-Puteri, M. D. P. T., Wiwengku, R. T. P., Setiawati, A., & Hendra, P. (2023). In vitro and in vivo anti hyperglycemic evaluation of *Sterculia quadrifida* bark through the inhibition of alpha glucosidase. *Journal of Pharmaceutical Sciences and Community*, *20*(1), 15–21. https://doi.org/10.24071/jpsc.005153

Katja, D. G. (2020). Fitokimia dan aktivitas antioksidan ekstrak kulit batang *Chisocheton* sp. (C.DC) Harms (Meliaceae). *CHEMISTRY PROGRESS*, *13*(2), 117–122. https://doi.org/10.35799/cp.13.2.2020.31672

Luyen, N. T., Dang, N. H., Binh, P. T. X., Hai, N. T., & Dat, N. T. (2018). Hypoglycemic property of triterpenoid saponin PFS isolated from *Polyscias fruticosa* leaves. *Anais Da Academia Brasileira de Ciências*, *90*(3), 2881–2886. https://doi.org/10.1590/0001-3765201820170945

Ogunyemi, O. M., Gyebi, G. A., Saheed, A., Paul, J., Nwaneri-Chidozie, V., Olorundare, O., Adebayo, J., Koketsu, M., Aljarba, N., Alkahtani, S., Batiha, G. E.-S., & Olaiya, C. O. (2022). Inhibition mechanism of alpha-amylase, a diabetes target, by a steroidal pregnane and pregnane glycosides derived from Gongronema latifolium Benth. *Frontiers in Molecular Biosciences*, *9*(86799), 1–19.

Perkumpulan Endokrinologi Indonesia. (2021). *Pedoman pengelolaan dan pencegahan diabetes melitus tipe 2 dewasa di Indonesia—2021*. PB Perkeni. https://pbperkeni.or.id/unduhan

Puteri, M. D. P. T. G., Tjiptadi, F. M., Hendra, P., & Santoso, F. (2020). Lemongrass (*Cymbopogon citratus*) ethanolic extract exhibited activities that inhibit *α* -glucosidase enzymes and postprandial blood glucose elevation. *Makara Journal of Science*, *24*(4), 219–227. https://doi.org/10.7454/mss.v24i4.1154

Radjah, S. Y., Setio Putri, K. S., & Elya, B. (2021). Elastase inhibitory activity, determination of total polyphenol and determination of total flavonoids and pharmacognosy study of Faloak plant (*Sterculia quadrifida* R.Br) from East Nusa Tenggara-Indonesia. *Pharmacognosy Journal*, *13*(3), 758–764. https://doi.org/10.5530/pj.2021.13.97

Rahimi-Madiseh, M., Malekpour-Tehrani, A., Bahmani, M., & Rafieian-Kopaei, M. (2016). The research and development on the antioxidants in prevention of diabetic complications. *Asian Pac. J. of Trop. Med.*, *9*(9), 825–831. https://doi.org/10.1016/j.apjtm.2016.07.001

Rollando, R., Warsito, W., Masruri, M., & Widodo, W. (2020). Potential therapeutic use of *Sterculia quadrifida* R.Br and *Sterculia foetida* Linn.: Review. *Asian Journal of Plant Sciences*, *19*(4), 325–334. https://doi.org/10.3923/ajps.2020.325.334

Sato, V. H., Chewchinda, S., Goli, A. S., Sato, H., Nontakham, J., & Vongsak, B. (2023). Oral glucose tolerance test (OGTT) evidence for the postprandial anti-hyperglycemic property of *Salacca zalacca* (Gaertn.) Voss seed extract. *Molecules*, *28*(6775), Article 19. https://doi.org/10.3390/molecules28196775

Shamsudin, N. F., Ahmed, Q. U., Mahmood, S., Shah, S. A. A., Sarian, M. N., Khattak, M. M. A. K., Khatib, A., Sabere, A. S. M., Yusoff, Y. M., & Latip, J. (2022). Flavonoids as antidiabetic and anti-inflammatory agents: A review on structural activity relationship-based studies and meta-analysis. *International Journal of Molecular Sciences*, *23*(12605), 1–35. https://doi.org/10.3390/ijms232012605

Sieniawska, E. (2015). Activities of tannins – from *in vitro* studies to clinical trials. *Natural Product Communications*, *10*(11), 1877–1884. https://doi.org/10.1177/1934578X1501001118

Siswadi, S., Rianawati, H., Saragih, G. S., & Hadi, D. S. (2014). The potency of Faloak's (*Sterculia quadrifida*, R.Br.) active compounds as natural remedy. *International Seminar Proceedings "Forests & Medicinal Plants for Better Human Welfare," 1*, 73–79. https://doi.org/10.5281/ZENODO.3353788

Siswadi, S., & Saragih, G. S. (2021). Phytochemical analysis of bioactive compounds in ethanolic extract of *Sterculia quadrifida* R.Br. *AIP Conference Proceedings 2353, 030098 (2021)*, 030098. https://doi.org/10.1063/5.0053057

Sornalakshmi, V., Tresina, S. P., Paulpriya, P., Packia, L. M., & Mohan, V. R. (2016). Oral glucose tolerance test (OGTT) in normal control and glucose induced hyperglycemic rats with hedyotis leschenaultiana DC. *International Journal of Toxicological and Pharmacological Research*, *8*(1), 59–62.

Susanto, F. H. (2019). Potensi fraksi aktivitas antibakteri dan antiradikal dari kulit batang Faloak (*Sterculia quadrifida* R.Br). *Majalah Farmasi Dan Farmakologi*, *23*(1), 25–28. https://doi.org/10.20956/mff.v23i1.6463

Tzanova, M., Atanasov, V., Yaneva, Z., Ivanova, D., & Dinev, T. (2020). Selectivity of current extraction techniques for flavonoids from plant materials. *Processes*, *8*(1222), Article 10. https://doi.org/10.3390/pr8101222

Weng, L., Chen, T., Huang, L., Lai, D., Kang, N., Fu, Y., & Weng, C. (2021). A nutraceutical combination of cinnamon, purple onion, and tea linked with key enzymes on treatment of type 2 diabetes. *Journal of Food Biochemistry*, *45*(12). https://doi.org/10.1111/jfbc.13971

Zhang, Q.-W., Lin, L.-G., & Ye, W.-C. (2018). Techniques for extraction and isolation of natural products: A comprehensive review. *Chinese Medicine*, *13*(20), 1–26. https://doi.org/10.1186/s13020-018-0177-x

Pharmaciana
Vol.14, No.3, Nov 2024, Page.299-308
ISSN: 2088 4559; e-ISSN: 2477 0256
DOI: 10.12928/pharmaciana.v14i3.30005

Nicotine-free vape liquids containing essential oils of peppermint, lavender, and tangerine: safety and efficacy profile

Rahmad Aji Prasetya[1,3*], Djamilah Arifiyana[2], Zain Budi Syulthoni[4]
[1]Department of Pharmacy Practice, Akademi Farmasi Surabaya
[2]Department of Pharmaceutical Sciences, Akademi Farmasi Surabaya
Jl. Ketintang Madya No.81, Surabaya, Indonesia
[3]Faculty of Mathematics and Natural Sciences, Universitas Negeri Surabaya
Komplek Universitas Negeri Surabaya Gedung C5-C6,
Jl. Ketintang Selatan, Surabaya, Indonesia
[4]Psychiatrist, Medical Doctor Profession Education Study Program, Faculty of Medicine and Health,
Institut Teknologi Sepuluh Nopember
Gedung Fakultas Kedokteran dan Kesehatan, Kampus ITS Sukolilo, Surabaya, Indonesia

Submitted: 06-09-2024 ***Reviewed: 13-11-2024*** ***Accepted: 18-11-2024***

ABSTRACT

Despite low nicotine levels, cigarettes and vape liquids can cause addiction, which makes quitting smoking difficult owing to withdrawal syndrome. Hence, we created a nicotine-free liquid vape using essential oils (EOs) like peppermint (*Mentha piperita*), lavender (*Lavandula latifolia*), and tangerine (*Citrus reticulata*) to substitute the nicotine in inducing relaxation without addiction. Thus, this study aimed to examine (1) the safety profile of this nicotine-free liquid vape by observing chemical characteristics using gas chromatography-mass spectrometry (GC-MS) and (2) its efficacy in reducing short-term anxiety in healthy volunteers who had previously used nicotine vape. The most complicated vape liquid formula (F4), containing propylene glycol, vegetable glycerin, with those three EOs, was injected into GC-MS, and the mass spectra were compared to the Wiley mass spectral library to identify the compound name. For the efficacy test, subjects who met inclusion criteria and fulfilled informed consent were randomly assigned to five groups (four groups received test liquids formula (F1-F4) while one group received placebo). Before and after using the vape liquid, subjects were asked to complete the State-Trait Anxiety Inventory (STAI) questionnaire to assess its anxiety-reduction effects. The result showed that nicotine-free vape liquids containing three EOs did not show any foreign substances that had never been encountered before, which means our product is safer than nicotine-containing vape liquids. This safety was also supported by all study subjects who did not report any adverse effects. The efficacy test showed that subjects who used vape liquids with essential oils (F1-F4) experienced a significant decrease in heart rate and systolic blood pressure. At the same time, 50% had a lower post-test STAI score, indicating a decrease in anxiety, although it was not statistically significant.

Keywords: vape liquids, *Mentha spicata*, *Lavandula latifolia*, *Citrus reticulata*, anxiety, GC-MS

Corresponding author:
Rahmad Aji Prasetya
Faculty of Mathematics and Natural Sciences, Universitas Negeri Surabaya
Komplek Universitas Negeri Surabaya Gedung C5-C6
Jl. Ketintang Selatan, Surabaya, Indonesia
Email: rahmadprasetya@unesa.ac.id

INTRODUCTION

The current trend in Indonesia shows a noticeable rise in the number of active smokers over time. According to data from the 2021 Global Adult Tobacco Survey (GATS) initiated by the Ministry of Health, the population of adult smokers rose from 60.3 million in 2011 to 69.1 million in 2021 (Kemenkes RI., 2022). Moreover, Indonesia holds the highest number of smokers in the Southeast Asia region, as stated in The Tobacco Control Atlas ASEAN Region 4th Edition (Drope et al., 2018). The World Health Organization (WHO) implements multiple strategies to combat the tobacco epidemic. One of these strategies involves substituting traditional tobacco cigarettes with electronic cigarettes, also known as the Electronic Nicotine Delivery System (ENDS) or vape. By utilizing this particular cigarette variant, individuals can effectively regulate their nicotine use, enabling active smokers to quit smoking (Bullen et al., 2013). Conversely, in Indonesia, vape utilization is experiencing a significant rise. According to the 2018 National Basic Health Research (Riskesdas) data, the prevalence of e-cigarette usage among the Indonesian population was 2.8%. The highest proportion of e-cigarette users was found in the 10-14 year age group, with a rate of 10.6%, followed closely by 15-19 year olds at 10.5% (Badan Penelitian dan Pengembangan Kesehatan, 2019). This indicates that nicotine exposure and addiction are increasing among young people.

Nicotine, found in both tobacco cigarettes and vape, is an active compound that induces a feeling of relaxation but is also highly addictive. Nicotine has been demonstrated to cause heart diseases through oxidative stress, fibrosis, and inflammation, in addition to the risks associated with dependency. Nicotine exerts persistent effects on the brain and central nervous system in several organs, which potentially causes stroke (Moheimani et al., 2017; Ramalingam et al., 2021). Particularly in pregnant women, nicotine may hamper blood circulation to the fetus, posing a risk to fetal development and potentially leading to adverse outcomes upon birth, such as disabilities or growth retardation (Rodrigues et al., 2022). Regardless of the low nicotine levels in cigarettes or vape liquids, they can still lead to addiction due to the interaction between nicotine and nicotine cholinergic receptors in the brain. As a result, users may develop tolerance and require higher doses of nicotine over time (Hall et al., 2015). Furthermore, those who are dependent or addicted to nicotine have significant challenges when attempting to suddenly cease smoking due to withdrawal syndrome, characterized by symptoms such as agitation, anxiety, and potential psychological disorders (McLaughlin et al., 2015). Therefore, it necessitates a method for reducing the symptoms of drug withdrawal in individuals seeking to overcome nicotine addiction.

Recently, we developed a nicotine-free liquid vape containing essential oils (EOs) like peppermint (*Mentha piperita*), lavender (*Lavandula latifolia*), and tangerine (*Citrus reticulata*). This vape liquid has been formulated and rigorously tested to ensure it meets quality standards regarding homogeneity, compatibility, viscosity, and acceptability (Prasetya & Imtihani, 2023). The addition of essential oil is expected to function as a substitute for nicotine, inducing a sense of relaxation without the risk of addiction. In other applications, these EOs have been proven to relax patients in several conditions. For instance, studies conducted on patients following abdominal surgery or endoscopic procedures demonstrated that peppermint EO can effectively alleviate both pain and anxiety (Akbari et al., 2019). Lavender and citrus oils possess the capacity to relieve symptoms of anxiety, enhance mood, optimize sleep quality, augment cognitive capacities, and aid in the reduction of blood pressure, discomfort, and muscular spasms in both adults and children (Beyliklioğlu & Arslan, 2019; Koulivand et al., 2013). However, there is no study examining their efficacy in reducing anxiety in the form of vape liquid. In terms of safety, vaping is comparatively less hazardous than smoking traditional tobacco cigarettes; nonetheless, it can still have adverse effects (Mcneill et al., 2015). One factor contributing to this is the release of aldehyde molecules when propylene glycol and glycerin are heated (Mcneill et al., 2015). Hence, this study aimed to (1) examine the safety profile of this nicotine-free liquid vape by observing the chemical characteristics using gas chromatography-mass spectrometry and (2) investigate, for the first time, its efficacy in reducing short-term anxiety among several volunteers who had previously used nicotine vape.

MATERIALS AND METHOD

Materials

This study began with the preparation of vape liquid ingredients such as propylene glycol (PG) and vegetable glycerin (VG) (pharmaceutical grade), 100% pure peppermint, tangerine, and lavender EOs (PT. Syailendra Bumi Investama), vanilla essence, and sucralose (food grade). A hand mixer (Philips) was used to make the liquid. Gas Chromatography-Mass Spectroscopy (GC-MS) analysis was performed using GC-MS QP-2010 Shimadzu with Rtx-5MS capillary column for pure EOs analysis. For vape liquid analysis, ISQ™ 7610 Single Quadrupole Thermo Scientific GC-MS with TriPlus™ RSH SMART Autosampler and the 5% phenyl phase Thermo Scientific™ TraceGOLD™ TG-5MS column were used.

Methods

Vape liquids preparation and formulation

All ingredients mentioned above were mixed directly with a hand mixer to make a liquid based on the formulas stated in Table 1. Each liquid was made for single use with a volume of approximately 10.5 mL.

Table 1. Nicotine-free vape liquids formula

Ingredients	F1	F2	F3	F4	Control
Propylene glycol	7 mL	7 mL	7 mL	7 mL	7 mL
Vegetable glycerin	3 mL	3 mL	3 mL	3 mL	3 mL
EO lavender	15 µL	-		8 µL	-
EO peppermint	-	15 µL	-	8 µL	-
EO tangerine	-	-	15 µL	8 µL	-
Vanilla essence	0.4 mL	0.4 mL	0.4 mL	0.4 mL	0.4 mL
Sucralose	0.3 mg	0.3 mg	0.3 mg	1 mg	0.3 mg

Vape liquid compound characterization

In this study, three EOs and the most complex formula (F4) sample were characterized and analyzed for their compound content using GC-MS. The operating conditions used for pure EOs analysis were an injector temperature of 250°C and an oven temperature of 50°C (2.0 min hold), 10°C/min to 240 °C (10 min hold). The pressure is set at 8.8 Psi, and the capillary column is used. Helium gas is used for the gas carrier with a flow rate of 1.0 mL/min. Meanwhile, the headspace sampling technique was used for vape liquid analysis. A liquid sample (1 mL) was placed in a crimp-closed headspace vial with a magnetic bi-metal cap and a toped silicone septum. The sample was first agitated for 2-3 minutes with a temperature of 250°C before being injected through an autosampler. The operating conditions for GC were almost the same as the EO analysis except for the carrier gas flow rate of 0.5 mL/min. After the sample is injected and analyzed by gas chromatography, it is then analyzed using mass spectrometry. Subsequent identification was performed by comparing their recorded mass spectra with those contained in the Wiley mass spectral library of the GC-MS data system.

Efficacy examination of vape liquids in reducing anxiety levels

This first stage clinical trial was an experimental pre-post randomized controlled study. Ethical approval for this study was obtained from the University of Muhammadiyah Lamongan Ethics Committee for Medical Research with certificate number 337/EC/KEPK-S2/10/2023. The subject's criteria included adult males/females aged 18 years and older, had vaped nicotine liquids at least six

months before, and were currently healthy with no history of asthma or other chronic respiratory disorders. Subjects who were willing (filling out informed consent) and met the inclusion criteria were randomly divided into five groups. Group 1 received a vape liquid product according to F1, Group 2 received F2, Group 3 received F3, Group 4 received F4, and Group 5 received negative control (placebo). The provision of vape liquid products was carried out in a double-blind manner to maintain the objectivity of the effectiveness measurement. Before and after data collection, a general practitioner will check subjects' vital signs, like temperature, blood pressure, heart rate, and SpO2, to ensure their health condition. To reduce the risk of allergies, subjects will be asked to drip vape liquid on the skin of the arm before use. If there was an allergic reaction, such as itching or redness, the subject could switch to another formula or be excluded from the study. Following the allergy check, subjects were allowed to use the assigned formula of vape liquids for around 10-15 minutes using their own devices, either mods or pods. To examine the efficacy of the vape liquid in producing a sense of relaxation and reducing anxiety levels, subjects were asked to fill out the State-Trait Anxiety Inventory (STAI) questionnaire before and after using the vape. STAI questionnaire is a tool utilized to assess both actual state anxiety and persistent trait anxiety. The scale assessment for state anxiety comprises 20 items that enquire about subjects' emotions, such as tension, dread, worry, and restlessness. The trait scale comprises 20 items designed to assess anxiety as a characteristic. The STAI questionnaire consists of four Likert scales for each item, and higher scores indicate greater anxiety (Beyliklioğlu & Arslan, 2019). In this work, we utilized a translated version of the STAI in Bahasa Indonesia that has undergone rigorous testing to establish its validity and reliability (Khoiriyah, 2021).

Data Analysis

The statistical analysis was determined by paired t-test and Wilcoxon test (for paired data that did not pass the normality test) to determine significant differences between pre and post-data. Meanwhile, unless stated otherwise, the Kruskal-Wallis test was used to examine group differences. Data analysis and visualization were performed using GraphPad Prism version 8.0.1 for Windows, GraphPad Software, San Diego, California USA, www.graphpad.com; $p<0.05$ was considered significant.

RESULT AND DISCUSSION

Nicotine-free vape liquid compound characterization

The GC-MS examination of the compound content in F4 vape liquid containing three essential oils revealed 37 peaks on the chromatogram with concentrations higher than 0.01% (Figure 1). The main compounds (relative percentage >3%) found in the vape liquid were (R)-(-)-2-amino-1-propanol (peak #1&2), D-limonene (peak #13), eucalyptol (peak #14), linalool (peak #18), cyclohexanone (peak #23&25), levomenthol (peak #26), and linalyl acetate (peak #31). The complete list of the identified components is shown in Table 2. The first and second peaks were identified as (R)-(-)-2-Amino-1-propanol, which was probably formed by the pyrolysis mechanism of propylene glycol and glycerol. Further decomposition and oxidation of PG and VG due to thermal conditions yielded several compounds such as acetone, propanoic acid, and butanoic acid (peak #4, 6, and 8, respectively), which accounted for around 12% of vape liquid composition in total (Li et al., 2021; Liang et al., 2022).

By using the headspace sampling technique, the sample was first heated and turned into aerosol before being auto-injected. This method successfully separated the liquid components from the 3 EOs used in the nicotine-free vape liquid (F4). For instance, compounds found in this study, such as ß-myrcene, 3-octanol, o-cymene, D-limonene, trans-linalool oxide, linalool, limonene oxide, trans-, 1,2-dihydro linalool, terpinene-4-ol, a-Terpineol, and linalyl acetate, have been proven contained in lavender as stated by Dong et al. (2020). Our finding about compounds commonly found in peppermint was also in line with Shahbazi's (2015) study, including ß-myrcene, limonene, menthone (Cyclohexanone,5-methyl-2-(1-methyl ethyl)-, cis-) and its derivate, levomenthol, and pulegone. Meanwhile, compounds like eucalyptol, linalool, a-terpineol, sabinene (Bicyclo[3.1.0] hexane,4-methylene-1-(1-methylethyl)-),

octacosane, heptacosane were commonly contained in tangerine or citrus essential oils (Mahmood et al., 2017; Yabalak et al., 2022).

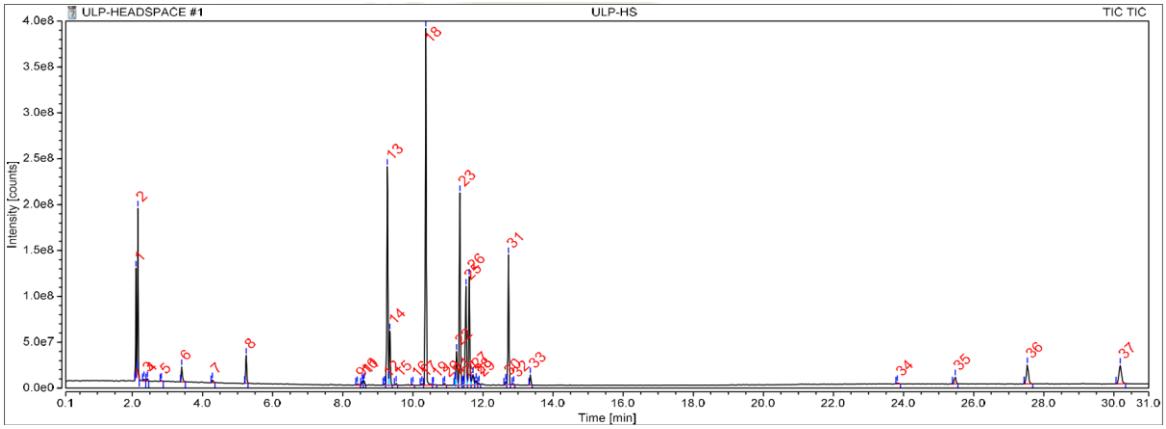

Figure 1. Chromatogram of GC analysis of nicotine-free vape liquid formula with 3 EOs (F4)

Table 2. Identified compounds of nicotine-free vape liquid formula with 3 EOs (F4) by GC-MS

Peak number	Retention time	Compound name	SI	Prob. (%)	Relative area (%)
1	2.100	(R)-(-)-2-Amino-1-propanol	79.2	91.34	3.40
2	2.155	(R)-(-)-2-Amino-1-propanol	80.3	49.15	5.47
3	2.332	Propanamide, 2-hydroxy-	72.2	88.12	0.16
4	2.427	Acetone	60.2	29.73	0.16
5	2.821	L-Alanine, N-acetyl-	56.8	39.39	0.09
6	3.406	Propanoic acid, 2-oxo-	73.4	29.56	1.16
7	4.280	Propanamide, 2-hydroxy-	67.8	55.63	0.22
8	5.246	Butanoic acid, ethyl ester	90.2	94.91	1.77
9	8.419	Bicyclo[3.1.0]hexane, 4-methylene-1-(1-methylethyl)-	68.7	18.00	0.13
10	8.562	ß-Myrcene	77.2	31.24	0.25
11	8.613	3-Octanol	74.4	61.36	0.28
12	9.195	o-Cymene	71.0	28.86	0.12
13	9.273	D-Limonene	93.1	37.45	13.79
14	9.345	Eucalyptol	93.0	82.50	3.53
15	9.521	a-Pinene	71.7	12.47	0.13
16	10.001	trans-Linalool oxide (furanoid)	65.8	19.44	0.08
17	10.259	Cyclohexene, 1-methyl-4-(1-methylethylidene)-	64.2	5.67	0.15
18	10.372	Linalool	92.6	70.69	22.13
19	10.583	Limonene oxide, trans-	67.2	18.44	0.10
20	10.906	1,2-Dihydrolinalool	67.9	22.15	0.12
21	11.205	Isopulegol	83.4	31.03	0.18
22	11.249	Bicyclo[2.2.1]heptan-2-one, 1,7,7-trimethyl-, (1S)-	91.9	43.42	2.47
23	11.341	Cyclohexanone, 5-methyl-2-(1-methylethyl)-, cis-	94.1	44.43	12.44
24	11.433	endo-Borneol	69.0	27.79	0.14
25	11.514	Cyclohexanone, 5-methyl-2-(1-methylethyl)-, cis-	90.1	43.64	7.68
26	11.606	Levomenthol	94.8	44.83	7.22

Peak number	Retention time	Compound name	SI	Prob. (%)	Relative area (%)
27	11.715	Terpinen-4-ol	80.9	33.75	1.12
28	11.804	Cyclohexanol, 5-methyl-2-(1-methylethyl)-, (1a,2a,5a)-	78.2	19.95	0.33
29	11.892	a-Terpineol	67.0	5.34	0.14
30	12.647	Pulegone	74.9	28.19	0.24
31	12.729	Linalyl acetate	89.6	22.14	7.56
32	12.875	2-Cyclohexen-1-one, 3-methyl-6-(1-methylethyl)-	69.2	56.57	0.09
33	13.354	Cyclohexanol, 5-methyl-2-(1-methylethyl)-, acetate	85.3	27.92	0.64
34	23.826	Digitoxin	58.0	11.41	0.14
35	25.472	Dotriacontane	76.4	15.41	0.82
36	27.530	Octacosane	83.3	10.89	2.57
37	30.180	Heptacosane	82.8	9.69	2.98
				Total	100

*SI = Similarity Index

The results of GC-MS analysis on pure peppermint EO without solvents (Figure 2) showed the presence of menthone (peak #4), L-(-)-menthol (peak #5, 6, and 8), limonene (peak #2), beta-pinene (peak #1), and pulegone (peak #7) compounds with similarity index of 98, 99, 94, 90, and 92, respectively. Likewise, the mixture of lavender and tangerine EOs (Figure 3) has been proven to contain compounds similar to previous results, including limonene (peak #1), linalool (peak #2), camphor (peak #3), and linalyl acetate (peak #4) with similarity index of 96, 97, 93, and 97, respectively. Taken together, both compound analysis results of nicotine-free vape liquid and pure EOs used as raw materials did not show any foreign substances that had never been encountered before. This indicates that our product has a better safety level than nicotine-containing vape liquids available on the market.

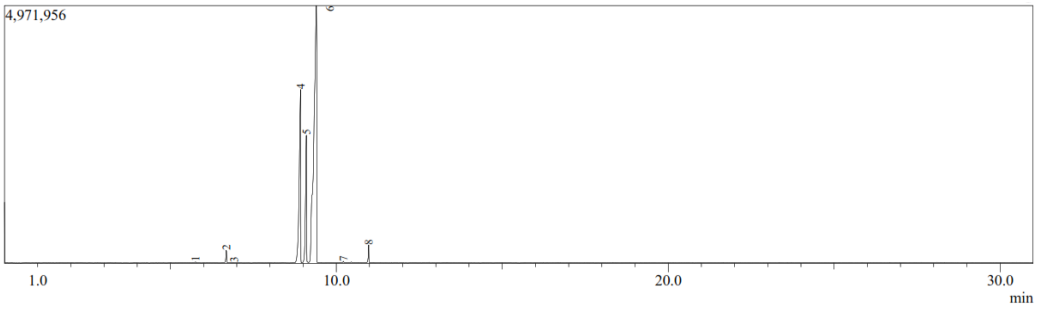

Figure 2. Chromatogram of GC analysis of EO peppermint

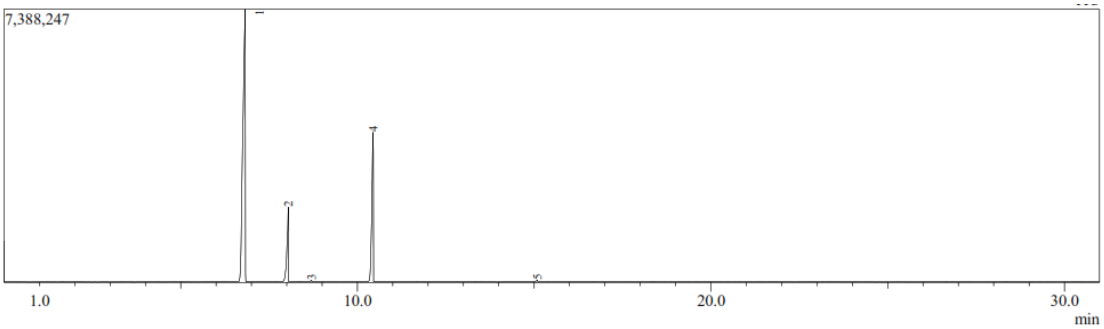

Figure 3. Chromatogram of GC analysis of mixed EOs lavender and tangerine

Efficacy examination of vape liquids in reducing anxiety levels

There were 32 participants who signed up voluntarily, but only 30 were eligible and randomized to 5 groups equally (6 participants in each group). Most of them were students with an average age of 22 years old and used pods (83.3%) as their vaping devices. There was actually one female who enrolled in this study, but she did not pass the health screening due to a history of asthma (Table 3). Then, the result of the efficacy examination showed that 50% of subjects who used vape liquid containing essential oils (F1-F4) experienced a decrease in anxiety levels, as indicated by a lower post-test STAI score. Unfortunately, statistical analysis revealed no significant difference in STAI scores, both between before and after using nicotine-free vape liquid and between the control and test vape liquid (F1-F4). The full results can be seen in Figure 4.

Table 3. Sociodemographic data of the subjects (n=30)

Variable	Frequency	%
Gender		
Male	30	100
Female	0	0
Age (year)		
18-24	26	86.7
25-37	4	13.3
Occupation		
Student	24	80
Private employee	5	16.7
Entrepreneur	1	3.3
Type of vape device		
Mods	25	83.3
Pods	5	16.7

The absence of a significant change in the anxiety levels of the subjects could be caused by several things, including the relatively short treatment so that it did not have a significant impact. The typical user of an electronic cigarette vaped between 60 and 90 puffs in a day (Yingst et al., 2020). The subjects in this study only used vape for ten minutes or about ten to fifteen puffs. In another study related to interventions for reducing stress and anxiety, a decrease in anxiety levels was only observed after the treatment was administered for at least four weeks (Ponzo et al., 2020). The interaction between the treatment subjects during data collection can also affect the anxiety levels of the research subjects. The emotions of the subjects can be influenced by others during data collection. This is in line with a study on the influence of emotional contamination on a social group (Herrando & Constantinides, 2021). In this study, a decrease in anxiety levels was still observed, although it was not statistically significant. This decrease aligns with the findings of other studies that used essential oils such as lavender and peppermint in inhalers, which can reduce anxiety levels in patients in the Intensive Care Unit (ICU) (Karimzadeh et al., 2021).

Table 4 depicted that subjects who vaped with liquid containing essential oil(s) experienced a significant ($p<0.001$) decrease in heart rate and systolic blood pressure but not in diastolic blood pressure. Meanwhile, the control group also showed a decrease in those parameters but not significant ($p>0.05$). This was in line with a study using lavender as inhaled aromatherapy for patients before angiography (Ziyaeifard et al., 2017). Furthermore, regarding acceptability, the subjects said the vape liquid products they tried were well-accepted. Besides, no side effects were experienced by all of the research subjects when using this nicotine-free vape liquid, such as allergic reactions, shortness of breath, or a burning sensation in the respiratory tract.

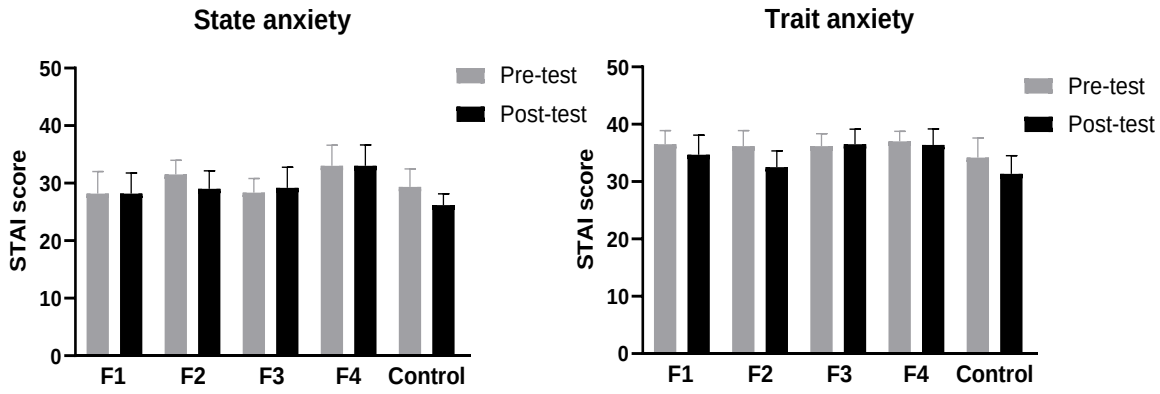

Figure 4. State anxiety (left) and trait anxiety (right) score differences between groups according to the STAI questionnaire. Data are presented in average ± standard error of the mean (SEM)

Table 4. Hemodynamic monitoring data of the subjects

Variables		Control group (n=6) ± SEM	F1-F4 groups (n=24) ± SEM	p-value*
Heart rate (beat/min)	pre-test	91.00±3.31	94.46±2.58	0.55
	post-test	87.67±4.33	87.92±2.85	0.65
	p-value	0.26	**0.0009*** **	
Blood pressure				
Systole (mmHg)	pre-test	119.80±5.05	117.1±3.38	0.75
	post-test	115.20±7.91	109.5±2.38	0.60
	p-value	0.54	**0.0009*** **	
Diastole (mmHg)	pre-test	74.67±5.91	73.83±2.18	0.48
	post-test	80.83±8.92	71.00±1.74	0.39
	p-value	0.32	0.10	

*p-value was analyzed between control and treatment (F1-F4) groups using the Mann-Whitney test
***p<0.001

However, this study has limitations, such as a small sample size in each group and the protocol for measuring anxiety levels. Further examination of liquid vape efficacy should be performed for a longer duration to see whether the liquid can produce relaxed feelings and lessen nicotine addiction. The procedure for measuring anxiety could be improved by allowing each subject to use the liquid without communicating with others to avoid emotional contamination and bias when fulfilling the questionnaire.

CONCLUSION

To conclude, we reported the safety profile for the first time based on the results of GC-MS analysis, which proved that no foreign compounds were found in a nicotine-free vape liquid as it contained in other commercial vape liquids. This safety is also supported by all study subjects who did not report any adverse effects. Regarding the efficacy of this liquid, it can be said that some subjects experienced lower anxiety levels, indicated by lower scores on the post-test STAI questionnaire, though not significant, and decreased heart rate and systolic blood pressure.

ACKNOWLEDGEMENT

This research received funding from the Akademi Farmasi Surabaya's internal research scheme and the Directorate of Vocational Education, Ministry of Education, Culture, Research, and Technology through the Junior Lecturer Research (PDP) Scheme 2024.

REFERENCES

Akbari, F., Rezaei, M., & Khatony, A. (2019). Effect of peppermint essence on the pain and anxiety caused by intravenous catheterization In cardiac patients: a randomized controlled trial. *Journal of Pain Research*, *12*, 2933. https://doi.org/10.2147/JPR.S226312

Badan Penelitian dan Pengembangan Kesehatan. (2019). *Laporan Nasional Riskesdas 2018*.

Beyliklioğlu, A., & Arslan, S. (2019). Effect of Lavender oil on the anxiety of patients before breast Surgery. *Journal of PeriAnesthesia Nursing*, *34*(3), 587–593. https://doi.org/10.1016/J.JOPAN.2018.10.002

Bullen, C., Howe, C., Laugesen, M., McRobbie, H., Parag, V., Williman, J., & Walker, N. (2013). Electronic cigarettes for smoking cessation: a randomised controlled trial. *Lancet (London, England)*, *382*(9905), 1629–1637. https://doi.org/10.1016/S0140-6736(13)61842-5

Dong, G., Bai, X., Aimila, A., Aisa, H., & Maiwulanjiang, M. (2020). Study on Lavender Essential Oil Chemical Compositions by GC-MS and Improved pGC. *Molecules*, *25*(14), 3166. https://doi.org/10.3390/molecules25143166

Drope, J., Schluger, N., Cahn, Z., Drope, J., Hamill, S., Islami, F., Liber, A., Nargis, N., & Stoklosa, M. (2018). The tobacco atlas. sixth edition. consumption. In *American Cancer Society and Vital Strategies* (Issue March).

Hall, F. S., Der-Avakian, A., Gould, T. J., Markou, A., Shoaib, M., & Young, J. W. (2015). Negative affective states and cognitive impairments in nicotine dependence. *Neuroscience & Biobehavioral Reviews*, *58*, 168–185. https://doi.org/10.1016/J.NEUBIOREV.2015.06.004

Herrando, C., & Constantinides, E. (2021). Emotional contagion: a brief overview and future directions. *Frontiers in Psychology*, *12*. https://doi.org/10.3389/fpsyg.2021.712606

Karimzadeh, Z., Azizzadeh Forouzi, M., Rahiminezhad, E., Ahmadinejad, M., & Dehghan, M. (2021). The effects of Lavender and Citrus aurantium on anxiety and agitation of the conscious patients in intensive care units: a parallel randomized placebo-controlled trial. *BioMed Research International*, *2021*, 1–8. https://doi.org/10.1155/2021/5565956

Kemenkes RI. (2022). *Perokok dewasa di Indonesia meningkat dalam sepuluh tahun terakhir - badan kebijakan pembangunan kesehatan*. 3 Juni.

Khoiriyah, S. N. (2021). Perbedaan tingkat kecemasan mahasiswa Lulusan SMA dam MA dalam Menghadapi Pelajaran Bahasa Arab pada Fakultas Ushuluddin dan Humaniora UIN Walisongo Semarang Angkatan 2018. In *Skripsi*. Universitas Islam Negeri Walisongo Semarang.

Koulivand, P. H., Ghadiri, M. K., & Gorji, A. (2013). Lavender and the nervous system. *Evidence-Based Complementary and Alternative Medicine*, *2013*, 1–10. https://doi.org/10.1155/2013/681304

Li, Y., Burns, A. E., Tran, L. N., Abellar, K. A., Poindexter, M., Li, X., Madl, A. K., Pinkerton, K. E., & Nguyen, T. B. (2021). Impact of e-liquid composition, coil temperature, and puff topography on the aerosol chemistry of electronic cigarettes. *Chemical Research in Toxicology*, *34*(6), 1640–1654. https://doi.org/10.1021/acs.chemrestox.1c00070

Liang, J., Zhang, D., Cao, Y., Xue, K., Xia, Y., & Qi, Z. (2022). Insight into pyrolysis mechanism of 1,2-propylene glycol: based on density functional theory and wavefunction analysis. *Journal of Molecular Graphics and Modelling*, *116*, 108277. https://doi.org/10.1016/j.jmgm.2022.108277

Mahmood, R., Ahmad, S., Jaskani, M. J., & Ahmad, R. (2017). Topographicallocation of orchards modulates the biochemical composition of essential oils in citrus fruit peel. *Pakistan Journal of Agricultural Sciences*, *54*(3), 635–643. https://doi.org/10.21162/PAKJAS/17.6417

McLaughlin, I., Dani, J. A., & De Biasi, M. (2015). Nicotine Withdrawal. In *Current Topics in Behavioral Neurosciences* (Vol. 24, pp. 99–123). Springer, Cham. https://doi.org/10.1007/978-3-319-13482-6_4

Mcneill, A., Brose, L. S., Calder, R., Hitchman, S. C., Hajek, P., & H, M. (2015). E-cigarettes : an evidence update A report commissioned by Public Health England. In *Public Health England*. Public Health England.

Moheimani, R. S., Bhetraratana, M., Peters, K. M., Yang, B. K., Yin, F., Gornbein, J., Araujo, J. A., & Middlekauff, H. R. (2017). Sympathomimetic effects of acute e-cigarette use: role of nicotine and non-nicotine constituents. *Journal of the American Heart Association*, *6*(9). https://doi.org/10.1161/JAHA.117.006579

Ponzo, S., Morelli, D., Kawadler, J. M., Hemmings, N. R., Bird, G., & Plans, D. (2020). Efficacy of the digital therapeutic mobile app bioBase to reduce stress and improve mental well-being among university students: randomized controlled trial. *JMIR MHealth and UHealth*, *8*(4), e17767. https://doi.org/10.2196/17767

Prasetya, R. A., & Imtihani, H. N. (2023). Formulasi dan evaluasi Likuid Vape tanpa Nikotin dengan Kandungan Minyak Atsiri Pepermin (Mentha spicata), Jeruk (Citrus reticulata) dan Lavender (Lavandula angustifolia). *Journal of Herbal, Clinical and Pharmaceutical Science (HERCLIPS)*, *5*(01), 34. https://doi.org/10.30587/herclips.v5i01.6380

Ramalingam, A., Budin, S. B., Mohd Fauzi, N., Ritchie, R. H., & Zainalabidin, S. (2021). Targeting mitochondrial reactive oxygen species-mediated oxidative stress attenuates nicotine-induced cardiac remodeling and dysfunction. *Scientific Reports*, *11*(1), 13845. https://doi.org/10.1038/s41598-021-93234-4

Rodrigues, V. da S. T., Miranda, R. A., Soares, P. N., Peixoto, T. C., de Oliveira, E., Manhães, A. C., de Moura, E. G., & Lisboa, P. C. (2022). Neonatal nicotine exposure changes insulin status in fat depots: sex-related differences. *Journal of Developmental Origins of Health and Disease*, *13*(2), 252–262. https://doi.org/10.1017/S2040174421000131

Shahbazi, Y. (2015). Chemical composition and in vitro antibacterial activity of Mentha spicata essential oil against common food-borne Pathogenic Bacteria. *Journal of Pathogens*, *2015*, 1–5. https://doi.org/10.1155/2015/916305

Yabalak, E., Erdoğan Eliuz, E. A., & Nazlı, M. D. (2022). Evaluation of Citrus reticulata essential oil: Chemical composition and antibacterial effectiveness incorporated gelatin on E. coli and S. aureus. *International Journal of Environmental Health Research*, *32*(6), 1261–1270. https://doi.org/10.1080/09603123.2021.1872059

Yingst, J., Foulds, J., Veldheer, S., Cobb, C. O., Yen, M. S., Hrabovsky, S., Allen, S. I., Bullen, C., & Eissenberg, T. (2020). Measurement of electronic cigarette frequency of use among smokers participating in a randomized controlled trial. *Nicotine and Tobacco Research*, *22*(5), 699–704. https://doi.org/10.1093/ntr/nty233

Ziyaeifard, M., Azarfarin, R., Faritous, Z., Dehdashtian, E., Baghestani, ; Amir, Ziyaeifard, P., & Yousefi, Z. (2017). Evaluation of lavender oil inhalation effects on blood pressure and heart rate in patients undergoing coronary Angiography. *Iranian Heart Journal*, *18*(4), 29–33.

Pharmaciana
Vol.14, No.3, Nov 2024, Page. 309–323
ISSN: 2088 4559; e-ISSN: 2477 0256
DOI: 10.12928/pharmaciana.v14i3.27639

Gastroprotective activity of Banana peel (*Musa paradisiaca* var. sapientum) methanol extract purified on aspirin-induced gastric ulceration in Rats

Jastria Pusmarani[1]*, Risky Juliansyah Putri[2], Citra Dewi[2], Difa Fitriani[3], Setyo Purwono[4], Zullies Ikawati[5]

[1]Department of Pharmacology and Clinical Pharmacy of Universitas Mandala Waluya, Jl. A. H. Nasution no. G37 Kambu district, Kendari, South-East Sulawesi, Indonesia
[2]Department of Phytochemical of Universitas Mandala Waluya, Jl. A. H. Nasution no. G37 Kambu district, Kendari, South-East Sulawesi, Indonesia
[3]Department of Pharmacy of Universitas Mandala Waluya, Jl. A. H. Nasution no. G37 Kambu district, Kendari, South-East Sulawesi, Indonesia
[4]Department of Pharmacology and Therapy of Universitas Gadjah Mada, Jl. Farmako, Sekip Utara, Mlati, Kabupaten Sleman, Daerah Istimewa Yogyakarta, Indonesia
[5]Department of Pharmacology and Clinical Pharmacy of Universitas Gadjah Mada, Jl.Sekip Utara,. Mlati, Kabupaten Sleman, Daerah Istimewa Yogyakarta, Indonesia

Submitted: 23-01-2024 ***Reviewed: 21-02-2024*** ***Accepted: 10-09-2024***

ABSTRACT

Banana (*Musa paradisiaca* var. sapientum) is the world's most popular fruit-bearing crop, with rising consumption and waste. This study aimed to measure the metabolite compound and evaluate the gastroprotective properties of a banana peel-purified methanol extract. Animals test used in this study were divided into six groups: Group One received NaCMC 0.5%, Group Two received sucralfate, Group Three received aspirin 1000 mg/kg body weight, and groups four, five, and six received PBP at doses of 200 mg/kg body weight, 400 mg/kg body weight, and 600 mg/kg body weight, respectively, for seven days. Except for group 1, all groups were induced with aspirin at 1000 mg/kg body weight on the eighth day. The result of this study exhibited banana peel containing total phenolic, flavonoid, and tannin compounds with concentrations of 33.45 mg GAE/g, 19.92 mg QE/g, and 0.16 %, respectively. The results showed that pure extract of *Musa paradisiaca* var. sapientum fruit peel can reduce the incidence of gastric ulcers by decreasing the ulcer index ($p<0.05$). The results suggested that *Musa paradisiaca* var. sapientum peel has a gastroprotective effect against aspirin-induced gastric ulceration.

Keywords: *Musa paradisiaca* var. sapientum peel, Gastric ulcer, purified extract

.

Corresponding author:
Jastria Pusmarani
Universitas Mandala Waluya
Jl. A. H. Nasution no. G37 Kambu district, Kendari, South-East Sulawesi, Indonesia
Email: triapusmarani20@gmail.com

INTRODUCTION

Peptic ulcers are lesions that develop in the stomach or the nearby part of the small intestine known as the duodenum, and they are among the most prevalent ailments affecting the upper digestive system (Malik et al., 2018). The prevalence of peptic ulcer disease is estimated at 5–10% in the general population (Lanas & Chan, 2017). Peptic ulcers are caused by mucosal damage, which is mostly caused by platelet agglutination inhibitors such as long-term use of nonsteroidal anti-inflammatory drugs (NSAIDs), *Helicobacter pylori* (H. *pylori*) infection, alcohol consumption, and long-term use of tobacco (Wang and Wei, 2022; Jang et al., 2022). In addition, peptic ulcers may be induced by submucosal erosion, decreased cyclooxygenase, and deformation of the stomach mucosal layer (Ibrahim & Allam, 2022). Moreover, peptic ulcers result from disruptions in the body's defensive mechanisms, which include blood circulation, mucus level, mucosal membranes, cell renewal, and endogenous defense enzymes (Yaghoobi & Armstrong, 2022).

Aspirin is one of the NSAIDs that might cause gastric damage in the form of chronic inflammation produced by gastric acid stimulation because it breaks down the gastric mucosal barrier. Additionally, gastric acid can directly damage the mucosal epithelial cells, resulting in inflammation, bleeding, and gastric ulcers. Intestinal microorganisms, bile, and other stimulating factors have all been implicated in the process of aspirin-induced mucosal damage (Washio et al., 2016). Patients with a medical history of peptic ulcers or previous bleeding who are above 65 years old, who are taking anticoagulants or long-term steroids, and who consume high dosages of NSAIDs or combinations of NSAIDs are the most vulnerable to developing ulcers induced by NSAIDs (Narayanan et al., 2018).

Antacids, acid inhibitory agents, cytoprotective agents, histamine-2 (H_2) receptor antagonists, muscarinic receptor (M1) antagonists, *Helicobacter pylori* eradication drugs, and triple therapy regimens are the most often used pharmaceuticals to treat peptic ulcers (Dipiro et al., 2020). Typical adverse effects associated with these medications consist of joint discomfort, gynecomastia, erectile dysfunction, and systemic alkalosis (Handa et al., 2014). Nonetheless, prolonged use of proton pump inhibitors (PPIs) can lead to several adverse outcomes as they suppress gastric acid secretion, creating an environment conducive to the growth of ingested microbial pathogens and infections (Kuna et al., 2019). An earlier research study reported that the use of PPIs could increase the risk of acquiring enteric infections such as Campylobacter and Salmonella, as well as developing community-acquired pneumonia (Lambert et al., 2015).

Currently, numerous investigations are underway to explore the potential of natural substances in improving pharmaceuticals with minimal adverse effects. Bananas are widely consumed globally, with a production exceeding 100 million tons worldwide in 2013 (Vu et al., 2018). Some of the metabolite compounds identified in banana peel include tannins, flavonoids, polyphenols, terpenoids and phenolic (Thomas and Krishnakumar, 2017; Pusmarani et al., 2019; Kibria et al., 2019). When compared to other fruit peels like watermelon, melon, papaya, and pineapple, banana peel has a high phenolic concentration (Morais et al., 2015). Various metabolite compounds, such as terpenoids flavonoids, and phenolics, play important roles in human health as antioxidants and gastroprotective agents (Jabbar, 2022; Li et al., 2022; Al Amri and Hossain (2018) reported that the extract methanol from banana peel had higher antioxidant activity related to gastroprotective activity.

Kapadia et al. (2015) discovered that banana peels contained therapeutic compounds. Banana peels have various activities, such as antibacterial, antibiotic, and antioxidant (Rita et al., 2020). Furthermore, various pharmacological activities of banana peel include hepatoprotective, cholesterol-lowering, and anti-ulcerogenic activities (Berawi and Bimandama, 2018; Pusmarani et al., 2022; Aziakpono et al., 2021). The research that has been carried out has shown extracts of banana peel (*Musa sapientum*) protect the stomach mucosa against erosion and have ulcer-healing capabilities (Onasanwo et al., 2013). Therefore, based on these facts, this study aims to assess the gastroprotective activities of banana peel extract purified on aspirin-induced gastric ulceration in rats.

MATERIALS AND METHODS

Materials

Banana fruit peels (*Musa paradisiaca* var. sapientum) were obtained from the Poleang district, Bombana regency, Southeast Sulawesi. The plants were determined at the Biology Laboratory, Faculty of Teacher Training and Education, Halu Oleo University.

Methods

Extraction of Banana peel

A 5-kilogram dry peel of ripe banana was placed in a maceration vessel. The extraction of the sample was used through maceration and methanol as the solvent and left at room temperature for 24 hours. This method was repeated for 3x24 hours, or until the solvent was clear. The extract of banana peels was then filtered five times with filter paper. A rotary rotavapor was used to evaporate the macerate. After getting the extract, it was concentrated and weighed on an analytical balance. Then, the methanol extract of banana peel was calculated for its yield.

Purification extract of Banana peel

Liquid-liquid extraction was used to purify the banana peel extract through a separatory funnel. The viscous banana peel extract was dissolved in distilled water, mixed with *n*-hexane, transferred to a separating funnel, and shaken until the solution separated. This process was repeated until the solvent's yellow color was removed. Ethyl acetate was used to elute the n-hexane fraction until the solution was separated into two parts. The ethyl-acetate as an insoluble fraction was eluted by hot water and then concentrated as a viscous banana peel extract containing total phenolic, flavonoid, and tannin compounds using a rotary evaporator.

Determination of total phenolic content

Measurement of the overall phenolic content of the pure extract obtained from banana peels using the Folin-Ciocalteu method through spectrophotometry (Hossain et al., 2014). Gallic acid served as the standard for the experiment. The crude extract and the standard were mixed with the 7.5% sodium carbonate and Folin Ciocalteau reagent. The resulting mixture's absorbance was gauged at 775 nm. A standard curve is used to determine phenolic compounds and is reported as gallic acid equivalents (GAE) in milligrams per gram dry weight (mg/g extracted substance). The analysis of the sample was conducted three times to ensure accuracy.

Determination of total flavonoid content

The determination of flavonoid content in the purified extract obtained from banana peel was conducted through a colorimetric aluminum chloride test (Baba & Malik, 2015). In the experiment, quercetin served as the standard for the assay. The crude extract and the standard were combined with sodium nitrite, aluminum chloride, and distilled water. The mixture extract and standard were then incubated, followed by the addition of NaOH and thorough mixing. After cooling down, the absorbance of the mixtures was read at 415 nm. Using the calibration curve, the flavonoid compound was assessed and written as milligrams of quercetin equivalent per gram of dry weight (mg QE/g). Sample was analyzed three times to ensure accuracy.

Determination of tannin content

To determine the tannin content, an insoluble compound called polyvinylpolypyrrolidone (PVPP) was employed. PVPP is known for its ability to bind tannins (Pulipati et al., 2014). For the analysis of tannin content, a standard tannin solution was utilized. The crude extract was prepared by dissolving the extract with a content of 1 mg in methanol. Then, the extract of 1 ml was mixed with 100 mg PVPP. The mixture was vortexed and incubated at 40^{o}C for 15 minutes, followed by centrifugation at 3000 rpm for 10 minutes. The resulting mixture was read at 725 nm. The tannin compound was calculated using a

calibration curve and reported a percentage of weight per weight (% w/w). The experiment was performed in triplicate to ensure accuracy.

In vivo study: gastroprotective effect of banana peel methanol extract purified animals

A total of thirty male rats with Wistar species, that have a weight range of 150-200 g with the age 2-3 months were obtained from the animal enclosure of the integrated research and Testing Laboratory unit Preclinical and Experimental Animal Development of Universitas Gadjah Mada, Indonesia. The animals were then separated randomly into six groups with each group consisting of five rats. The group consisted of negative control (rats receiving 0.5% of Na-CMC), a sucralfate-treated (dose: 120 mg/5 ml), an induced control group (with 1000 mg/kg body weight of aspirin), and three groups received 200, 400, and 600 mg/kg body weight of purified banana peel methanol extract, respectively. All rats were adapted and acclimatized for 7 days. All animals were fed rodent pellets as a standard diet and water *ad libitum*. Before testing, all rats were not fed for 18 hours with still received water ad libitum. The animals were kept into a cage at a stable temperature (25 ± 2 °C) and relative humidity (50-70%) with controlled light (12 hours dark/12 hours light cycle). All studies were approved by the Animal Care Ethics Committee of the Faculty of Medicine, Gadjah Mada University, Yogyakarta, Indonesia (KE/FK/108/EC/2019), following the National Institute of Health (NIH) "Guidelines for the Care and Use of Laboratory Animals" (NIH Publications No. 85-23, Revised 1985).

Dose preparation and route of administration

The first group was given NaCMC 0.5%. The second group was treated with sucralfate 120 ml/5 ml. All animals were not fed for 18 hours and only given a drink before treatment. The third group was given aspirin at a dosage of 1000 mg/kg body weight, while groups 4, 5, and 6 were treated with purified banana peel methanol extract at doses of 200 mg/kg body weight, 400 mg/kg body weight, and 600 mg/kg body weight, respectively. All animals received oral treatment for 7 days. All animals except for group 1 were administered a dose of aspirin at 1000 mg/kg body weight to induce gastric ulcers on the eighth day. After six hours, all rats were euthanized with ketamine overdose by injected intraperitoneally. The abdomen were then dissected, eliminated, rinsed, and cut open along the larger curvature. The gastric juice was obtained for analysis, and the stomach was thoroughly washed with normal saline to eliminate blood clots and stomach contents. Macroscopic examination of the stomach by measuring the gastric pH, the volume of gastric fluid, and the extent of ulceration was calculated with a vernier caliper (Mahurkar and Sayeed, 2015; Kadhem et al., 2018).

The number of scorings was used to determine the ulcer score. (Table 1) (Pusmarani et al., 2019). The method described by Cho & Ogle (1979) was used to calculate the ulcer index (mm) for each group. The ulcer index and percentage inhibition were calculated using formula (1) and formula (2):

$$\text{Ulcer Index (UI)} = \frac{Total\ of\ Ulcer\ score}{Total\ of\ ulcerated\ rats} \quad \text{..... (1)}$$

$$\%\ \text{Inhibition} = \frac{IU\ (Induced\ Group) - IU\ (treated\ group)}{IU\ (Induced\ Group)} \text{ x } 100\% \quad \text{..... (2)}$$

The determination process of gastric juice and pH

The gastric juice were obtained and then subjected to centrifugation at 1000 rpm for 10 minutes. The volume of supernatant was measured in milliliters, and its pH was determined by a pH meter (Ulser, 2016).

Histopathological evaluation of gastric damage

The method for determining the histologic assessment of gastric tissue called gastric histopathologic examination follows the method of Carleton et al. (1980). Each stomach was placed in formalin 10% at

room temperature for 24 hours. The stomach was embedded in a paraffin block using an automated embedding machine. Gastric tissue samples were cut into 5 mm slices for sectioning and colored using hematoxylin-eosin for histopathological examination of the gastric mucosa (Sisay and Jemere, 2020). The histology of the stomach rats observed edema, inflammatory cell infiltration, and necrotic changes to define all rat stomachs (Kathirvelu et al., 2019; Zaghlool et al., 2019).

Table 1. Number of scoring lesions formed of gastric

Number of Scoring	Number of lesions (mm)
1	< 1
2	1.00 -2.00
3	2.01-3.00
4	3.01-4.00
5	4.01-5.00
10	>5.00
Perforation	>25

Data Analysis

The mean value and standard deviation of means are described with numerical data. All statistical analyses were calculated with SPSS 25.00 software. Kruskal-Wall test was used to analyze the data. The Mann-Whitney test was used to compare the groups with the control group with statistical significance at the $p < 0.05$ levels.

RESULT AND DISCUSSION

In extract of methanol from banana peel, it was found to yield an extract of 7.07%. The total phenolics level in *Musa paradiasiaca* var. sapientum peel purified extract was analyzed using a slightly modified Folin-Ciocalteu method with the standard (gallic acid), and the total phenolics level was 33.45 mg GAE/g (Table 2). The flavonoid content of *Musa paradiasiaca* var. sapientum peel purified extract was measured by aluminum chloride assay with quercetin as a standard and showed a flavonoid level of 19.92 mg GAE/g. The tannin level in banana peel purified extract was measured using an insoluble polyvinyl-polypyrrolidone with tannin as a standard, and it was found to be 0.16%. In this study, the banana peel had the highest level of flavonoid when compared to total phenolic and tannin.

The absorption measurements of standard gallic acid, quercetin, and tannin were entered into Microsoft Excel to create a graph of concentration versus absorption, which served as a calibration curve for standard gallic acid solution (Figure 1, Figure 2, and Figure 3).

Table 2. Determination of total phenolic, flavonoid and tannin levels of banana (*Musa paradisiaca* var. sapientum) peel methanol extract purified

Metabolite Compounds	Replication	Absorbance	Metabolite compound content	Metabolite compound levels average±SD
Total Phenolic (mg GAE/g)	1	0.132	33.86	33.45±0.3554
	2	0.144	33.23	
	3	0.139	33.26	
Flavonoids (mg QE/g)	1	0.031	19.55	19.92±0.4549
	2	0.032	19.79	
	3	0.032	20.43	
Tannins (%)	1	0.046	0.17	0.16±0.01
	2	0.043	0.15	
	3	0.044	0.16	

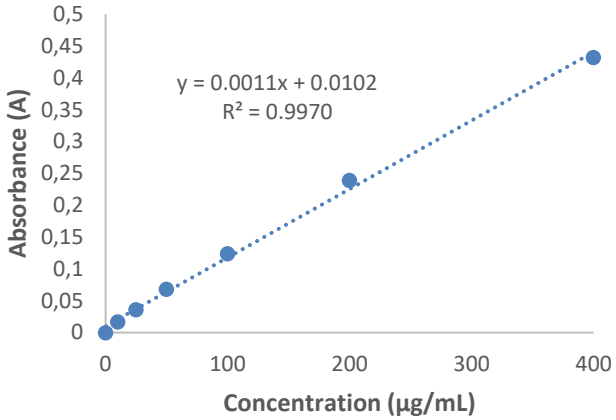

Figure. 1. Calibration curve of gallic acid at a maximum wavelength of 775 nm

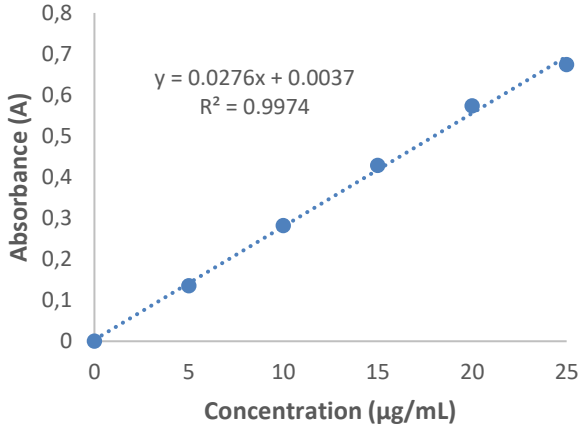

Figure 2. Calibration curve of quercetin at a maximum wavelength of 415 nm

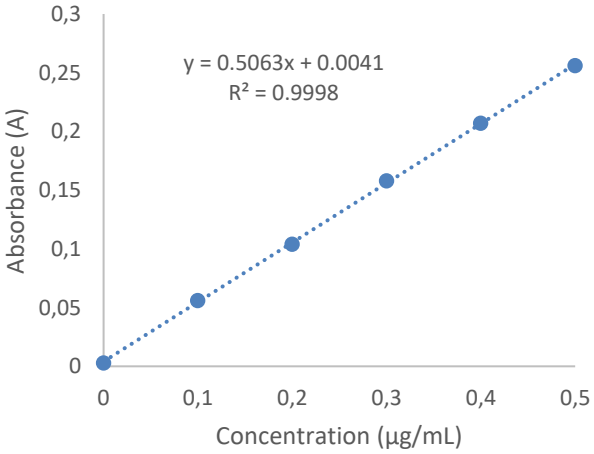

Figure 3. Calibration curve of tannin at a maximum wavelength of 725 nm

The gastroprotective effect of banana peel purified extract on gastric juice and pH is shown in Table 3. The findings of the research indicated that the purified methanol extract of *Musa paradisiaca* var. sapientum peel, administered with doses at 200 mg/kg and 400 mg/kg body weight (resulting in values of 2.63 ±0.727 and 1.61 ± 0.51, respectively), as well as sucralfate (with a value of 2.03 ±0.89), significantly decrease the volume of gastric juice when compared to the group that was induced with aspirin (1000 mg/kg body weight). The rising volume of gastric juice from the banana peel methanol extract purified was not statistically significantly different (Kruskal Wallis test, $p=0.475<0.05$) compared to the aspirin group. Based on some research results, one of the indicators that can be measured when a peptic ulcer occurs is a rise in gastric volume and the healing of gastric ulcers can be characterized by a decrease in the volume of stomach juice (Raish et al., 2021). Although the purification of banana peel extract raised the pH of the stomach, macroscopic and histopathologic observations showed that the extract was effective in promoting the healing of gastric ulcers.

The pH levels in the sucralfate group and banana peel methanol extract group were significantly increased compared to the other groups (Table 3). The pH value in the banana peel methanol extract group with doses of 200 mg/kg body weight (4.80±0.837), 400 mg/kg body weight (4.63± 2.663), and 600 mg/kg BW (4.87±0.641) was higher when compared to the induced group (4.20±0.837). Pre-treatment with purification banana peel extract 200 mg/kg BW, 400 mg/kg BW, and 600 mg/kg BW showed a significant increase in gastric fluid pH ($p=0.01<0.05$, $p=0.025<0.05$, and $p=0.01<0.05$, respectively) compared to group aspirin-induced ulcers. The increase in gastric fluid pH caused by the purified banana peel methanol extract showed no significant difference ($p < 0.05$) compared to the sucralfate group. The results agree with previous research that shows increasing the pH of gastric juices is associated with the healing process of gastric ulcers (Rahman et al., 2020).

Table 3 shows the effect of purified banana peel methanol extract at various doses on ulcers in rats before and six hours after receiving aspirin. The results indicate that oral aspirin administration causes damage to the gastric mucosa with an ulcer index of 7.6±3.362 (Figure 4). This damage is significantly different from the group receiving Na CMC ($p=0.005$, $p < 0.05$). These findings indicate that aspirin administration resulted in a marked ulcer index compared to the negative control group. Purified banana peel methanol extract with the dose of 200 mg/kg body weight substantially reduced ($p=0.018 < 0.05$) the ulcer index as compared to the induced group. Meanwhile, a purified banana peel methanol extract with a dose of 400 mg/kg BW significantly declined the ulcer index ($p=0.005<0.05$) compared to the induced group. Furthermore, purified banana peel methanol extract at a dose of 600 mg/kg body weight significantly reduced ($p=0.005<0.05$) the ulcer index as compared to the induced group. Moreover, purified banana peel methanol extract at a dose of 200, 400, and 600 mg/kg BW reduced the ulcer index 3.30±1.732, 0.00±0.000 and 0.00±0.000 giving 56.5%, 100%, and 100% protection, respectively.

Table 3. Gastroprotective activities of banana (*Musa paradisiaca* var. sapientum) peel extract purified

Animal group	Group	pH of gastric juice (Mean ± SD)	Volume of gastric juice (Mean ± SD)	Ulcer Index (Mean ± SD)	% inhibition
1	Na CMC 0.5%	5.20 ± 1.095	0.88 ± 0.565	0.00±0.000 [f]	0
2	Sucralfat (120 mg/5 ml)	4.40± 0.548	2.03 ±0.89	0.00±0.000 [f]	100
3	Aspirin (1000 mg/kg BW)	4.20±0.837	3.62 ± 1.31	7.60±3.362 [f]	0
4	Purified banana peel extract (200 mg/kg BW	4.80±0.837[e]	6.03 ±2.727[d]	3.30±1.732[a,f]	56.5
5	Purified banana peel extract (400 mg/kg BW)	4.63± 2.663[e]	2.63 ±0.727[d]	0.00±0.000[b,f]	100
6	Purified banana peel extract	4.87±0.641[e]	1.61 ± 0.51[d]	0.00±0.000[c,f]	100

(600 mg/kg BW)

[a,b,c] The aspirin, banana peel, and sucralfate groups demonstrated a significant reduction in ulcer index according to the Mann-Whitney test. [d,e] There was no significant difference in pH and gastric volume between the banana peel and sucralfate groups according to the Kruskal-Wallis test. There were significant differences in the ulcer index between the banana peel and the standard drug sucralfate, as indicated by the Kruskal-Wallis test.

According to our study, a purified banana peel extract significantly decreased the ulcer index after aspirin administration (Kruskal-Wallis test, $p = 0.000 < 0.05$), demonstrating that banana peel has gastroprotective activity against aspirin-induced gastric ulcers. Figure 4 shows the representation of the stomachs of rats after aspirin-induced gastric ulcers. Aspirin (1000 mg/kg body weight) induced superficial or deep erosions, inhibited prostaglandins, and decreased mucus.

Histopathological examination of the control group (Na CMC control group) demonstrated no significant damage to the stomach mucosa, such as necrosis in the tunica mucosa and submucosa, edema in the submucosa, plasma cell infiltration, and limfosit in the tunica mucosa and submucosa (Figure 5). The purified extract of the banana peel with doses of 200, 400, and 600 mg/kg BW, respectively were represented protects the gastric mucosa better, as evidenced by no specific pathological changes, no edema with infiltration in plasma cells or infiltration in the tunica mucosa and submucosa, and it has a comparable protective ulcer gastric effect with sucralfate groups (Figure 5). Aspirin 1000 mg/kg body weight as an inducer of necrosis ulcerative bleeding in the tunica mucosa-submucosa, edema in the tunica submucosa with neutrophil infiltration, lymphocyte and plasma cell tunica mucosa and submucosa (Figure 5).

An imbalance between pepsin, stomach acid, and the components of the gastrointestinal tract is responsible for maintaining the mucous membranes of the gastrointestinal tract, leading to peptic ulcers. The defense of gastric mucosal integrity involves balancing harmful factors such us hydrochloric acid (HCl) and pepsin with protective factors such as mucus and bicarbonate secretion, prostaglandins, mucosal blood flow, and nitric oxide (Yandrapu & Sarosiek, 2015). An agent exhibited a capacity to restore balance by reducing the secretion of gastric ulcers may play a role as an anti-ulcerative agent (Ezekwesili et al., 2014). Aspirin belongs to the class of non-steroidal anti-inflammatory drugs (NSAIDs) and works by inhibiting the activity of the cyclooxygenase (COX) enzyme, which leads to reduced synthesis of prostaglandins. This reduction in prostaglandins can increase gastric acid secretion, thereby increasing the risk of developing ulcers.
(Cryer & Mahaffey, 2014).

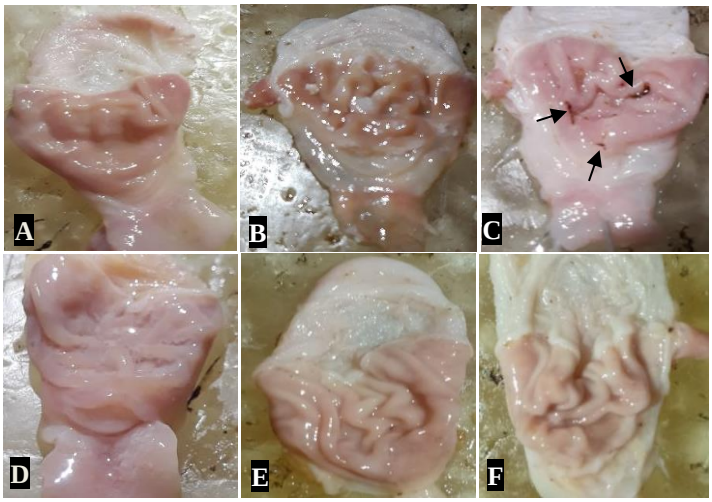

Figure 4. Macroscopic observation of stomach; (A) NaCMC group; (B) Sucralfate (120mg/5 mL) group; (C) Aspirin group (1000 mg/kg BW); (D) purified banana peel extract

200 mg/kg BW; (E) purified banana peel extract 400 mg/kg BW; (F) purified banana peel extract 600 mg/kg BW

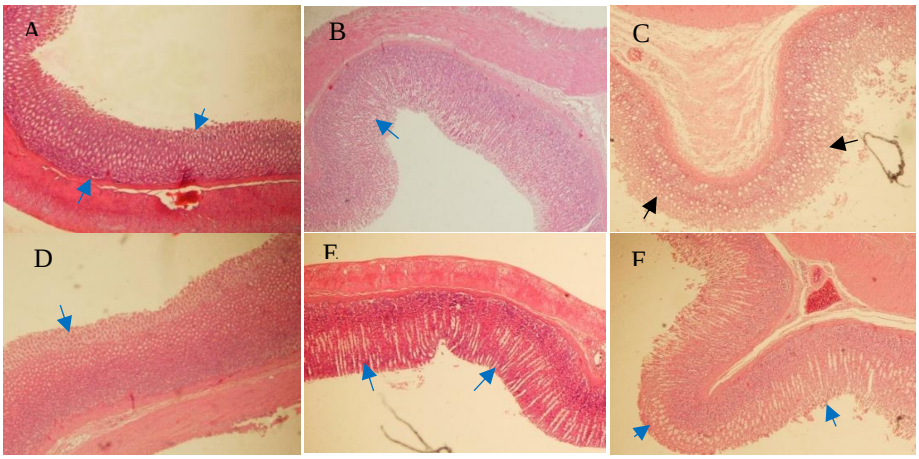

Figure 5. Microscopic of mucosa gastric: (A) Microscopic section of the control group Na CMC; (B) Microscopic section of group sucralfate (120mg/5 mL); (C) Microscopic section of aspirin (1000 mg/kg BW) group as the marker severe ulceration, necrosis, and hemorrhage; (D), (E), and (F) Microscopic section of received by *Musa paradisiaca* var. sapientum peel methanol extract purified with doses 200 mg/kg BW, 400 mg/kg BW, and 600 mg/kg BW, respectively and it was described normal gastric mucosa. The blue arrow indicates no change in gastric mucosal cell-specific pathology

The level of histologic damage to the stomach is microscopically classified into three categories: mild, moderate, and severe damage. In mild damage, there were changes in the gastric epithelium in one place where signs of inflammation were found, namely the spread of inflammatory cells in the lamina propria, and erosion was found, namely the release of some epithelial cells in the superficial part. In moderate damage, it was found that gastric epithelial changes occurred in several places (multifocal). In severe damage, changes in the gastric epithelium accompanied by signs of inflammation in the mucosa as in mild damage, but the changes that occur have been mild damage, but the changes that occur are evenly distributed (diffuse) throughout the epithelial (Sakura et al., 2017).

For many years, traditional medicine has employed natural products to treatment various ailments. The use of herbal drugs in complementary and alternative medicine (CAM) to address gastrointestinal issues is growing in both developed and developing nations. The use of medicinal plants as safe and effective therapies is supported by scientific evidence, as recommended by the World Health Organization (WHO) (Hervé et al., 2018). Medicinal/herbal plants and extracts are useful in the treatment of gastric ulcers with no noticeable side effects and at a low cost (Gohar & Zaki, 2014; Zheng et al., 2014; Saiah et al., 2018). Banana peel is a plant that has been shown to treat gastric ulcers. It contains various metabolite compounds that contribute to the healing of gastric ulcers (Mohammed et al., 2021).

The potential anti-ulcer capacity of purified methanol extract of banana peel (Musa paradisiaca var. sapientum) was investigated in this study using aspirin-induced ulceration models in rats. The study measured ulcer index, percent inhibition, pH, and volume of gastric juice. The ulcer index is a macroscopic marker to assess the extent of stomach ulceration or gastric damage in animal models. (Saheed et al., 2015).

Our results indicated no statistically significant differences in pH and gastric juice volume. It might be due to a reduced substance component or a higher dose is necessary. The volume of acid in gastric juice is a representation of gastric secretion, which includes various substances such as hydrochloric

acid (HCl), pepsinogen, bicarbonate, intrinsic factor, and protein. The decrease in the concentration of hydrogen ions in gastric juice indicated the high pH of gastric juice.

In this study, *Musa paradisiaca* var. sapientum peel showed gastroprotective activity (Kruskal Wallis test, $p=0.000<0.05$) against aspirin-induced gastric ulcer. This study's findings are comparable to those of prior research conducted by Fayyaz et al. (2021) and Pusmarani et al. (2019). Furthermore, similar to a result by Gogola (2020), the ethanolic extract of various banana peels, such as *Musa acuminata*, *Musa parasiaca* L., and *Musa acuminata Colla* cv. exhibits antioxidant and gastroprotective properties against aspirin-induced gastric ulcers. Moreover, Abdullah et al. (2014) revealed that banana peel (*Musa acuminata*) had antiulcerogenic properties, which were associated with metabolite components identified in the banana peel and pulp, such as saponins, flavonoids, and triterpenes.

This study presented that *Musa paradisiaca* var. sapientum peels contain phenolic, flavonoid, and tannin compounds. Additionally, flavonoids, polyphenols, terpenoids, saponins, and alkaloids were also found in banana peel (Pusmarani, Putri et al., 2019). Several phenolic compounds observed in banana peel include gallic acid, catechin, epicatechin, tannins, and anthocyanins (Singh et al., 2016). The medicinal plants and their chemical components identified by Kuna et al. (2019) exhibit preventive and therapeutic effects on peptic ulcers.

Plant metabolites known as phenolic compounds or polyphenols are molecules found in plants that are similar to the more well-known phenol groups (Harborne, 1989). Phenolic compounds were known to possess various physiological functions, including gastroprotective, vasodilator, antioxidant, antiplatelet aggregation, and cardioprotective properties (Sharifi-Rad et al., 2021; Shahidi and Ambigaipalan, 2015; Chiu et al., 2021). Polyphenols have been found to treat gastric ulcers through their antioxidant properties, which prevent tissue damage caused by free radicals (Ahmed et al., 2016).

Tannins possess astringent properties that can cause the precipitation of proteins in mucosal membranes and skin. These compounds have been shown to reduce gastric secretion, enhance the production of the mucus layer, and protect the gastric mucosa pH (Benchikh, 2018).

Saponins are metabolites that, through an anti-secretory mechanism, inhibit acid secretion and total acid production while decreasing the pH of gastric juice (Awaad et al., 2013). Another potential of saponin compounds' anti-ulcerogenic properties involves minimizing stomach mucosa's inflammatory responses and promoting mucin synthesis (M. Sharifi-Rad et al., 2018).

Flavonoids are the largest group of plant phenolic compounds, constituting more than 50% of the approximately 8,000 known polyphenols in the natural world (Puri & Hall, 1998). In addition, Flavonoids are the most widely distributed group of phenolic compounds, found in almost all parts of plants, particularly in photosynthesizing cells (Kumar & Pandey, 2013). Our investigation focused on *Musa paradisiaca* var. sapientum peel, which contains flavonoid compounds. Flavonoids in banana peel reduced mast cell histamine secretion, prevented lipid peroxidation, preserved the gastric mucosal glycoprotein moiety, and increased nitric oxide (NO) activity (Awaad et al., 2013).

Another study found that banana peel contains leucocyanidin as a natural flavonoid derived from unripe banana (*Musa sapientum*) that promotes cell proliferation, accelerates wound healing, strengthens the mucosal layer, and protects the gastric mucosa from erosion (Lewis et al., 1999; Lewis and Shaw, 2001). Furthermore, the antiulcer properties of bananas were attributed to the active component leucocyanidin, which could be responsible for promoting mucosal maintenance, cell proliferation, mucus secretion, and preventing the release of hydrochloric acid (HCl), ultimately leading to ulcer healing (Onasanwo et al., 2013). On the other hand, hydroxy ethylated leucocyanidin and tetra-allyl leucocyanidin, which are synthetic analogs of leucocyanidin, were found to have gastroprotective effects in rats with aspirin-induced erosions by increasing the thickness of the gastric mucus (Kumar et al., 2013). In a study by Obioma et al. (2018), unripe *Musa paradisiaca* ethanolic extract was found to have the potential to heal ulcers and may be suggested as part of the diet for individuals who are at a high risk of developing gastric ulcers due to aspirin treatment.

Natural antioxidants derived from herbs have been found to offer significant protection against a variety of diseases, including gastric ulcers (Palle et al., 2018). Purified banana peel extract demonstrated

free radical scavenging activities against DPPH with the highest antioxidant effect and the smallest IC_{50} values of 139.498 ppm (Jami'ah et al., 2018). Meanwhile, banana peel (*Musa paradisiaca*) was shown to have antioxidant activity by increasing OH radical scavenging ability, Fe^{2+} chelating ability, and MDA inhibition when the concentration of the extract was increased, paving the way for gastric ulcer treatments (IM et al., 2014).

These explanations for our findings, coupled with the histopathological data, revealed the purified banana peel extract's beneficial effects on treating aspirin-induced gastric ulcers. Therefore, gastroprotective benefits may be attributed to decreasing gastric acid production, protecting the gastric mucosal lining, or eradicating H. *pylori*. The gastroprotective activity of the purified extract from *Musa paradisiaca* var. sapientum peel is attributed to the presence of bioactive components with anti-ulcer activities, such as phenolics, flavonoids, tannins, leucocyanidin, and saponins (Farzaei et al., 2015; Pereira and Maraschin, 2015). Additionally, banana peel extract may enhance the protection of mucosal tissues and promote ulcer healing because of the presence of aqueous polysaccharides, which are major agents that coat the mucosa.

CONCLUSION

In conclusion, the banana peel purified extract contained total phenolic, flavonoid, and tannin compounds that are associated with banana peel's gastroprotective properties. In this study, it was demonstrated that purified banana peel extract exhibits a superior gastroprotective effect against aspirin-induced ulcers compared to standard medication (sucralfate).

ACKNOWLEDGEMENT

The financial support for this research was provided by the Indonesian Ministry of Education, Culture, Research, and Technology, and the authors gratefully acknowledge this support.

REFERENCES

Abdullah, F. C., Rahimi, L., Zakaria, Z. A., & Ibrahim, A. L. (2014). Hepatoprotective, antiulcerogenic, cytotoxic and antioxidant activities of Musa acuminata peel and pulp. Novel Plant Bioresources: Applications in Food, Medicine and Cosmetics, 371-382. https://doi.org/10.1002/9781118460566.ch26

Ahmed, O. E. I., Hashim, N. M., Yousif, M., Ibrahim, A. A. A., & Ismail Adam, H. A. (2016). Ahmed, O. E. I., Hashim, N. M., Yousif, M., Ibrahim, A. A. A., & Ismail Adam, H. A. (2016). Gastroprotective effects of (+)-catechin hydrate on ethanol-induced gastric ulcer in rats. Cienc Tec Vitivinic, 31. *Cienc Tec Vitivinic*, *31*.

Al Amri, F. S., & Hossain, M. A. (2018). Comparison of total phenols, flavonoids and antioxidant potential of local and imported ripe bananas. *Egyptian Journal of Basic and Applied Sciences*, *5*(4), 245–251. https://doi.org/ 10.1016/j.ejbas.2018.09.002

Awaad, A. S., El-meligy, R. M., & Soliman, G. A. (2013). Natural products in treatment of ulcerative colitis and peptic ulcer. *Journal of Saudi Chemical Society*, *17*(1), 101–124. https://doi.org/10.1016/j.jscs.2012.03.002

Aziakpono, O. M., Ofili, C. C., Chisom, M. U., Johnson, U. A., John, O. A., Sylvanus, M. C., Ogbonnaya, M., Chizoba, N. G., & Harrison, O. U. (2021). Anti-Ulcer Activities of Methanolic Extract of Musa Paradisiaca. *Journal of Advances in Medical and Pharmaceutical Sciences*, *23*(6), 10–17. https://doi.org. 10.9734/jamps/2021/v23i630240

Baba, S. A., & Malik, S. A. (2015). Determination of total phenolic and flavonoid content, antimicrobial and antioxidant activity of a root extract of Arisaema jacquemontii Blume. *Journal of Taibah University for Science*, *9*(4), 449–454. https://doi.org/10.1016/j.jtusci.2014.11.001

Benchikh, F. (2018). *Pharmacological effects of Myrtus communis L. on the gastrointestinal tract of rats and mice*.*Thesis*. Université Ferhat Abbas Sétif 1.

Berawi, K. N., & Bimandama, M. A. (2018). The effect of giving extract etanol of kepok banana peel (Musa Acuminata) toward total cholesterol level on male mice (Mus Musculus L.) strain

deutschland-denken-yoken (ddy) Obese. *Biomedical & Pharmacology Journal*, *11*(2). https://doi.org/10.13005/bpj/1431

Carleton, H. M., Drury, R. A. B., & Wallington, E. A. (1980). *Carleton's histological technique*. Oxford University Press, USA.

Chiu, H.-F., Venkatakrishnan, K.: K, Golovinskaia, O., & Wang, C.-K. (2021). In Vitro and In Vivo Study of Gastroprotective Effect of Purified Exract Andrographis Paniculata. *Molecules*, *26*(7), 2090. https://doi.org/10.3390/molecules26072090

Cho, C. H., & Ogle, C. W. (1979). Cholinergic-mediated gastric mast cell degranulation with subsequent histamine H1-and H2-receptor activation in stress ulceration in rats. *European Journal of Pharmacology*, *55*(1), 23–33. https://doi.org/10.1016/0014-2999(79)90144-4

Cryer, B., & Mahaffey, K. W. (2014). Gastrointestinal ulcers, role of aspirin, and clinical outcomes: pathobiology, diagnosis, and treatment. *Journal of Multidisciplinary Healthcare*, *7*, 137. https://doi.org/10.2147/JMDH.S54324

Dipiro, J., Yee, G., Haines, S., Nolin, T., & Ellingrod, V. (2020). *Pharmacotherapy: a pathophysiologic approach. 11th Editi*. New york: McGraw-Hill Companies.

Ezekwesili, C. N., Ghasi, S., Adindu, C. S., & Mefoh, N. C. (2014). Evaluation of the anti-ulcer property of aqueous extract of unripe Musa paradisiaca Linn. peel in Wistar rats. *African Journal of Pharmacy and Pharmacology*, *8*(39), 1006–1011.

Farzaei, M. H., Abdollahi, M., & Rahimi, R. (2015). Role of dietary polyphenols in the management of peptic ulcer. *World Journal of Gastroenterology: WJG*, *21*(21), 6499. https://doi.org/10.3748/wjg.v21.i21.6499

Fatimah, C, A., Rahimi, L., Zakaria, Z. A., & Ibrahim, A. L. (2014). Hepatoprotective, antiulcerogenic, cytotoxic and antioxidant activities of Musa acuminata peel and pulp. *Novel Plant Bioresources: Applications in Food, Medicine and Cosmetics*, 371–382. https://doi.org/10.1002/9781118460566.ch26

Fayyaz, A., Samad, A., Waseem, U., Shafique, S., Nasreen, S., & Hassan, S. (2021). Gastric mucosal damage with aspirin: results of experimental models in adult albino rats. *International Journal of Community Medicine and Public Health*, *8*(1), 50. https://doi.org/10.18203/2394-6040.ijcmph20205447

Gogola, D. (2020). Phytochemical screening, antioxidant and gastro-protective activity studies on the fruit peels of selected varieties of Banana. *Herbal Medicines Journal (Herb Med J)*, *5*(2), 45–59. https://doi.org/10.22087/hmj.v5i2.763

Gohar, A. A., & Zaki, A. A. (2014). Assessment of some herbal drugs for prophylaxis of peptic ulcer. *Iranian Journal of Pharmaceutical Research: IJPR*, *13*(3), 1081.

Handa, O., Naito, Y., Fukui, A., Omatsu, T., & Yoshikawa, T. (2014). The impact of non-steroidal anti-inflammatory drugs on the small intestinal epithelium. *Journal of Clinical Biochemistry and Nutrition*, *54*(1), 2–6. https://doi.org/10.3164/jcbn.13-84

Harborne, J. B. (1989). General procedures and measurement of total phenolics. *Methods in Plant Biochemistry*, *1*, 1–28. https://doi.org/10.1016/B978-0-12-461011-8.50007-X

Hervé, E. E., Bernard, G. N., Léandre, K. K., Paul, Y. A., & Etienne, E. E. (2018). Acute toxicity and gastric anti-ulcer activity of an aqueous extract of the leaves of Macaranga barteri Mll. Arg (Euphorbiaceae) on rat models. *Journal of Medicinal Plants Research*, *12*(9), 96–105. https:doi.org/10.5897/JMPR2017.6547

Hossain, M. D., Sarwar, M. S., Dewan, S. M. R., Hossain, M. S., Shahid-Ud-Daula, A. F. M., & Islam, M. S. (2014). Investigation of total phenolic content and antioxidant activities of Azadirachta indica roots. *Avicenna Journal of Phytomedicine*, *4*(2), 97.

Ibrahim, M. F. G., & Allam, F. A. F. A. (2022). Potential stem cell—Conditioned medium and their derived exosomes versus omeprazole in treatment of experimental model of gastric ulcer. *Acta Histochemica*, *124*(4), 151896. https://doi.org/10.1016/j.acthis.2022.151896

IM, F., Birnin-Yauri, A. U., & Jemaima, J. (2014). In vitro antioxidant properties of musa paradisiacal

peel aqueous extract. *Journal of Scientific and Innovative Research*, *3*(6), 563–568. https://doi.org/10.31254/jsir.2014.3603

Jabbar, A. A. (2022). Gastroprotective and Immuno-supportive Role of Alcea kurdica against Stress Induced Lesion in Japanese Quails. *Baghdad Science Journal*, 19 (4),716-724. https://doi.org/10.21123/bsj.2022.19.4.0716

Jami'ah, S. R., Ifaya, M., Pusmarani, J., & Nurhikma, E. (2018). Uji aktivitas antioksidan ekstrak metanol kulit pisang raja (Musa paradisiaca sapientum) dengan metode DPPH (2, 2-difenil-1-pikrilhidrazil). *Jurnal Mandala Pharmacon Indonesia*, *4*(1), 33–38. https://doi.org/10.35311/jmpi.v4i1.22

Jang, E., Park, M., Jeong, J. E., Lee, J. Y., & Kim, M. G. (2022). Frequently reported adverse events of rebamipide compared to other drugs for peptic ulcer and gastroesophageal reflux disease. *Scientific Reports*, *12*(1), 7839. https://doi.org/10.1038/s41598-022-11505-0

Kadhem, M. A., Abdul-Niby, A. A., & Khassaf, H. K. (2018). Study the effect of ethanolic extract of Anethum graveolens L. on aspirin induced Gastric Ulcer in Male Guinea Pigs. *Research Journal of Pharmacy and Technology*, *11*(9), 3793–3798. https://doi.org/10.5958/0974-360X.2018.00695.9

Kapadia, S. P., Pudakalkatti, P. S., & Shivanaikar, S. (2015). Detection of antimicrobial activity of banana peel (Musa paradisiaca L.) on Porphyromonas gingivalis and Aggregatibacter actinomycetemcomitans: An in vitro study. *Contemporary Clinical Dentistry*, *6*(4), 496. https://doi.org/10.4103/0976-237X.169864

Kathirvelu, P., Cheriyan, B. V., Jagan, N., Viswanathan, S., Kumar, S. V., & Kamalakannan, P. (2019). Gastroprotective and Antioxidant effect of Petroleum ether Extract of Eupatorium triplinerve Vahl. *Research Journal of Pharmacy and Technology*, *12*(11), 5163–5166. https://doi.org/10.5958/0974-360X.2019.00893.X

Kibria, A. A., Kamrunnessa, Rahman, M. M., & Kar, A. (2019). Extraction and Evaluation of Phytochemicals from Banana Peels (Musa sapientum) and Banana Plants (Musa paradisiaca) . *Malaysian Journal of Halal Research*, *2*(1), 22–26. https://doi.org/10.2478/mjhr-2019-0005

Kumar, M., Gautam, M. K., Singh, A., & Goel, R. K. (2013). Healing effects of Musa sapientum var. paradisiaca in diabetic rats with co-occurring gastric ulcer: cytokines and growth factor by PCR amplification. *BMC Complementary and Alternative Medicine*, *13*(1), 1–9. https://doi.org/10.1186/1472-6882-13-305

Kumar, S., & Pandey, A. K. (2013). Chemistry and biological activities of flavonoids: an overview. *The Scientific World Journal*, *2013*. https://doi.org/10.1155/2013/162750

Kuna, L., Jakab, J., Smolic, R., Raguz-Lucic, N., Vcev, A., & Smolic, M. (2019). Peptic ulcer disease: a brief review of conventional therapy and herbal treatment options. *Journal of Clinical Medicine*, *8*(2), 179. https://doi.org/10.3390/jcm8020179

Lambert, A. A., Lam, J. O., Paik, J. J., Ugarte-Gil, C., Drummond, M. B., & Crowell, T. A. (2015). Risk of community-acquired pneumonia with outpatient proton-pump inhibitor therapy: a systematic review and meta-analysis. *PloS One*, *10*(6), e0128004. https://doi.org/10.1371/journal.pone.0128004

Lanas, A., & Chan, F. K. L. (2017). Peptic ulcer disease. *The Lancet*, *390*(10094), 613–624. https://doi.org/10.1016/S0140-6736(16)32404-7

Lewis, D. A., Fields, W. N., & Shaw, G. P. (1999). A natural flavonoid present in unripe plantain banana pulp (Musa sapientum L. var. paradisiaca) protects the gastric mucosa from aspirin-induced erosions. *Journal of Ethnopharmacology*, *65*(3), 283–288. https://doi.org/10.1016/S0378-8741(99)00005-7

Lewis, D. A., & Shaw, G. P. (2001). A natural flavonoid and synthetic analogues protect the gastric mucosa from aspirin-induced erosions. *The Journal of Nutritional Biochemistry*, *12*(2), 95–100. https://doi.org/10.1016/S0955-2863(00)00133-9

Li, C., Wang, L., Zhao, J., Wei, Y., Zhai, S., Tan, M., Guan, K., Huang, Z., & Chen, C. (2022). Lonicera rupicola Hook. f. et Thoms flavonoids ameliorated dysregulated inflammatory responses, intestinal barrier, and gut microbiome in ulcerative colitis via PI3K/AKT pathway. *Phytomedicine*, *104*, 154284. https://doi.org/10.1016/j.phymed.2022.154284

Mahurkar, N., & Sayeed Ul Hasan, S. M. (2015). Synergistic Antiulcer Effect of Melatonin and

Esomeprazole Combination in Pylorus Ligation, Ethanol, Aspirin induced Peptic Ulcers. *Asian Journal of Pharmaceutical Research*, *5*(1), 10–14. https://doi.org/10.5958/2231-5691.2015.00002.7

Malik, T. F., Gnanapandithan, K., & Singh, K. (2018). *Peptic ulcer disease*.

Mohammed, M. A., El-Hadi, A. E., Mohammed, E. A., Abbas, F. S., Musa, K. O., Al-Ameen, M. Y., Ahmed, A. M., Gassab, M. T. I., Hassan, H. M., & Abdelgadir, A. A. (2021). *Gastro-protective Effects of Green Banana (Musa cavendishii Lamb.) Pulp Powder on Aspirin-induced Gastric Ulcer in Albino Rats*.

Morais, D. R., Rotta, E. M., Sargi, S. C., Schmidt, E. M., Bonafe, E. G., Eberlin, M. N., Sawaya, A. C. H. F., & Visentainer, J. V. (2015). Antioxidant activity, phenolics and UPLC–ESI (–)–MS of extracts from different tropical fruits parts and processed peels. *Food Research International*, *77*, 392–399. https://doi.org/10.1016/j.foodres.2015.08.036

Narayanan, M., Reddy, K. M., & Marsicano, E. (2018). Peptic ulcer disease and Helicobacter pylori infection. *Missouri Medicine*, *115*(3), 219.

Obioma, N. E., Kelechi, O. J., Miracle, N. T., Ogbonnaya, E., & Offor, N. (2018). Ulcer healing effect of ethanolic extract of unripe musaparadisiaca on aspirin induced gastric ulceration in adult wistar rats. *European Journal of Pharmaceutical and Medical Research*, *5*(12), 58–62.

Onasanwo, S. A., Emikpe, B. O., Ajah, A. A., & Elufioye, T. O. (2013). Anti-ulcer and ulcer healing potentials of Musa sapientum peel extract in the laboratory rodents. *Pharmacognosy Research*, *5*(3), 173–178. https://doi.org/10.4103/0974-8490.112423

Palle, S., Kanakalatha, A., & Kavitha, C. N. (2018). Gastroprotective and antiulcer effects of Celastrus paniculatus seed oil against several gastric ulcer models in rats. *Journal of Dietary Supplements*, *15*(4), 373–385. https://doi.org/10.1080/19390211.2017.1349231

Pereira, A., & Maraschin, M. (2015). Banana (Musa spp) from peel to pulp: ethnopharmacology, source of bioactive compounds and its relevance for human health. *Journal of Ethnopharmacology*, *160*, 149–163. https://doi.org/10.1016/j.jep.2014.11.008

Pulipati, S., Babu, P. S., & Narasu, M. L. (2014). Quantitative determination of tannin content and evaluation of antibacterial activity of Amaranthus tricolor (L). *Int J Biol Pharm Res*, *5*, 623–626.

Puri, B., & Hall, A. (1998). *Phytochemical dictionary: a handbook of bioactive compounds from plants*. CRC press.

Pusmarani, J., Ifaya, M., Isrul, M., & Saleh, A. (2019). Gastroprotective effect of Lannea Coromandelica Stem Bark in Rat induced by aspirin. *Research Journal of Pharmacy and Technology*, *12*(4), 1646–1648. https://doi.org/10.5958/0974-360X.2019.00275.0

Pusmarani, J., Ifaya, M., & Putri, R. J. (2022). Hepatoprotector Effect of Banana Peel (Musa paradisiaca Sapientum) on Paracetamol Induced Rats. *Jurnal Farmasi Galenika (Galenika Journal of Pharmacy)(e-Journal)*, *8*(2), 109–116. https://doi.org/10.22487/j24428744.2022.v8.i2.15968

Pusmarani, J., Putri, R. J., Dewi, C., Purwono, S., & Ikawati, Z. (2019). Non Specific and Specific Parameter Standardization Of Banana Peel (Musa paradisciata Sapientum) and Andrographis Paniculata. *International Summit on Science Technology and Humanity*, 658–664.

Rahman, Z., Dwivedi, D. K., & Jena, G. B. (2020). Ethanol-induced gastric ulcer in rats and intervention of tert-butylhydroquinone: involvement of Nrf2/HO-1 signaling pathway. *Human & Experimental Toxicology*, *39*(4), 547–562. https://doi.org/10.1177/0960327119895559

Raish, M., Shahid, M., Bin Jardan, Y. A., Ansari, M. A., Alkharfy, K. M., Ahad, A., Abdelrahman, I. A., Ahmad, A., & Al-Jenoobi, F. I. (2021). Gastroprotective effect of sinapic acid on ethanol-induced gastric ulcers in rats: involvement of Nrf2/HO-1 and NF-κB signaling and antiapoptotic role. *Frontiers in Pharmacology*, *12*, 622815. https://doi.org/10.3389/fphar.2021.622815

Rita, S. W., Swantara, I. M. D., Asih, I., & Puspawati, N. M. (2020). Antibacterial activity and antioxidant capacity of selected local banana peel (Musa sp.) methanol extracts cultivated in Bali. *Int. J. Agric. Environ. Biores*, *5*, 242–251. https://doi.org/10.35410/IJAEB.2020.5519

Saheed, S., Olarewaju, S. A., Taofeeq, G., Olatunde, S. T., & Alanamu, A. A. (2015). Combined administration of Spondias mombin and Ficus exasperata leaf extracts stall Indomethacin-mediated

gastric mucosal onslaught in rats. *African Journal of Traditional, Complementary and Alternative Medicines*, *12*(1), 45–51. https://doi.org/10.4314/ajtcam.v12i1.7

Saiah, W., Halzoune, H., Djaziri, R., Tabani, K., Koceir, E. A., & Omari, N. (2018). Antioxidant and gastroprotective actions of butanol fraction of Zingiber officinale against diclofenac sodium-induced gastric damage in rats. *Journal of Food Biochemistry*, *42*(1), e12456. https://doi.org/10.1111/jfbc.12456

Sakura, Y. W., Jayawardhita, A. A. G., Kardena, I. M., & Sudimartini, L. M. (2017). Perbandingan gambaran histopatologi lambung tikus putih (Rattus norvegicus) jantan yang diberi amoxicillin dikombinasikan dengan asam mefenamat dan deksametason. *Indonesia Medicus Veterinus*, *6*(3), 246–253.

Shahidi, F., & Ambigaipalan, P. (2015). Phenolics and polyphenolics in foods, beverages and spices: Antioxidant activity and health effects–A review. *Journal of Functional Foods*, *18*, 820–897. https://doi.org/10.1016/j.jff.2015.06.018

Sharifi-Rad, J., Quispe, C., Zam, W., Kumar, M., Cardoso, S. M., Pereira, O. R., Ademiluyi, A. O., Adeleke, O., Moreira, A. C., & Živković, J. (2021). Phenolic bioactives as antiplatelet aggregation factors: the pivotal ingredients in maintaining cardiovascular health. *Oxidative Medicine and Cellular Longevity*, *2021*. https://doi.org/10.1155/2021/2195902

Singh, B., Singh, J. P., Kaur, A., & Singh, N. (2016). Bioactive compounds in banana and their associated health benefits–A review. *Food Chemistry*, *206*, 1–11. https://doi.org/10.1016/j.foodchem.2016.03.033

Sisay Zewdu, W., & Jemere Aragaw, T. (2020). Evaluation of the anti-ulcer activity of hydromethanolic crude extract and solvent fractions of the root of Rumex nepalensis in Rats. *Journal of Experimental Pharmacology*, 325–337. https://doi.org/10.2147/JEP.S258586

Thomas, A., & Krishnakumar, K. (2017). Banana peel: pharmacological activities: a Review. *International Journal of Innovative Research and Advanced Studies*, *4*(5), 62–64.

Ulser, T. (2016). Antiulcer activity of Musa paradisiaca [banana] tepal and skin extracts in ulcer induced albino mice. *Malaysian Journal of Analytical Sciences*, *20*(5), 1203–1216. https://doi.org/10.17576/mjas-2016-2005-27

Vu, H. T., Scarlett, C. J., & Vuong, Q. V. (2018). Phenolic compounds within banana peel and their potential uses: A review. *Journal of Functional Foods*, *40*, 238–248. https://doi.org/10.1016/j.jff.2017.11.006

Wang, Z., & Wei, Y. (2022). SEMA3D Plays a critical role in peptic ulcer disease-related Carcinogenesis Induced by H. pylori Infection. *International Journal of General Medicine*, *15*, 1239. https://doi.org/10.2147/IJGM.S343635

Washio, E., Esaki, M., Maehata, Y., Miyazaki, M., Kobayashi, H., Ishikawa, H., Kitazono, T., & Matsumoto, T. (2016). Proton pump inhibitors increase incidence of nonsteroidal anti-inflammatory drug–induced small bowel injury: a randomized, placebo-controlled trial. *Clinical Gastroenterology and Hepatology*, *14*(6), 809-815.e1. https://doi.org/10.1016/j.cgh.2015.10.022

Yaghoobi, M., & Armstrong, D. (2022). Peptic ulcer disease. In *Yamada's Textbook of Gastroenterology* (pp. 924–976). Wiley. https://doi.org/10.1002/9781119600206.ch49

Yandrapu, H., & Sarosiek, J. (2015). Protective factors of the gastric and duodenal mucosa: an overview. *Current Gastroenterology Reports*, *17*(6), 24. https://doi.org/10.1007/s11894-015-0452-2

Zaghlool, S. S., Abo-Seif, A. A., Rabeh, M. A., Abdelmohsen, U. R., & Messiha, B. A. S. (2019). Gastro-protective and anti-oxidant potential of Althaea officinalis and solanum nigrum on pyloric ligation/indomethacin-induced ulceration in rats. *Antioxidants*, *8*(11), 512. https://doi.org/10.3390/antiox8110512

Zheng, Y.-F., Xie, J.-H., Xu, Y.-F., Liang, Y.-Z., Mo, Z.-Z., Jiang, W.-W., Chen, X.-Y., Liu, Y.-H., Yu, X.-D., Huang, P., & Su, Z.-R. (2014). Gastroprotective effect and mechanism of patchouli alcohol against ethanol, indomethacin and stress-induced ulcer in rats. *Chemico-Biological Interactions*, *222*, 27–36. https://doi.org/https://doi.org/10.1016/j.cbi.2014.08.008

Pharmaciana
Vol.14, No.3, Nov 2024, Page. 324-336
ISSN: 2088 4559; e-ISSN: 2477 0256
DOI: 10.12928/pharmaciana.v14i3.28229

Analysis of pharmaceutical technical staff needs at hospital X in Bandung using the WISN method

Angela Alysia Elaine[1*], Imam Adi Wicaksono[2], Falerina Puspita [3], Hijrah Mutaqin Zainuddin[3]
[1]Professional Pharmacist Program, Faculty of Pharmacy, Padjadjaran University
Hegarmanah, Kec. Jatinangor, Kabupaten Sumedang, West Java, Indonesia
[2]Department of Pharmacology and Clinical Pharmacy, Faculty of Pharmacy, Padjadjaran University
Hegarmanah, Kec. Jatinangor, Kabupaten Sumedang, West Java, Indonesia
[3]Pharmacy Installation of Hospital X, Bandung, Indonesia

Submitted: 16-01-2024 ***Reviewed: 26-03-2024*** ***Accepted: 31-05-2024***

ABSTRACT

One of the essential and inseparable health services in hospitals is pharmaceutical services. Pharmaceutical services in hospitals are carried out by the Hospital Pharmacy Installation (*Instalasi Farmasi Rumah Sakit*/IFRS). The implementation of pharmaceutical services in hospitals must be supported by adequate, skilled, and competent human resources so that pharmaceutical service activities can run well and are high quality for patients. The lack of human resources for pharmaceutical services will result in excessive workload and reduced quality of pharmaceutical services. One method widely used to determine the number of staff needs is the Workload Indicators of Staffing Needs (WISN). Analysis of the need for pharmaceutical technical staff at Hospital X in Bandung City was carried out using the WISN method. The data used for the analysis were obtained from interviews, observations, and data collection on pharmaceutical services from the pharmacy installation of the Hospital X. The results of the WISN analysis showed that the need for pharmaceutical technical personnel for central pharmacy installations providing outpatient and inpatient services is 87 people, the total need for the emergency room pharmacy satellite is 6 people, the operating room pharmacy satellite is 6 people, and the pharmacy warehouse is 3 people. From the results of WISN ratio, the number of pharmaceutical technical staff available for the central pharmacy installation, emergency room pharmacy satellite, and operating room pharmacy satellite are still inadequate for the existing workload (WISN ratio < 1). In contrast, for the pharmaceutical warehouse, it is adequate (WISN ratio = 1). Therefore, Hospital X needs to consider adding existing pharmaceutical technical staff to support more optimal pharmaceutical services at the hospital.

Keywords: pharmaceutical technical staff, pharmaceutical installation, pharmaceutical services, workload, WISN

Corresponding author:
Angela Alysia Elaine
Professional Pharmacist Program, Faculty of Pharmacy, Padjadjaran University
Hegarmanah, Kec. Jatinangor, Kabupaten Sumedang, West Java, Indonesia
Email: angela19001@mail.unpad.ac.id

INTRODUCTION

A hospital is a health service facility that provides comprehensive individual health services through promotive, preventive, curative, rehabilitative, and palliative health services by providing inpatient, outpatient, and emergency services (Pemerintah Republik Indonesia, 2023). One of the important health services in hospitals is pharmaceutical services. According to Minister of Health Regulation (*Peraturan Menteri Kesehatan*) Number 72 of 2016 concerning Pharmaceutical Service Standards in Hospitals, pharmaceutical services are a direct and responsible service to patients related to pharmaceutical preparations to achieve definite results and improve the patient's quality of life. Pharmaceutical services in hospitals are carried out by the Hospital Pharmacy Installation or *Instalasi Farmasi Rumah Sakit* (IFRS) (Kementerian Kesehatan RI, 2016). Hospital Pharmacy Installation is an installation in a hospital led by a pharmacist and assisted by other pharmaceutical staff to provide pharmaceutical services, including management of pharmaceutical supplies and clinical pharmacy services (Agustini et al., 2023; Siregar, 2004).

The implementation of pharmaceutical services in hospitals must be supported by adequate, skilled, and competent human resources (HR) so that pharmaceutical service activities can run well and are of high quality for patients. Human resources for pharmaceutical services are known as pharmaceutical personnel, which can consist of pharmacists and pharmaceutical technical staff. Pharmaceutical Technical Staff or *Tenaga Teknis Kefarmasian* (TTK) are personnel who assist pharmacists in carrying out pharmaceutical work. Pharmaceutical technical staff can consist of undergraduate pharmacists, intermediate pharmacy experts, and pharmaceutical analysts. The availability of the number of pharmaceutical technical staff in hospital pharmaceutical installations must be fulfilled following the hospital classification and licensing provisions determined by the Minister of Health to achieve the targets and objectives of the pharmaceutical installation (Govule et al., 2015; Kuswandani et al., 2021). The lack of human resources for pharmaceutical services will result in excessive workload and reduced quality of pharmaceutical services. The decline in the quality of standard pharmaceutical services is characterized by the failure to achieve minimum service standard indicators in health facilities (Gialama et al., 2019; Rensiner et al., 2018; Yulaika, 2018). Decreased service quality can have an impact on increasing service waiting times, decreasing patient satisfaction, and increasing the occurrence of medication errors (Govule et al., 2015; Kuswandani et al., 2021). Therefore, hospitals need to consider and plan the availability of pharmaceutical technical staff based on the function and workload of each pharmaceutical service unit (Akbar et al., 2020).

Currently, there are several methods for calculating the number of health workers needed so that the workload is not excessive. The Indonesian Ministry of Health recommends three methods, namely the ratio of health workers per population, the standard number of health workers based on health facilities, and the WISN method developed by the World Health Organization (WHO) (Kementerian Kesehatan RI, 2016; WHO, 2023). The WISN method will help to calculate the estimated number of workers/health workers needed based on workload or activity standard. The WISN method is an effective way to accurately determine the necessary number of pharmaceutical technical staff in each work unit (Wahyu Ningsih et al., 2020). The WISN method has several advantages, including being easy to use, fast, being able to carry out calculations more accurately based on workload, and being comprehensive (Cucu et al., 2019; Kuswandani et al., 2021).

Hospital X in Bandung is a general hospital classified as class B which has 300 beds, 10 installations of medical services, 5 installations of non-medical services, and 1 unit of non-medical service. One of the medical service installations in Hospital X is a pharmacy installation. The pharmacy installation at Hospital X includes the central pharmacy installation, which provides pharmaceutical services for inpatient and outpatient care, emergency room pharmacy satellite, operating room pharmacy satellite, and pharmacy warehouse. The pharmacy installation in Hospital X provides 24-hour services, except pharmacy warehouse. The pharmacy installation at Hospital X has 9 pharmacists and 40 pharmaceutical technical staff. Health services and the number of prescriptions continue to increase every day, causing the workload in pharmaceutical installations to increase. Therefore, this research aims to analyze the

number of pharmaceutical technical personnel needed based on the existing workload using the WISN method.

MATERIALS AND METHOD

Materials

The data required to calculate the number of pharmaceutical technical staff required consists of the number of working days in a year: the number of holidays and national leave in a year; the number of days of leave or permission due to illness, training, or other reasons; type of pharmaceutical service activities at Hospital X; the number of prescription services and other services in a year; as well as currently available total of staff.

Methods

Data collection

This is descriptive research to determine the number of pharmaceutical technical staff needed based on the existing workload in pharmacy installation at Hospital X to improve pharmaceutical services at Hospital X. Data collection was carried out by observation, interviews with pharmaceutical technical staff, as well as data from pharmaceutical services at Hospital X in the period on September 2022 – August 2023. The types of pharmaceutical work carried out by pharmaceutical staff and how long it takes to do each job were obtained through observation. Details of the pharmaceutical work observed refer to Minister of Health Regulation 72/2016 concerning Pharmaceutical Service Standards in Hospitals. There are three ways to calculate the workload of pharmaceutical technical staff, that are work sampling, time and motion study, and daily log (Lubis et al., 2022). The frequency of carrying out pharmaceutical work and estimates of the time required were also obtained through interviews with pharmaceutical staff. Interview were carried out using random sampling by asking questions related to the pharmaceutical work being carried out and the estimated time required.

Workload indicator of staffing needs method

Determination of Available Working Time (AWT)

Available Working Time (AWT) is the time available for pharmaceutical technical staff to work within one year. AWT can be determined from working days in a year minus annual leave days, national holidays, and leave/permission days due to illness or training activities. Available working time can be determined using the following formula (WHO, 2023).

$$AWT = A – (B + C + D + E)$$

In this formula AWT is the total available working time; A is the number of possible working days in a year; B is the number of days off for public holidays in a year; C is the number of days off for annual leave in a year; D is the number of days off due to sick leave in a year; E is the number of days off due to other leave, such as training, etc., in a year. The AWT results are then multiplied by the working hours in one day to get the available working time in hours.

Determination of workload component

The workload components of pharmaceutical technical staff were determined based on interviews and observations of the work activities of pharmaceutical technical personnel in the pharmaceutical installations center, emergency room pharmacy satellite, operating room pharmacy satellite, and pharmacy warehouses (WHO, 2023).

Determination of activity standard

Activity standard is the time required by pharmaceutical technical staff to complete an activity that is a workload component by standards. Activity standard data was obtained through data from Hospital X pharmacy installation, observations, interviews, and calculations (WHO, 2023).

Determination of standard workload

Standard workload is the amount of work in a health service workload component that can be carried out by a health worker in a year. Standard workload calculations can be done by assuming that a health worker carries out all components of the workload in one year (Aulia et al., 2019). Standard workload calculations can be done using the mention equation 1 (WHO, 2023).

$$\text{Standard workload} = \frac{\text{Available working time}}{\text{Average working time}} \quad \text{.....(1)}$$

Calculating the number of pharmaceutical technical staff based on standard health service workload can be done using the following equation.

$$\text{Number of staff needs for health care activities (A)} = \frac{\text{Quantity of activities}}{\text{Standard workload}} \quad \text{.....(2)}$$

Calculating the number of pharmaceutical technical staff based on supporting activities workload can be done using the following equation 3.

$$\text{Number of staff needs for supporting activities (B)} = \frac{1}{1-\text{total of supporting activities}} \quad \text{.....(3)}$$

Calculating the number of pharmaceutical technical staff based on individual additional activities workload can be done using the following equation 4.

$$\text{Number of staff needs for individual activities (C)} = \frac{\text{Total of individual additional activities}}{\text{Available working time}} \quad \text{.....(4)}$$

Determination of total of pharmaceutical technical staff needs

The number of pharmaceutical technical staff needed can be calculated from data calculated from the number of staff needed for health services, supporting activity, and additional activity (WHO, 2023). Calculations can be done using the following equation 5.

$$\text{Total of pharmaceutical technical staff needs} = A \times B + C \quad \text{.....(5)}$$

Determination of WISN ratio

The results of calculating the need for pharmaceutical technical staff using the WISN method are expressed in the WISN ratio. The WISN ratio can see whether the existing number of pharmaceutical technical staff is following the existing workload or is insufficient so that the workload of each pharmaceutical technical staff is exceeded (WHO, 2023). The WISN ratio can be determined using the following equation 6.

$$\text{WISN Ratio} = \frac{\text{Total of current pharmaceutical technical staff}}{\text{Total value of calculation pharmaceutical technical staff}} \quad \text{.....(6)}$$

Data Analysis

The data that has been collected is processed using Microsoft Excel to carry out WISN method calculations. The data that has been processed will be presented in tabular form and interpreted according to the results of the WISN method established by WHO.

RESULT AND DISCUSSION

Since becoming a Regional General Hospital, Hospital X had an increase in visits and the number of health services, including pharmaceutical services. The higher the level of health services in the hospital, the more prescriptions or requests for pharmaceutical supplies must be provided by pharmaceutical staff. This can cause an increase in workload if not accompanied by the addition of the appropriate number of human resources. One method that is easy and comprehensive to use in determining the number of pharmaceutical technical staff needs is the Workload Indicator Staffing Needs (WISN) method. The WISN method can help hospital management determine the appropriate number of health workers, such as doctors, pharmaceutical staff, nurses, and others, to aid in developing health services in hospitals (Jing et al., 2022). Through the WISN method, it can be seen the difference between the number of pharmaceutical technical staff available and the number of pharmaceutical technical staff needed based on the workload carried out (Doosty et al., 2019; McQuide et al., 2013). WISN method is a method that is widely used because it is easy to do using available data, easy to use for all health staff, and realistic for providing human resource allocation (WHO, 2023).

The initial step in the WISN method is to determine available working time (AWT). Pharmaceutical technical staff do not work every day for one year. There are several days and times when staff do not do work. Therefore, it is necessary to determine available working time which shows the staff time available in one year to do their work at the hospital. Available working time can be expressed in days per year, hours per year, or minutes per year (Sungkonoputri & Dhamanti, 2023; WHO, 2023). Based on the results of the study, pharmaceutical technical staff at Hospital X worked for 6 days in 1 week and every working day worked for 6.5 hours. Available working time for pharmaceutical technical staff in a year is 1748.5 hours/year or equivalent to 104,910 minutes/year. Available working time was obtained from the results of working days in one year minus the number of annual leave days, national holidays, and the average day of leave due to illness or training. Data and results of Available working time can be seen in Table 1.

Table 1. Available working time of pharmaceutical technical staff in Hospital X

Factor	Total	Annotation
Number of working days (A)	312	days/year
National holiday leave (B)	15	days/year
Mass leave (C)	8	days/year
Annual leave (D)	12	days/year
Leave due to illness / training / other reasons (E)	8	days/year
Daily working hours (F)	6.5	hours/day
Available working time (AWT) AWT = [A – (B+C+D+E)] x F	269 1748.5 104,910	day/year hour/year minute/year

In deciding the number of pharmaceutical technical staff needed, it is necessary to group the available workload components. Based on WHO, workload components can be grouped into three, (a) health service activities refer to pharmaceutical services (especially direct pharmaceutical services to patients) carried out by pharmaceutical technical staff; (b) supporting activities, refer to important work that can support health service activities and is carried out by all pharmaceutical technical personnel; (c) individual additional activities, refer to specific responsibilities and tasks assigned to only a few pharmaceutical technical staff. Adding a list of workload components that are rarely worked on or

require little work time makes an insignificant difference in the final calculation results. Although detailing workload components can improve calculation accuracy, it also increases the burden and costs, time, and effort in WISN calculations (Gialama et al., 2019; WHO, 2023). The next step in the WISN method after determining available working time and workload components is determining activity standards. Activity standards are the time required by trained pharmaceutical technical staff to perform pharmaceutical services according to professional standards. Activity standards are divided into service standards for health care activities and allowance standard for supporting and additional activities for health care. Supporting activities are carried out by all pharmaceutical technical staff, while additional activities are only carried out by a few assigned staff (WHO, 2023).

Determination of the number of pharmaceutical technical staff needs is carried out for each functional unit of pharmaceutical services, namely the central pharmacy installation, emergency room pharmacy satellite, operating room pharmacy satellite, and pharmacy warehouse. The central pharmaceutical installation is a pharmaceutical installation at the hospital X which serves the need for pharmaceutical supplies for inpatient and outpatient care. From September 2022 to August 2023, the number of prescriptions served outpatient and inpatient at Hospital X amounted to 39.537 prescriptions and 220,331 prescriptions respectively. The number of prescription services continues to increase causing the workload to increase. The results of calculating the need for pharmaceutical technical staff based on the workload showed in the Table 2, the pharmaceutical technical staff needed in the central pharmacy installation is around 87 people. However, currently there are 27 pharmaceutical technical staff available at the central pharmacy installation.

The WISN results can be analyzed in two ways, including (1) by looking at the difference between the number of existing staff and the number of staff needed or (2) calculating the ratio of the difference in the number of staff. If the WISN ratio result is equal to 1, this shows that the current number of staff is balanced with staff needs so that the workload is also balanced. If the WISN ratio result is less than one, then the number of staff currently available is not sufficient for the existing workload. If the WISN ratio result is more than 1, it shows that the number of existing staff exceeds the workload that must be done (overstaffing) (Agustini et al., 2023; WHO, 2023). The WISN ratio of the difference in the number of available pharmaceutical technical personnel in central pharmacy installation and the total calculation results is 0,31. Based on WHO provisions, the available number of health workers is inadequate for the existing workload, causing every pharmaceutical technical staff at Hospital X to have an excessive workload (Gialama et al., 2019; WHO, 2023).

The pharmacy installation at Hospital X has two satellites that assist pharmaceutical services at the hospital. The two satellites are the emergency room pharmacy satellite and the operating room pharmacy satellite. The emergency room pharmacy satellite performs pharmaceutical service activities in the emergency room. Currently, the emergency room pharmacy satellite is run by 4 pharmaceutical technical staff. Each work shift is filled by 1 pharmaceutical technical staff. However, an analysis of the need for pharmaceutical technical staff based on workload in Table 3, shows that around 6 people are needed to carry out pharmaceutical services in the emergency room pharmacy satellite. The result of the WISN ratio for emergency room pharmacy satellites is 0.66, which means that the number of staff available is not commensurate with the workload that must be carried out.

The operating room pharmacy satellite at Hospital X aims to provide pharmaceutical services in the central surgical installation. The operating room pharmacy satellite is currently also run by 4 pharmaceutical technical staff with one work shift filled by one staff. Based on the results of the analysis using the WISN method in Table 4, the number of pharmaceutical technical staff required to carry out pharmaceutical services based on the workload in the operating room satellite pharmacy is 6 people. The number of staff available is still inadequate for the existing workload, as indicated by a WISN ratio value of less than 1 (WISN ratio 0.66) (Purwanti & Syam, 2024; WHO, 2023).

Table 2. The result of pharmaceutical technical staff needs analysis in Hospital X central pharmacy installation by WISN method

Healthcare Activities	Activity Standard (min/activities)		Standard Workload (min)	Number of Staff Needs
Acceptance, assessment, and input of outpatient prescription	3		34970	1.13
Preparation, checking, and etiquette labeling of outpatient prescription	17		6171	6.41
Distribution of outpatient drugs to patients	5		20982	1.88
Acceptance, assessment, and input of inpatient prescription	3		34970	6.30
Preparation, checking, and etiquette labeling of inpatient prescription	15		6994	31.50
Inpatient concoction drug services	20		5246	2.20
Distribution of pharmaceutical supplies to the nurse	10		10491	21
Medication concocting	20		5246	0.41
Dispensing of sterile preparations and/or total parenteral nutrition (TPN)	30		3497	0.45
Total of pharmaceutical technical staff needs for health services				71.29
Supporting Activities	Activity standard (min)	Activity Category	Total of Activity standard (min)	Number of Staff Needs
Shift change	10	Daily	30	0.077
Shift report	10	Daily	30	0.077
Pharmaceutical supply stock checking	60	Monthly	60	0.007
Stok opname (SO)	390	Annual	780	0.007
		Total of supporting activities		0.17
Total of pharmaceutical technical staff needs for supporting activities				1,20
Additional Activities	Activity standard (min)	Number of Activities	Frequency (per year)	Number of Staff Needs
Narcotics and psychotropic stock cheking	10	2	807	269
Return of medication from the inpatient room	15	1	2421	605.25
Room and refrigerator temperature report	3	1	538	26.9
Input requests pharmaceutical supply needs to pharmaceutical warehouses	10	1	156	26
Receipt and check of pharmaceutical supplies from pharmaceutical warehouses	30	1	156	78
Storage of pharmaceutical supplies from warehouses and stock card updates	60	3	156	468
Emergency trolley checking	30	1	2	1
		Total of additional activities		1474.15
Total of pharmaceutical technical staff needs for additional activities				0.84
Total of pharmaceutical technical staff needs for central pharmacy installation (people)				86.55

Table 3. The result of pharmaceutical technical staff needs analysis in Hospital X emergency room pharmacy satellite by WISN method

Healthcare Activities	Activity standard (min/activities)	Standard Workload (min)	Number of Staff Needs
Acceptance, assessment, and input of discharge patient prescription from the ER	3	34970	0.02
Preparation, checking, and etiquette labeling of discharge patient prescription from the ER	17	6171	0.11
Distribution of outpatient drugs to patients	5	20982	0.03
Acceptance, assessment, and input of pharmaceutical supply for ER	3	34970	1.23
Preparation of demand for pharmaceutical supply from ER	5	20982	2.04
Distribution of pharmaceutical supplies to the ER nurse	3	34970	1.23
Total of pharmaceutical technical staff needs for health services			4.66

Supporting Activities	Activity standard (min)	Activity Category	Total of Activity standard	Number of Staff Needs
Shift change	10	Daily	30	0.077
Shift report	10	Daily	30	0.077
Pharmaceutical supply stock checking	60	Monthly	60	0.007
Stok opname (SO)	390	Annual	780	0.007
		Total of supporting activities		0.17
Total of pharmaceutical technical staff needs for supporting activities				1.20

Additional Activities	Activity standard (min)	Number of Activities	Frequency (per year)	Number of Staff Needs
Reports of narcotics and psychotropic use in the ER	10	1	269	44.83
Room and refrigerator temperature report	5	1	807	67.25
Preparation of birth packages (partus set)	5	1	1345	112.08
Input requests pharmaceutical supply needs to pharmaceutical warehouses	3	1	156	7.8
Receipt and check of pharmaceutical supplies from pharmaceutical warehouses	15	1	156	39
Storage of pharmaceutical supplies from warehouses and stock card updates	30	1	156	78
Emergency trolley checking	30	1	2	1
			Total of additional activities	349.97
Total of pharmaceutical technical staff needs for additional activities				0.20
Total of pharmaceutical technical staff needs for ER pharmacy satellite (people)				5.81

Table 4. The result of pharmaceutical technical staff needs analysis in Hospital X operating room pharmacy satellite by WISN method

Healthcare Activities	Activity standard (min/activities)		Standard Workload (min)	Number of Staff Needs
Preparation of surgical packages and pharmaceutical supplies requirements	30		3497	3.29
Carry out input and return of pharmaceutical supplies used for operations	15		6994	1.64
Total of pharmaceutical technical staff needs for health services				4.93
Supporting Activities	Activity standard (min)	Activity Category	Total of Activity standard	Number of Staff Needs
Shift change	10	Daily	30	0.077
Shift report	10	Daily	30	0.077
Pharmaceutical supply stock checking	60	Monthly	60	0.007
Stok opname (SO)	390	Annual	780	0.007
		Total of supporting activities		0.17
Total of pharmaceutical technical staff needs for supporting activities				1.20
Additional Activities	Activity standard (min)	Number of Activities	Frequency (per year)	Number of Staff Needs (people
Reports of narcotics and psychotropic use in the OR	10	1	269	44.83
Room and refrigerator temperature report	5	1	807	67.25
Preparation of birth packages (partus set)	3	1	156	7.8
Input requests pharmaceutical supply needs to pharmaceutical warehouses	15	1	156	39
Receipt and check of pharmaceutical supplies from pharmaceutical warehouses	30	1	156	78
Storage of pharmaceutical supplies from warehouses and stock card updates	30	1	2	1
			Total of additional activities	237.88
Total of pharmaceutical technical staff needs for additional activities				0.14
Total of pharmaceutical technical staff needs for OR pharmacy satellite (people)				6.06

The pharmacy warehouse has the main responsibility for managing pharmaceutical supplies at Hospital X. The pharmacy warehouse plays a role in planning, procurement, storage, distribution, and administration related to the management of pharmaceutical supplies. Based on the results of the WISN analysis, the pharmaceutical warehouse requires 3 pharmaceutical technical personnel as shown in Table 5. Currently, the pharmaceutical warehouse at Hospital X has 3 pharmaceutical technical staff. The WISN ratio is 1 and shows that the current workforce is balanced or adequate for the existing workload (Purwanti & Syam, 2024; WHO, 2023).

Table 5. The result of pharmaceutical technical staff needs analysis in Hospital X pharmacy warehouse by WISN method

Healthcare Activities	Activity standard (min/activities)	Standard Workload (min)	Number of Staff Needs
Acceptance of pharmaceutical supply requests from the central pharmacy installation	10	10491	0.01
Process of mutation/input of pharmaceutical supply in the SIMRS system	60	1749	0.09
Preparation of pharmaceutical supplies according to central pharmacy installation request	180	583	0.27
Distribution of pharmaceutical supplies to central pharmacy installation	30	3497	0.04
Double check of pharmaceutical supply in central pharmacy installation	120	874	0.18
Acceptance of pharmaceutical supply requests from pharmacy satellites	10	10491	0.03
Process of mutation/input of pharmaceutical supply in the SIMRS system	30	3497	0.09
Preparation of pharmaceutical supplies according to pharmacy satellite request	90	1166	0.27
Distribution of pharmaceutical supplies to pharmacy satellites	30	3497	0.09
Double check of pharmaceutical supply in pharmacy satellites	60	1749	0.18
Acceptance of pharmaceutical supply requests from inpatient room	15	6994	0.10
Preparation of pharmaceutical supplies according to inpatient room request	30	3497	0.21
Total of pharmaceutical technical staff needs for health services			1.56

Supporting Activities	Activity standard (min)	Activity Category	Total of Activity standard	Number of Staff Needs
Storage and updating of incoming drug stock cards	160	Daily	160	0.410
Storage and updating of stock cards for medical equipment/consumable medical materials	160	Daily	160	0.410
Enter drug invoices	60	Daily	60	0.154
Enter invoices for medical equipment/consumable medical materials	60	Daily	60	0.154
Coordinate the management of pharmaceutical supplies, medical devices and consumable medical materials	60	Weekly	120	0.059
Storage of invoice documents / drug order letters	30	Weekly	30	0.015
Storage of invoice documents/orders letters for	30	Weekly	30	0.015

medical devices and consumable medical materials				
Storage of invoices for requests for pharmaceutical supplies from the inpatient room	30	Weekly	30	0.015
Storage of report documents	30	Weekly	30	0.015
Check stock of generic drugs	60	Monthly	60	0.007
Check stock of non-generic drugs	60	Monthly	60	0.007
Check stock of medical devices	60	Monthly	60	0.007
Check stock of consumable medical materials	60	Monthly	60	0.007
			Total of supporting activities	0.03
Total of pharmaceutical technical staff needs for supporting activities				1.03

Additional Activities	**Activity standard (min)**	**Number of Activities**	**Frequency (per year)**	**Number of Staff Needs**
Receipt and inspection of invoices with physical form of pharmaceutical inventory	5	2	4304	717.33
Receipt and inspection of invoices with physical form of medical devices / consumable medical materials	5	2	4304	717.33
Monitoring and reporting temperature	5	1	538	44.83
Make plans for the need for pharmaceutical supplies, medical devices, consumable medical materials, and drugs for the health program	240	2	52	416
Make orders for the need for pharmaceutical supplies, medical devices, consumable medical materials, and drugs for the health program	30	1	208	104
Evaluate offers of pharmaceutical supplies	60	2	12	24
Making expired pharmaceutical supply reports	60	1	12	12
Making vaccine reports to the Public Health Office (*Dinas Kesehatan*)	60	1	12	12
Making an IUD report	60	1	12	12
Making activity reports in the pharmacy warehouse	60	1	12	12
Making reports for product recalls	30	1	12	6
Creation of empty pharmaceutical supply reports	60	1	12	12
Creation of new item reports	60	1	12	12
			Total of additional activities	**2101.5**
Total of pharmaceutical technical staff needs for additional activities				**1.20**
Total of pharmaceutical technical staff needs for pharmacy warehouse (people)				**2.80**

CONCLUSION

Based on WISN calculations, the required number of pharmaceutical technical personnel in the central pharmacy installation is 87 people, the emergency room pharmacy satellite is 6 people, the operating room pharmacy satellite is 6 people, and the pharmacy warehouse is 3 people. The analysis result shows the number of pharmaceutical technical staff needed at Hospital X using the WISN method, the current number of pharmaceutical technical personnel in the central pharmacy installation, emergency room pharmacy satellite, and operating room pharmacy satellite are still not following with the existing workload (WISN ratio value < 1). Meanwhile, the pharmaceutical warehouse currently has pharmaceutical technical staff that is appropriate to the existing workload (WISN ratio value = 1). Therefore, Hospital X can consider increasing the number of pharmaceutical technical personnel to improve the existing pharmaceutical services at Hospital X so that patient satisfaction and patient treatment can be achieved more optimally. Hospital X also can improve their human resource management so that the currently available pharmaceutical staff do not experience excessive workload which results in worsening service.

REFERENCES

Agustini, T. T., Muharni, S., & Dwiputri, Y. M. (2023). Analisis kebutuhan tenaga kerja berdasarkan metode workload indicators staffing need (Wisn) di Depo Farmasi rawat jalan Rsud Arifin Achmad provinsi Riau. *Jurnal Penelitian Dan Pengkajian Ilmiah Eksakta*, *2*(1), 110–115. https://doi.org/10.47233/jppie.v2i1.797

Akbar, M.I., Ali, L., & Ratnawati. (2020). Kajian kebutuhan tenaga dokter umum dengan menggunakan metode Workload Indicator Staff Need (WISN) di poli umum dan unit gawat darurat (UGD) RSUD Kabupaten Buton Utara. *MIRACLE Journal Of Public Health*, *3*(2), 153–162. https://doi.org/10.36566/mjph/Vol3.Iss2/173

Aulia, R.E., M.H. Asiana Gabril, & Riantina Luxiarti. (2019). Description of medical record staff based on method workload indicator staff need in Kuningan medical Center Hospital. *Jurnal Kesehatan Mahardika*, *6*(2), 42–50. https://doi.org/10.54867/jkm.v6i2.47

Cucu, C., Nuraeni, H., & Muryani, A. (2019). Analisis beban kerja perawat di ruang rawat inap rumah sakit gigi mulut Universitas Padjadjaran tahun 2018. *Jurnal Sistem Kesehatan*, *4*(4), 164–172. https://doi.org/10.24198/jsk.v4i4.22983

Doosty, F., Maleki, M., & Yarmohammadian, M. (2019). An investigation on workload indicator of staffing need: A scoping review. *Journal of Education and Health Promotion*, *8*(1), 22. https://doi.org/10.4103/jehp.jehp_220_18

Gialama, F., Saridi, M., Prezerakos, P., Pollalis, Y., Contiades, X., & Souliotis, K. (2019). The implementation process of the Workload Indicators Staffing Need (WISN) method by WHO in determining midwifery staff requirements in Greek Hospitals. *European Journal of Midwifery*, *3*(January). https://doi.org/10.18332/ejm/100559

Govule, P., Mugisha, J. F., Katongole, S. P., Maniple, E., Nanyingi, M., & Onzim, R. A. D. (2015). Application of workload indicators of staffing needs (WISN) in determining health workers' requirements for mityana general hospital. *International Journal of Public Health Research*, *3*(5), 254–263.

Jing, Q., Xing, Y., Duan, M., Guo, P., Cai, W., Gao, Q., Gao, R., Ji, L., & Lu, J. (2022). Study on the rehabilitation therapist estimation under institutional perspective by applying the workload indicators of staffing needs in theaging context. *Frontiers in Public Health*, *10*. https://doi.org/10.3389/fpubh.2022.929675

Kementerian Kesehatan RI. (2016). *Peraturan Menteri Kesehatan RI Nomor 72 Tahun 2016 tentang Standar Pelayanan Kefarmasian di Rumah Sakit*.

Kuswandani, F., Lestari, D., & F. Balafif, F. (2021). Workload analysis of pharmacy technicians at pharmacy department of Universitas Padjadjaran dental and oral Hospital using workload indicators of staffing needs. *Indonesian Journal of Clinical Pharmacy*, *10*(3), 198–208. https://doi.org/10.15416/ijcp.2021.10.3.198

Lubis, A. D. S., Girsang, E., Mutiara, M. S., & Ulina Karo-karo. (2022). Analysis of pharmaceutical personnel needs on workload with method wisn (workload indicator of staffing need) in hospital pharmaceutical installation hospital royal prima. *International Journal of Health and Pharmaceutical (IJHP)*, *2*(2), 250–258. https://doi.org/10.51601/ijhp.v2i2.27

McQuide, P. A., Kolehmainen-Aitken, R.-L., & Forster, N. (2013). Applying the workload indicators of staffing need (WISN) method in Namibia: challenges and implications for human resources for health policy. *Human Resources for Health*, *11*(1), 64. https://doi.org/10.1186/1478-4491-11-64

Pemerintah Republik Indonesia. (2023). *Undang-Undang Republik Indonesia Nomor 17 Tahun 2023 tentang Kesehatan*.

Purwanti, D. I., & Syam, N. S. (2024). Analisis perhitungan jumlah kebutuhan SDM menggunakan metode workload indicators of staffing need (WISN) di instalasi central sterile supply department (CSSD) Rumah Sakit Swasta. *International Journal of Healthcare Research*, *6*(2), 23–34. https://doi.org/10.12928/ijhr.v6i2.9602

Rensiner, R., Azwar, V. Y., & Putra, A. S. (2018). Analisis faktor kualitas pelayananterhadap kepuasan pasien rawat jalan RSUD DR. Achmad Darwis. *Jurnal Kesehatan Andalas*, *7*, 1. https://doi.org/10.25077/jka.v7i0.817

Siregar, C. J. . (2004). *Farmasi rumah sakit teori dan penerapan*. Jakarta EGC.

Sungkonoputri, L., & Dhamanti, I. (2023). Analysis of nurse needs using workload indicator staff need (WISN) method. *Jurnal Aisyah : Jurnal Ilmu Kesehatan*, *8*(3). https://doi.org/10.30604/jika.v8i3.2158

Wahyu Ningsih, S., Hakam, F., & Asriati, Y. (2020). Analisis kebutuhan tenaga rekam medis menggunakan metode workload indicator staff need (WISN) di UPTD Puskesmas Weru Tahun 2020. *Jurnal Manajemen Informasi Dan Administrasi Kesehatan (JMIAK)*, *3*(2). https://doi.org/10.32585/jmiak.v3i2.1005

WHO. (2023). *WISN workload indicators of staffing need User's manual* (second edition (ed.)).

Yulaika, N. (2018). Perencanaan tenaga teknis kefarmasian berdasarkan analisis beban kerja menggunakan metode WISN di RSIA KM. *Jurnal Administrasi Kesehatan Indonesia*, *6*(1), 46. https://doi.org/10.20473/jaki.v6i1.2018.46-52

Pharmaciana
Vol.14, No.3, Nov 2024, Page. 337-345
ISSN: 2088 4559; e-ISSN: 2477 0256
DOI: 10.12928/pharmaciana.v14i3.27001

The potential of swiftlet bird's nest extract (*Aerodramus fucipaghus*) as an antioxidant in serum formulation

Naniek Widyaningrum[1*], Chintiana Nindya Putri[1], Thendi Abdul Arief[1], Nada Aini Sofa[1], Monica Virdaus[2]

[1]Professional Pharmacy Education Program, Sultan Agung Islamic University, Semarang
Jl Kaligawe Raya Km 4, No.Km.4, Terboyo Kulon, Kec. Genuk, Semarang, Central Java, Indonesia
[2]Pharmaceutical Science Study Program, Sultan Agung Islamic University, Semarang
Jl Kaligawe Raya Km 4, No.Km 4, Terboyo Kulon, Kec. Genuk, Semarang, Central Java, Indonesia

Submitted: 22-08-2023 ***Reviewed: 02-08-2024*** ***Accepted: 06-11-2024***

ABSTRACT

The white swiftlet bird's nest (*Aerodramus fucipaghus*) constitutes one of nature's treasures endowed with diverse health benefits. The swiftlet bird's nest is a potential source of antioxidants, capable of counteracting free radicals contributing to premature ageing. It can be harnessed as a serum formulation featuring small molecules, facilitating deeper skin penetration, efficient delivery of highly concentrated active agents, and expedited resolution of skin issues. This study aimed to ascertain the swiftlet bird's nest serum's physical properties, physical stability, and antioxidant activities. Serum formulations span a range of concentrations: 10%, 20%, 30%, and 40%. Physical attributes of the serum, including organoleptic properties, homogeneity, pH, spreadability, and viscosity, were observed. Serum stability was assessed over a 21-day storage period. The antioxidant activity of the serum was gauged via DPPH assay, determining the IC_{50} values. The serum, across varying concentrations, exhibited commendable physical characteristics, satisfying stipulated criteria. Antioxidant activity was detected in the serum across a spectrum of concentrations, revealing IC_{50} values of 250.00±1.58 µg/mL, signifying a range from weak to strong efficacy (90.137±0.4 µg/mL). The swiftlet bird's nest serum with its concentration variants demonstrated physical stability during the 21-day storage duration. Drawing from the research, it can be deduced that the swiftlet bird's nest holds promise for development into a serum formulation that fulfils both physical and stability criteria, endowed with robust antioxidant activity. Notably, the swiftlet bird's nest serum in formula 4 at a 40% concentration exhibited good physical, stability and potent antioxidant activity, manifesting an IC_{50} value of 90.137±0.4 µg/mL.

Keywords: swiftlet bird's nest, *Aerodramus fucipaghus*, serum, antioxidant, DPPH

Corresponding author:
Naniek Widyaningrum
Professional Pharmacy Education Program, Sultan Agung Islamic University
Jl Kaligawe Raya Km 4, No.Km.4, Terboyo Kulon, Kec. Genuk, Semarang, Central Java, Indonesia
Email: naniek@unissula.ac.id

INTRODUCTION

The white swiftlet bird's nest (*Aerodramus fucipaghus*) is a natural treasure extensively harvested by Asian nations. Indonesia, in particular, is the world's largest exporter, contributing over 75% of the global supply of swiftlet bird's nests. Revered for its myriad health benefits, the swiftlet bird's nest serves as a dietary supplement renowned for its roles in skin lightening, prebiotic functions, and even burn wound healing (Chan et al., 2015; Anggraini & Kasmawati, 2017; Babji & Daud, 2019; Acharya & Satheesh, 2023).

The swiftlet bird's nest constitutes a promising source of antioxidants. Prior studies have revealed the antioxidant activity of swiftlet bird's nest at a concentration of 4 ppm, yielding an IC_{50} value of 4.0240 mg/g (Nadia et al., 2017). The glycoproteins within the swiftlet bird's nest function to counteract Reactive Oxygen Species (ROS) such as H2O2, thereby mitigating the escalation of free radicals and concurrently enhancing the antioxidant activity of the enzyme catalase (Dewi, 2020).

Free radicals constitute the foremost contributors to premature ageing, inducing skin pigmentation, collagen degradation, and damage to DNA, mitochondria, proteins, and lipid membranes (Krutmann et al., 2017; Nakai & Tsuruta, 2021). Skin ageing poses a prevalent concern within modern society. The emergence of fine wrinkles on the face, heightened skin dryness, and alterations in skin colouration characterise skin ageing. Premature ageing is brought about by free radicals, such as those originating from cigarette smoke, pollution, and exposure to UV rays (Zahruddin & Damayanti, 2018).

Antioxidants can impede the oxidation of oxidant molecules. Superoxide dismutase is a natural antioxidant synthesised by the body. Additionally, natural antioxidants can be obtained from natural sources, exemplified by vitamins A, C, and E, which derive from natural substances (Silvia, 2018). The human body lacks an abundant reserve of antioxidants; thus, additional antioxidants are required to inhibit the process of premature ageing.

Swiftlet bird's nest can be developed into cosmetic formulations, including serums. Serums are preparations with small molecules capable of penetrating the skin's deeper layers, delivering highly concentrated active ingredients, proving effective and swift in addressing various skin issues (Thakre, 2017).

This research aimed to harness the potential of white swiftlet bird's nest (*Aerodramus fucipaghus*) as an antioxidant serum. Serum possesses a lightweight texture, facilitating easy application to the face while refraining from leaving an oily residue on the skin. The serum is formulated across 10%, 20%, 30%, and 40% concentrations

.

MATERIALS AND METHOD

Materials

The instruments employed encompassed UV-Vis Spectrophotometer (Agilent Technologies Carry 60 UV-Vis), Brookfield Viscometer, pH meter (Mettler Toledo), analytical balance (Dj. Series Excellent Scale), aluminum foil, and glassware. The utilized materials comprised 2,2-diphenyl-1-picrylhydrazyl (DPPH), methanol, and distilled water (aqua dest). All employed chemical substances were of analytical grade (p.a). White swiftlet bird's nest (*Aerodramus fucipaghus*) was employed as the active ingredient for the serum formulation. Excipients for the serum formulation consisted of Carbopol (Sigma-Aldrich), propylene glycol (Sigma-Aldrich), glycerin (Sigma-Aldrich), and nipagin (Sigma-Aldrich) obtained from PT Medikalab Indo Raya, Semarang.

Method

Sample preparation

The swiftlet bird's nest was thoroughly washed and cleaned to remove impurities and subsequently air-dried until completely dry. The dried white swiftlet bird's nest (*Aerodramus fucipaghus*) was finely blended to minimize the surface area, thereby enhancing the contact between the swiftlet nest particles and the solvent and optimizing the extraction of active compounds. The powdered swiftlet bird's nest

was then soaked in distilled water using a low-temperature water bath (maximum 71°C) for 10 minutes to facilitate expansion, after which it was finely ground (Anggraini & Kasmawati, 2017).

Preparation of white swiftlet bird's nest extract serum

The swiftlet bird's nest serum was formulated in four different concentrations, as outlined in Table 1. The swiftlet bird's nest serum production followed the methodology established in the referenced research study (Kurniawati & Wijayanti, 2018) with slight modifications. Carbopol was hydrated in distilled water overnight to form a gel, which was then stirred thoroughly to achieve uniformity and prevent clumps. Glycerin was gradually added while continuously stirring (mass 1). Nipagin was dissolved in propylene glycol (mass 2). Masses 1 and 2 were mixed, followed by the addition of the extract according to its concentration. Distilled water was added to reach the desired final volume.

Table 1. The formula for white swiftlet bird's nest extract serum

Materials	Concentration			
	F1	F2	F3	F4
Swiftlet Bird's Nest (*Aerodramus fuciphagus*)	10%	20%	30%	40%
Glycerin	15	15	15	15
Carbopol	0.5	0.5	0.5	0.5
Nipagin	0.2	0.2	0.2	0.2
Propylene Glycol	3	3	3	3
Distilled Water	ad 100	ad 100	ad 100	ad 100

Evaluation of physical properties of white swiftlet bird's nest extract serum

Organoleptic test

Visual observation of the preparation regarding the formulated serum's form, color, and aroma. Typically, serums exhibit a transparent white color and possess a moderately viscous texture.

Homogeneity test

This test was conducted by applying a serum sample onto a glass slide. The serum should exhibit a homogeneous composition without coarse particles (Kurniawati & Wijayanti, 2018).

pH Test

pH observation of the serum was conducted by immersing a pH meter into the formulation.

Viscosity Test

Viscosity testing was performed by placing a 100 mL sample in a Brookfield viscometer with the spindle immersed up to a specific limit, rotating at 60 rpm. An optimal facial serum viscosity typically falls within 230-1150 cps (Wijayanti & Faizatun, 2011).

Physical stability of the serum

The evaluation of the physical stability of the formulation was conducted to ensure that the preparation retained consistent properties post-production and continued to meet predefined criteria throughout storage. The serum's physical stability test involved observing the serum's organoleptic characteristics after storage for 21 days at room temperature (15-30°C (Ariyanti et al., 2020).

Antioxidant activity of swiftlet bird's nest serum

Determination of wavelength and operating time

Antioxidant activity is carried out by DPPH method (Rispriandari et al., 2024). A solution of 0.1 mM DPPH was prepared by dissolving 10 mg of DPPH powder in 250.0 mL of methanol. The maximum wavelength and blank were determined by adding 2 mL of 0.1 mM DPPH solution to 2 mL

of methanol p.a. The mixture was then measured using a UV-Vis spectrophotometer at 400 to 600 nm wavelengths. To determine the operating time, 50 µL of a standard vitamin C solution was added to 4 mL of 0.1 mM DPPH solution. The mixture was homogenized using a stirrer for 1 minute, and its absorbance was measured at 0, 5, 10, 15, 20, 25, 30, 35, 40, 45, 50, 55, and 60 minutes at the maximum wavelength (Widyowati et al., 2014).

Determination of antioxidant potential

A standard solution at a 100 µg/mL concentration was prepared by dissolving 10 mg of vitamin C in 100 mL of methanol. A dilution series was prepared at concentrations of 1 µg/mL, 4 µg/mL, 7 µg/mL, 10 µg/mL, and 13 µg/mL. For each concentration, 2.0 mL of 0.1 mM DPPH solution was added to a volumetric flask containing 2 mL of the standard solution. Test solutions were prepared by dissolving 25 mg in 50 mL of methanol to achieve a concentration of 500 µg/mL, followed by dilution series at concentrations of 50 µg/mL, 100 µg/mL, 150 µg/mL, 200 µg/mL, and 250 µg/mL. Again, for each concentration, 2.0 mL of 0.1 mM DPPH solution was added to a volumetric flask containing 2 mL of the test solution. Both test and standard solution flasks were vortexed for 30 seconds and then incubated for 30 minutes in a dark room. Absorbance was measured using a UV-Vis spectrophotometer at the predetermined maximum wavelength. The obtained absorbance results were substituted into the following equation 1.

$$\%\text{Inhibition} = \frac{Blank\ Absorbance - Sample\ Absorbance}{Blank\ Absorbance}\ x\ 100\ \% \quad \text{.....(1)}$$

The values of the extract or standard concentration, along with their respective inhibition percentages, were plotted on the x and y axes using the equation 2.

$$y = a + bx \quad \text{.....(2)}$$

A linear regression equation was employed to determine the IC_{50} values of each sample by expressing the y-value as 50 and the x-value as IC_{50}. The IC_{50} value indicated the sample concentration required to reduce 50% of the DPPH free radicals.

Data Analysis

Data analysis was conducted using SPSS. Viscosity, spreadability, and adhesion data were assessed using the Shapiro-Wilk test to ascertain their normal distribution. Homogeneity was examined using the Levene test. Normally distributed and homogenous data were further analyzed through parametric One-Way ANOVA followed by Post Hoc Tests. Non-normally distributed data was assessed using Kruskal-Wallis and Mann-Whitney tests. Stability data were analyzed using Repeated Measures ANOVA.

RESULT AND DISCUSSION

Physical properties of white swiftlet bird's nest extract serum

The white swiftlet bird's nest extract (*Aerodramus fuciphagus*) utilized in this research was obtained from a bird nest breeding facility in Sukamara Regency, Southeast Kalimantan. White swiftlet bird's nest extract was formulated into a serum preparation and subsequently subjected to physical property tests, encompassing organoleptic assessment, homogeneity, pH, viscosity, spreadability, and adhesion. Organoleptic test results revealed that the white swiftlet bird's nest extract serum exhibited a dull white color, carried a distinct swiftlet bird's nest aroma (musty), and possessed a dense texture akin to serum (Figure 1, Table 2).

Figure 1. White swiftlet bird's nest serum

Based on the observations (Figure 1), formula 1 with a 10% concentration yields a serum color that is clearer and brighter. As the concentration of white swiftlet bird's nest extract increases, the resulting serum color tends to become a darker dull white.

Table 2. The results of organoleptic and homogeneity tests on the serum

Formula	Color	Aroma	Form	Homogeneity
F1	Dull White	Distinct	Viscous	Homogeneous
F2	Dull White	Distinct	Viscous	Homogeneous
F3	Dull White	Distinct	Viscous	Homogeneous
F4	Dull White	Distinct	Viscous	Homogeneous

Homogeneity testing was conducted to observe whether the preparation is uniform by examining the presence of large or coarse particles in the serum. The test results for the preparation (Table 2) indicate the absence of coarse particles, thus confirming that the white swiftlet bird's nest serum (*Aerodramus fuciphagus*) is considered homogeneous.

Table 3. The pH test results of the serum

Formula	Day				p-Value
	1	7	14	21	
F1	5.03±0.1	4.93±0.4	4.97±0.2	5.05±0.5	0.024
F2	4.84±0.4	4.91±0.3	4.87±0.1	4.99±0.4	
F3	4.92±0.2	4.64±0.5	4.66±0.1	4.70±0.3	
F4	4.97±0.1	4.87±0.3	4.66±0.5	4.64±0.3	

The results of the physical test on the white swiftlet bird's nest extract serum (Table 3) at various concentrations reveal pH values ranging from 4.64 to 5.05, falling within the pH range suitable for topical formulations, which is 4 to 5.5 (Thakre, 2017). pH measurement determines whether the formulated product is safe and non-irritating when applied to the skin. An excessively low pH value can lead to skin irritation due to its acidic nature, while a high pH value can cause skin dryness (Putri & Anindhita, 2022). At varying concentrations, the antioxidant serum with white swiftlet bird's nest extract significantly influences the resulting pH with a significance value of 0.024 ($p<0.05$). Meaningful differences are observed between the 10% (F1) concentration and the 30% (F3) and 40% (F4) concentrations. Across the serum formulations at different concentrations, no significant difference was observed between pH and storage time with $p=0.324$ ($p>0.05$). The results of the spreadability test for the white swiftlet bird's nest extract serum (*Aerodramus fuciphagus*) can be observed as follows Table 4.

The spreadability test aimed to determine the ability of the serum preparation to spread. The spreadability test results (Table 4) for various formulations meet the criteria for good serum spreadability: having a diameter within the range of 4-7.5 cm (Montenegro et al., 2015). The analysis of the white swiftlet bird's nest serum formula (*Aerodramus fuciphagus*) at various concentrations

reveals a significant difference with a significance value of 0.004 ($p<0.05$). Meaningful differences are observed between concentrations F1 and F4 and between F1 and F3. The spreadability of the serum during a 21-day storage period indicates good stability across various concentrations, with no significant difference observed at $p=0.553$ ($p>0.05$) concerning storage time. The spreadability value is inversely proportional to viscosity, where an increase in formulation thickness leads to a decrease in spreadability (Mudhana & Pujiastuti, 2021).

Table 4. The Results of the spreadability test (cm) on the serum

Formula	Day				p-Value
	1	7	14	21	
F1	6.8 ±0.1	6.8 ±0.3	7±0.2	7±0.1	0.004
F2	5.5±0.2	5.8±0.4	5.8±0.4	5.9±0.6	
F3	5±0.2	5.2±0.5	5.2±0.6	5±0.3	
F4	5.2±0.1	5±0.2	5±0.2	5±0.3	

The viscosity values of the swiftlet bird's nest extract serum (Table 5) indicate that higher extract concentrations result in thicker serum viscosity and lower spreadability values. In the viscosity test, the data analysis reveals significance between the serum formulations at 10% and 40% concentrations. The higher the extract concentration, the higher the viscosity. The viscosity of the formulation can be influenced by various factors, including temperature changes, variations in manufacturing conditions, and raw material quality (Thakre, 2017), including the concentration of the active ingredient (Mardhiani et al., 2018). The concentration of added swiftlet bird's nest extract in the serum impacts viscosity due to the texture of swiftlet bird's nest being similar to agar, necessitating a balance with increased water phase to achieve the desired viscosity. Stability analysis of the serum across all four formulations reveals no significant difference, with $p=0.506$ ($p>0.05$), in viscosity during a 21-day storage period.

Table 5. The results of the serum viscosity test (cps)

Formula	Day				p-Value
	1	7	14	21	
F1	224±0.6	256±0.5	273±0.6	274±0.7	0.003
F2	362±0.2	421±0.4	421±0.6	425±0.3	
F3	4210±0.2	4430±0.6	4060±0.6	4020±0.4	
F4	7392±0.3	7283±0.2	7308±0.6	7308±0.5	

Antioxidant activity of white swiftlet bird's nest extract serum

The results of the antioxidant test using the DPPH method on the White Swiftlet Bird's Nest Extract Serum (*Aerodramus fuciphagus*) at concentrations of 10%, 20%, 30%, and 40% can be observed in the following Table 6. The antioxidant activity test on the white swiftlet bird's nest extract serum (*Aerodramus fuciphagus*) uses the DPPH method (Sabandar et al., 2023), which involves a nitrogen radical compound. The DPPH reaction mechanism operates through electron transfer. The DPPH method is chosen due to its simplicity, ease of use, sensitivity, and requirement of only a tiny sample (Rahmawati et al., 2016). Antioxidant activity in this reaction can be observed through the change of colour from purple to yellow. Before reading the absorbance, the sample solution is incubated for 30 minutes to allow the donation reaction between the free radicals and the sample solution to be tested for its antioxidant activity (Martiani et al., 2017).

The antioxidant test results using the DPPH method on the white swiftlet bird's nest extract serum (*Aerodramus fuciphagus*) at concentrations of 10% (F1), 20% (F2), 30% (F3), and 40% (F4) are 250.00±1.58 µg/mL, 132.31±0.74 µg/mL, 118.57±0.37 µg/mL, and 90.13±0.4 µg/mL respectively.

These results will be compared with the positive control, a commercially available serum (Vitamin C Serum), and the negative control in the form of the serum base.

Table 6. The results of the antioxidant activity test on the serum

Formula	Concentration (µg/mL)	% Inhibition	lC50 (µg/mL)
F1	50	12.033±0.06	250.00±1.58
	100	21.352±0.12	
	150	29.240±0.08	
	200	36.792±0.14	
	250	53.058±0.16	
F2	50	27.237±0.07	132.31±0.74
	100	41.492±0.05	
	150	52.870±0.06	
	200	68.341±0.15	
	250	85.395±0.23	
F3	50	30.521±0.09	118.57±0.37
	100	47.487±0.05	
	150	60.444±0.15	
	200	66.666±0.17	
	250	85.351±0.28	
F4	50	40.2597±0.26	90.137±0.4
	100	50.7499±0.38	
	150	66.1113±0.43	
	200	81.0967±0.64	
	250	92.5357±0.48	
Control (+): Vitamin C Serum			138.17±0.4
Control (-): Base (Placebo)			2415.37±0.59

From the antioxidant test results on the white swiftlet bird's nest extract serum using the DPPH method (Table 6), it can be observed that the serum formulation exhibits antioxidant activity ranging from strong to weak. At a concentration of 10%, the white swiftlet bird's nest serum shows weak antioxidant activity with an IC_{50} value of 250.00±1.58 µg/mL. The limited antioxidant effect of the swiftlet bird's nest might be attributed to the relatively small amount of peptide bonds that have undergone hydrolysis, subsequently reducing the number of amino groups and consequently decreasing its pharmacological effectiveness (Ramachandran et al., 2018). The weak antioxidant effect of the white swiftlet bird's nest serum formulation can also be attributed to the relatively low concentration or content of the swiftlet bird's nest used in the 10% concentration formulation. The white swiftlet bird's nest serum formulation at 20% and 30% exhibits moderate antioxidant activity with IC_{50} values of 132.31±0.74 µg/mL and 118.57±0.37 µg/mL, respectively. The formulation at 40% concentration shows vigorous antioxidant activity with an IC_{50} value of 90.13±0.4 µg/mL. Compared to the positive control (Vitamin C Serum) with an IC_{50} value of 138.17±0.4 µg/mL, the white swiftlet bird's nest serum at a 20% extract concentration already falls within the range of commercially available serums. In the case of the negative control, the obtained IC_{50} value is 2415.37±0.59 µg/mL, indicating the absence of antioxidant activity in the negative control formulation (Base) due to the absence of white swiftlet bird's nest (*Aerodramus fuciphagus*) content.

Swiftlet bird's nests contain various amino acids, including cysteine, methionine, histidine, tyrosine, tryptophan, and phenylalanine (Ali et al., 2019). Hydrophobic amino acids, including tyrosine, activate the antioxidant in the white swiftlet bird's nest. The mechanism of free radical inhibition by the amino acid tyrosine involves the activity of the ROO• group, which acts as a proton

donor in the tyrosine peptide. The ROO• radical acquires a proton from the hydroxyl group of tyrosine, forming a neutral molecule ROOH. Tyrosine transforms into a new radical, which can resonate to become a stable ketone group (Esfandi et al., 2019).

White swiftlet bird's nest (*Aerodramus fuciphagus*) contains Epidermal Growth Factor (EGF), which can be utilized as an anti-ageing agent. EGF functions by improving skin texture and tissue, leading to skin rejuvenation. EGF plays a significant role in regenerating skin cells, accelerating the metabolism of the skin layers, and repairing dead skin cells (Rohmah, 2019). Hence, aside from being a nutritious and healthy dietary source, swiftlet bird's nest can also be developed into various cosmetic formulations within the beauty industry.

CONCLUSION

Based on the research, it can be concluded that a swiftlet bird's nest can be developed into a serum formulation that meets the physical and stability criteria with potent antioxidant activity. The swiftlet bird's nest serum in formula 4 at a concentration of 40% exhibited good physical, stability and potent antioxidant activity, with an IC_{50} value of 90.137±0.4 µg/mL.

ACKNOWLEDGEMENT

The authors would like to thank the Faculty of Pharmacy, Universitas Islam Sultan Agung, which has facilitated and helped research until it can be completed well.

REFERENCES

Acharya, C., & Satheesh, N. (2023). Edible Bird's Nest (EBN): production, processing, food and medicinal importance. *Agricosemagazine*, *4*(3), 20–25

Ali, A. A. M., Noor, H. S. M., Chong, P. K., & Abdul Salam Babji, S. J. L. (2019). Comparison of amino acids profile and antioxidant activities between edible bird nest and chicken egg. *Malaysian Applied Biology*, *48*(2), 63–69

Anggraini, D., & Kasmawati, L. Y. (2017). Formulasi gel sarang burung walet putih (Aerodramus fushipagus) dan uji penyembuhan luka bakar derajat II pada mencit. *Jurnal Sains Farmasi & Klinis*, *4*(1), 55. https://doi.org/10.29208/jsfk.2017.4.1.172

Ariyanti, E. L., Handayani, R. P., & Yanto, E. S. (2020). Formulasi sediaan serum antioksidan dari ekstrak sari Tomat (Solanum lycopersicum L.) dan ekstrak Kayu Manis (Cinnamomum burmannii) sebagai perawatan kulit. *Journal of Holistic and Health Sciences*, *4*(1), 50–57. https://doi.org/10.51873/jhhs.v4i1.80

Babji, A. S., & Daud, N. A. (2019). Physicochemical properties of Glycan within Swiftlet's Nest (Aerodramus fuciphagus) as potential prebiotic. *Acta Scientific Medical Sciences*, *3*(9), 9–13

Chan, G. K. L., Wong, Z. C. F., Lam, K. Y. C., Cheng, L. K. W., Zhang, L. M., Lin, H., Dong, T. T., & Tsim, K. W. K. (2015). Edible bird's nest, an Asian health food supplement, possesses skin lightening activities: identification of N-Acetylneuraminic acid as active ingredient. *Journal of Cosmetics, Dermatological Sciences and Applications*, *05*(04), 262–274. https://doi.org/10.4236/jcdsa.2015.54032

Dewi, M. E. (2020). Manfaat konsumsi sarang Burung Walet. *Jurnal Kedokteran Ibnu Nafis*, *9*(1), 12–16. https://doi.org/10.30743/jkin.v9i1.43

Esfandi, R., Walters, M. E., & Tsopmo, A. (2019). Antioxidant properties and potential mechanisms of hydrolyzed proteins and peptides from cereals. *Heliyon*, *5*(4), e01538. https://doi.org/10.1016/j.heliyon.2019.e01538

Krutmann, J., Bouloc, A., Sore, G., Bernard, B. A., & Passeron, T. (2017). The skin aging exposome. *Journal of Dermatological Science*, *85*(3), 152–161. https://doi.org/10.1016/j.jdermsci.2016.09.015

Kurniawati, zizah Y., & Wijayanti, E. D. (2018). *Karakteristik sediaan serum wajah dengan variasi konsentrasi sari rimpang temu giring (Curcuma heyneana) terfermentasi Lactobacillus bulgaricus.*

Akademi Farmasi Putra Indonesia Malang
Mardhiani, Y. D., Yulianti, H., Azhary, D. P., & Rusdiana, T. (2018). Formulasi dan stabilitas sediaan serumdari ekstrak kopi hijau (Coffea Canephora Var. Robusta)sebagai antioksidan. *Indonesia Natural Research Pharmaceutical Journal Universitas 17 Agustus 1945 Jakarta*, *2*(2), 19–33
Martiani, I., Azzahra, I. F., & Perdana, F. (2017). Aktivitas antioksidan ekstrak N-Heksan, etil asetat, dan Metanol Daun Dewandaru (Eugenia uniflora L.). *Jurnal Ilmiah Farmako Bahari*, *8*(2), 31. https://doi.org/10.52434/jfb.v8i2.78
Montenegro, L., Rapisarda, L., Ministeri, C., & Puglisi, G. (2015). Effects of lipids and emulsifiers on the Physicochemical and Sensory properties of cosmetic emulsions containing Vitamin E. *Cosmetics*, *2*(1), 35–47. https://doi.org/10.3390/cosmetics2010035
Mudhana, A. R., & Pujiastuti, A. (2021). Pengaruh trietanolamin dan asam stearat terhadap mutu fisik dan stabilitas mekanik krim sari buah Tomat. *Indonesian Journal of Pharmacy and Natural Product*, *4*(2), 113–122. https://doi.org/10.35473/ijpnp.v4i2.1342
Nadia, N., M., Babji, A. S., Ayub, M. K., & Nur 'Aliah, D. (2017). Effect of enzymatic hydrolysis on antioxidant capacity of cave edible bird's nests hydrolysate. *International Journal of ChemTech Research*, *10*(2), 1100–1107
Nakai, K., & Tsuruta, D. (2021). What are reactive oxygen species, free radicals, and oxidative stress in skin diseases? *International Journal of Molecular Sciences*, *22*(19), 10799. https://doi.org/10.3390/ijms221910799
Putri, W. E., & Anindhita, M. A. (2022). Optimization of cardamom fruit ethanol extract gel with combination of HPMC and Sodium Alginate as the gelling agent using Simplex Lattice Design. *Jurnal Ilmiah Farmasi*, 107–120. https://doi.org/10.20885/jif.specialissue2022.art13
Rahmawati, R., Muflihunna, A., & Sarif, L. M. (2016). Analisis aktivitas antioksidan produk sirup buah Mengkudu (Morinda citrifolia L.) dengan metode DPPH. *Jurnal Fitofarmaka Indonesia*, *2*(2), 97–101. https://doi.org/10.33096/jffi.v2i2.177
Ramachandran, R., Babji, A. S., & Wong, I. P. (2018). Effect of heating on antioxidant activity on edible bird nest. *International Seminar on Tropical Animal Production (ISTAP)*
Rispriandari, A. A., Sarmoko, S., Setyono, J., & Wisesa, S. (2024). Inhibition breast carcinogenesis via PI3K/AKT pathway using bioactive compounds of Strychnine tree (Strychnos nux-vomica): in silico study. *Pharmaciana*, *14*(2), 133. https://doi.org/10.12928/pharmaciana.v14i2.28242
Rohmah, S. D. (2019). Formulasi krim sarang Burung Walet Putih (Aerodramus Fuciphagus) dengan basis Tipe A/M sebagai pencerah kulit wajah. *Jurnal Mahasiswa Farmasi Fakultas Kedokteran Universitas Tanjungpura*, *1*(1)
Sabandar, A. H., Kasmiyati, S., & Djohan, D. (2023). The determination of antioxidant and lead content of hemiparasite Dendrophthoe vitellina (F. Muell) Tiegh on Nutmeg. *Pharmaciana*, *13*(3), 338. https://doi.org/10.12928/pharmaciana.v13i3.26780
Silvia, D. (2018). Pengumpulan data base sumber antioksidan alami alternatif berbasis pangan Lokal di Indonesia. *Surya Octagon Interdisciplinary Journal of Technology*, *1*(2), 181–198. https://doi.org/10.31219/osf.io/7n38k
Thakre, A. D. (2017). Formulation and development of de pigment serum incorporating fruits extract. *International Journal of Innovative Science and Research Technology*, *2*(12), 330–382
Widyowati, H., Ulfah, M., & Sumantri, S. (2014). Uji aktivitas antioksidan ekstrak etanolik herba Alfalfa (Medicago sativa L.) dengan metode DPPH (1,1-Diphenyl-2 Picrylhidrazyl). *Jurnal Ilmu Farmasi Dan Farmasi Klinik*, *11*(1), 25–33. https://doi.org/10.31942/jiffk.v11i1.1285
Wijayanti, C. ., & Faizatun. (2011). *Formulasi sediaan serum gel vitamin C dan vitamin E menggunakan HPMC (Hydroxy Propyl Methyl Cellulosa) sebagai gelling agent*. Jakarta: Universitas Pancasila
Zahruddin, A., & Damayanti, D. (2018). Penuaan kulit: patofisiologi dan manifestasi klinis. *Berkala Ilmu Kesehatan Kulit Dan Kelamin*, *30*(3), 208–215. https://doi.org/10.20473/bikk.V30.3.2018.208-215

Pharmaciana
Vol.14, No.3, Nov 2024, Page. 346–355
ISSN: 2088 4559; e-ISSN: 2477 0256
DOI: 10.12928/pharmaciana.v14i3.28208

Use of bitter melon seed oil (*Momordica charantia*) to improve the photoprotective effect of sunscreen formulations

Lina Winarti*, Ema Prastiwi Refayani
Department of Pharmaceutical, Faculty of Pharmacy, University of Jember
Jl.Kalimantan I/2 Kampus Tegal Boto Jember Indonesia

Submitted: 13-01-2024 ***Reviewed: 12-07-2024*** ***Accepted: 18-11-2024***

ABSTRACT

Bitter melon seed oil (BMSO) was identified as having the potential as an anti-UV radiation agent due to alpha-oleo stearic acid, flavonoids, tannins, polyphenols, and phytosterols, which have the potential as antioxidants. Antioxidants are the main protection for the skin from the dangers of solar radiation, making BMSO a good quality if developed in sunscreen cream. This research aims to determine the effect of adding variations in the concentration of BMSO on the physical characteristics and in vitro photoprotective effectiveness of oxybenzone and octyl methoxycinnamate cream. Sunscreen creams are made with each BMSO concentration of 0%, 6%, 8%, 10%, and 12%. The result shows that the greater the concentration of BMSO added, the lower the viscosity and pH values, the %TP (percentage of transmission pigmentation) and %TE (percentage of transmission erythema), while the spreadability and SPF (sun protection factor) values of the cream increase. The best formula contains the highest concentration of BMSO (12%). The characteristics of the best formula are a slightly yellowish, soft cream and a slight smell typical of bitter melon. The spreadability value of the best formula cream is 6.6 ± 0.1 cm, pH is 6.57 ± 0.01, and viscosity is 88.3 ± 4.1 dPa.s, SPF value is 24.27 ± 0.28, %TE is 0.931 ±0.084, and %TP is 0.981±0.0001. These results show that BMSO has the potential to be an active ingredient in sunscreen to reduce the negative effects of using synthetic sunscreen, such as allergenic and irritant.

Keywords: BMSO, oxybenzone, octyl metoxycinamates, sunscreen

Corresponding author:
Lina Winarti
Department of Pharmaceutical, Faculty of Pharmacy, University of Jember
Jl.Kalimantan I/2 Kampus Tegal Boto Jember Indonesia
Email:lina.winarti@unej.ac.id

INTRODUCTION

The skin possesses a natural defense system that guards against radiation from sunlight. It thickens the stratum corneum and generates the hormone melanin as a protective response to radiation exposure (Brenner & Hearing, 2008). Sunlight, at appropriate exposure levels, contributes to vitamin D synthesis by converting 7-dehydrocholesterol into cholecalciferol (vitamin D3), which aids in calcium absorption (Wacker & Holick, 2013). However, if exposure to solar radiation exceeds the skin's natural protection, it can lead to various health issues, including erythema, inflammation, premature aging, and cancer (Amaro-Ortiz et al., 2014).

Alongside its inherent defenses, the skin requires additional protection, such as sunscreen. *Sunscreen* is a cosmetic formulation designed primarily to absorb radiation from direct sunlight on the skin (Chao et al., 2010). Typically formulated as a cream, sunscreen allows for easy application, does not leave a sticky residue, acts directly on local tissues, and can be easily washed off with water compared to other formulations like gels or ointments (Sharon et al., 2013).

Two types of UV protection exist UV-A (ultraviolet-A) and UV-B (ultraviolet-B) absorbers (Holick, 2016). Oxybenzone serves as a filter for both UV-A and UV-B rays. However, oxybenzone has been associated with allergies and endocrine disruptors associated with Hirschsprung's disease and causes various toxic effects in coral and fish (DiNardo & Downs, 2018). Octylmethoxycinnamate functions as a UV-B absorber but does not protect against UV-A rays. Therefore, combining oxybenzone with octylmethoxycinnamate in the formulation can enhance sunscreen effectiveness (Tamara et al., 2019).

Recent findings have led to banning oxybenzone (BP-3) and octylmethoxycinnamate in Key West and Hawaii due to their harmful effects on marine life. However, their implications for human health still require thorough examination (Suh et al., 2020). Despite this, oxybenzone remains in popular sunscreen brands to achieve a higher SPF. Consequently, this research aims to utilize low concentrations of oxybenzone, octylmethoxycinnamate, and BMSO to improve SPF. BMSO, along with various vegetable oils such as coconut oil, sunflower oil, and avocado oil, typically has an SPF below 10 (Ranjithkumar et al., 2016), necessitating the combination with other chemical or physical agents to enhance SPF.

Oils have inherent properties that protect the skin from the adverse effects of sunlight (Montenegro & Santagati, 2019). BMSO contains conjugated α-linolenic acid and bioactive substances like tocopherols and polyphenolic compounds. Conjugated α-linolenic acid offers numerous potential benefits as an antioxidant, anti-inflammatory, anti-atherosclerotic, and antitumor. It can reduce serum lipid levels in vitro and in vivo (Yoshime et al., 2016). Both conjugated α-linolenic acid and bioactive compounds such as tocopherols and phenolic shielding prevent the development of free radicals induced by solar radiation (Rajaram, 2014). The inclusion of BMSO allows for a decrease in the concentration of oxybenzone needed, minimizing its adverse effects without compromising the photoprotective efficiency of the final formulation, as BMSO synergistically interacts with oxybenzone and octylmethoxycinnamate to absorb UV rays.

The application of BMSO in sunscreen cosmetic formulations has yet to be previously researched. Given this context, the researcher will assess the sunscreen cream formulations that combine BMSO with oxybenzone and octylmethoxycinnamate. The research aims to determine the effect of BMSO addition on sunscreen's physical characteristics and in vitro photoprotective effectiveness.The sunscreen cream will be tested for its effectiveness in vitro by calculating the SPF (Sun Protection Factor), %TE, and %TP values, as well as testing the physical characteristics of the sunscreen cream, which is composed of organoleptic tests, pH, viscosity, spreadability, and homogeneity.

MATERIALS AND METHOD

Materials

BMSO comes from Ethereal Ingredients Private Limite, India, oxybenzone (cosmeutical grade, Thornhill), octylmethoxycinnamate (cosmeutical grade, MFCI), propylene glycol, edetate sodium,

triethanolamine, petrolatum, cetyl alcohol, stearic acid, glyceryl monostearate, and nipagin are technical grade.

Methods

Formulation

In this research, five formulations of sunscreen cream were prepared. Each formula is accompanied by the active ingredients of BMSO, oxybenzone, and octylmethoxycinnamate with a ratio of F1 (0:2:5), F2 (6:2:5), F3 (8:2:5), F4 (10:2: 5), and F5 (12:2:5) (Muliyawan & Suriana, 2013).

Sunscreen preparation

The ingredients for cream formulations are categorized into two sections: the water phase and the oil phase. The water phase includes edetate sodium, propylene glycol, nipagin, triethanolamine, and distilled water, while the oil phase contains petrolatum, glyceryl monostearate, stearic acid, cetyl alcohol, and oxybenzone. The oil phase is heated in a water bath to a temperature between 70-75˚C, after which oxybenzone is gradually incorporated until a uniform mixture is achieved. Next, the oil phase is transferred into a heated mortar and combined with the water phase while stirring continuously until a creamy texture is formed. Depending on the variants indicated in Table 1, octyl methoxycinnamate and BMSO oil are then added.

Table 1. BMSO formulation

Materials	Function	Concentration (%)				
		F1	F2	F3	F4	F5
BMSO	Chemical absorber	-	6.0	8.0	10.0	12.0
Oxybenzone	Chemical absorber	2.0	2.0	2.0	2.0	2.0
Octy lmetoxynamate	Chemical absorber	5.0	5.0	5.0	5.0	5.0
Sodium edetate	Chelating agent	0.05	0.05	0.05	0.05	0.05
Triethanolamine	Emulsifying agent	1.0	1.0	1.0	1.0	1.0
Stearic acid	Emulsifying agent	3.0	3.0	3.0	3.0	3.0
Glyceril monostearate	Emulsifying agent	3.0	3.0	3.0	3.0	3.0
Petrolatum	Emollient agent	5.0	5.0	5.0	5.0	5.0
Cetyl alcohol	Stiffening agent	3.0	3.0	3.0	3.0	3.0
Propylene glycol	Co-solvent	7.0	7.0	7.0	7.0	7.0
Methylparaben	Preservative agent	0.1	0.1	0.1	0.1	0.1
Distilled water	Vehicle	ad 100	ad 100	ad 100	ad 100	ad 100

Physicochemical characteristic evaluation

Organoleptic test

The organoleptic test for the type of sunscreen cream preparation was carried out visually by observing the color of, the texture, and the aroma of the cream.

Spreadabilty test

One gram of cream place into a round glass scale. Then on the top side of the material is placed a pair of round glass and added a load of 5 grams every 1 minute until constant diameter. Spreadability is measured based on the diameter of the preparation (Sabale et al., 2011).

Homogenity test

Homogeneity test was carried out by smeared the cream on the object glass and then observed for the presence or absence of coarse grains (Ardhany & Novaryatiin, 2019).

Viscosity test

This viscosity test was carried out by placing 100 grams of cream in a beaker glass, then installing rotor number 2. The test was carried out with a Viscotester VT-04 (Simões et al., 2018).

pH

The pH meter was dipped into the test cream. The number seen on the screen is stable or stagnant, recorded as the pH of the cream (Mukhlishah & Ningrum, 2019).

In vitro photoprotective effectiveness

Determination of SPF value

A 0.5-gram portion of cream was dissolved in isopropanol within a 25 mL volumetric flask to achieve a concentration of 20,000 ppm. The resulting sample solution was then diluted to a concentration of 10,000 ppm. Subsequently, the absorbance of the sample was recorded using a UV-Vis spectrophotometer over a wavelength range of 290-400 nm in 5 nm intervals (Fonseca & Nobre, 2013). The area under the curve (AUC) was computed using the formula provided in equation (1).

$$AUC = \frac{Aa + Ab}{2} \times dPa - b \quad \text{.....(1)}$$

where Aa: λa absorbance (nm); Ab: λa absorbance (nm); dPa – b: a and b wavelenght difference.

The SPF value is calculated by formula in the equation (2) (Mulyani et al., 2015).

$$\log SPF = \frac{AUC}{\lambda_n - \lambda_1} \quad \text{.....(2)}$$

where λ_n: higher absorbance; λ_1: smaller absorbance.

Determination of erythema transmission value (%TE)

Cream of 0.5 grams dissolved with isopropanol in a 25 mL volumetric flask to obtain a concentration of 20,000 ppm. Then the sample solution was diluted to a concentration of 10,000 ppm. The absorbance of the test solution was measured using UV-vis spectrophotometry at a wavelength of 292.5 – 337.5 nm, with an observation interval of 5 nm (Abdassah et al., 2015). The erytema transmision value calculated by formula in the equation (3).

$$\%TE = \frac{\sum T \times Fe}{\sum Fe} \quad \text{.....(3)}$$

where T: transmision percentage; Fe: erytema effectivity constant.
The categories of erythema transmission capability of sunscreen cream preparations can be seen in Table 2.

Determination of pigmentation transmission value (%TP)

A 0.5-gram sample was dissolved in isopropanol within a 25 mL volumetric flask to achieve a concentration of 20,000 ppm. Subsequently, the solution was diluted to reach a concentration of 10,000 ppm. The absorbance of the test solution was measured using UV-vis spectrophotometry at wavelengths ranging from 322.5 to 372.5 nm, with measurements taken at 5 nm intervals, allowing for the absorption values to be obtained and calculated using the formula in equation (4) (Abdassah et al., 2015).

$$\%TP = \frac{\sum T \times Fp}{Fp} \quad \text{.....(4)}$$

where T: transmision percentage; Fp: pigmentation effectivity constant.
The categories of pigmentation transmittance for sunscreen cream preparations can be seen in Table 2.

Table 2. %TP and %TE value categories

%TE	%TP	Categori
< 1	< 1 – 2	Total block
1 – 6	3 – 40	Ultra protection
6 – 12	45 – 86	Suntan
12 – 18		Fast tanning

Data Analysis

Spreadability, pH, viscosity, SPF value, percentage of erythema transmission, and percentage transmission of pigmentation in the cream were tested for normality and homogeneity of the data. If it has a p-value > 0.05, data analysis is continued with One-Way ANOVA and Least Significantly Different (LSD) if ANOVA difference is significant. The results are said to be significantly different if they have a p-value <0.05.

RESULT AND DISCUSSION

Organoleptic test

Organoleptic test on sunscreen cream aims to determine the physical characteristics of the cream by visual testing of color, texture and aroma. Cream preparations are expected to have a white color, soft texture, and odorless aroma (Direktorat Jenderal Kefarmasian dan Alat Kesehatan, 2020) related to the aesthetics of the preparation. The results of organoleptic observations it is known that the results of sunscreen cream preparations on F1, F2, and F3 have a white color. In contrast to F4 and F5, it shows a slightly yellowish white color (Figure 1). This was due to the addition of high concentrations of BMSO hence the color of the cream became slightly yellowish white. In addition, the formula that is given BMSO also has a distinctive aroma.

Cream is a mixture of oil and water, and a dispersing agent can disperse the oil called an emulsifier. The highest BMSO concentration was obtained through preliminary studies. In this study, the highest oil concentration that could technically produce a stable emulsion was evaluated by centrifugation at 3500 rpm for 30 minutes. If the cream breaks or the oil phase separates, it indicates that the BMSO added was too high. Therefore, the highest BMSO concentration used in this cream formulation does not produce an oily cream because it can be accommodated by the water phase with the help of an emulsifier.

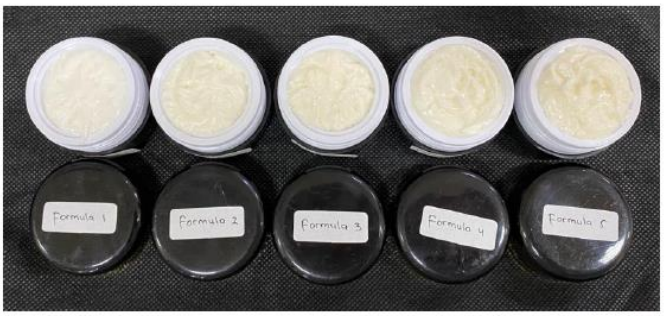

Figure 1. Cream formula appearance

Spreadability test

The diameter of each formula was 4.5 ± 0.1; 4.7 ± 0.1; 5.6 ± 0.1; 6.0 ± 0.1; and 6.6 ± 0.1 cm. Spreadability is said to be good if the results are 5-7 cm in diameter. Based on the tests, each formula meets the requirements. The addition of BMSO reducing the viscosity of the oxybenzone and octylmethoxycinnamate sunscreen cream, so that the lower the viscosity value, the thinner the cream, making it easier to spread when used ($p < 0.05$) (Widyaningrum et al., 2012).

Homogeneity evaluation

The homogeneity assessment is designed to verify that the ingredients in the sunscreen cream are distributed evenly without any lumps or coarse particles present. A homogeneous cream preparation signifies that all components are thoroughly blended. Cream formulations must be homogeneous to ensure comfort and prevent irritation during skin application. The findings from the homogeneity assessment indicated that all samples of sunscreen cream were homogeneous.

Viscosity evaluation

The viscosity assessment was conducted to gauge the thickness of the sunscreen cream. The thickness influences the cream's ability to spread uniformly when applied to the skin. The anticipated viscosity range is 50-150 dPa.s (Lachman et al., 1987). For formulations F1 to F5, the recorded viscosity values were 117.6 ± 2.5; 113.3 ± 1.5; 105.6 ± 5.1; 97.3 ± 2.5; and 88.3 ± 4.1 dPa.s, respectively. The observed reduction in viscosity of the preparations was attributed to the increased concentration of BMSO ($p < 0.05$) based on the LSD test. Consequently, while the SPF is expected to rise, the percentages of TP and TE are projected to decline, as the formulation with the highest BMSO concentration offers improved UV blocking. These outcomes align with the spreadability test results.

Acidity testing

The pH level of the sunscreen should correspond to that of the skin. Sunscreen with a highly acidic formulation can irritate the skin. Conversely, a pH level that is too alkaline can lead to dryness and flakiness of the skin (Ali & Yosipovitch, 2013). As the concentration of BMSO increases, the pH of the cream decreases due to an acidic pH (pH=4.0) of the BMSO. The pH values of the creams were respectively 6.96 ± 0.01, 6.84 ± 0.01, 6.75 ± 0.01, 6.66 ± 0.01, and 6.57 ± 0.01. All formulations met the quality standards for effective sunscreen cream, albeit with a p-value <0.05 in the LSD test.

In vitro effetiveness evaluation

In vitro effectiveness, assessment BMSO is incorporated into the sunscreen cream due to its content of antioxidants, such as conjugated α-linolenic acid, and bioactive components like tocopherols and phenolic compounds that help protect against and mitigate the generation of free radicals induced by light exposure (Yoshime et al., 2016). A limitation of using BMSO alone is its inability to achieve a high SPF rating. Moreover, combining BMSO with oxybenzone and octylmethoxycinnamate aims to minimize the adverse effects associated with these ingredients, which can lead to skin irritation and other toxic reactions (Serpone et al., 2002).

SPF value

Based on the SPF value, sunscreen creams are grouped into several categories, including Minimum SPF (2-3) can result in tanning, Moderate SPF (4-6) can cause tanning, Extra SPF (6-8) results in limited tanning, Maximum SPF (8-15) tanning does not occur, SPF Ultra (> 15) does not result in tanning (Osterwalder & Herzog, 2010). The increase in the SPF value indicated that the addition of BMSO is effective to give protection from tanning. The higher the SPF value, the better the effectiveness of the sunscreen preparation and the greater the absorption of UV radiation. Between formulas showed significant differences in LSD test due to variations in the concentration of BMSO ($p < 0.05$).

Table 3. *In vitro* effectiveness of BMSO with oxybenzone and octylmethoxycinnamate

Formula	SPF	SPF Categories	% TE	% TP	%TE and %TP Categories
F1	5.66 ± 0.24	Extra	0.990 ± 0.0002	0.991 ± 0.0001	Total block
F2	9.86 ± 0.36	Maximal	0.88 ± 0.0001	0.988 ± 0.0007	Total block
F3	11.49 ± 0.57	Maximal	0.986 ± 0.0001	0.987 ± 0.0005	Total block
F4	16.14 ± 0.28	Ultra	0.984 ± 0.0002	0.984 ± 0.0001	Total block
F5	24.27 ± 0.28	Ultra	0.931 ± 0.084	0.981 ± 0.0001	Total block

Various vegetable oils have been researched for their ability to absorb UV light. Thus, it is suggested to utilize vegetable oil to decrease the amounts of organic UV filters (octyl-methoxycinnamate, butyl methoxydibenzoylmethane, and bemotrizinol) found in sunscreen formulations. Studies have shown that pomegranate oil (1% w/w) and shea oil (1% w/w) achieve a higher SPF than formulations containing organic UV filter components. The physical properties of the cream remained consistent, as Montenegro and Santagati (2019) reported. Findings from the studies on pomegranate and shea oil support the idea that incorporating bitter melon seed oil into sunscreen formulations could be a practical approach for creating products with reduced levels of organic UV filters.

Erythema transmission value (%TE)

According to Table 3, all tested formulas protect total erythema, indicating that the cream serves as a sunblock against UV rays and can be understood as effectively preventing skin redness, as demonstrated by %TE values of less than 1%. A lower %TE value signifies superior effectiveness as a sunscreen in shielding the skin from erythema (Ahmad, 2015). The sunscreen formula with the highest concentration of bitter melon seed oil (BMSO) recorded the lowest %TE value, marking it as the most effective in protecting the skin from erythema. Significant differences were observed among the formulas in the LSD test, attributed to varying concentrations of BMSO ($p < 0.05$). The formula with the highest BMSO concentration contained elevated levels of conjugated α-linolenic acid and bioactive compounds such as tocopherols and phenolic compounds, which aid in guarding the skin from solar radiation.

Pigmentation transmision value (%TP)

According to Table 3, all formulas exhibit a pigmentation transmission percentage of less than 1-2%, all falling within the same total block category. A lower percentage of transmission for pigmentation implies a superior capacity of the sunscreen cream to inhibit pigmentation resulting from UV radiation (Ahmad, 2015). The reduction in pigmentation attributed to BMSO is linked to alpha-oleo stearic acid, which functions as an anti-UV agent by absorbing UV rays, thus preventing their penetration into the skin. There were significant differences among the formulas in the LSD test, attributable to the varying concentrations of BMSO ($p < 0.05$).

BMSO is composed of lipids, polyunsaturated fatty acids (PUFAs), phytosterols, and tocopherols (Aruna et al., 2016; Fernandes et al., 2015; Jing et al., 2012). The composition of BMSO includes 30%-60% of the α-allosteric acid (Aruna et al., 2016; Khoddami & Roberts, 2015; Saha et al., 2012). It also holds significant amounts of the conjugated fatty acid α-eleostearic acid, a positional and geometric isomer of α-linolenic acid. Conjugated α-linolenic acid represents a positional and geometric isomer of octadecatrienoic fatty acid with three conjugated double bonds (Melo et al., 2014). The UV absorbance of compounds with extended conjugated double bonds can be estimated using Woodward Fieser's rule. Shifts in the wavelength may occur in a bathochromic or hypochromic manner, influenced by the extent of conjugation, the presence of donating groups, and electron-withdrawing groups (Gauglitz & Vo-Dinh, 2003). Based on the Woodward–Fieser rule and the

Structure-Activity Relationship, the conjugated fatty acids in BMSO triglycerides are also noted for their UV absorption capabilities (Wagemaker et al., 2011), which can be advantageous in sunscreen formulations.

Additionally, α-linolenic acids offer several potential health benefits, such as antioxidant and anti-inflammatory properties. Furthermore, along with a high concentration of conjugated α-linolenic acids, BMSO contains tocopherols and polyphenolic compounds (Anjum et al., 2013; Nyam et al., 2009). Tocopherol aids in photoprotection by enhancing glutathione production and mitigating lipid peroxidation, as well as reducing levels of reactive oxygen species (ROS) and malondialdehyde (MDA) (Delinasios et al., 2018; Wu et al., 2014). Consequently, BMSO plays a vital role in sunscreen formulations by synergistically absorbing UV light, providing antioxidants, and exhibiting anti-aging and anti-inflammatory effects.

The UV absorption capability of BMSO can enhance the SPF value. Simultaneously, its antioxidant properties may help neutralize free radicals that lead to redness or erythema (Sutriningsih & Astuti, 2017), limit melanin production, and reduce the occurrence of skin pigmentation following UV exposure (Suhaenah et al., 2019). Therefore, an increase in the amount of BMSO within oxybenzone and octyl methoxycinnamate cream will decrease the % TP and % TE.

CONCLUSION

It is found that the greater the concentration of BMSO added to the formula, the greater the in vitro SPF value, while the % TE and % TP is getting smaller which indicate BMSO will give an addition protection to the skin by absorbed the radiation to be not transmitted into the skin. It will avoid the negative effect of UV radiation such as pigmentation, erythema, skin aging cause by free radicals, and reduce the content of organic sunscreen.

ACKNOWLEDGEMENT

The authors may acknowledge Universitas Jember for the research facility.

REFERENCES

Abdassah, M., Aryani, R., Surachman, E., & Muchtaridi, M. (2015). In-vitro assessment of effectiveness and photostability avobenzone in cream formulations by combination ethyl ascorbic acid and alpha tocopherol acetate. *Journal of Applied Pharmaceutical Science*, 070–074. https://doi.org/10.7324/JAPS.2015.50611

Ahmad, I. (2015). Penentuan nilai persentase eritema dan pigmentasi ekstrak herba Suruhan (Peperomia pellucida L.) secara in vitro. *Jurnal Sains Dan Kesehatan*, *1*(2), 90–95. https://doi.org/10.25026/jsk.v1i2.22

Ali, S., & Yosipovitch, G. (2013). Skin pH: from basic science to basic skin care. *Acta Dermato Venereologica*, *93*(3), 261–267. https://doi.org/10.2340/00015555-1531

Amaro-Ortiz, A., Yan, B., & D'Orazio, J. (2014). Ultraviolet radiation, aging and the skin: prevention of damage by topical cAMP manipulation. *Molecules*, *19*(5), 6202–6219. https://doi.org/10.3390/molecules19056202

Anjum, F., Shahid, M., Bukhari, S., & Anwar, S. (2013). Study of quality characteristics and efficacy of extraction solvent/technique on the antioxidant activity of bitter gourd seed. *Food Processes Technology*, *4*(2), 1–9

Ardhany, S. D., & Novaryatiin, S. (2019). Antibacterial activity of ethanolic extract Bawang Dayak (Eleutherine Bulbosa (Mill.) Urb) in cream against propionibacterium acnes. *International Journal of Applied Pharmaceutics*, *11*(5), 1–4. https://doi.org/10.22159/ijap.2019.v11s5.T0020

Aruna, P., Venkataramanamma, D., Singh, A. K., & Singh, R. P. (2016). Health benefits of punicic acid: a review. *Comprehensive Reviews in Food Science and Food Safety*, *15*(1), 16–27. https://doi.org/10.1111/1541-4337.12171

Brenner, M., & Hearing, V. J. (2008). The protective role of melanin against UV damage in human skin. *Photochemistry and Photobiology*, *84*(3), 539–549. https://doi.org/10.1111/j.1751-1097.2007.00226.x

Chao, Y., Xue-min, W., Yi-mei, T., Li-jie, Y., Yin-fen, L., & Pei-lan, W. (2010). Effects of sunscreen on human skin's ultraviolet radiation tolerance. *Journal of Cosmetic Dermatology*, *9*(4), 297–301. https://doi.org/10.1111/j.1473-2165.2010.00525.x

Delinasios, G. J., Karbaschi, M., Cooke, M. S., & Young, A. R. (2018). Vitamin E inhibits the UVAI induction of "light" and "dark" cyclobutane pyrimidine dimers, and oxidatively generated DNA damage, in keratinocytes. *Scientific Reports*, *8*(1), 423. https://doi.org/10.1038/s41598-017-18924-4

DiNardo, J. C., & Downs, C. A. (2018). Dermatological and environmental toxicological impact of the sunscreen ingredient oxybenzone/benzophenone-3. *Journal of Cosmetic Dermatology*, *17*(1), 15–19. https://doi.org/10.1111/jocd.12449

Direktorat Jenderal Kefarmasian dan Alat Kesehatan. (2020). *Farmakope Indonesia edisi VI*. Jakarta: Kementrian Kesehatan Republik Indonesia

Fernandes, L., Pereira, J. A., Lopéz-Cortés, I., Salazar, D. M., Ramalhosa, E., & Casal, S. (2015). Fatty acid, vitamin E and sterols composition of seed oils from nine different pomegranate (Punica granatum L.) cultivars grown in Spain. *Journal of Food Composition and Analysis*, *39*, 13–22. https://doi.org/10.1016/j.jfca.2014.11.006

Fonseca, A., & Nobre, R. (2013). Determination of sun protection factor by UV-Vis spectrophotometry. *Health Care Current Reviews*, *1*(1), 1–4. https://doi.org/10.4172/2375-4273.1000108

Gauglitz, G., & Vo-Dinh, T. (Eds.). (2003). *Martin Hof in Handbook of Spectroscopy*. Wiley-VCH Verlag GmbH & Co. KGaA

Holick, M. F. (2016). Biological effects of sunlight, ultraviolet radiation, visible light, infrared radiation and vitamin D for health. *Anticancer Research*, *36*(3), 1345–1356

Jing, P., Ye, T., Shi, H., Sheng, Y., Slavin, M., Gao, B., Liu, L., & Yu, L. (Lucy). (2012). Antioxidant properties and phytochemical composition of China-grown pomegranate seeds. *Food Chemistry*, *132*(3), 1457–1464. https://doi.org/10.1016/j.foodchem.2011.12.002

Khoddami, A., & Roberts, T. H. (2015). Pomegranate oil as a valuable pharmaceutical and nutraceutical. *Lipid Technology*, *27*(2), 40–42. https://doi.org/10.1002/lite.201500002

Lachman, L., Lieberman, H. A., & Kanig, J. L. (1987). *The theory and practice of industrial pharmacy*. Philadephia: Lippincott Williams & Wilkins

Melo, I. L. P. de, Carvalho, E. B. T. de, & Mancini-Filho, J. (2014). Pomegranate seed oil (Punica granatum L.): a source of punicic acid (conjugated α-linolenic acid). *Journal Human Nutrition & Food Science*, *2*(1), 1–11. https://doi.org/10.47739/2333-6706/1024

Montenegro, L., & Santagati, L. M. (2019). Use of vegetable oils to improve the sun protection factor of sunscreen formulations. *Cosmetics*, *6*(2), 25. https://doi.org/10.3390/cosmetics6020025

Mukhlishah, N. R. I., & Ningrum, D. M. (2019). Uji sifat fisik dan iritasi ekstrak etanol buah Rukem (Flacourtia rukam) dalam sediaan sunscreen basis gel. *Pharmaceutical & Traditional Medicine*, *3*(2), 56–61

Muliyawan, D., & Suriana, N. (2013). *A-Z tentang kosmetik*. Jakarta: Elex Media Komputindo

Nyam, K. L., Tan, C. P., Lai, O. M., Long, K., & Che Man, Y. B. (2009). Physicochemical properties and bioactive compounds of selected seed oils. *LWT - Food Science and Technology*, *42*(8), 1396–1403. https://doi.org/10.1016/j.lwt.2009.03.006

Osterwalder, U., & Herzog, B. (2010). The long way towards the ideal sunscreen—where we stand and what still needs to be done. *Photochemical & Photobiological Sciences*, *9*(4), 470–481. https://doi.org/10.1039/b9pp00178f

Rajaram, S. (2014). Health benefits of plant-derived α-linolenic acid. *The American Journal of Clinical Nutrition*, *100*, 443S-448S. https://doi.org/10.3945/ajcn.113.071514

Ranjithkumar, J., Sameesh, A., & Ramakrishnan, K., H. (2016). Sun screen efficacy of Punica granatum (Pomegranate) and Citrullus colocynthis (Indrayani) seed oils. *International Journal of Advanced Research in Biological Sciences (IJARBS)*, *3*(10), 198–206.

https://doi.org/10.22192/ijarbs.2016.03.10.027
Sabale, V., Sabale, P., & Kunjwani, H. (2011). Formulation and in vitro evaluation of the topical antiageing preparation of the fruit of Benincasa hispida. *Journal of Ayurveda and Integrative Medicine*, *2*(3), 124. https://doi.org/10.4103/0975-9476.85550
Saha, S. S., Patra, M., & Ghosh, M. (2012). In vitro antioxidant study of vegetable oils containing conjugated linolenic acid isomers. *LWT - Food Science and Technology*, *46*(1), 10–15. https://doi.org/10.1016/j.lwt.2011.11.008
Serpone, N., Salinaro, A., Emeline, A. V., Horikoshi, S., Hidaka, H., & Zhao, J. (2002). An in vitro systematic spectroscopic examination of the photostabilities of a random set of commercial sunscreen lotions and their chemical UVB/UVA active agents. *Photochemical & Photobiological Sciences*, *1*(12), 970–981. https://doi.org/10.1039/b206338g
Sharon, N., Anam, S., & Yuliet. (2013). Formulasi krim antioksidan ekstrak etanol Bawang Hutan (Eleutherine palmifolia L. Merr.). *Online Jurnal of Natural Science*, *2*(3), 111–122
Simões, A., Veiga, F., Vitorino, C., & Figueiras, A. (2018). A tutorial for developing a topical cream formulation based on the quality by design approach. *Journal of Pharmaceutical Sciences*, *107*(10), 2653–2662. https://doi.org/10.1016/j.xphs.2018.06.010
Suh, S., Pham, C., Smith, J., & Mesinkovska, N. A. (2020). The banned sunscreen ingredients and their impact on human health: a systematic review. *International Journal of Dermatology*, *59*(9), 1033–1042. https://doi.org/10.1111/ijd.14824
Suhaenah, A., Widiastuti, H., & Arafat, M. (2019). Potensi ekstrak etanol biji Alpukat (Persea americana Mill.) sebagai tabir sSurya. *Ad-Dawaa' Journal of Pharmaceutical Sciences*, *2*(2). https://doi.org/10.24252/djps.v2i2.11560
Sutriningsih, & Astuti, I. W. (2017). Uji antioksidan dan formulasi sediaan masker peel -off dari ekstrak biji alpukat (Persea americana Mill.) dengan perbedaan konsentrasi pva (polivinil alkohol). *Indonesia Natural Research Pharmaceutichal Journal*, *1*(9), 67–75
Tamara, N., Angkasa, C., Ginting, C. N., Chiuman, L., & Lister, I. N. E. (2019). Determination sunscreen potential based on sunflower seed oil (Helianthus annuus) in cream preparation with combination of oxybenzone and octyl methoxycinnamate by in vitro method. *American Academic Scientific Research Journal for Engineering, Technology, and Sciences*, *60*(1), 33–39
Wacker, M., & Holick, M. F. (2013). Sunlight and Vitamin D. *Dermato-Endocrinology*, *5*(1), 51–108. https://doi.org/10.4161/derm.24494
Wagemaker, T. A. L., Carvalho, C. R. L., Maia, N. B., Baggio, S. R., & Guerreiro Filho, O. (2011). Sun protection factor, content and composition of lipid fraction of green coffee beans. *Industrial Crops and Products*, *33*(2), 469–473. https://doi.org/10.1016/j.indcrop.2010.10.026
Widyaningrum, N., Murrukmihadi, M., & Ekawati, S. K. (2012). Pengaruh konsentrasi ekstrak etanolik daun Teh Hijau (Camellia sinesis L.) dalam sediaan krim terhadap sifat fisik dan aktivitas antibakteri. *Sains Medika : Jurnal Kedokteran Dan Kesehatan*, *4*(2), 147. https://doi.org/10.30659/sainsmed.v4i2.371
Wu, C.-M., Cheng, Y.-L., Dai, Y.-H., Chen, M.-F., & Wang, C.-C. (2014). α-Tocopherol protects keratinocytes against ultraviolet A irradiation by suppressing glutathione depletion, lipid peroxidation and reactive oxygen species generation. *Biomedical Reports*, *2*(3), 419–423. https://doi.org/10.3892/br.2014.236
Yoshime, L. T., de Melo, I. L. P., Sattler, J. A. G., de Carvalho, E. B. T., & Mancini-Filho, J. (2016). Bitter gourd (Momordica charantia L.) seed oil as a naturally rich source of bioactive compounds for nutraceutical purposes. *Nutrire*, *41*(1), 12. https://doi.org/10.1186/s41110-016-0013-y

Pharmaciana
Vol.14, No.3, Nov 2024, Page. 356-369
ISSN: 2088 4559; e-ISSN: 2477 0256
DOI: 10.12928/pharmaciana.v14i3.28892

Optimization of self-nanoemulsifying drug delivery system of rifampicin for nebulization using cinnamon oil as oil phase

I Komang Aan Adi Ricardo, Dewa Ayu Arimurni*
Sekolah Tinggi Farmasi Mahaganesha
Jl. Tukad Barito Timur no. 57, Renon, Denpasar-Bali, Indonesia

Submitted: 28-03-2024 ***Reviewed: 13-04-2024*** ***Accepted: 02-08-2024***

ABSTRACT

Lung delivery can overcome the problems related to the effectiveness of tuberculosis treatment by increasing the drug concentration at the target site. Rifampicin as the first-line antibiotic for tuberculosis has low water solubility and is unstable in gastric which hinders its effectiveness. Self-nanoemulsifying drug delivery system (SNEDDS) is a strategy known to improve the solubility and stability of such drugs. This study aimed to obtain the optimum formula of rifampicin SNEDDS intended for lung nebulization using essential oil as an oil phase. Several essential oils are known to have effective antibacterial on *Mycobacterium tuberculosis*. However, a high capability to solubilize the drug is required for SNEDDS formulation. Cinnamon oil, tween 80, and transcutol P were chosen as SNEDDS components for optimization using a D-optimal mixture based on the physicochemical characteristics. The optimum formula comprised 12.65% cinnamon oil, 75.00% tween 80, and 12.35% transcutol P which dispersed easily to form a highly transparent emulsion in normal saline under 1 minute. Upon dilution with saline, the optimal SNEDDS can produce a homogenous nanometer droplet (169.2±19.771 nm, PDI of 0.258±0.070) with acceptable pH for lung administration. It also has a viscosity similar to water (0.94±0.01 cP) which allows it to be nebulized easily (aerosol output rate of 0.14±0.02 g/min). Although the diluted SNEDDS has a zeta potential of -2.533±0.268 mV, it was stable for up to 4 hours during the nebulization. These results indicate the potential of cinnamon oil-based rifampicin SNEDDS to be an alternative in the pulmonary delivery of rifampicin via nebulization.

Keywords: SNEDDS, rifampicin, cinnamon oil, nebulizer, D-optimal mixture design

Corresponding author:
Dewa Ayu Arimurni
Sekolah Tinggi Farmasi Mahaganesha
Jl. Tukad Barito Timur no. 57, Renon, Denpasar-Bali, Indonesia
Email: dewaayuarimurni@gmail.com

INTRODUCTION

Tuberculosis is a disease caused by *Mycobacterium tuberculosis* that mainly affects the lungs (Kemenkes RI, 2020). According to the Global Tuberculosis Report 2023, tuberculosis was the world's second-highest cause of death from a single infectious agent in 2022. There were 7.5 million new tuberculosis cases diagnosed and reported, with the total number of deaths reaching 1.30 million cases (WHO, 2023). Tuberculosis is a curable disease but can be fatal if not treated properly. Nowadays, the recommended treatment for pulmonary tuberculosis includes the daily oral administration of four first-line drugs (rifampicin, isoniazid, pyrazinamide, and ethambutol) for two months in the initial phase, followed by rifampicin and isoniazid for four months in the continuation phase (Kemenkes RI, 2020). Nevertheless, the efficacy of these regimens is restricted by several issues, such as constraints of drug dose, undesirable drug effects, and low patient compliance from the lengthy treatment duration that can cause multi-drug-resistant tuberculosis (Shah et al., 2017).

Rifampicin, a semisynthetic derivative of rifamycin, has a bactericidal activity on mycobacteria by inhibiting RNA synthesis (Katzung, 2018). Although rifampicin is a first-line drug for tuberculosis treatment, high oral dosages of rifampicin may be restricted due to the increased risk of systemic toxicities such as hepatic toxicity and gastrointestinal discomforts (Somasundaram et al., 2014). Delivering rifampicin directly to the lungs is one of the promising approaches to improve the effectiveness of anti-tubercular therapy with a smaller dose and to reduce resistance by maximizing drug concentration at the target site (Khadka et al., 2023). The lung provides a vast surface area, which when paired with small particles/droplets from an inhaled aerosol results in fast systemic absorption. The lung has a lesser amount of efflux transporters and lower enzymatic activity than the oral route which increases stability and concentration of the drug in the target site. There have been reports of several types of drug delivery systems for rifampicin inhalation, including microparticle systems (Parikh et al., 2014), micellar systems (Grotz et al., 2019), and solid lipid nanoparticles (SLN) (Maretti et al., 2019). However, more research is required before the clinical application.

According to the AARC (2023), three types of aerosol generators are commonly used for inhaled drug delivery which include nebulizers and pressurized metered-dose inhalers (pMDI) to deliver liquid medications, and dry powder inhalers (DPI) for micronized powder medications. pMDI requires the patient's ability to use this type of inhaler and improper operation reduces the effectiveness of drug therapy. Meanwhile, dry powder formulations require high energy to produce and sometimes face problems such as poor powder flowability and high agglomeration due to high cohesivity between particles leading to poor aerosolization (Shah et al., 2017). Unlike pMDI, a nebulizer does not require active cooperation from the patient, although it takes a long time to administer the drug due to the higher amount/volume of drug that needs to be administered. The drug delivered via nebulization could be in a dispersed form such as suspension or solution that is easier to produce (Wang et al., 2024).

Based on the Biopharmaceutics Classification System (BCS), rifampicin is classified into BCS Class II, which means the drug has high permeability and low solubility (Tsume et al., 2014). One of the strategies that can be used to improve the solubility of rifampicin is to formulate it into a self-nano emulsifying drug delivery system (SNEDDS) dosage form. SNEDDS is a mixture of oil, surfactant, co-surfactant, and drugs that form oil-in-water nanoemulsion under gentle agitation followed by the addition of aqueous media (Divate et al., 2021). In addition to enhancing the solubility of hydrophobic drugs, SNEDDS can also improve the physical and chemical stability of the preparation as it is formulated without water, making it suitable for rifampicin which is unstable to water (Priani et al., 2017). To make it suitable for nebulization, SNEDDS can be diluted/reconstituted using an aqueous vehicle such as water for injection or normal saline to produce nanoemulsion. Nanoemulsion produced by SNEDDS is known to have a superior inhalation and aerosolization performance than other formulations such as nanoparticles, solid lipid nanoparticles, liposomes, and micelles due to its similar viscosity to water (Elbardisy et al., 2022). Therefore, SNEDDS was chosen as a delivery system to deliver rifampicin via nebulization to the lungs. Oil is a key component in SNEDDS. The oil phase contributes to the increased solubility of hydrophobic drugs. Furthermore, several oils are known a high antibacterial effect on *Mycobacterium tuberculosis* such as cinnamon oil, clove oil, and peppermint oil

(Gautam et al., 2023; Sawicki et al., 2018; Vidya Raj et al., 2022). Therefore, selecting oil components that have a high capability to solubilize rifampicin is important. The oil phase also influenced other SNEDDS component's selection. In recent years, the D-optimal mixture design has emerged as a preferred statistical experimental design and modeling method in pharmaceutical formulation studies. This method was applied when the independent variables are the components of a mixture, and the dependent variable is the function of the proportion of each component. D-optimal mixture design allows investigation of the interrelations between the mixture components and response with the least number of experiments (Carneiro et al., 2020). Therefore, components of SNEDDS need to be screened and optimized by a D-optimal mixture design approach to reduce the cost, unpredictability result, and time-consuming process (Sopyan et al., 2022).

Based on the background above, SNEDDS is likely an ideal way to improve the pharmacological effect of rifampicin. This study aimed to obtain the optimum formula of rifampicin SNEDDS targeted to lungs using various concentrations of selected essential oil, surfactant, and co-surfactant by applying the D-optimal mixture design and evaluating its physicochemical characteristics for lung administration.

MATERIALS AND METHODS

Materials

Rifampicin was purchased from PT. Phapros Tbk, cinnamon oil, clove oil, and peppermint oil were purchased from PT. Darjeeling Sembrani Aroma, tween 80 (Brataco), transcutol P (Moellhausen), normal saline (Otsuka), aquadest (Brataco), methanol p.a (Merck).

Methods

Solubility study of rifampicin

Saturation solubility of rifampicin was tested in several oils, including cinnamon oil, clove oil, and peppermint oil. An excess quantity of rifampicin was put into a microtube that each contained 1 mL of different oil. The mixtures were vortexed using a vortex mixer (OHAUS) and sonicated with a water bath sonicator (GT SONIC) for 10 minutes each to ensure appropriate mixing and solubilization of the rifampicin in the oil. Then, mixtures were centrifuged at 6,000 rpm for 10 minutes to separate the undissolved drug using a mini centrifuge (OHAUS Frontier 5306). Aliquots of supernatant were diluted with methanol and rifampicin dissolved in oils was quantified with a UV-visible spectrophotometer (Thermofisher Genesys 10) at 475 nm. Meanwhile, the surfactant (tween 80) and co-surfactant (transcutol P) employed in this study are chosen based on previous research conducted by (Mantena et al., 2015).

GC-MS analysis of selected oil

The volatile components of the selected oil were analyzed by GC-MS (Shimadzu QP2010SE with GC-2020 plus) equipped with InertCap 5MS/Sil column (30 m x 0.32 mm I.D., 0.5 µm) after being diluted to 1% acetone. The operating conditions were helium as the carrier gas, 3 mL/min of flow rate, 1:5 split ratio, 44.5 kPa pressure, and 200℃ ion source temperature. Column temperature was programmed at 50℃ for 5 minutes, increased to 250℃ at a rate of 10℃/min, and maintained for 10 minutes. The mass range was set from 45-500 amu!.

Optimization of rifampicin SNEDDS

Formula optimization was performed by entering the lower and upper limit values of rifampicin SNEDDS composition as shown in Table 1. Lower and upper limit values of the factors were determined by preliminary experiments (data was not shown). Values of other experimental conditions such as the amount of rifampicin, stirring rate, stirring type, and sonication time were kept constant. D-optimal mixture design was then used to analyze the effect of each composition on a physicochemical characteristic of the resulted SNEDDS such as emulsification time, percent transmittance, viscosity, pH, and aerosol output rate in Design Expert® Version 13 software.

Table 1. The lower and upper limit of rifampicin SNEDDS composition

Composition	Lower limit (%)	Upper limit (%)
Cinnamon oil	5	20
Tween 80	75	90
Transcutol P	5	20

Preparation of rifampicin SNEDDS

Oil phase, surfactant, co-surfactant, and drug (rifampicin 100 mg/mL) were mixed with a magnetic stirrer (IKA C-MAG HS 7) at 1,200 rpm for 90 minutes and sonicated for 15 minutes. The mixtures were allowed to stand at room temperature for 24 hours to reach equilibrium.

SNEDDS characterizations

Organoleptic

The organoleptic test for rifampicin SNEDDS preparation includes observation of the color, smell, and the presence or absence of phase separation (Aisy et al., 2021).

Emulsification time

An amount of 1 mL of the SNEDDS was diluted with 100 mL of normal saline (1:100 dilution) under continuous stirring (100 rpm) at ambient temperature. The time required to form a nanoemulsion (a clear-transparent mixture) was expressed as the emulsification time (Winarti, 2016).

Percent transmittance

The SNEDDS mixture was diluted 1:50 with normal saline using a magnetic stirrer. The percent transmittance was measured at 650 nm using a UV-visible spectrophotometer (Thermofisher Genesys 10) with normal saline as the blank (Sahumena et al., 2019).

Viscosity

The rifampicin SNEDDS formula was diluted at a 1:100 ratio with normal saline. The nanoemulsion formed was evaluated using an Ostwald viscometer at 25℃. Record the time it takes for the emulsion to pass the first and second lines (Fithri et al., 2017).

pH

Initially, the sample was diluted 100 times with normal saline to form a nanoemulsion. The pH meter (HANNA Hi 2211) electrodes were then inserted into the emulsion, and the resulting value was recorded (Annisa et al., 2023).

Aerosol output rate

The medicine compartment of the OneMed nebulizer 405A was loaded with five milliliters of nanoemulsion made from 1:100 dilution of SNEDDS with normal saline. The aerosol output rate (g/min) was measured by dividing the weight (gram) of the drug nebulized by the nebulization time using equation 1 (Shah et al., 2017). $W_{initial}$ is the weight of the nebulizer cup containing the sample before nebulization, W_{left} is the weight of the nebulizer cup after nebulization, and t is the time needed to nebulize the sample to dryness (Asmawi et al., 2023).

$$\text{aerosol output rate (g/min)} = \frac{[(\text{Winitial} - \text{Wleft})]}{(\text{t})} \text{ x } 100 \qquad (1)$$

Globule size and zeta potential analysis

The rifampicin SNEDDS optimum formula was diluted at a 1:100 scale with normal saline and then put into a particle size analyzer/PSA (Malvern zetasizer nano ZS series). The evaluation was conducted at a temperature of 25℃ (Shah et al., 2017).

Centrifugation test

The optimum formula was diluted 1:100 with normal saline then centrifuged at 6,000 rpm for 30 minutes. Signs of drug precipitation and phase separation were visually evaluated (Rehman et al., 2022).

Freeze-thaw test

The optimum formula was kept under freezing temperature for 24 hours, then thawed at room temperature for 24 hours (1 cycle). After 6 cycles, the formula is tested for significant changes in physicochemical parameters (emulsification time, percent transmittance, viscosity, pH, and aerosol output rate) and compared with the condition before the freeze-thaw cycle (Hajrin et al., 2024).

Nanoemulsion stability test

The optimum formula was reconstituted by diluting with normal saline at a ratio of 1:50 and then stored at a cold temperature. The nanoemulsion was then observed every 1 hour for any sign of phase separation and its percent transmittance.

Data Analysis

The D-optimal mixture design approach was employed to obtain the optimum concentration of selected oil phase, surfactant, and co-surfactant as independent variables in rifampicin SNEDDS formulation on dependent variables or responses including emulsification time, percent transmittance, viscosity, pH, and aerosol output rate. The correlation between each SNEDDS composition and the response will be explained by the best-fitted model given by the software. Design Expert also displays the mathematical equation of the model to describe the contribution of each SNEDDS composition to the response. Furthermore, the composition of the selected oil, surfactant, and co-surfactant in the optimized formula was determined through numerical optimization. In this method, a desired goal was set for each dependent variable (in range, minimize, maximize, or targeted). Then, the optimization option was utilized to choose the optimal formula determined by the desirability value. The solution with the highest desirability value is selected as the optimum formula (Beandrade, 2018). A paired sample t-test was performed to analyze the mean difference of each response before and after the freeze-thaw test. If the p-value <0.05, the data were significantly different (Purnomo & Syamsul, 2017).

RESULT AND DISCUSSION

Solubility study of rifampicin

Drug solubility in oil, surfactant, and co-surfactant is an important aspect of SNEDDS formulation. The solubility of rifampicin in several oils is presented in Figure 1. Oil with a higher drug solubilization capacity has a greater potential for drug loading. In this study, rifampicin shows the highest solubility in cinnamon oil (176.56±10.65 mg/mL) compared to other oils, thus cinnamon oil was chosen as the oil phase. According to the research conducted by Mantena et al. (2015) rifampicin has a higher solubility in tween 80 (86.84±1.84 mg/mL) and transcutol P (80.46±2.93 mg/mL), among other surfactants and co-surfactants used. Therefore, cinnamon oil, tween 80, and transcutol P were selected for further study.

Identification of oil components

Cinnamon oil, the selected oil phase in this study was analyzed for its chemical compounds using gas chromatography-mass spectrometry (GC-MS). In our research, the main compounds of cinnamon oil were cinnamaldehyde (73.82%), caryophyllene (16.64%), and p-Cymene (5.04%). These compounds exhibit anti-*Mycobacterium tuberculosis* action, with the minimum inhibitory concentration (MIC) value of cinnamaldehyde (3.12 µg/mL), caryophyllene (100.00 µg/mL), and p-Cymene (91.66 µg/mL) (Andrade-Ochoa et al., 2015).

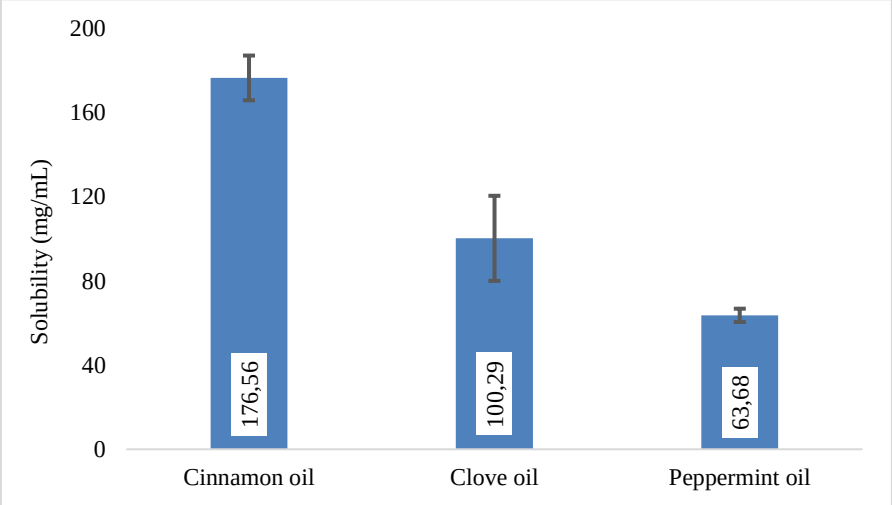

Figure 1. The solubility of rifampicin in several oils

SNEDDS characterizations

The rifampicin SNEDDS composition of each experimental run is displayed in Table 2. Under the D-optimal mixture design, a total of 16 experimental runs were to be performed (with 5 replication points and 5 lack-of-fits points). The model was built using Design Expert® Version 13 software. Figure 2 shows that all experimental runs produced a red-brown, distinctive aroma of rifampicin SNEDDS, and there is an absence of phase separation.

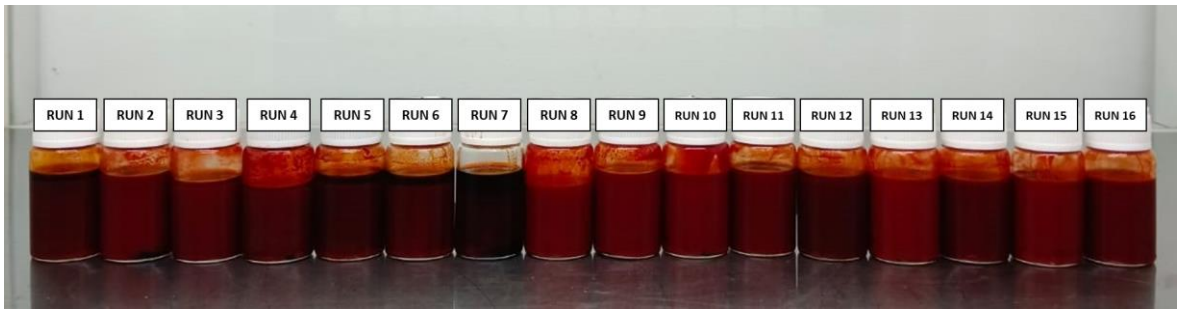

Run 1 (11.25% CIN : 81.25% T80 : 7.5% TC), Run 2 (12.5% CIN : 75% T80 : 12.5% TC), Run 3=Run 10 (5% CIN : 75% T80 : 20% TC), Run 4=Run 6 (5% CIN : 90% T80 : 5% TC), Run 5=Run 12 (20% CIN : 75% T80 : 5% TC), Run 7=Run 13 (5% CIN : 82.5% T80 : 12.5% TC), Run 8=Run 14 (12.5% CIN : 82.5% T80 : 5% TC), Run 9 (15% CIN : 77.5% T80 : 7.5% TC), Run 11 (11.25% CIN : 77.5% T80 : 11.25% TC), Run 15 (7.5% CIN : 77.5% T80 : 15% TC), Run 16 (7.5% CIN : 85% T80 : 7.5% TC)
CIN= cinnamon oil, T80= tween 80, TC= transcutol P

Figure 2. The visual appearance of rifampicin SNEDDS

As presented in Table 2 the emulsification times of all experimental runs ranged from 37.33 to 49.33 seconds. This indicates that the prepared SNEDDS can be emulsified spontaneously and meet the criteria for a good SNEDDS (emulsification time <1 minute) (Reddy & Gubbiyappa, 2022). Percent transmittance refers to the quantity of light that can pass through a material represented as a percentage. This parameter can indicate whether the dispersed droplets are in the nano range or not (Nuari et al., 2021; Wiwiek et al., 2017). If the droplet size gets smaller, the percent transmittance value will be higher (close to 100%), and vice versa. In this study, the percent transmittance value of all formulations ranged

from 18.09 to 92.14%, this suggests that not all the droplets of the resulting SNEDDS formulations have reached nanosized. Viscosity is one of the aspects that influence the nebulizer output. The higher the viscosity of drugs, the flow rate would decrease (Hailu et al., 2020). The rifampicin SNEDDS formulation has a viscosity ranging from 0.93 to 0.95 cP at a temperature of 25℃ indicating good flowability and suitability for pulmonary administration (viscosity <3.9 cP) (Arbain et al., 2018). The pH is a crucial factor in determining the tolerance of nebulized drugs. All formulations met the criteria for lung administration (pH 4.5-8.7), with pH values ranging from 5.69 to 6.40 (Shah et al., 2017). The aerosol output rate is the mass rate of drugs exiting the aerosol generator. This is an important parameter to ensure therapeutic comfort in nebulization (Shah et al., 2017). The higher the aerosol output rate value, the less time is required for nebulization. In this study, the aerosol output rate value of all formulations ranged from 0.12 to 0.15 g/min.

Table 2. D-optimal mixture design runs for rifampicin SNEDDS composition and physicochemical characteristic result

RUN	SNEDDS compositions			Characteristics				
	CIN (%)	T80 (%)	TC (%)	ET (sec)	%T (%)	Viscosity (cP)	pH	AOR (g/min)
1	11.25	81.25	7.5	49.00	65.72	0.95	6.40	0.14
2	12.5	75	12.5	40.00	87.06	0.93	6.02	0.15
3	5	75	20	37.33	37.25	0.93	5.81	0.14
4	5	90	5	49.33	89.95	0.93	5.92	0.13
5	20	75	5	46.67	89.02	0.93	5.69	0.13
6	5	90	5	44.33	88.35	0.93	5.96	0.13
7	5	82.5	12.5	43.00	87.79	0.93	5.83	0.13
8	12.5	82.5	5	48.00	91.92	0.93	5.83	0.12
9	15	77.5	7.5	43.67	80.44	0.93	5.95	0.15
10	5	75	20	38.67	18.09	0.93	6.01	0.14
11	11.25	77.5	11.25	45.00	52.88	0.93	5.99	0.15
12	20	75	5	46.67	92.14	0.94	5.81	0.15
13	5	82.5	12.5	46.67	72.62	0.93	6.14	0.14
14	12.5	82.5	5	39.67	77.05	0.93	5.82	0.13
15	7.5	77.5	15	40.33	76.65	0.94	5.87	0.15
16	7.5	85	7.5	43.00	51.03	0.93	5.71	0.13

CIN= cinnamon oil, T80= tween 80, TC= transcutol P, ET= emulsification time, %T= percent transmittance, AOR= aerosol output rate

Design Expert® Version 13 software was used to analyze the resulting data in Table 2 by choosing a suitable regression model for each response (emulsification time, percent transmittance, viscosity, pH, and aerosol output rate) to describe the influence of each SNEDDS composition. Table 3 shows that the best-fitting models for explaining the influence of independent variables on observed responses are the linear model for emulsification time, the special cubic model for percent transmittance, and the quadratic model for aerosol output rate due to the model's p-value <0.05 (significant), and non-significant lack of fit (p>0.05) (Akbar et al., 2022; Astuti et al., 2017). Meanwhile, no model in the software can explain the relationship between the SNEDDS composition on viscosity and pH. This indicates that the viscosity and pH parameters on rifampicin SNEDDS are not influenced by variations in the independent variables. A mathematical equation that explains the quantitative effects of each SNEDDS composition and their interaction on the observed response is presented in Table 3. The positive sign of the coefficient represents the synergistic effect, whereas the negative sign represents an antagonistic effect of independent variables on the dependent variables. The larger the coefficient value of the factor suggests the more influential the factor is toward the response, and vice versa (Yadav et al., 2020).

Numerical optimization of rifampicin SNEDDS

Based on the ideal criteria of rifampicin SNEDDS formulation targeted to the lungs, the optimal formula should be able to quickly form nanoemulsions with a clear appearance, have a good flow property, pH ranging from 4.5 to 8.7, and have a high aerosol output rate. Therefore, to optimize the composition of cinnamon oil, tween 80, and transcutol P, the goals for percent transmittance and aerosol output rate were set to maximize, the pH was set to in range (5.69-6.40), while emulsification time and viscosity were set to minimize. Based on these criteria, Design Expert® Version 13 creates three solution formulas. The solution with the highest desirability value (0.856) which contained 12.65% cinnamon oil, 75.00% tween 80, and 12.35% transcutol P was selected as the optimum formula and will be used for further investigation. Three replicates of the optimum formula were prepared and characterized similarly to the previous 16 experimental runs with the addition of other physicochemical characteristics tests including globule size, zeta potential, and stability studies. Then, the optimum formula was confirmed by comparing the predicted values provided by the software with the actual values.

Table 3. Determination of the mixture model and mathematical equation generated by Design Expert®

Response (Y)	Mixture model	Mathematical equation	Lack of fit
Emulsification time	Linear (p=0.0130)	Y=0.420699A+0.498805B-0.040405C	Not significant (p=0.7330)
Percent transmittance	Special cubic (p=0.0095)	Y=-96.06273A-1.01839B-136.99257C +1.35201AB+22.34251AC+1.84426BC -0.290683ABC	Not significant (p=0.1188)
Aerosol output rate	Quadratic (p=0.0244)	Y=0.009406A+0.001392B-0.002607C -0.000122AB+0.000295AC+0.000038BC	Not significant (p=0.7451)
Viscosity		N/A*	
pH		N/A*	

Cinnamon oil (A), Tween 80 (B), Transcutol P (C), *N/A= not available

Table 4 showed that the actual values for all responses were within the 95% prediction interval (PI) range, suggesting that the software can reliably predict the values of all responses in the optimum formula. The optimum formula produced SNEDDS with good characteristics includes forming nanoemulsion spontaneously with a clear appearance, having a pH within the range of pH values for nebulized drugs, and easily coming out of the aerosol generator due to its low viscosity. In SNEDDS formulation, the emulsion droplet size is an important factor. A smaller droplet size is favored because it provides a larger surface area for the absorption of drugs (Avachat & Patel, 2015).

As shown in Table 5, the rifampicin SNEDDS optimum formula had a droplet size of 169.2±19.771 nm, meeting the SNEDDS formulation criteria of <200 nm (Fitria et al., 2021). In addition, this particle size also meets the criteria for drug delivery to reach the pulmonary alveolus, where *Mycobacterium tuberculosis* resides (Costa et al., 2016). Polydispersity index (PDI) is a homogeneity parameter of particle size with a value range between 0.0 and 1.0. The smaller the PDI value, the more homogeneous the droplet size in a formulation, and vice versa. The optimum formula had a PDI value of 0.258±0.070 which indicates that the formula is monodispersed (PDI value ≤0.5) (Darusman et al., 2023). Zeta potential is a crucial aspect in determining the stability of SNEDDS. A good zeta potential value for SNEDDS formulation is higher than ±30 mV. In this system, the repulsive force between particles is high, preventing particle aggregation (Syukri et al., 2020). The optimum formula had a zeta potential value of -2.533±0.268 mV. A negative value may be due to hydroxyl groups present in the structure of

the surfactant and cosurfactant used in this study. These negatively charged particles can avoid the mucus layer interaction (biological barrier for pulmonary drug delivery) because the mucus has a negative charge, while positively charged particles will interact with mucus, be entrapped then cleared by the mucociliary clearance mechanism. Thus positively charged particles may have a lower deposition in the deeper lung area (Vu et al., 2024). To be deposited in the lower part of the lungs (alveolar and terminal bronchiolus) which has no mucus, the repulsion from mucus is needed to change the airway direction of the aerosolized particles, making it easier to reach the deeper lung and deposited under sedimentation/Brownian motion mechanism (Majid et al., 2012). Low zeta potential values can result from normal saline that is used to dilute the SNEDDS in this study. Normal saline contains many electrolytes that can disrupt the surface charge of SNEDDS droplets. This occurs because counter ions in the diffusion layer can be repelled into the inner layer, decreasing the zeta potential (Lu et al., 2018). Normal saline is often used to reconstitute nebulized solution to provide a dosage form with suitable tonicity for lung administration. Moreover, the droplets produced by SNEDDS with tween 80 as surfactant are often stabilized by the steric repulsion due to long polyoxyethylene head groups of the tween 80 molecules which cause them to have a low to zero zeta potential (Suryani et al., 2019)

Table 4. Results of model confirmation and physicochemical characteristics of the optimum formula of rifampicin SNEDDS before and after freeze-thaw test

Response	Prediction value	95% PI	Before stability test	After stability test	p-value
Emulsification time (seconds)	42.234	37.95-46.52	40.67±1.53	42.67±1.53	0.321
Percent transmittance (%)	92.100	60.42-123.77	93.11±0.25	92.51±0.02	0.055
Aerosol output rate (g/min)	0.157	0.14-0.17	0.14±0.02	0.14±0.01	0.667
Viscosity (cP)	0.932	0.93-0.94	0.94±0.01	0.93±0.02	0.423
pH	5.923	5.69-6.16	5.91±0.01	5.90±0.02	0.270

Table 5. The results of globule size and zeta potential analysis of the optimum formula

Characterization	Value
Droplet size	169.2±19.771 nm
PDI	0.258±0.070
Zeta potential	-2.533±0.268 mV

Stability is one of the important aspects to consider while developing pharmaceutical preparations, including SNEDDS. The instability of drug products could affect the therapeutic efficacy and cause a toxic effect (Pratiwi et al., 2018). Based on Table 4, no statistically significant changes were noticed in each response after the freeze-thaw stability test (p-value>0.05). These findings show that the optimum formula is thermodynamically stable. Furthermore, results from the centrifugation test showed no signs of drug precipitation and phase separation, meaning the SNEDDS is capable of producing is kinetically stable nanoemulsion.

Another parameter that can be used to evaluate the stability of reconstituted SNEDDS preparations is percent transmittance. The good percent transmittance value for nanoemulsion is >80% which shows that the size of oil droplets which encapsulate the drug is still in the nanometer range <100 nm (Syukri et al., 2020). Figure 3 showed that reconstitution of rifampicin SNEDDS with normal saline which was stored at a cold temperature was stable for up to 4 hours with no visible drug precipitation even after centrifugated at 6000 rpm for 30 minutes, although the transmittance percentage of the resulting nanoemulsion fell to 80%. However, this shows that the reconstituted SNEDDS is still safe to use, as

the duration of nebulization is generally < 30 minutes. Therefore, to ensure the effectiveness and safety of treatment, this liquid is recommended to be used immediately after reconstitution.

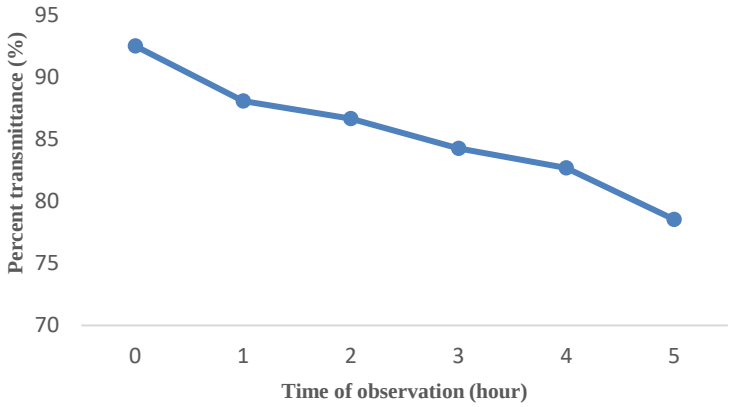

Figure 3. The stability profile of reconstituted rifampicin SNEDDS in normal saline

CONCLUSION

The optimum formula of rifampicin SNEDDS consisted of 12.65% cinnamon oil, 75.00% tween 80, and 12.35% transcutol P. This formula produces a stable preparation with good physicochemical characteristics of SNEDDS. These results indicate the potential of cinnamon oil-based rifampicin SNEDDS to be an alternative in the pulmonary delivery of rifampicin via nebulization and need to be further evaluated to prove its effectiveness.

ACKNOWLEDGEMENT

We acknowledge support by Sekolah Tinggi Farmasi Mahaganesha for providing facilities used in this study.

REFERENCES

AARC. (2023). *Pulmonary disease aerosol delivery devices: a guide for physicians, nurses, pharmacists, and other health care professionals* (4th ed.). American Association for Respiratory Care.

Aisy, Z. H. R., Puspita, O. E., & Shalas, A. F. (2021). Optimasi formula nanoemulsi nifedipin dengan metode self-nanoemulsifying drug delivery system (SNEDDS). *Pharmaceutical Journal of Indonesia*, *6*(2), 85–95. https://doi.org/10.21776/ub.pji.2021.006.02.3

Akbar, N. D., Nugroho, A. K., & Martono, S. (2022). Artikel review: optimasi formulasi SNEDDS dengan simplex lattice design dan box behnken design. *Jurnal Ilmiah Farmako Bahari*, *13*(1), 90. https://doi.org/10.52434/jfb.v13i1.1216

Andrade-Ochoa, S., Nevárez-Moorillón, G. V., Sánchez-Torres, L. E., Villanueva-García, M., Sánchez-Ramírez, B. E., Rodríguez-Valdez, L. M., & Rivera-Chavira, B. E. (2015). Quantitative structure-activity relationship of molecules constituent of different essential oils with antimycobacterial activity against Mycobacterium tuberculosis and Mycobacterium bovis. *BMC Complementary and Alternative Medicine*, *15*(1), 332. https://doi.org/10.1186/s12906-015-0858-2

Annisa, R., Mutiah, R., Yuwono, M., & Hendradi, E. (2023). The development formulation of eleutherine palmifolia extract-loaded self nanoemulsifying drug delivery system (SNEDDS) using D-optimal mixture design approach. *International Journal of Applied Pharmaceutics*, *15*(5), 269–276. https://doi.org/10.22159/ijap.2023v15i5.47645

Arbain, N. H., Basri, M., Salim, N., Wui, W. T., & Abdul Rahman, M. B. (2018). Development and characterization of aerosol nanoemulsion system encapsulating low water soluble quercetin for lung cancer treatment. *Materials Today: Proceedings*, *5*, S137–S142. https://doi.org/10.1016/j.matpr.2018.08.055

Asmawi, A. A., Salim, N., Abdulmalek, E., & Abdul Rahman, M. B. (2023). Size-controlled preparation of docetaxel- and curcumin-loaded nanoemulsions for potential pulmonary delivery. *Pharmaceutics*, *15*(2), 652. https://doi.org/10.3390/pharmaceutics15020652

Astuti, I. Y., Marchaban, M., Martien, R., & Nugroho, A. E. (2017). Design and optimization of self nano-emulsifying drug delivery system containing a new anti-inflamatory agent pentagamavunon-0. *Indonesian Journal of Chemistry*, *17*(3), 365. https://doi.org/10.22146/ijc.22640

Avachat, A. M., & Patel, V. G. (2015). Self nanoemulsifying drug delivery system of stabilized ellagic acid–phospholipid complex with improved dissolution and permeability. *Saudi Pharmaceutical Journal*, *23*(3), 276–289. https://doi.org/10.1016/j.jsps.2014.11.001

Beandrade, M. U. (2018). Formulasi dan karakterisasi SNEDDS ekstrak Jinten Hitam (Nigella Sativa) dengan fase minyak ikan Hiu Cucut botol (Centrophorus Sp) serta uji aktivitas imunostimulan. *JPSCR : Journal of Pharmaceutical Science and Clinical Research*, *3*(1), 50. https://doi.org/10.20961/jpscr.v3i1.15506

Carneiro, A. F., Carneiro, C. N., de N Pires, L., Teixeira, L. S. G., Azcarate, S. M., & de S Dias, F. (2020). D-optimal mixture design for the optimization of extraction induced by emulsion breaking for multielemental determination in edible vegetable oils by microwave-induced plasma optical emission spectrometry. *Talanta*, *219*, 121218. https://doi.org/10.1016/j.talanta.2020.121218

Costa, A., Pinheiro, M., Magalhães, J., Ribeiro, R., Seabra, V., Reis, S., & Sarmento, B. (2016). The formulation of nanomedicines for treating tuberculosis. *Advanced Drug Delivery Reviews*, *102*, 102–115. https://doi.org/10.1016/j.addr.2016.04.012

Darusman, F., Dwiatama, A., & Priani, S. E. (2023). Formulasi dan karakterisasi self-nanoemulsifying drug delivery System (SNEDDS) esomeprazol magnesium trihidrat. *Jurnal Sains Farmasi & Klinis*, *10*(1), 10. https://doi.org/10.25077/jsfk.10.1.10-20.2023

Divate, M. P., Bawkar, S. U., Chakole, R. D., & Charde, M. S. (2021). Self nano-emulsifying drug delivery system: a review. *Journal of Advanced Scientific Research*, *12*(3 Suppl 2), 1–12. https://doi.org/10.55218/JASR.s2202112301

Elbardisy, B., Boraie, N., & Galal, S. (2022). Tadalafil nanoemulsion mists for treatment of pediatric pulmonary hypertension via nebulization. *Pharmaceutics*, *14*, 2717. https://doi.org/10.3390/pharmaceutics14122717

Fithri, N. A., Mardiyanto, M., Novita, R. P., & Andrean, V. (2017). Furosemide self nano emulsifying drug delivery system (SNEDDS) formulation comprising of capryol-90, polysorbate-80, and peg-400 with simplex-lattice-design. *Science and Technology Indonesia*, *2*(4), 85–88. https://doi.org/10.26554/sti.2017.2.4.85-88

Fitria, A., Hanifah, S., Chabib, L., Uno, A. M., Munawwarah, H., Atsil, N., Pohara, H. A., Weuanggi, D. A., & Syukri, Y. (2021). Design and characterization of propolis extract loaded self-nano emulsifying drug delivery system as immunostimulant. *Saudi Pharmaceutical Journal*, *29*, 625–634.

Gautam, S., Qureshi, K. A., Jameel Pasha, S. B., Dhanasekaran, S., Aspatwar, A., Parkkila, S., Alanazi, S., Atiya, A., Khan, M. M. U., & Venugopal, D. (2023). Medicinal plants as therapeutic alternatives to combat mycobacterium tuberculosis: a comprehensive review. *Antibiotics*, *12*(3), 541. https://doi.org/10.3390/antibiotics12030541

Grotz, E., Tateosian, N. L., Salgueiro, J., Bernabeu, E., Gonzalez, L., Manca, M. L., Amiano, N., Valenti, D., Manconi, M., García, V., Moretton, M. A., & Chiappetta, D. A. (2019). Pulmonary delivery of rifampicin-loaded Soluplus Micelles against Mycobacterium tuberculosis. *Journal of Drug Delivery Science and Technology*, *53*, 101170.https://doi.org/ 10.1016/j.jddst.2019.101170

Hailu, N., Postema, M., Krejcar, O., & Assefa, D. (2020). Nebulization criteria and quantification. *Fluids*, *5*(2), 91. https://doi.org/10.3390/fluids5020091

Hajrin, W., Subaidah, W. A., & Juliantoni, Y. (2024). Formulasi dan karakterisasi nanoemulsi dari ekstrak biji buah Makasar (Brucea javanica (L) Merr). *Indonesian Journal of Pharmaceutical Science and Technology*, *11*(1), 117–125.

Katzung, B. G. (2018). *Basic & Clinical Phamacology* (14th ed.). McGraw-Hill Education

Kemenkes RI. (2020). *Pedoman Nasional Pelayanan Kedokteran Tata Laksana Tuberkulosis*. Kementerian Kesehatan Republik Indonesia

Khadka, P., Dummer, J., Hill, P. C., Katare, R., & Das, S. C. (2023). A review of formulations and preclinical studies of inhaled rifampicin for its clinical translation. *Drug Delivery and Translational Research*, *13*, 1246–1271. https://doi.org/10.1007/s13346-022-01238-y

Lu, Y., Qi, J., & Wu, W. (2018). Lipid nanoparticles: In vitro and in vivo approaches in drug delivery and targeting. In *Drug Targeting and Stimuli Sensitive Drug Delivery Systems* (pp. 749–783). Elsevier. https://doi.org/10.1016/B978-0-12-813689-8.00020-3

Majid, H., Madl, P., Hofmann, W., & Alam, K. (2012). Implementation of charged particles deposition in stochastic lung model and calculation of enhanced deposition. *Aerosol Science and Technology*, *46*(5), 547–554. https://doi.org/10.1080/02786826.2011.645957

Mantena, A. D., Mantena, A. D., & Nerella, A. (2015). Formulation, optimization and in vitro evaluation of rifampicin Nanoemulsions. *International Journal of Pharmaceutical Sciences and Drug Research*, *7*(6), 451–455.

Maretti, E., Rustichelli, C., Gualtieri, M. L., Costantino, L., Siligardi, C., Miselli, P., Buttini, F., Montecchi, M., Leo, E., Truzzi, E., & Iannuccelli, V. (2019). The impact of lipid corona on rifampicin intramacrophagic transport using inhaled solid lipid nanoparticles surface-decorated with a mannosylated surfactant. *Pharmaceutics*, *11*, 508. https://doi.org/ 10.3390/pharmaceutics11100508

Nuari, Y. R., Wahyuningsih, I., & Prabawati, S. (2021). Self-Nanoemulsifying drug delivery system (SNEDDS) of piroxicam. *Pharmaciana*, *11*(2), 185. https://doi.org/10.12928/pharmaciana.v11i2.20973

Parikh, R., Patel, L., & Dalwadi, S. (2014). Microparticles of Rifampicin: comparison of pulmonary route with oral route for drug uptake by alveolar macrophages, phagocytosis activity and toxicity study in Albino Rats. *Drug Delivery*, *21*(6), 406–411. https://doi.org/10.3109/10717544.2013.851302

Pratiwi, L., Fudholi, A., Martien, R., & Pramono, S. (2018). Physical and chemical stability test of SNEDDS (Self-nanoemulsifying Drug Delivery System) and nanoemulsion ethyl acetate fraction of garcinia mangostana L. *Majalah Obat Tradisional*, *23*(2), 84. https://doi.org/10.22146/mot.28533

Priani, S. E., Nurrayyan, & Darusman, F. (2017). Formulation self nano emulsifying drug delivery system glimepiride using oleic acid as oil phase. *Pharmaciana*, *7*(2), 267–276. http://dx.doi.org/10.12928/pharmaciana.v7i2.7387

Purnomo, H., & Syamsul, E. S. (2017). *Statistika farmasi (aplikasi praktis dengan SPSS)*.

Reddy, M. R., & Gubbiyappa, K. S. (2022). Formulation development, optimization and characterization of Pemigatinib-loaded supersaturable self-nanoemulsifying drug delivery systems. *Future Journal of Pharmaceutical Sciences*, *8*(1), 45. https://doi.org/10.1186/s43094-022-00434-4

Rehman, F. U., Farid, A., Shah, S. U., Dar, M. J., Rehman, A. U., Ahmed, N., Rashid, S. A., Shaukat, I., Shah, M., Albadrani, G. M., Kamel, M., Altyar, A. E., Abdel-Daim, M. M., & Shah, K. U. (2022). Self-emulsifying drug delivery systems (SEDDS): measuring energy dynamics to determine thermodynamic and kinetic stability. *Pharmaceuticals*, *15*(9), 1064. https://doi.org/10.3390/ph15091064

Sahumena, M. H., Suryani, S., & Rahmadani, N. (2019). Formulasi self-nanoemulsifiying drug delivery system (SNEDDS) asam mefenamat menggunakan VCO dengan kombinasi surfaktan tween dan span. *Journal Syifa Sciences and Clinical Research*, *1*(2), 37–46. https://doi.org/10.37311/jsscr.v1i2.2660

Sawicki, R., Golus, J., Przekora, A., Ludwiczuk, A., Sieniawska, E., & Ginalska, G. (2018). Antimycobacterial activity of Cinnamaldehyde in a Mycobacterium tuberculosis(H37Ra) Model. *Molecules*, *23*(9), 2381. https://doi.org/10.3390/molecules23092381

Shah, K., Chan, L. W., & Wong, T. W. (2017). Critical physicochemical and biological attributes of nanoemulsions for pulmonary delivery of rifampicin by nebulization technique in tuberculosis treatment. *Drug Delivery*, *24*(1), 1631–1647. https://doi.org/10.1080/10717544.2017.1384298

Somasundaram, S., Ram, A., & Sankaranarayanan, L. (2014). Isoniazid and Rifampicin as Therapeutic Regimen in the Current Era: A Review. *Journal of Tuberculosis Research*, *2*, 40–51. https://doi.org/10.4236/jtr.2014.21005

Sopyan, I., Gozali, D., Sriwidodo, & Guntina, R. K. (2022). Design-expert software (DOE): an application tool for optimization in pharmaceutical preparations formulation. *International Journal of Applied Pharmaceutics*, 55–63. https://doi.org/10.22159/ijap.2022v14i4.45144

Suryani, Sahumena, M. H., Alfiandi, Putrawansya, L. R. P., Mallarangeng, A. N. T. A., Aswan, M., & Ruslin. (2019). The self-nanoemulsifying Drug delivery systems formulation of mefenamic acid. *Asian Journal of Pharmaceutics*, *13*(4), 287.

Syukri, Y., Nugroho, B. H., & Istanti, I. (2020). Penggunaan D-optimal mixture design untuk optimasi dan formulasi self-nano emulsifying drug delivery system (SNEEDS) asam mefenamat. *Jurnal Sains Farmasi & Klinis*, *7*(3), 180. https://doi.org/10.25077/jsfk.7.3.180-187.2020

Tsume, Y., Mudie, D. M., Langguth, P., Amidon, G. E., & Amidon, G. L. (2014). The biopharmaceutics classification system: subclasses for in Vivo Predictive Dissolution (IPD) methodology and IVIVC. *European Journal of Pharmaceutical Sciences*, *57*, 152–163. https://doi.org/10.1016/j.ejps.2014.01.009

Vidya Raj, C. K., Venugopal, J., Muthaiah, M., Chadha, V. K., Brammacharry, U., Swappna, M., Sangeetha, A. V., Dhandapani, S. P., Kareedhi, V. R., Calivarathan, L., Karthick, M., & Jayapal, K. (2022). In-vitro anti-Mycobacterium tuberculosis effect of Eugenol. *Indian Journal of Tuberculosis*, *69*(4), 647–654. https://doi.org/10.1016/j.ijtb.2021.09.016

Vu, H.-D., Vu, T.-H., Mai, N. L., Pande, D. C., Dao, D. V., Rehm, B. H. A., Nguyen, N.-T., Grant, G. D., Tran, C.-D., Zhu, Y., & Dau, V. T. (2024). In-flight electro-neutralisation electrospray for pulmonary drug delivery. *Nano Today*, *55*, 102217. https://doi.org/10.1016/j.nantod.2024.102217

Wang, B., Wang, L., Yang, Q., Zhang, Y., Qinglai, T., Yang, X., Xiao, Z., Lei, L., & Li, S. (2024). Pulmonary inhalation for disease treatment: basic research and clinical translations. *Materials Today Bio*, *25*, 100966.https:// doi.org.10.1016/j.mtbio.2024.100966

WHO. (2023). *Global Tuberculosis Report 2023*. World Health Organization

Winarti, L. (2016). Formulation of Self-Nanoemulsifying Drug Delivery System of Bovine Serum Albumin using HLB (Hydrophilic-Lipophilic Balance) Approach. *Indonesian Journal of Pharmacy*, *27*(3), 117. https://doi.org/10.14499/indonesianjpharm27iss3pp117

Wiwiek, I. A., Martodihardjo, S., . S., . J., Ngurah Budiana, I. G. M., & . M. (2017). Preparation and in-vitro characterization of Self-Nano emulsifying system of C- Phenylcalix-[4]-Resorcinaryl Octacinnamate and C-Methylcalix-[4]-Resorcinaryl Octabenzoate as ultraviolet absorbers. *Bali Medical Journal*, *6*(3), 569. https://doi.org/10.15562/bmj.v6i3.699

Yadav, P., Rastogi, V., & Verma, A. (2020). Application of Box–Behnken design and desirability function in the development and optimization of self-nanoemulsifying drug delivery system for enhanced dissolution of ezetimibe. *Future Journal of Pharmaceutical Sciences*, *6*(1), 7. https://doi.org/10.1186/s43094-020-00023-3

Pharmaciana
Vol.14, No.3, Nov 2024, Page. 370-381
ISSN: 2088 4559; e-ISSN: 2477 0256
DOI: 10.12928/pharmaciana.v14i3.27936

Optimization of nanoemulsion hair serum from chia seed oil using the Simplex Lattice Design method

Mayu Rahmayanti*, Reza Putri Oktavia, Faidatul Amalina, Safa Aulia Nur Fadila, Ginanjar Putri Nastiti, Sadli Syarifuddin
Departement of Pharmacy, Faculty of Medicine and Health Science, UIN Maulana Malik Ibrahim Malang
Jl. Locari Tlekung, Batu, East Java, Indonesia

Submitted: 14-12-2023 ***Reviewed: 02-07-2024*** ***Accepted: 06-10-2024***

ABSTRACT

Hair loss is a hair problem that men and women often experience. Chia seed oil (*Salvia hispanica* L.) contains linolenic acid, which can stimulate the sebum glands. This research aims to determine the composition of the optimum formula for chia seed oil nanoemulsion hair serum using the Simplex Lattice Design (SLD) method to prove that the characteristics and physical stability of the optimum formula meet the requirements for good preparation. The optimization method was carried out with the help of Design Expert 13 software to optimize the formula by varying Tween 80 (X1) and propylene glycol (X2). The characteristic parameters observed include organoleptic parameters such as pH, viscosity, homogeneity, emulsion type, particle size, zeta potential, polydispersity index, and percent transmittance. The physical stability test was carried out using a 6-cycle test method for organoleptic parameters, pH, and homogeneity. Optimization results show that the optimum composition consists of Tween 80 33.52% and propylene glycol 46.48%. The preparation meets all physical characteristic tests. Physical stability did not significantly change in the pH test, with a significance value of 0.027 in the paired t-test. Based on the research results, it can be concluded that the optimum surfactant and cosurfactant composition in the optimum formula based on optimization using SLD is Tween 80 (33.52%) and propylene glycol (46.48%) with a desirability value of 0.947. The optimum formula for preparing chia seed oil nanoemulsion hair serum meets good physical characteristics and stability requirements.

Keywords: chia seed oil, nanoemulsion, *Salvia hispanica* Linn, Simplex Lattice Design

Corresponding author:
Mayu Rahmayanti
Departement of Pharmacy, Faculty of Medicine and Health Science, UIN Maulana Malik Ibrahim Malang
Jl. Locari Tlekung, Batu, East Java, Indonesia
Email: mayu31@farmasi.uin-malang.ac.id

INTRODUCTION

Hair loss is one of the most common hair problems. Hair loss does not pose a severe threat to human life, but it impacts self-confidence and the function of hair on the skin, especially the scalp. Hair loss is caused by abnormalities in the hair shaft cycle, which cause damage to the hair follicles, thereby causing hair growth failure. Hair loss problems can occur in both men and women (Magfirah et al., 2022).

Technological advances to overcome hair problems and research that continues to be studied increase knowledge and innovation in the use of herbal plants in cosmeceutical hair care products. Hair serum, or hair serum, is a product used to style and coat the hair's surface and has a thicker consistency than air (Vakhariya et al., 2022). Consumer interest in herbal products continues to increase globally (Gamage et al., 2022). The chia plant (*Salvia hispanica* L.) originates from northern Guatemala and is widely cultivated in Mexico. Chia seeds contain 39% oil and have the highest α-linolenic acid content at 68%; this level is higher than the content in flax seeds, namely 57% (Segura-Campos et al., 2014). Linolenic acid, or omega 3, is a polyunsaturated fatty acid that can be absorbed into the skin and stimulate hair growth through its mechanism as a sebum gland stimulant (Sofwan et al., 2017).

According to research by (Rahmayanti et al., 2023), chia seed oil hair emulsion is weak as an active ingredient, making it less stable during storage. Hence, it needs to be reformulated into a more stable dosage form. Nanoemulsions are kinetically and thermodynamically more stable. An optimization process is undoubtedly needed to create the best formula for a cosmetic product. Optimization can be done using several methods, including a mixture. The method in mixture design is simplex lattice design (SLD). This method is considered more effective in time and can minimize the costs used (Hidayat et al., 2020).

Several previous studies have been carried out regarding the optimization of nanoemulsion formulas using the SLD method, one of which is research on the optimization of eel fish oil nanoemulsion formulas using the SLD method, where in this study, good significant results were obtained. Namely, there was no significant difference between the results of direct observation of the preparation and the value predictions of the Design expert software version 10.0.1.0 (Az-Zahra et al., 2022); however, from several existing studies regarding the optimization of nanoemulsion formulas, there has been no research regarding the optimization of chia seed oil nanoemulsion hair serum formulas. Hence, this research needs to be developed. Based on the description above, it is necessary to conduct research on optimizing the halal nanoemulsion hair serum formula from chia seed oil (*Salvia hispanica* L.) using the Simplex Lattice Design (SLD) method.

MATERIALS AND METHOD

Materials

The ingredients used in the research were chia seed oil (*Salvia hispanica* L.) (CV. Happy Green), Tween 80 (Chimica Panzeri), propylene glycol (Bratachem), methylparaben (Golden Era), propylparaben (Golden Era), span 80 (Bratachem), sodium metabisulfite (Purolanssss), and distilled water (Bratachem). The tools used in the research were software Design Expert 13-trial, UV-Vis spectrophotometry (Shimadzu), Particle Size Analyzer (PSA) (Microtac Nanotrac Wave II), oven (Memmert UN30), Refrigerator (Samsung), benchtop pH meter (Metler Toledo), Brookfield spindle viscometer number 40 (Ametek).

Methods

Formula rationalization

The method used in the formula rationalization process is to look for literature studies regarding what materials are suitable for use in this research, compatibility between materials is seen from the characteristics of the materials through handbooks of pharmaceutical excipients, journals that support the use of materials, and also other literature studies. The basis for selecting materials is related to compatibility, solubility, toxicity, and also the range of use and usefulness of the material. Active ingredient used in optimizing this formula is chia seed oil. The linolenic acid content in chia seed oil is a stimulant agent for the sebaceous glands that stimulates hair growth (Rahmayanti et al., 2023). The

combination of Tween 80 and Span 80 surfactants was chosen to produce HLB 12 with an O/W emulsion type; besides, both are nonionic surfactants, so toxicity and side effects are lower. Propylene glycol was chosen as a cosurfactant to help reduce interfacial tension and help increase the diffusion rate of topical preparations. The combination of propylparaben and methylparaben preservatives was chosen to increase efficacy and reduce side effects. The antioxidant Sodium Metabisulfite was used in this research to prevent oxidation processes that may occur during heating.

Formula optimization using design expert 13

The chia seed oil nanoemulsion hair serum preparation formula was optimized using Design Expert software version 13. The research direction used in this research was optimization to optimize the formula with the best characteristics. One method in mixture design is simplex lattice design (SLD). This method is an optimization method used to determine the best formula for a mixture of ingredients that have been determined, with the proportion of the total amount of different ingredients having to be 1 (Hidayat et al., 2020). Formula optimization was carried out by varying variable X which was the independent variable, Tween 80 (X1) and propylene glycol (X2) while variable Y was the physical characteristics test response. This method is carried out by entering data on the upper and lower limits for the use of variable After the data is entered into the software via the new design menu, then optimization, mixture and simplex lattice. The software will provide an overview of the test results of various combinations of variable X and their influence on variable Y mathematically. Then the software will provide an initial recommendation formula and predictions of quantitative physical evaluation data test results. Every 2 ingredients that are varied will produce 8 formulas, of which 3 are the same formula. This formula equation functions to support the accuracy of the data predicted by the Design Expert software.

Validation and verification

The nanoemulsion hair serum preparation was validated to ensure the preparation complies with the optimum formula results from the Design Expert software by repeating the preparation in triplicate three times. Verification is carried out by comparing the predicted results with the results.

The experiment uses a parametric one sample t-test if the data is distributed normal and non-parametric Wilcoxon tests if the data is not normally distributed. Normality testing is carried out for each preparation evaluation result. The software used for the verification process is SPSS software (Noor, 2018).

Procedure for making nanoemulsion hair serum

In the chia seed oil nanoemulsion hair serum formulation, the concentration of chia seed oil used is 7.5%, methyl paraben 0.18%, propyl paraben 0.02%, sodium metabisulfite 0.075%, distilled water ad 100%. For the use of optimized materials, the concentration is written in the range, namely Tween 80 5-80% and propylene glycol 1-10%, while for the use of Span 80 the amount of use adjusts the results of the HLB calculation to produce an HLB value of 12 when combined with Span 80. The selection of range and concentration has been adjusted to the literature and the reasons for selecting ingredients at the formula rationalization stage. All ingredients needed in the formulation are weighed, then dissolve the propyl paraben and methyl paraben in propylene glycol (mixture 1). Mixture 1 was added with chia seed oil and then homogenized using a magnetic stirrer at 1000 rpm for 30 minutes. A mixture of 2, namely the water phase, was made by heating Tween 80 and distilling water at a temperature of 50^{o}C, then homogenizing using a stirrer at 1000 rpm for 30 minutes at a temperature of 50^{o}C. then homogenized using a stirrer at 1000 rpm for 30 minutes at 50oC. The oil and water phases were mixed using a magnetic stirrer at a speed of 1000 rpm for 70 minutes. Then, it was sonicated using a bath-type sonicator for 90 minutes.

Physical evaluation of hair serum nanoemulsion preparations

Organoleptic test

The organoleptic test was performed by visually observing the hair serum nanoemulsion preparation. Good organoleptic results include precise, transparent preparations and no phase separation (Collins et al., 2023).

Homogeneity test

The homogeneity test is carried out to see whether less homogeneous particles or coarse particles are scattered in the preparation. A good preparation has homogeneous characteristics and does not contain scattered coarse particles (Collins et al., 2023).

pH test

The pH test is carried out so that the preparation has a pH that matches the skin's pH and does not cause irritation. The pH range of good topical preparations is between 4.5 and 7.0 (Sanaji & Liananda3, 2019). pH testing is carried out using a benchtop pH meter, by calibrating the pH meter with a standard buffer of pH 4.00; 7.00; and 9.00 then rinsed the electrode with distilled water and dry using tissue. After that, pH measurements are carried out by: dip the pH into the nanoemulsion preparation until the pH value appears on the screen pH meter (Handayani et al., 2018).

Viscosity test

The viscosity test is carried out to determine the viscosity level of the resulting preparation. A suitable dosage viscosity range is between 10 and 2000 cPs (Nicolini et al., 2021). This test uses tools Brookfield spindle viscometer number 40 with a rotation speed of 1 rpm. Then, the measurement results visible on the viscometer are viewed and analyzed meets the requirements for good viscosity acceptance or not (Az-Zahra et al., 2022).

Particle size test, zeta potential test, and polydispersity test

This test was carried out using a PSA apparatus with a dilution of 1:250 using Aqua Pro injection to determine whether the nanoemulsion preparation met the requirements for a good nanoemulsion, namely 10-1000 nm (Handayani et al., 2018). The particle size test, zeta potential test, and polydispersity tetst uses a Particle Size Analyzer (PSA) tool. The method is to dilute 1 mL of the nanoemulsion preparation in 250 mL of Aqua Pro injection, the diluted preparation is placed in a cuvette and the data coming out of the PSA device is observed. (Az-Zahra et al., 2022).

Emulsion type test

This test is carried out to determine the type of emulsion formed, including the type of oil in water (O/W) or water in oil (W/O). This test was carried out using a painting method using methylene blue.

Percent transmittance test

This test was carried out using UV-vis spectrophotometry with a dilution of 1:100 using aqua deion solvent. The aim is to see the clarity of the nanoemulsion; the acceptance range is 90–100% (Aprilya et al., 2021).

Physical stability test

The physical stability test was carried out using the cycling test method. The test was carried out by storing the preparation at a low temperature of 4ºC and a high temperature of 40ºC. With six cycle repetitions, each storage time is 48 hours (Ma'arif et al., 2023). The chia seed oil nanoemulsion hair serum formulation was stored at a low temperature of 4º C in the refrigerator and a high temperature of 40º C in the oven. The cycle was repeated for 6 cycles where each cycle was stored for 48 hours and observed whether there were any changes or instability that occurred in the nanoemulsion preparation.

After the preparation was stored for 6 cycles, the preparation was observed organoleptically, pH, and homogeneity to determine the stability of the preparation (Pratiwi et al., 2018).

Data Analysis

Data were analyzed using SPSS with one sample t-test to verify the predicted and experimental data if the data is usually distributed and the Wilcoxon if it is not normally distributed. Further data analysis was carried out on stability data using paired t-test samples. The p-value>0.05 indicates that the data is not significantly different. Based on the results of the pH response normality test, particle size, zeta potential, polydispersity index and percent transmittance data normally distributed so it uses a one sample t-test. Whereas for viscosity response data is not normally distributed in the normality test so Wilcoxon test was used. The results of data analysis show the significance value of the pH response 0.500; particle size response 0.500; viscosity response 0.276; zeta potential response 0.500; polydispersity index response 0.500; and the percent transmittance response is 0.500. The p value>0.05 indicates that there is no significant difference between prediction results with experimental results (Taufik et al., 2023).

RESULT AND DISCUSSION

Results of formula rationalization

Rationalization, in this case, means designing the ingredients used in the dosage formulation based on valid and relevant literature (Illu, 2020). The results of the rationalization of the formula are shown in Table 1.

Table 1. Nanoemulsion hair serum formula

Raw Material	Function
Chia Seed Oil	Active ingredients
Tween 80	Surfactant
Span 80	Surfactant
Propylene glycol	Cosurfactant
Methylparaben	Preservative
Propylparaben	Preservative
Sodium metabisulfite	Antioxidant
Aquadest	Solvent

Simplex Lattice Design (SLD) method formula optimization results

The simplex lattice design method requires researchers to enter the material components to be optimized by determining the upper and lower limits for each material. The mixed designs can contain anywhere from 2 to 30 materials or components where all components must have the same range. The results of the expert design formula are shown in Table 2.

The material components used in this research are compound X1, Tween 80, with a lower limit of 1 and an upper limit of 35%. Component X2 is propylene glycol, with a lower limit of 5% and an upper limit of 80% (Rowe et al., 2009). The total used for these two materials was 80. The determination of the total of these materials was adjusted to the researcher's wishes. Every two materials or components entered will produce eight runs of the prediction formula, as presented in Table 2. In addition, in these 8 formulas there are 3 similar formulas, this formula equation serves to increase the accuracy of the formulas produced by Design Expert. The responses entered will be coded with the letter Y. The value of each response is obtained from the laboratory experiments' results.

Table 2. Formula design expert results

Run	X1	X2	Y1	Y2	Y3	Y4	Y5	Y6
	Tween 80 (%)	Propylene glycol (%)	pH	Particle size (nm)	Viscosity (cPs)	Zeta potential (mV)	Polydis-persity index	Transmittance (%)
1	1	79	4.48	374.88	68.57	5.8	0.1181	25.508
2	35	45	6.40	104.40	157.27	16.5	0.1231	95.423
3	18	62	6.16	807.95	102.07	53.7	0.0233	69.039
4	9.5	70.5	5.62	172.70	96.16	9.6	0.1172	30.716
5	1	79	4.48	374.88	68.57	5.8	0.1181	25.508
6	35	45	6.40	104.40	157.27	16.5	0.1231	95.423
7	18	62	6.16	807.95	102.07	53.7	0.0233	69.039
8	26.5	53.5	6.26	307.26	117.20	5.9	0.3440	59.245

Design expert prediction optimum formula recommendation results

The optimum formula results were obtained after the selected model was significant, and analysis was carried out on each response. Determining the optimum formula is based on the formula that has the highest desirability value. The desirability value refers to the value of the optimization objective function. This value shows the program's ability to determine the formula according to the parameters set by the researcher. A desirability value close to 1 indicates that the formula is increasingly optimal. The results of the Design Expert's optimal prediction formula are presented in Table 3. In the optimization results, the optimum formula is shown in the gray area where the resulting desirability value is 0.947, which indicates that the desirability value is close to 1, which means the formula is the most optimal predicted formula result.

Optimum formula validation and verification results

Validation was carried out on the optimum hair serum nanoemulsion formula by preparing three replications, and the results were obtained, as shown in Table 4. Then, the stage continued with verification by comparing the predicted results with experimental results using the parametric one-sample t-test if the data was distributed normally and the Wilcoxon test if the data was not normally distributed. The test was carried out with the help of SPSS version 20 software. The results of the data analysis showed a significant value for the pH response of 0.500, particle size response of 0.500, viscosity response of 0.276, potential zeta response of 0.500, polydispersity index response of 0.500, and the percent transmittance response of 0.500. In the viscosity response test, the data obtained in the replication was not normally distributed, so the test was carried out using the Wilcoxon method. The p-value> 0.05 indicates no significant difference between the predicted and experimental results (Taufik et al., 2023). The optimum formula verification results are shown in Table 4.

Table 3. Design Expert 13 optimal prediction formula

Material Components (X)		Predicted Value of Response Variable (Y)						
Tween 80 (%)	Propylene glycol (%)	pH	Particle size (nm)	Viscosity (cPs)	Zeta potential (mV)	Polydis-persity index	Trans-mittance (%)	Desirability Value
33.52	46.48	6.37	176.958	147.14	17.125	0.287	90.00	0.947 (suggested)
26.50	53.50	6.29	454.576	116.00	32.079	0.344	75.85	0.626
13.26	66.74	5.92	605.654	99.37	33.635	0.023	49.18	0.325

Table 4. Optimum formula verification results

Response Parameters (Y)	Prediction	Experiment Results ($\bar{X}$ ± SD)	*p-value*	Information
pH	6.37	6.43 ± 0.015	0.500	Not significant difference
Particle size (nm)	176.96	130.29 ± 19.542	0.500	Not significant difference
Viscosity (cPs)	147.14	145.20 ± 1.617	0.297	Not significant difference
Zeta Potential	17.13	36.70 ± 29.444	0.500	Not significant difference
Polydispersity Index	0.287	0.274 ± 0.148	0.500	Not significant difference
Percent Transmittance (%)	90.00	95.16 ± 3.314	0.500	Not significant difference

Note: $\bar{X}$ = average
SD = Standard Deviation

Optimum formula characteristic results

Physical characteristics were carried out to compare the physical parameter values of the optimum hair serum nanoemulsion chia seed oil formula obtained with the predetermined acceptance range. Observation data are presented in Table 5.

Based on the results of physical characteristic tests on the optimum formula for chia seed oil nanoemulsion hair serum preparations, the optimum formula meets all physical characteristic tests for each parameter. In the organoleptic test, the light yellow color of the preparation was due to the composition of ingredients, which were mostly yellow, including chia seed oil, which had a clear yellow color, Span 80, which had a yellow color, and Tween 80, which had a yellow color. Adding propylene glycol as a cosurfactant can make the preparation more straight forward. The addition of appropriate surfactants and cosurfactants plays a role in reducing the interfacial tension between the oil and water phases so that phase separation does not occur and a homogeneous preparation is obtained in the homogeneity test (Figure 1).

Figure 1. Observation results of homogeneity and organoleptic tests of preparations

Table 5. Optimum formula characteristic test results

Parameter	Optimum Formula ($\bar{X}$ ± SD)	Acceptance
Organoleptic	Light yellow, liquid, characteristic smell of chia seed oil, clear, and no phase separation	-
Homogeneity	Homogeneous	Homogeneous
pH	6.43 ± 0.015	4.5 – 7
Particle size (nm)	130.29 ± 19.542	10 – 1000
Emulsion type	Oil in water (O/W)	Oil in water (O/W)
Viscosity (cPs)	145.20 ± 1.617	10 – 2000 cPs
Zeta potential (mV)	36.70 ± 29.444	(-30 mV) – (+30 mV)
Polydispersity Index	0.274 ± 0.148	0 – 1
Transmittance (%)	95.160 ± 3.314	90 %-100%

Note: $\bar{X}$ = average
SD = Standard Deviation

The physical appearance of the preparation is shown in Figure 2. The results obtained in the organoleptic test meet the characteristics of nanoemulsion, namely clarity and transparency. The organoleptic characteristics of a preparation can influence consumer acceptance of the product (Xu et al., 2022). In the optimum formula formulation, the preparation is replicated three times to increase the accuracy of the formula created and show that the test results obtained are not biased. As shown in Figure 2, the first bottle is the optimum formula for replication 1, then the next bottles are the optimum formula for replication 2 and 3.

In the pH test, it is known that the preparation meets the required pH range, namely by the topical pH of the skin. The Tween 80 surfactant used in this research has a pH that tends to be alkaline, namely (6–8), so increasing the concentration of Tween 80 surfactant tends to increase the pH value of the preparation. Meanwhile, the cosurfactant used, namely propylene glycol, tends to have an acidic pH (3-6), so the optimum composition between the use of surfactant and cosurfactant can produce a pH that meets the requirements (Bagiana et al., 2017).

Figure 2. Physical appearance of the optimum hair serum nanoemulsion chia seed oil formula

In the test using the Particle Size Analyzer (PSA) instrument, three test data were obtained, namely the particle size test, polydispersity index test, and zeta potential test. In the particle size test, it was discovered that the preparation had nano-sized particles by the standardized acceptance criteria. Tween 80 surfactants play a role in reducing particle size by reducing the amount of free energy between surfaces and forming a mechanical barrier that prevents particle aggregation (Pratiwi et al., 2018). Propylene glycol cosurfactant itself functions to prevent nanosized particles from recombining through

a steric barrier formation mechanism so that the right combination of surfactant and cosurfactant will produce a nanoemulsion preparation with a stable nanometer size. The polydispersity index value in this preparation is classified as monodisperse because it has a polydispersity index value of <0.3, which means the particle size is uniform. The particle size distribution is narrow, so the preparation will be more stable in storage (Handayani et al., 2018). The polydispersity index tends to be influenced by the stirring speed, where the right stirring speed will produce a dosage value with a good polydispersity index (Faizatun et al., 2020). The zeta potential value of the chia seed oil nanoemulsion preparation meets the required criteria, namely >30 mV; this indicates that the preparation has good electrostatic stability (Handayani et al., 2018). The use of surfactants and cosurfactants does not influence the negative charge on the zeta potential value; this is because Tween 80 and propylene glycol are nonionic compounds (no charge); the negative charge is produced from the collision of droplets with the dispersing phase containing hydroxyl ions (OH-), thus creating preparations tend to have a negative charge.

In the emulsion type test, the preparation was an O/W emulsion type. For topical use, the O/W emulsion-type nanoemulsion was more suitable because it was not sticky and, as a hair serum, did not leave crusts on the scalp (Rahmayanti et al., 2023). The type of O/W emulsion is influenced by the highest concentration of nanoemulsion constituents, which tend to be polar, namely Tween 80, a hydrophilic nonionic surfactant, and propylene glycol, which is polar. The correct surfactant and cosurfactant composition influences the HLB value, so the oil phase can be dispersed evenly in the distilled water because the surface tension can be reduced. This makes methylene blue, which is polar, completely soluble to produce an O/W emulsion type (Dzakwan & Priyanto, 2019). The HLB value used in this research is HLB 12, which can produce O/W type nanoemulsions.

In the viscosity test, the chia seed oil nanoemulsion hair serum preparation was in accordance with the acceptance criteria for a good preparation. Viscosity is the main parameter of rheology, which is related to flow resistance (Nicolini et al., 2021). Components that influence the viscosity of the preparation are Tween 80 and propylene glycol, where increasing the concentration will cause the viscosity of the preparation to also increase. Tween 80's mechanism for increasing viscosity is by reducing the movement between globules, which causes the globule diameter to decrease and the particle size to become smaller, which causes the surface area to become larger and the resistance of the nanoemulsion to also increase so that the viscosity increases (Zulfa et al., 2019). The increase in viscosity is also influenced by propylene glycol, a cosurfactant, which will help increase the bond between the surfactant, oil phase, and water phase, which causes resistance to flow to become greater (Yuliani et al., 2016). The use of cosurfactant and surfactant composition in this optimum formula is correct, as proven by the viscosity value of the preparation, which meets the requirements.

Optimum formula physical stability test results

Stability testing is one of the quality parameters. It is carried out to determine the ability of a product to survive within specified specification limits throughout the storage and use period. Several factors can influence the stability of a product, namely temperature and time. In this research, stability tests were carried out at 4ºC and 40ºC for six cycles, where one cycle consisted of 48 hours (Ma'arif et al., 2023). The stability test results are shown in Table 6.

The physical stability test using the cycling test method shows that the preparation remains stable during the storage period in the homogeneity and organoleptic tests. In the descriptive pH test, there was a decrease in pH. The significance of the data determined with a paired t-test was carried out. The requirements for carrying out a parametric paired t-test are that the data is normally distributed and homogeneous. Based on the normality test results using Shapiro Wilk, the p-value before stability was 0.637; after stability, it was 0.463. The homogeneity test shows a p-value of 0.519. The p value > 0.05 in the normality and homogeneity test indicates that the resulting data is normally and homogeneously distributed. Testing continued with the paired t-test; in this test, a tailed sig.2 value of 0.27 was obtained. The p-value > 0.05 indicates that the pH test data before and after physical stability did not show a

significant change. It means that the nanoemulsion hair serum preparation is also pH stable using the cycling test method during the storage period. A stable preparation indicates that the components used are correct; apart from that, the oxidation process can also be inhibited by the presence of the antioxidant sodium metabisulfite through its interaction with the carbonyl group in the material to produce melanoidin, thereby preventing the oxidation process from occurring (Taufik et al., 2023).

Table 6. Optimum Formula characteristic test results

Parameter	Cycle-0 ($\bar{X}$ ± SD)	Cycle-6 ($\bar{X}$ ± SD)
Organoleptic	Light yellow, liquid, characteristic smell of chia seed oil, clear, and no phase separation	Light yellow, liquid, characteristic smell of chia seed oil, clear, and no phase separation
Homogeneity	Homogeneous	Homogeneous
pH	6.43 ± 0.015	6.37 ± 0.021

Note: $\bar{X}$ = average
SD = Standard Deviation

CONCLUSION

The optimum composition of surfactant (Tween 80) and cosurfactant for the preparation of chia seed oil nanoemulsion hair serum (*Salvia hispanica* L.) based on formula optimization using the Simplex Lattice Design (SLD) method is 33.52%: 46.48% with a desirability value of 0.947. The optimum formula's physical characteristics and stability for the chia seed oil nanoemulsion hair serum preparation fulfill all the physical parameter requirements for good preparation.

ACKNOWLEDGEMENT

Thanks to the Research Unit and Community Service (UPPM) FKIK UIN Malang, who has funded research with a budget for DIPA FKIK UIN Maulana Malik Ibrahim Malang.

REFERENCES

Aprilya, A., Rahmadevi, R., & Meirista, I. (2021). Formulasi nanoemulsi dengan bahan dasar minyak ikan (Oleum Iecoris Aselli). *Jurnal Sains Dan Kesehatan*, *3*(3), 370–375. https://doi.org/10.25026/jsk.v3i3.309

Az-Zahra, A. P., Wijayanti, F., Ramadhanti, L., & Faizal, I. A. (2022). Formulasi dan evaluasi nanoemulsi minyak ikan Sidat dengan menggunakan metode Sonikasi. *Pharmaqueous*, *4*(2).

Bagiana, I. K., Suwarmi, & Inayah. (2017). Optimasi tween 80 dan span 80 dalam sediaan krim ekstrak etanol daun Iler (Coleus atropurpureus (L) Benth) dan aktivitas antibakteri Staphylococcus aureus ATC 25923. *Majalah Farmasi Indonesia*, *10*(2), 896–905.

Collins, E., Rollando, & Monica, E. (2023). Pembuatan serum penumbuh rambut kombinasi minyak Kemiri (Aleurites moluccanus) dan ekstrak buah Apel (Pyrus malus L.). *Jurnal Farmasi Ma Chung: Sains, Teknologi, Dan Klinis Komunitas*, *1*(1), 32–41. https://doi.org/10.33479/jfmc.v1i(1).6

Dzakwan, M., & Priyanto, W. (2019). Peningkatan kelarutan fisetin dengan teknik kosolvensi. *Parapemikir : Jurnal Ilmiah Farmasi*, *8*(2), 5. https://doi.org/10.30591/pjif.v8i2.1388

Faizatun, F., Gangga, E., Anindita, S., Martati, T., & Miftahurrohmah, N. (2020). Formulation of NLC Gel from Callus Mulberry leaf extract induced by NAA and BAP. *Jurnal Ilmu Kefarmasian Indonesia*, *18*(1), 123–129. https://doi.org/10.35814/jifi.v18i1.814

Gamage, D. G. N. D., Dharmadasa, R. M., Abeysinghe, D. C., Wijesekara, R. G. S., Prathapasinghe, G. A., & Someya, T. (2022). Global perspective of plant-based cosmetic industry and possible contribution of Sri Lanka to the development of herbal cosmetics. *Evidence-Based Complementary and Alternative Medicine*, *2022*, 1–26. https://doi.org/10.1155/2022/9940548

Handayani, F. S., Nugroho, B. H., & Munawiroh, S. Z. (2018). Optimasi formulasi nanoemulsi minyak biji anggur energi rendah dengan d-optimal mixture design (DMD). *Jurnal Ilmiah Farmasi*, *14*(1), 17–34. https://doi.org/10.20885/jif.vol14.iss1.art03

Hidayat, I. R., Zuhrotun, A., & Sopyan, I. (2020). Design-expert software sebagai alat optimasi formulasi sediaan farmasi. *Majalah Farmasetika*, *6*(1). https://doi.org/10.24198/mfarmasetika.v6i1.27842

Illu, J. (2020). Pengaruh rasionalisasi terhadap relasi interpersonal. *Phronesis: Jurnal Teologi Dan Misi*, *2*(1), 74–82. https://doi.org/10.47457/phr.v2i1.33

Ma'arif, B., Rani Azzahara, Fahrul Rizki, Arief Suryadinata, Abdul Wafi, Novia Maulina, & Hajar Sugihantoro. (2023). Formulasi dan karakterisasi nanoemulsi ekstrak etanol 70% daun Semanggi (Marsilea crenata C. Presl.). *Medical Sains : Jurnal Ilmiah Kefarmasian*, *8*(2), 733–746. https://doi.org/10.37874/ms.v8i2.731

Magfirah, M., Hamdi Angka, M., & Rizka. (2022). Pemanfaatan kembang Sepatu sebagai shampountuk perawatan rambut rontok. *Jurnal DiMas*, *4*(1), 25–28. https://doi.org/10.53359/dimas.v4i1.37

Nicolini, A., Gonçalves Maciel, V., da Silva Andrade Neto, J., Roca Bragança, S., & Maldaner Jacobi, M. (2021). Rheological behavior of fresh latex polymeric mortar by squeeze-flow technique. *Construction and Building Materials*, *267*, 121175. https://doi.org/10.1016/j.conbuildmat.2020.121175

Noor, S. M. (2018). *Optimasi titik lebur pada sediaan lipstik kulit Buah Naga Merah (Hylocereus polyrhizius) menggunakan metode D-Optimal Mixture. (Skripsi)*. Universitas Brawijaya.

Pratiwi, L., Fudholi, A., Martien, R., & Pramono, S. (2018). Physical and chemical stability test of SNEDDS (Self-nanoemulsifying Drug Delivery System) and nanoemulsion ethyl acetate fraction of garcinia mangostana L. *Majalah Obat Tradisional*, *23*(2), 84. https://doi.org/10.22146/mot.28533

Rahmayanti, M., Nastiti, G. P., & Fitri, M. A. (2023). Formulasi dan uji stabilitas sediaan hair Emulsion minyak Biji Chia (Salvia hispanica) dengan kombinasi tween 80 dan span 80 sebagai emulgator. *Jurnal Mandala Pharmacon Indonesia*, *9*(1), 10–19. https://doi.org/10.35311/jmpi.v9i1.356

Rowe, R. C., Sheskey, P. J., & Quinn, M. E. (2009). *Handbook of pharmaceutical excipients* (Sixth Edit). USA: Pharmaceutical Press.

Rusdi, M. (2017). Karakteristik ukuran partikel dan indeks polidispersitas formulasi nanoemulsi pewarna alam ekstrak kayu Secang (Caesalpinia Sappan Linn). *Jurnal Pertanian Terpadu*, *5*(2), 114–127. https://doi.org/10.36084/jpt..v5i2.132

Sanaji, J. B., & Liananda3, M. S. K. dan F. R. (2019). Pengaruh konsentrasi tween 80 sebagai Surfaktan terhadap karakteristik fisik sediaan Nanoemulgel ibuprofen. *Indonesian Journal of Chemical Science and Technology*, *6*(2), 89–91.

Segura-Campos, M. R., Ciau-Solís, N., Rosado-Rubio, G., Chel-Guerrero, L., & Betancur-Ancona, D. (2014). Physiocemical Characterization of chia (Salvia hispanica) Seed Oil from Yucatan Mexico. *Agricultural Sciences*, *05*(03), 220–226. https://doi.org/10.4236/as.2014.53025

Sofwan, A. G., Hafizullah, A., Adiansyah, A., & Tampubolon, R. R. (2017). Pengaruh minyak Sawit Merah (Rpo) dan minyak Zaitun murni (EVOO) terhadap pertumbuhan rambut pada Kelinci. *Jurnal Farmanesia*, *4*(2), 105–109. https://doi.org/10.51544/jf.v4i2.2710

Taufik, I. I., Soewandhi, S. N., & Nugraha, Y. P. (2023). Optimasi formula emulgel vitamin C dengan pendekatan Simplex Lattice Design. *Jurnal Sains Farmasi & Klinis*, *10*(1), 145. https://doi.org/10.25077/jsfk.10.1.145-154.2023

Vakhariya, R. R., Oza, S. A., Bhingardeve, C. S., Patil, S. J., Mujawar, S. F., & Mohite, D. S. K. (2022). Formulation, development and evaluation of Herbal hair serum: a classical approach to enhance hair quality. *International Journal of Pharmaceutical Sciences Review and Research*, 100–103. https://doi.org/10.47583/ijpsrr.2022.v76i02.017

Xu, L., Sun, D.-W., Tian, Y., Sun, L., Fan, T., & Zhu, Z. (2022). Combined effects of radiative and evaporative cooling on fruit preservation under solar radiation: sunburn resistance and temperature stabilization. *ACS Applied Materials & Interfaces*, *14*(40), 45788–45799. https://doi.org/10.1021/acsami.2c11349

Yuliani, S. H., Hartini, M., Stephanie, Pudyastuti, B., & Istyastono, E. P. (2016). Comparison of physical stability properties of pomegranate seed oil nanoemulsion dosage forms with long-chain triglyceride

and medium-chain triglyceride as the oil phase. *Traditional Medicine Journal*, *21*(2), 93–98.

Zulfa, E., Novianto, D., & Setiawan, D. (2019). Formulasi nanoemulsi natrium diklofenak dengan variasi kombinasi tween 80 dan span 80: kajian karakteristik fisik sediaan. *Media Farmasi Indonesia*, *14*(1), 1471–1477.

Pharmaciana
Vol.14, No.3, Nov 2024, Page. 382-395
ISSN: 2088 4559; e-ISSN: 2477 0256
DOI: 10.12928/pharmaciana.v14i3.29237

Development of standardized green coffee bean extract (*Coffea canephora*) into effervescent granules as an antioxidant supplement

Andre Wijaya, Farida Lanawati Darsono*, Kuncoro Foe
Faculty of Pharmacy, Widya Mandala Surabaya Catholic University,
Jl. Raya Kalisari Selatan No 1, Surabaya, East Java, Indonesia

Submitted: 25-06-2024 ***Reviewed: 25-09-2024*** ***Accepted: 08-11-2024***

ABSTRACT

This study aims to obtain the optimum formula for green coffee extract effervescent granules (EG-GCE). Dry extract is obtained by percolation using water as a solvent and a spray dryer drying system. Specific and non-specific standardization is carried out to ensure the quality of dry green coffee extract. The dose of the dried extract of green coffee used in the granule effervescent was 250 mg each sachet. EG-GCE was formulated using wet granulation method. The quality of effervescent granules was determined based on physical quality tests and the effectiveness of antioxidant power (IC_{50} value) with DPPH reagent using a microplate reader. The optimum effervescent granule formula uses a factorial design method combining monohydrate citric acid and tartaric acid. As a response includes water content, flow rate, and effervescent granule dissolution time test. Furthermore, the data from the parametric experiments between bets and between formulas were analyzed using the One Way ANOVA (Yate's Treatment) statistical method. The test will continue using the Tukey post-hoc test method if there is a significant difference in the statistical analysis between formulas. The pH value of resulting EG-GCE products was within the range of 5.46-6.07, moisture content: 3.12-3.67%, flow rate: 25.78-28.53 g/s, angle of repose: 25.65-30.13°, Hausner ratio: 1.14-1.22, Carr's index: 12.50–17.83%, dissolving effervescent granule time test: 1.00-1.33 min. This study demonstrated that citric acid monohydrate, tartaric acid, and their interaction affected the moisture content, flow rate, and effervescent time of EG-GCE. The proportion of citric acid monohydrate (9.94%) and tartaric acid (17.46%) was found to be the optimum formula of EG-GCE, with the following responses: moisture content 3.26%, flow rate 25.72 g/s, and dissolving effervescent granule time test 1.19 min. The optimum formula show strong antioxidant activity with IC_{50} free of radical scavenging 56.56 ± 0.97 µg/mL.

Key words: antioxidant**,** effervescent granules, green coffee, factorial design, citric acid monohydrate, tartaric acid

Corresponding author:
Farida Lanawati Darsono
Faculty of Pharmacy, Widya Mandala Catholic University Surabaya
Jl. Raya Kalisari Selatan No 1, Surabaya, East Java, Indonesia
Email: farida@ukwms.ac.id

INTRODUCTION

Oxidative stress is a condition with a decrease in endogenous antioxidant capacity and an increase in free radicals (reactive oxygen species - ROS) (Di Domenico et al., 2019). Free radicals are unstable reactive molecular species formed from natural metabolic processes that act as reducing agents or oxidants (Flieger et al., 2021). Free radicals have an impact on the pathogenesis of many diseases due to prolonged oxidative stress conditions triggered by increased free radicals causing cell damage (Flieger et al., 2021). Therefore, exogenous antioxidant supplementation is needed, such as bioactive polyphenolic compounds which can ward off free radicals to prevent oxidative stress conditions. One of the polyphenolic compounds that has antioxidant properties is chlorogenic acid (Boccellino & D'Angelo, 2020; Galanakis et al., 2020; Lammi & Arnoldi, 2021).

Pimple et al (2020) stated that chlorogenic acid is often found in robusta coffee beans at a concentration of around 7-14%. Green coffee has higher antioxidant activity because it does not undergo a roasting process, which risks degrading chlorogenic acid polyphenolic compounds (Asbaghi et al., 2020). The two types of coffee that dominate the global market include arabica coffee (*Coffea arabica*) and robusta coffee (*Coffea canephora*) (Cui et al., 2020; Faria et al, 2020).

Green coffee contains polyphenol compounds (Ohishi et al., 2021) which show stability at temperatures of 160-200 °C, so during the drying process with an oven at a temperature of 45°C it does not affect the stability of polyphenol compounds (Abrahão et al., 2019 ; Piñón-Balderrama et al., 2020).

Robusta coffee contains the highest levels of chlorogenic acid compared to other coffee species (Pereira et al., 2021). Based on previous research, the chemical compounds found in green coffee include chlorogenic acid (6.7-9.2%), and caffeine (0.9-1.3%) (Pimpley et al., 2020). Green coffee was chosen because it has a higher polyphenol content than roasted coffee (Asbaghi et al., 2020).

Considering that green coffee robusta (*Coffea canephora*) contains high levels of chlorogenic acid, this research carried out the development of a health supplement formula containing dry extract of green coffee robusta (*Coffea canephora*) at a selected dose of 250 mg per sachet in the form of effervescent granules (Gorji et al., 2019 ; Sudeep & Shyam Prasad, 2021). Dry extract of green coffee may reduce the degradation of secondary metabolites caused by microorganisms in extract containing high water content (Lima et al., 2020) reported that the green coffee extract (GCE) formulated as effervescent granules may increase the release, absorption, and bioavailability of the bioactive compounds.

The development of green coffee into quality effervescent granules is largely determined by the composition of the acid source and base source. The combination of acid sources commonly used is citric acid monohydrate and tartaric acid (Bertuzi, 2021). Citric acid monohydrate can increase the stability and extend the storage period of effervescent granule preparations (Bertuzi, 2021). Meanwhile, sodium bicarbonate can cause a stronger effervescent reaction (Bertuzi, 2021). In effervescent formulations, the amount of tartaric acid used in the formula must be higher than citric acid, to achieve the correct stoichiometric equivalence, where tartaric acid is a diprotic acid, while citric acid is a triprotic acid (Bertuzi, 2021). The ideal combination of acid sources with a composition of citric acid monohydrate, tartaric acid, and sodium bicarbonate in a ratio of 1:2:3.4. An incorrect ratio will cause citric acid to form a sticky powder mixture making it difficult to granulate, while tartaric acid tends to produce brittle granules. In this study, the manufacture of effervescent granules used the wet granulation method because this method can provide better uniformity of active ingredients and improve the flow properties and porosity of the granules (Bertuzzi, 2021).

Based on the above, it is necessary to optimize the combination of acid sources to produce an optimal effervescent granule dosage formula using the factorial design method. The first factor is citric acid monohydrate and the second factor is tartaric acid with the selected responses including flow rate, water content, and dissolving time. The response of water content and dissolving granule effervescent time was chosen because both affect the granule flow rate, where the granule flow rate gets worse when the water content is high (Maysarah et al, 2020). The concentration of citric acid monohydrate used for formula optimization with a lower limit level (-1) of 8% an upper limit level (+1) of 12% and a concentration of tartaric acid for the lower limit level (-1) of 16% and an upper limit level (+1) of 24%. Determining the specification range in the optimization process refers to general requirements in the

literature and compendiums and is also based on test results on the innovator's product. This study aimed to obtain the optimum formula for effervescent granules containing green coffee extract.

MATERIALS AND METHODS

In this study green coffee bean (*Coffea canephora*) dry extract was obtained from PT. Haldin Pacific Semesta (Indonesia). The dry extract was prepared by spray drying method without fillers and preservatives. Other materials used in this study were as follows: citric acid monohydrate (Weifang Ensign Industry Co., Ltd., China), tartaric acid (Badische Anilin- und SodaFabrik, Germany), sodium bicarbonate (Chruch and Dwilight Co., Inc., USA), PVP K-30 (Badische Anilin- und SodaFabrik, Germany), maltodextrin (Qin Huang Dao LiHua Starch Co., Ltd., China), aspartame (Shandong Tianjiao Biotech Co., Ltd., China), ethanol, and distilled water.

Standardization of dry extracts

The main ingredient used in this research is a dry water extract of green coffee (*Coffea canephora*) obtained from PT. Haldin Pacific Semesta, Bekasi. The quality of the dry extract obtained needs to be guaranteed before use, using specific (i.e visual form, color, smell, flavor, pH of 1% w/v solution, water soluble extract level, and ethanol soluble extract level) and non-specific standardization (i.e total ash content, acid insoluble ash content, water content).

.

Factorial experimental design

The number of effervescent granules of green coffee extract (EG-GCE) formula was determined according to a complete 2^2 factorial design. The factors studied in this study were citric acid monohydrate (8-12%) as X_A and tartaric acid (16-24%) as X_B. Both factors studied were independent of each other. The following responses were evaluated: flow rate (Y_1), moisture content (Y_2), and effervescent time (Y_3).

Formulation of EG-GCE

In this study, effervescent granules was formulated using wet granulation method. The proportion of citric acid monohydrate and tartaric acid as an acid source was 1:2, whereas sodium bicarbonate was used as a base source, as used by previous investigator. The optimum proportion of citric acid monohydrate and tartaric acid as an acid source was analysed by factorial design using Design Expert 12.0.3. The resulting EG-GCE was evaluated, including organoleptic, pH value after reconstitution, flow properties, moisture content, and dissolving effervescent time. According to the factorial experimental design, EG-GCE was formulated in four different formula (Table 1). Citric acid monohydrate, tartaric acid, and sodium bicarbonate were mixed and heated at 60 ^oC for approximately 3 hours. The purpose of heating is to remove hydrates, which reduces the risk of hygroscopicity and makes formulation easier. The mixture was subsequently crushed and mixed with other excipients. The mixture of excipients and GCE was mixed and binded with ethanolic solution of PVP K-30. The mixture was then sieved through mesh number 18 sieve. The wet granules obtained was then driedat 45 ^oC for approximately 3 hours or until the moisture content measured was lower than 5%.Finally, the EG-GCE was sieved with a mesh number 20 sieve.

Table 1. Formula of EG-GCE

Ingredients	Weight (g)			
	Formula-1(F-1)	Formula a(Fa)	Formula b(Fb)	Formula ab(Fab)
Green coffee extract	0.25	0.25	0.25	0.25
Citric acid monohydrate	**0.32**	**0.48**	**0.32**	**0.48**
Tartaric acid	**0.64**	**0.64**	**0.96**	**0.96**
Sodium bicabonate	1.24	1.24	1.24	1.24
Aspartame	0.12	0.12	0.12	0.12
PVP K-30	0.08	0.08	0.08	0.08
Maltodextrin	ad 4	ad 4	ad 4	ad 4
Water for reconstitution	250 mL	250 mL	250 mL	250 mL

Evaluation of the quality of EG-GCE before reconstitution

Organoleptic

The organoleptic test was carried out visually, namely by observing the physical form of the green coffee dry extract effervescent granule (EG-GCE) preparation before it was dissolved, including observing the color, shape, and odor of the EG-GCE preparation. The organoleptic requirements for EG-GCE are that they are granular, yellowish-white, and have a distinctive coffee aroma.

Flow rate test

The purpose of the flow rate test is to determine the flow of granules directly (Maysarah et al., 2020). Flow speed tests were carried out using the funnel method referring to (Taylor & Aultons, 2022) with modifications. A total of 100 grams of effervescent granules were weighed and placed in a funnel with the end closed after that the funnel cover was opened, and the effervescent granules were allowed to flow until they ran out. The granule flow time is calculated using a stopwatch fromthe time the funnel cover is opened and stopped when the granules have finished flowing. The flow rate test was carried out three times in replication using equation 1. Effervescent granules have good flow properties if the granule flow rate is more than 10 grams/second (Tanjung et al, 2023). The flow rate specification for EG-GCE based on requirements is 27.50 ± 2.00 grams/second (U.S Pharmacopeia, 2020). The following Equation 1 is used to calculate the flow rate.

$$\text{Flow rate} = \text{Granule weight} / \text{Flow time} \quad \text{.....(1)}$$

Angle of repose

The purpose of the angle of repose test is to determine the flow of granules indirectly (Maysarah et al., 2020). The angle of repose test was carried out using the funnel method referring to (Taylor & Aulton, 2021) with modifications. A total of 100 grams of effervescent granules were weighed and placed in a funnel with the end closed after the funnel cover opened, and the effervescent granules were allowed to flow until they ran out, after which the angle formed was measured. The angle of repose test was carried out three times in replication using equation 2. Effervescent granules have good flow properties when forming an angle of repose between 25-40º (Taylor & Aulton, 2021; U.S Pharmacopeia, 2020). The Equation 2 used to calculate the angle of repose:

$$\tan \alpha = \text{cone height} / \text{radius of the base of the cone} \quad \text{.....(2)}$$

Hausner ratio

The Hausner ratio test aims to determine the flow properties of granules indirectly which are influenced by friction between particles (Taylor & Aulton, 2021). The Hausner ratio test is determined based on the compressible density and bulk density parameters. The compressible density and bulk density of the effervescent granules are determined first. A measuring cup with a volume of 100 mL is weighed (W1), then the effervescent granules are slowly added to the 100 mL mark (V1) and weighed again (W2). Next, the mouth of the measuring cup is plugged, the measuring cup is installed on the test tool, and the motor is run for the first 5 minutes, and the volume is measured (V5), and then the motor is run again until the twelve minute and the volume is measured (V12). Next, calculate the bulk density first and then the compressible density, and then calculate the Hausner ratio using Equation 3. The Hausner ratio specification for EG-GCE is 1.00-1.25 (U.S Pharmacopeia, 2020). The following Equation 3 is used to calculate the Hausner ratio.

Hausner ratio = *Tapped Density* (ρt) / *Bulk Density* (ρb) ……....(3)

Carr's Index

The purpose of the Carr's index test is to determine the flow properties of granules indirectly, and the compressibility of granule preparations based on the compressible density parameters and bulk density of granule preparations referring to (Taylor and Aultons, 2022) with modifications. The compressible density and bulk density of the effervescent granules are determined first. A measuring cup with a volume of 100 mL is weighed (W1), then the effervescent granules are slowlyadded to the 100 mL mark (V1) and weighed again (W2). Next, the mouth of the measuring cup is plugged, the measuring cup is installed on the test tool, and the motor is run for the first 5 minutes, and the volume is measured (V5), and then the motor is run again until the twelve minute and the volume is measured (V12). The change in volume that occurs (compressible volume) is recorded as (V2). After obtaining the results, they first calculate the bulk density and compressed density and then calculate Carr's index using equation 4. The Carr's index test was carried out three times in replication. The Carr's index specification for EG-GCE based on requirements is 1-20% (U.S Pharmacopeia, 2020). The Equation 4 is used to calculate the Carr's index:

$$\text{Carr's index} = \frac{\rho t - \rho b}{\rho t} \times 100 \quad \text{.....(4)}$$

Water content test

The purpose of the water content test is to determine the water content in the preparation. The water content test was carried out using a Moisture Analyzer tool referring to (Lima et al., 2020) with modifications. Approximately 3 grams of EG-GCE were put into the sample container, then the tool was run until the tool gave water content test results. The water content test was carried out three times in replication. The water content requirement for effervescent granules is ≤ 5% (Giyatmi & Lingga, 2019). The water content specification for EG-GCE based on requirements is 3.40 ± 0.30%.

Evaluation of the quality of green coffee dry extract effervescent granules (EF-GCE) after reconstitution

Organoleptic

The organoleptic test was carried out visually, namely by observing the physical form of the green coffee dry extract effervescent granule (EG-GCE) preparation after being dissolved, including observing the color, shape, and taste of the EG-GCE preparation after being dissolved, as well as observing the effervescent reaction through a microscope which was marked by the appearance of carbon dioxide gas bubbles. The organoleptic requirements for the EG-GCE solution are that it is a yellowish-white solution, has a sweet and sour taste, and forms carbon dioxide gas.

pH Value

The pH test used a pH meter refers to the research of (Jain & Patil, 2020) with modifications. The purpose of the pH test is to determine the acidity level of a preparation. Before taking pH measurements, the electrode is rinsed first with distilled water and dried. After that, calibration was done using a buffer solution of pH 4.0, 7.0, and 9.0. The calibrated electrode must be dried first so that can be used to measure the pH of the EG-GCE solution. The pH test was carried out by dissolving one sachet (4 grams) the EG-GCE in 250 mL of water at approximately 25 ℃ and continuing with pH testing. The pH test was carried out three times in replication. The pH specification for the EG-GCE solution based on the requirements is 6.00 ± 1.00.

Dissolving effervescent granule test

The dissolving effervescent granule time test aims to determine the time required for the preparation to dissolve completely in water. In this study, the late time test refers to the research of (Maysarah et al., 2020) with modifications. The dissolving effervescent granule was carried out by dissolving one sachet (4 grams) of EG-GCE granules in 250 mL of water at a temperature of approximately 25℃, the granules were considered to have dissolved when the release of carbon dioxide gas stopped. The solubility test was carried out three times in replication. The dissoving effervescent granule specification for EG-GCE based on requirements is 1.00 ± 0.50 minutes.

Antioxidant activity test

The antioxidant activity test in this research will be carried out on the optimum formula obtained based on the results of data analysis with the Design Expert program. Antioxidant activity test using the DPPH method refers to research by (Tasew et al., 2020) with modifications. The following are the stages of preparing the test solution.

Preparation of ascorbic test solution

In this study, ascorbic acid was used as a positive control. The stock solution was prepared by weighing 10 mg of ascorbic acid and dissolving it with 10 mL of mixed solvent (1,000 µg/mL). The ascorbic acid solution was then diluted using a volumetric flask to obtain four different concentrations, namely 75.00 µg/mL, 37.50 µg/mL, 18.75 µg/mL, and 9.38 µg/mL.

Preparation of green coffee dry extract (GCE) test solution

The main solution of dry green coffee extract is made by weighing 250 mg of GCE and dissolving it with 100 mL of mixed solvent (2,500 µg/mL). The first stock solution of GCE was then diluted using a volumetric flask to obtain four different concentrations, namely 75.00 µg/mL, 37.50 µg/mL, 18.75 µg/mL, and 9.38 µg/mL.

Preparation of dry green coffee extract effervescent garnule (EG-GCE) test solution

The test solution was made by dissolving one sachet of the preparation (equivalent to 250 mg of GCE) with 100 mL of mixed solvent (2,500 µg/mL). The test solution of EG-GCE was diluted using a volumetric flask to obtain four different concentrations, namely 75.00 µg/mL, 37.50 µg/mL, 18.75 µg/mL, and 9.38 µg/mL.

Mixing Test Solution and DPPH solution

DPPH stock solution is made by weighing 25 mg of DPPH dissolved in 25 mL of methanol, then vortexing until completely dissolved. After that, the DPPH stock solution was diluted by pipetting 1 mL of DPPH of the first stock solution and adding methanol to 25 mL (Tasew et al., 2020). Each diluted test solution reacted with a DPPH solution in a ratio of 1:4, while the control contained mixed solvent methanol: water (1:1% v/v) and DPPH solution. The mixture of the test solution and DPPH solution was left for thirty minutes in a dark place at room temperature until the reaction was complete. After that, the absorbance was observed using a UV-Vis spectrophotometer at a wavelength of 517 nm. The analysis was carried out three times in replication.

Statistical analysis

The experimental results were analyzed by one way ANOVA at a confidence level of 95% using IBM SPSS Statistics 25.0. The optimum formula of EG-GCE was determined by Yate's treatment using Design Expert version 12.0.3.

RESULT AND DISCUSSION

Results of standardization of green coffee dry extract (GCE)

The dry extract of green coffee (*Coffea canephora*) organoleptically has a brownish-green color and a distinctive coffee odor. The dry extract of green coffee is acidic with a pH value of 5.11 ± 0.03. The purpose of determining the levels of water-soluble extracts and ethanol-soluble extracts is to determine the compound content in certain solvents according to their level of polarity. The test results show that the percentage of water-soluble extract levels is higher than ethanol-soluble extract levels, which means that green coffee has a higher solubility in water than in ethanol solvent. The full results of the standardization of dried extracts can be seen in Table 2.

The active compound profile of GCE (*Coffea canephora*): chlorogenic acid was observed using thin layer chromatography under UV 254 and VIS 366 nm light. The active substance profile in the extract using the mobile phase Chloroform: Methanol: Formic Acid (44.1: 2.5: 2.15 %v/v) and the stationary phase silica gel 60 GF_{254} showed that green coffee extract contained chlorogenic acid. The stain detected under 366 nm has a value of Rf 0.37 for a fluorescent blue color is chlorogenic acid. The theoretical Rf values for the active substances chlorogenic acid was 0.40 respectively (Bojić et al., 2013). The complete result of the TLC profile can be seen in Figure 1. The Rf value that is different from the theoretical Rf value is likely due to modifications to the analysis process and the type of solvent used. However, we can still say that green coffee bean extract still contains chlorogenic acid, which has anti-acne properties.

Table 2. Results of standardization of green coffee (*Coffea canephora*) **dry extract (GCE)**

Standardization Parametre	Result
Non Specific	
Total Ash Content (%)	8.89 ± 0.04
Acid Insoluble Ash Content (%)	0.26 ± 0.04
Water Soluble Ash Content (%)	8.19 ± 0.11
Water content (%)	3.45 ± 0.18
Specific	
Organoleptic	
• Form	Powder Brownish
• Color	greenTypical
• Smell	coffee
• Flavor	Bitter
pH (1% w/v solution)	5.11 ± 0.03
Water Soluble Extract Level (%)	92.03 ± 0.46
Ethanol Soluble Extract Level (%)	30.96 ± 0.68

Evaluation results of green coffee dry extract effervescent granules (EG-GCE) before reconstitution

Organoleptic

Organoleptic examination of the EG- GCE preparation was carried out visually as the preparation was yellowish-white in color, granular in shape, and hada distinctive coffee odor. The results of the organoleptic examination of the green coffee dry extract effervescent granule preparation can be viewed at Figure 2.

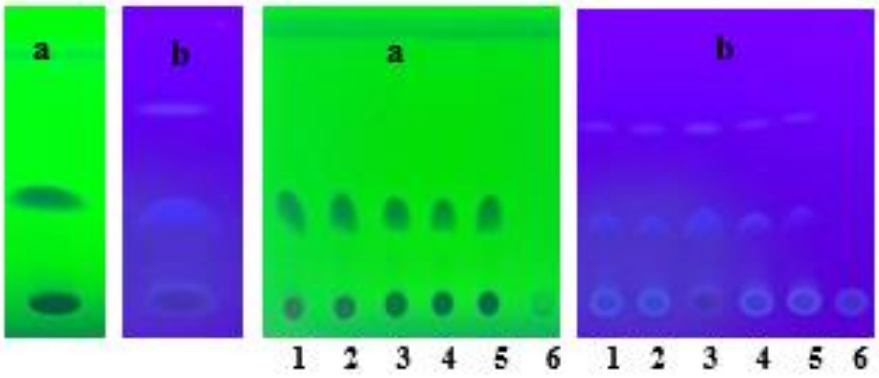

Figure 1. Thin layer chromatography results of GCE and EF with mobile phase chloroform: methanol: formic acid (44.1: 2.5: 2.15 mL) under 254 nm UV light (a) and 366 nm UV light (b), 1 (formula -1); 2 (formula a); 3 (GCE); 4 (formula b); 5 (formula ab); 6 (formula blank)

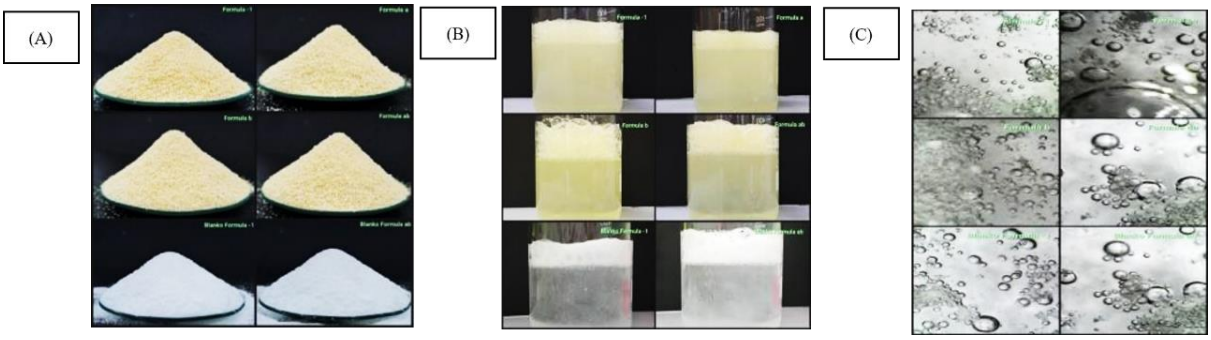

Figure 2. EG-GCE before reconstitution (A) and after reconstitution (B) with carbon dioxide gas bubbles observed at 1000x magnification (C) using digital microscope TRM-DM1000

pH Measurement

The pH measurement was carried out to determine the acidity of EG-GCE after reconstitution. The four formulas gave significantly different pH values ($F_{value} > F_{0.05}$), which may be attributed to the different proportions of acid species. This findings was in agreement with Lowry-Brönsted theory stating that acids may act as a substance donating H^+, and hence the addition of acidic solute into water will result in an increased hydronium ion concentration (Aultons & Taylor, 2022). The pH values of all EG-GCE formula met the pHrequirement, i.e. within the range of 5-7 (Giyatmi & Lingga, 2019).

Flow properties

The test results for all flow property parameters (flow rate, angle of repose, Hausner ratio, Carr index) show significant differences between the formulas (Table 3). Based on statistical analysis, it was found that F_{value} of all parameters of flow properties was greater than the $F_{0.05\ (table)}$. In addition, all formula demonstrated a good flow properties of granules. Granules are considered to have good flow rates if they can flow at >10 g/s, angle of repose <350, Hausner ratio <1.25, and Carr's index <20% (Taylor & Aulton, 2021) According to (Qiu et al., 2017), the flow properties of granules are complex and affected by several factors including humidity, particle shape and size. The resulting water content value meets specifications: 3.40 ± 0.30%.

Based on the results of the quality control of flow properties that has been carried out in terms of the parameters of flow speed and angle of repose, all formulas are declared to have good flow properties when viewed from the Hausner ratio and Carr's index parameters, formula -1, formula a, and formula b stated to be quite good.

Table 3. Flow properties parameters of EG-GCE

Parameter	F-1	Fa	Fb	Fab	Fvalue	F0.05
pH	6.07 ± 0.05	5.94 ± 0.04	5.85 ± 0.05	5.46 ± 0.12	82.03	
Flow rate (g/s)	28.53 ± 1.05	26.48 ± 0.93	28.35 ± 0.53	25.78 ± 0.47	18.14	
Angle of repose (^{0})	25.65 ± 0.89	27.47 ± 0.53	30.13 ± 0.56	29.56 ± 0.44	63.61	3.10
Hausner ratio	1.21 ± 0.01	1.22 ± 0.01	1.20 ± 0.02	1.14 ± 0.01	51.54	
Carr's index (%)	17.58 ± 0.49	17.83 ± 0.75	16.75 ± 1.25	12.50 ± 0.55	55.36	
Water Content (%)	3.16 ± 0.22	3.12 ± 0.06	3.28 ± 0.09	3.67 ± 0.14	18.66	

Evaluation results of green coffee dry extract effervescent granules (EG-GCE) afterreconstitution
Organoleptic

Organoleptic examination of the EF-GCE after reconstitution, provided specifications for the preparation being yellowish white in color, in solution form and with a sweet and sour taste, and producing carbon dioxide gas (Figure 2)**.**

pH Measurement

The purpose of pH measurements is to determine the acidity level of EG-GCE after reconstitution. The pH test results for each formula were -1 (6.07 ± 0.05), a (5.94 ± 0.04), b (5.85 ± 0.05), ab (5.46) respectively. ± 0.12), blank -1 (6.40 ± 0.03), blank ab (5.04 ± 0.07). The resulting pH value is in accordance with the specifications for the EG-GCE preparation, in the range of 6.00 ± 1.00. The four formulas give significantly different pH values ($F_{value} > F_{0.05}$), which may be attributed to the different proportions of acid species. This findings was in agreement with Lowry-Brönsted theory stating that acids may act as a substance donating H^+, and hence the addition of acidic solute into water will result in an increased hydronium ion concentration (Taylor & Aulton, 2021). The pH values of all EG-GCE formula met the pH requirement, i.e. within the range of 5-7 (Giyatmi & Lingga, 2019).

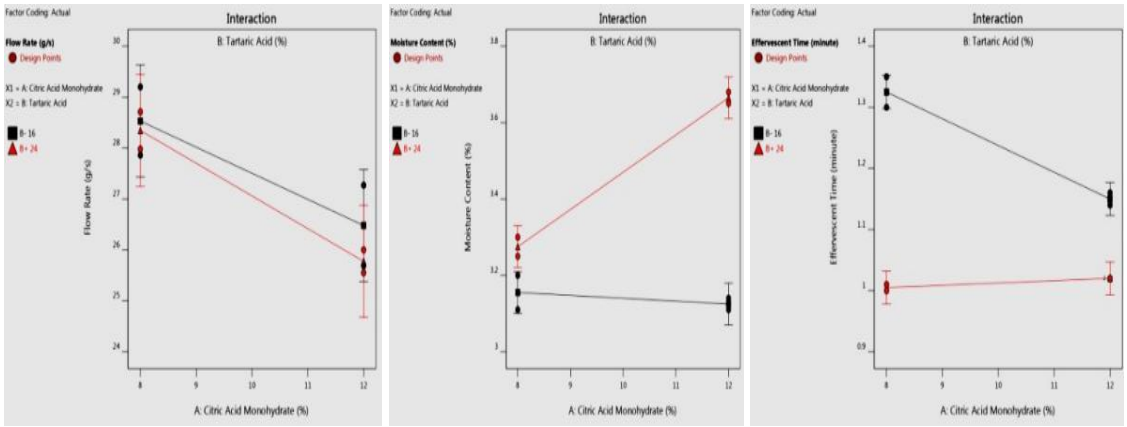

Figure 3. Interaction of X_A and X_B on Y_1, Y_2, and Y_3

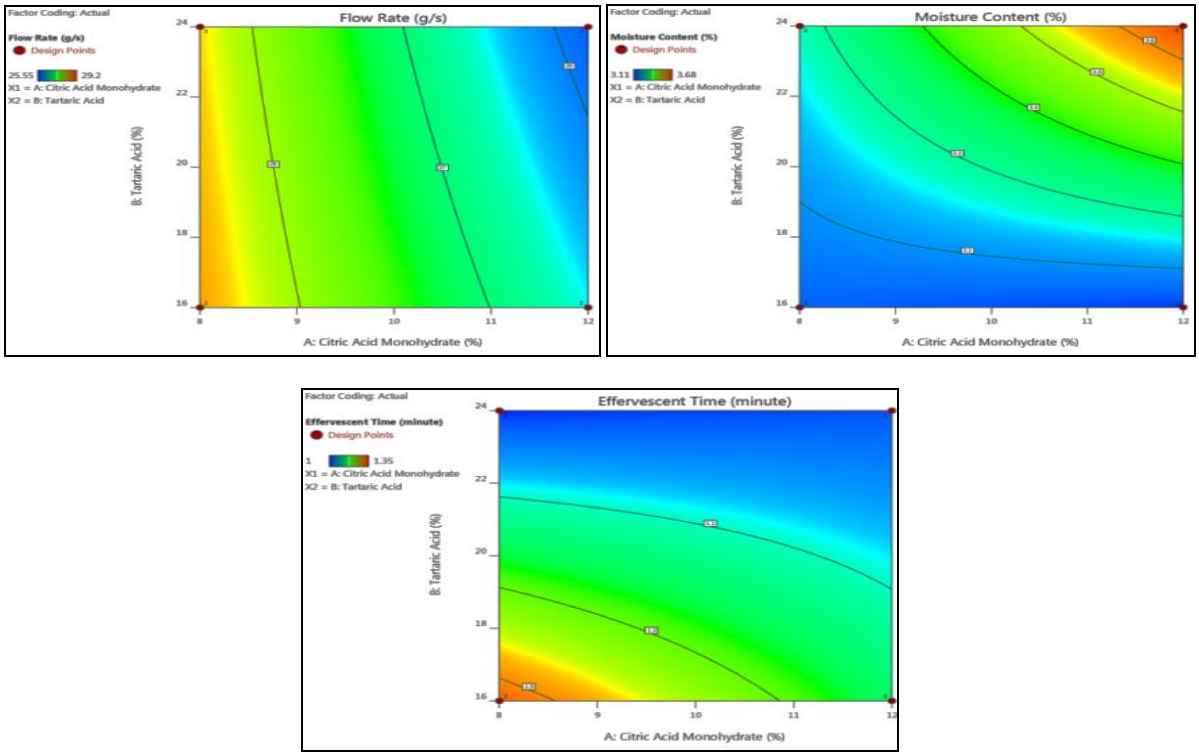

Figure 4. Contour plot of Y_1, Y_2, and Y_3

Formula optimization flow rate response

The flow rate test aims to ensure that granules may flow adequately through processing equipment, since poor flowability can lead to large weight variability among unit dose (sachet) in production scale (Qiu et al., 2017). In this study, all formula met the flow rate requirements, i.e. within the range of >10 g/s (Table 3). The polynomial equation for the flow rate was found to be $Y_1 = 27.28 - 1.16\ X_A - 0.22\ X_B - 0.13\ X_AX_B$. The equation suggested that citric acid monohydrate had more significant effect on the decreased flow rate than tartaric acid. According to (Rowe et al., 2020) citric acid monohydrate has orthorhombic crystal form, while tartaric acid is monoclinic. The difference in the crystal form of these two acidic substances may lead to a difference or change of flow rate (Qiu et al., 2017). Electrostatics forces, particle size, particle size distribution, and moisture content have also been shown to influence the flow rate (Gad, 2007; Qiu et al, 2017). In this study, it was also found that the interaction of citric acid monohydrate and tartaric acid did not affect the flow rate of the granules. (Figure 3 and 4).

Moisture content response

Effervescent granules should comply with the quality requirements related to moisture content, that is below 5% (Giyatmi & Lingga, 2019). The moisture content of all EG-GCE formula prepared in this study was within the range of 3.12-3.67% (Table 3). The polynomial equation for the moisture content was found to be $Y_2 = 3.31 + 0.09\ X_A + 0.17\ X_B + 0.11\ X_AX_B$. This equation suggested that tartaric acid exhibited more significant effect on the increased value of moisture content. This may be due to the hygroscopicity properties of the tartaric acid which is higher than citric acid monohydrate (Bertuzi, 2021). According to (Wilson & Koeberle, 2018; Kalman, 2021), hygroscopicity is the capacity of a chemical substance to adsorb and desorb water. Thus the increased concentration of tartaric acid which is highly hygroscopic excipient in the EG-GCE formula may enhance the water content in granules. This may be attributed to the increased capacity adsorption of water in the atmosphere. In this study, we found that the interaction of citric acid monohydrate and tartaric acid had no influence on the

moisture content of granules. In this study, all formulas had water content that met the requirement because the drying process of the wet granule mass was carried out at a relative humidity (RH) ≤ 25% with a temperature of around 25^0C, thereby preventing the effervescent granules from absorbing water from the surrounding air.(Figure 4 and 5).

Dissolving granule time test response

Dissolving granule time evaluation aims to determine the dissolving time of EG-GCE in water. Effervescent granules should meet the quality requirements regarding to the effervescent time, that is less than 5 minutes (Taylor & Aulton, 2021). In this study, the effervescent time of EG-GCE wasfound to be within the range of 1.00-1.33 min (Table 3). Upon reconstitution of EG-GCE in water, citric acid monohydrate and tartaric acid will react with sodium bicarbonate, which in turn will produce its sodium salt, water, and $CO_{2(g)}$ The conversion of weak acid to its sodium salt leads to an increased ionic dissociation constant which is subsequently followed by the improved solubility of granules (Taylor & Aulton, 2021). The polynomial equation demonstrating the effervescent time of this EG-GCE was $Y_3 = 1.13 - 0.04\ X_A - 0.11\ X_B + 0.05\ X_AX_B$. The equation suggested that tartaric acid had more significant effect on the decreased effervescent time of granules. This may be due to the anhydrous form of tartaric acid as a substance used in this study. According to (Taylor & Aulton, 2021), the anhydrous form of a substance has a faster-dissolved rate than its respective hydrate form. This may explain our findings that tartaric acid had more significant effect on the effervescent time, compared with citric acid monohydrate. In thisstudy, the interaction of citric acid monohydrate and tartaric acid did not affect the effervescent time significantly (Figure 4 and 5).

Optimum formula

Based on the contour plot of the responses used in this study (Figure 5), it was found that the proportion of citric acid monohydrate and tartaric acid was responsible for the determination of optimum formula of EG-GCE. The contour plot was then overlaid (superimposed) to obtain the optimum formula (Figure 6). The yellow area is the prediction of the optimum formula of EG- GCE. The software recommended an optimum formula containing a combination of citric acid monohydrate (9.94%) and tartaric acid (17.46%), with a predicted flow rate between 25.62-29.29 g/s, moisture content between 3.11-3.29%, and effervescent time between 1.15-1.24 min. The suggested optimum formula was then prepared and the responses of this formula were verified. The optimum formula of EG-GCE showed a moisture content of 3.26%, flow rate of 25.72 g/s, and effervescent time of 1.19 min. All responses were within the predicted range and met the effervescent granules requirements.

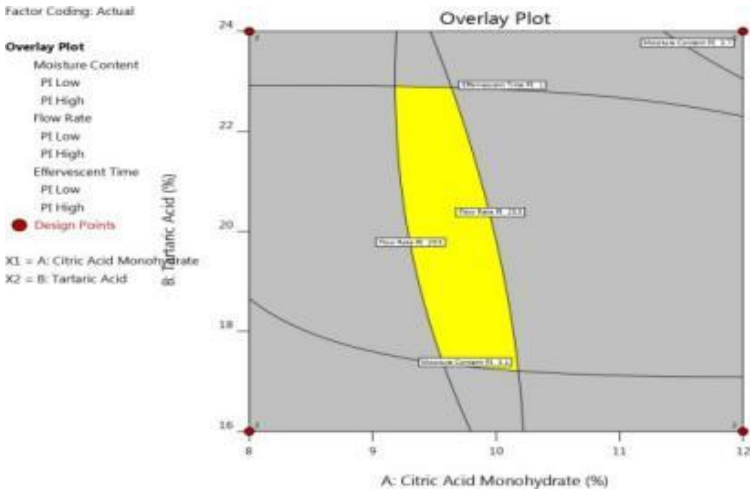

Figure 5. Superimposed (overlay plot) of EG-GCE

DPPH scavening activity of EG-GCE

Antioxidant activity tests were carried out on GCE and EG to determine the effect of formulation on GCE antioxidant activity. The results of the antioxidant activity test can be seen in Figure 6 with synthetic antioxidant compounds (ascorbic acid) as positive controls. The difference in IC_{50} values for antioxidants occurs due to space obstructions caused by other additives or excipients that cover the hydroxyl, phenol, carbonyl, and aromatic amide groups, inhibiting their antioxidant activity (Faria et al., 2020). The results of this study are by the observations of the IC_{50} of antioxidants using the DPPH method, which was reported by (Faria et al, 2020), where green coffee robusta thick extract has a stronger antioxidant IC_{50} compared to green coffee robusta thick extract, which is encapsulated with maltodextrin: gum arabic (1:1). The Blois antioxidant activity classification system can be divided into four classification, very strong antioxidants (IC_{50} < 50 µg/mL), strong antioxidants (50 µg/mL ≤ IC_{50} ≤ 100 µg/mL), moderate antioxidants (101 µg/mL ≤ IC_{50} ≤ 150 µg/mL), and weak antioxidants (IC_{50} > 150 µg/mL) (Faria et al., 2020). Based on this classification, ascorbic acid as a positive control has very strong antioxidant activity (37.36±0.29 µg/mL), while GCE and EG-GCE are classified as having strong antioxidant activity (IC_{50} antioxidant 51.40±1.18 µg/mL and 56.56±0.97 µg/mL. Statistical analysis using the one-way ANOVA method for the IC_{50} values of vitamin C, GCE, and EC-GCE gave a significant difference of F_{count} (368.52) > F_{table} (5.14).

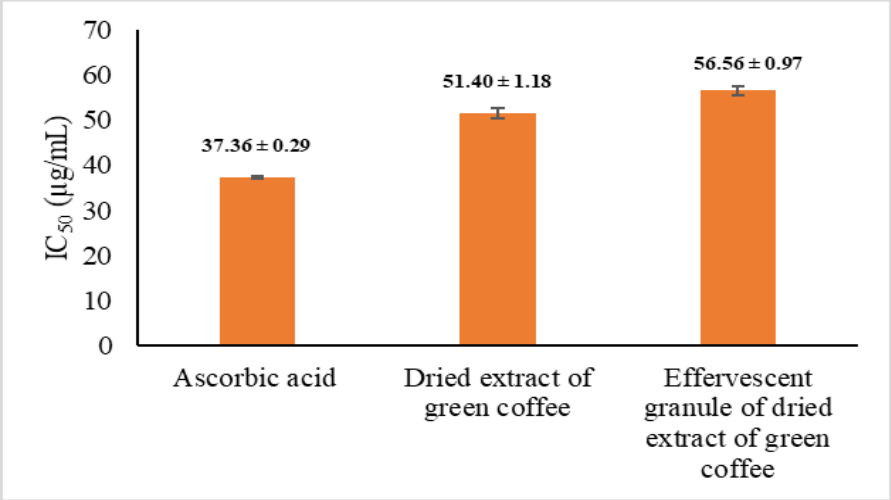

Figure 6. IC_{50} Antioxidant of ascorbic acid, GCE, and EG-GCE

CONCLUSION

EG-GCE has been formulated successfully as effervescent granules by wet granulation method and evaluated. The optimum formula, containing a combination of citric acid monohydrate (9.94%) and tartaric acid (17.46%), was obtained by factorial design method and has been verified, with the following parameters: moisture content 3.26%, flow rate 25.72 g/s, and effervescent time 1.19 min. The optimum formula show strong antioxidant activity with IC_{50} free of radical scavenging 56.56 ± 0.97 µg/mL.

ACKNOWLEDGMENTS

The author expresses his gratitude for the research facilities provided by the Faculty of Pharmacy, Widya Mandala Catholic University, Surabaya.

REFERENCES

Abrahão, F. R., Rocha, L. C. R., Santos, T. A., Carmo, E. L. do, Pereira, L. A. S., Borges, S. V., Pereira,

R. G. F. A., & Botrel, D. A. (2019). Microencapsulation of bioactive compounds from espresso spent coffee by spray drying. *LWT*, *103*, 116–124. https://doi.org/10.1016/j.lwt.2018.12.061

Asbaghi, O., Sadeghian, M., Rahmani, S., Mardani, M., Khodadost, M., Maleki, V., Pirouzi, A., Talebi, S., & Sadeghi, O. (2020). The effect of green coffee extract supplementation on anthropometric measures in adults: A comprehensive systematic review and dose-response meta-analysis of randomized clinical trials. *Complementary Therapies in Medicine*, *51*(March), 102424. https://doi.org/10.1016/j.ctim.2020.102424

Bertuzi, G. (2021). Effervescent granulation. In D. M. Parikh (Ed.), *Handbook of Pharmaceutical Granulation Technology* (4th Editio). CRC Press

Boccellino, M., & D'Angelo, S. (2020). Anti-obesity effects of polyphenol intake: Current status and future possibilities. *International Journal of Molecular Sciences*, *21*(16), 1–24. https://doi.org/10.3390/ijms21165642

Bojić, M., Haas, V. S., Šarić, D., & Maleš, Ž. (2013). Determination of flavonoids, phenolic acids, and xanthines in mate tea (Ilex paraguariensis St.-Hil.). *Journal of Analytical Methods in Chemistry*, *2013*. https://doi.org/10.1155/2013/658596

Cui, L., Hanika, K., Visser, R. G. F., & Bai, Y. (2020). Improving pathogen resistance by exploiting plant susceptibility genes in coffee (Coffea spp.). *Agronomy*, *10*(12), 1–20. https://doi.org/10.3390/agronomy10121928

Di Domenico, M., Pinto, F., Quagliuolo, L., Contaldo, M., Settembre, G., Romano, A., Coppola, M., Ferati, K., Bexheti-Ferati, A., Sciarra, A., Nicoletti, G. F., Ferraro, G. A., & Boccellino, M. (2019). The role of oxidative stress and hormones in controlling obesity. *Frontiers in Endocrinology*, *10*(August), 1–13. https://doi.org/10.3389/fendo.2019.00540

Faria, W. C. S., Silva, A. A. da, Veggi, N., Kawashita, N. H., Lemes, S. A. de F., Barros, W. M. de, Cardoso, E. da C., Converti, A., Moura, W. de M., & Bragagnolo, N. (2020). Acute and subacute oral toxicity assessment of dry encapsulated and non-encapsulated green coffee fruit extracts. *Journal of Food and Drug Analysis*, *28*(2), 337–355. https://doi.org/10.38212/2224-6614.1067

Flieger, J., Flieger, W., Baj, J., & Maciejewski, R. (2021). Antioxidants: classification, natural sources, activity/capacity measurements, and usefulness for the synthesis of nanoparticles. *Materials*, *14*(15). https://doi.org/10.3390/ma14154135

Gad, S. C. (2007). Pharmaceutical manufacturing handbook: production and processes. In *Pharmaceutical Manufacturing Handbook: Production and Processes*. https://doi.org/10.1002/9780470259818

Galanakis, C. M., Aldawoud, T. M. S., Rizou, M., Rowan, N. J., & Ibrahim, S. A. (2020). Food ingredients and active compounds against the Coronavirus Disease (COVID-19) pandemic: a comprehensive review. *Foods*, *9*(11), 1–17. https://doi.org/10.3390/foods9111701

Giyatmi, & Lingga, D. K. (2019). The effect of citric acid and sodium bicarbonate concentration on the quality of effervescent of red ginger extract. *IOP Conference Series: Earth and Environmental Science*, *383*(1). https://doi.org/10.1088/1755-1315/383/1/012022

Gorji, Z., Varkaneh, H. K., Talaei, S., Nazary-Vannani, A., Clark, C. C. T., Fatahi, S., Rahmani, J., Salamat, S., & Zhang, Y. (2019). The effect of green-coffee extract supplementation on obesity: A systematic review and dose-response meta-analysis of randomized controlled trials. *Phytomedicine*, *63*, 153018. https://doi.org/10.1016/j.phymed.2019.153018

Jain, G., & Patil, U. (2020). Formulation, characterization and evaluation of behavioral effects of suspension and effervescent granules of evolvulus alsinoides Linn. and convolvulus pluricaulis choisy. *International Journal of Pharmaceutical Investigation*, *10*(4), 460–465. https://doi.org/10.5530/ijpi.2020.4.81

Kalman, H. (2021). Effect of moisture content on flowability: Angle of repose, tilting angle, and Hausner ratio. *Powder Technology*, *393*(November), 582–596. https://doi.org/10.1016/j.powtec.2021.08.010

Lammi, C., & Arnoldi, A. (2021). Food-derived antioxidants and COVID-19. *Journal of Food*

Biochemistry, *45*(1), 1–7. https://doi.org/10.1111/jfbc.13557

Lima, A. L., Pinho, L. A. G., Chaker, J. A., Sa-Barreto, L. L., Marreto, R. N., Gratieri, T., Gelfuso, G. M., & Cunha-Filho, M. (2020). Hot-melt extrusion as an advantageous technology to obtain effervescent drug products. *Pharmaceutics*, *12*(8), 1–20. https://doi.org/10.3390/pharmaceutics12080779

Maysarah, H., Sari, I., Faradilla, M., & Kwok, K. (2020). Formulation of effervescent granule from robusta green coffee bean ethanolic extract (coffea canephora). *Journal of Pharmacy and Bioallied Sciences*, *12*(6), S743–S746. https://doi.org/10.4103/jpbs.JPBS_258_19

Ohishi, T., Fukutomi, R., Shoji, Y., Goto, S., & Isemura, M. (2021). The beneficial effects of principal polyphenols from green tea, coffee, wine, and curry on obesity. *Molecules*, *26*(2). https://doi.org/10.3390/molecules26020453

Pereira, L. L., Marcate, J. P. P., Caliman, A. D. C., Guarçoni, R. C., & Moreli, A. P. (2021). Physical Classification and Sensory Coffee Analysis. In *Food Engineering Series*. https://doi.org/10.1007/978-3-030-54437-9_8

Pimpley, V., Patil, S., Srinivasan, K., Desai, N., & Murthy, P. S. (2020). The chemistry of chlorogenic acid from green coffee and its role in attenuation of obesity and diabetes. *Preparative Biochemistry and Biotechnology*, *50*(10), 969–978. https://doi.org/10.1080/10826068.2020.1786699

Piñón-Balderrama, C. I., Leyva-Porras, C., Terán-Figueroa, Y., Espinosa-Solís, V., Álvarez-Salas, C., & Saavedra-Leos, M. Z. (2020). Encapsulation of active ingredients in food industry by spray-drying and nano spray-drying technologies. In *Processes* (Vol. 8, Issue 8). MDPI AG. https://doi.org/10.3390/PR8080889

Qiu, Y., Zhang, G. G. Z., & Mantri, R. V. (Eds.). (2017). *Developing solid oral dosiage forms: Pharmaceutical Theory & Practice*. Academic Press

Rowe, Sheskey & Owen, 2020. (2006). On site service factor works for minetec. In *AusIMM Bulletin* (Issue 1)

Sudeep, H. V., & Shyam Prasad, K. (2021). Supplementation of green coffee bean extract in healthy overweight subjects increases lean mass/fat mass ratio: A randomized, double-blind clinical study. *SAGE Open Medicine*, *9*(14). https://doi.org/10.1177/20503121211002590

Tanjung, Y. P., Akmal, T., Julianti, A. I., Fauziyyah, A., & Riki, A. (2023). Lozenges formulation of Ciplukan (Physalis Angulata L.) fruit extract as an antioxidant with combination of filler agents avicel Ph 102–Ludipress. *International Journal of Applied Pharmaceutics*, *15*(Special Issue 2), 74–78. https://doi.org/10.22159/ijap.2023.v15s2.14

Tasew, T., Mekonnen, Y., Gelana, T., Redi-Abshiro, M., Chandravanshi, B. S., Ele, E., Mohammed, A. M., & Mamo, H. (2020). In vitro antibacterial and antioxidant activities of roasted and green coffee beans originating from different regions of Ethiopia. *International Journal of Food Science*, *2020*. https://doi.org/10.1155/2020/8490492

Taylor, K. M. G., & Aulton, M. E. (2021). *Aulton's pharmaceutics: the design and manufacture of medicines (6th ed)* (pp. 248–253)

U.S Pharmacopeia. (2020). *The United States Pharmacopeia, USP 43- National Formulary, NF 38*. Pharmacopeial Convention, Inc

Wilson & Koeberle, 2018. (2018). Pharmaceutical formulation the science and technology of dosage forms. In *Pharmacology of Ocular Therapeutics*

Pharmaciana
Vol.14, No.3, Nov 2024, Page. 396-407
ISSN: 2088 4559; e-ISSN: 2477 0256
DOI: 10.12928/pharmaciana.v14i3.28104

The effect of HPMC-K15M and guar gum as polymer-coated for sustained-released tablet: disintegration and release kinetics

Nining Nining*, Anisa Amalia, Raditya Naufal Riyanto
Faculty of Pharmacy and Science, Universitas Muhammadiyah Prof DR. Hamka,
Jl. Delima II, Malaka Sari-Duren Sawit, Jakarta, Indonesia

Submitted: 29-12-2023 ***Reviewed: 31-03-2024*** ***Accepted: 06-11-2024***

ABSTRACT

Polymeric coating films are able to control tablet drug release rate depending on polymer physicochemical properties. Guar gum and HPMC-K15M (GG/HPMC-K15M) can be a coating polymer in sustained-release tablets. This study aims to characterize the disintegration and drug release kinetics on theophylline sustained-release tablets coated with GG/HPMC-K15M. The film coating was made with variations of the GG/HPMC-K15M ratio of 1:3 (F1), 1:4 (F2), and 1:5 (F3). Granules were preformulated regarding LOD, granule size distribution, packing, and flow properties. Film coating was carried out using a liquid spraying method. Coated tablets were tested for quality examination, and the drug release kinetics model was determined based on in-vitro dissolution. Granule pre-formulation result shows that the granules have excellent packing and flow properties with an LOD of 4.59–5.33% and a size of 553.28–627.28 πm. Tablets provided uniform size characteristics with a weight variation of 333.38–339.56 mg (CV 1.32–3.43% and acceptance value 6.53–13.58), hardness of 11.61–18.86 kgf, friability of 0.103–0.186%, disintegration time of 20.69–27.36 min, and drug content of 98.51–98.55%. The theophylline was dissolved by 95.24% (6h in FI), 97.04% (7h in F2), and 99.79% (8h in F3); all formulas followed zero-order kinetic ($r^2 \sim 1$). Suitable quality theophylline tablets GG/HPMC-K15M coating have been successfully produced. Increasing the concentration ratio of HPMC-K15M in the coating solution resulted in a significant increase in disintegration time and a slowing of the drug release rate. The drug release kinetics of all formulations followed the zero-order kinetic model.

.

Keywords: dissolution, drug release kinetics, film coating, liquid spray, polymeric coating

Corresponding author:
Nining Nining
Universitas Muhammadiyah Prof DR. Hamka
Jl. Delima II, Malaka Sari-Duren Sawit, Jakarta, Indonesia
Email: nining@uhamka.ac.id

INTRODUCTION

Tablets provide many advantages, such as ease of administration, high patient compliance, and cost-effectiveness, making them one of the most preferred dosage forms. Coating is an essential step in the tablet manufacturing process regarding aesthetic and functional considerations (Seo et al., 2020). Film coating is the most widely used to solve various obstacles during drug production, distribution, storage, and clinical use compared to other types, such as sugar and press coating (Zaid, 2020). For example, film coating can regulate drug release from the dosage form in terms of time, speed, and location (Lee et al., 2020). It aims to facilitate the delivery of acid-sensitive drugs to the colon while minimizing adverse effects on the gastrointestinal system. Sustained-release tablets with film coating are commonly used to regulate the rate at which drugs dissolve in the gastrointestinal tract (Kapoor et al., 2019). Its tablet is designed to rapidly achieve therapeutic blood levels and sustain them within the therapeutic range through controlled release (Agustin & Ratih, 2015). Controlling the drug release rate is influenced by the physicochemical properties and the quantity of polymer utilized for surface coating (Seo et al., 2020; Shukla et al., 2019). Guar gum and hydroxypropyl methylcellulose (HPMC) are suitable polymers for this coating film.

Guar gum (GG) is obtained from *Cyamopsis tetragonoloba* (Leguminosae family) seeds, a water-soluble and non-ionic natural polysaccharide gum. Chemically, it consists of a linear polymer chain of (1 → 4)-ß-Ɗ-mannopyranosyl units, which have α-Ɗ-galactopyranosyl units linked by (1 → 6) bonds (George et al., 2018). Its use has been widely developed in various hydrophilic matrices as carriers to effectively control drug release by forming gels. GG expands in cold water and produces a colloidal dispersion so that its gel-forming network inhibits drug release from the preparation (Jana et al., 2019). HPMC, another polymer, has hydrophilic properties and is widely applied in modified-release tablet formulations. Its addition to the coating component can improve the mechanical properties of the tablet (Prusty & Patra, 2022). This polymer is commercially available in several grades depending on the viscosity and amount of substituents (Hirun, 2022). HPMC-K15M can control drug release for 24 hours in tablet matrix formulations with drug release mechanisms in the form of drug dissolution inside the hydrogel, drug diffusion across the hydrogel, and gel erosion (Yi et al., 2019).

Theophylline is a bronchodilator for treating asthma and stable chronic obstructive pulmonary disease (COPD) (Rahmawati et al., 2018). Sustained release preparations have become essential to dynamic changes in COPD pharmacotherapy over the last few years (Sharma & Kansal, 2023). After oral administration, theophylline changes rapidly and is completely retained in the digestive tract. The serum half-life of theophylline varies from 3 to 13, with an average range of 7-9 hours, and is toxic at doses of 7.5 mg/kg or higher (Palai et al., 2023).

Based on the explanation above, studying the disintegration characterization and drug release kinetics of sustained-release tablets coated with guar gum and HPMC-K15M is necessary. Guar gum, a natural gum, is favored over similar synthetic polymers because of its easy availability, lower toxicity, and cost-effectiveness (George et al., 2018). The incorporation of HPMC will enhance the limited properties of guar gum. Theophylline core tablets were produced using the wet granulation process, and the coating was applied using coating solutions comprising various ratios of guar gum and HPMC-K15M. The primary measurement to assess the coating performance of the two polymers is the disintegration and in-vitro dissolution.

MATERIALS AND METHOD

Materials

Materials consist of theophylline BPFI (BPOM, Indonesia), theophylline (Jilin Shulan Synthetic Pharm., China), HPMC K15M (Shanghai Honest Chem. China), explotab (Gujarat Overseas INC., India), lactose (DFE pharma, Germany), talc (Haicheng Xinda Mining, China), guar gum (Shreeji Agro, India), Mg stearate (Faci Asia Pacific, Singapore), povidone K30 (JH Nanhang LC., China), PEG 400 (PT. Purnomo Putra Kimia, Indonesia), ethanol and aquadest (Harum Kimia, Indonesia).

Methods

Theophylline Granules Preparation

Granules (300 mg in capsule) consist of 25% theophylline (75 mg, active ingredient), 5% PVP (15 mg, binder), 4% Explotab (12 mg, disintegrant), and 62% lactose (186 mg, filler). Theophylline and Explotab were mixed with a V-mixer (Tamaru) at 90 rpm for 10 min. Then, dissolved in 74 mL of distilled water, PVP was added slowly until a banana-breaking mixture was formed. The mixture was sieved with a #12 mesh sieve and dried at 60°C in the oven for 2 hours. The dry granules were sieved again with a #18 mesh sieve and mixed with 2% Mg stearate and 2% talc for evaluation.

Theophylline Granules Evaluation

Densities, Carr Index, and Hausner Ratio

Granules ± 50 g (w) were weighed and put into a 100 mL measuring cup installed on a tapped density tester (Tamaru). The initial volume (v_1) before tapping and the final volume (v_2) after tapping 500 times were recorded (Nining et al., 2020). Then, the bulk density, tapped density, Carr index, and Hausner ratio are calculated using equations (1), (2), (3), and (4).

$$\text{Bulk density (g/mL)} = \frac{W}{v_1} \quad \text{.....(1)}$$

$$\text{Tapped density (g/mL)} = \frac{W}{v_2} \quad \text{.....(2)}$$

$$\text{Carr index (\%)} = \frac{tapped\ density - bulk\ density}{tapped\ density} \text{ x } 100 \quad \text{.....(3)}$$

$$\text{Hausner ratio} = \frac{tapped\ density}{bulk\ density} \quad \text{.....(4)}$$

Flow rate and angle of repose

Granules ±100 g (w) were weighed and put into a funnel with the hole closed on the granule flow tester. Then, the funnel lid was opened, and the granules' flow time (t), the pile's diameter (d), and height (h) were recorded. The t data was used to calculate the flow rate, while the d and h data were used to calculate the angle of repose (Nining et al., 2020). Both are calculated using equations (5) and (6).

$$\text{Flow rate (g/s)} = \frac{w}{t} \quad \text{.....(5)}$$

$$\text{Angle of repose (°)} = tan^{-1}\frac{h}{r} \quad \text{.....(6)}$$

Loss on Drying (LOD)

Granules ± 1g (w_1) were weighed and placed in a weighing bottle that has been heated and weighed. The weighing bottle containing the sample with the lid open was heated at 105°C in the oven (Memmert) for 30 min. Then, the bottle was cooled in a desiccator with the lid closed and weighed. Its

procedure was repeated until a constant weight (w_2) was obtained, indicated by a weighing difference of no more than 0.50 g (Depkes RI, 2020). LOD was calculated using equation (7).

$$\text{LOD (\%)} = \frac{w_1 - w_2}{w_1} x\ 100 \quad \text{.....(7)}$$

Granule size distribution

Granule grouping was determined using the sieving method (Depkes RI, 2020). Mesh analytical sieves #12, #18, #20, #30, #40, and pans were weighed (w_1) and arranged vertically downwards from small to large numbers. Granules ±100.0 g were weighed and put into the top sieve, and the tool was run at 30 Hz for 25 minutes. Once completed, each sieve was weighed again (w_2), and the average granule size was calculated.

Theophylline tablet core compressing and coating process

The granules that have been evaluated were then put into the hopper of the tablet compressing machine (Rimek). The tablet weight and hardness were regulated using the upper and lower punch of the machine. If both were matched, the machine was run until the granules were finished. A 100 mL coating solution was prepared with the composition listed in Table 1. Both polymers were weighed and put into a glass beaker. Coating tablets was done by spraying the coating solution over the tablet's surface gradually and uniformly with a revolving coating pan (CP-2L). Afterwards, the tablets were rotated in the pan until they reached room temperature. The film-coated pills were weighed and kept in a clean, then dried container (Iswandana et al., 2018).

Table 1. Composition of theophylline tablet coating solution

Materials	Function	Coating component (%)		
		F1	F2	F3
Guar gum	Polymer	1	1	1
HPMC K15M	Polymer	3	4	5
PEG 400	Plasticizer	1	1	1
Ethanol 80% ad	Solvent	100	100	100

Theophylline coating tablets evaluation

Physical examination and size uniformity

Physical examination was done by observing the tablet's shape, colour, and size (Nining et al., 2020). The diameter and thickness of the tablet were measured with a calliper and recorded in mm.

Weights variation

Ten tablets as samples were prepared. Each tablet was weighed, and the estimated amount of drug in each tablet was calculated in percentage of the amount stated on the label. The acceptance value determines whether the preparation is the same (Depkes RI, 2020). Correlation coefficients can also be calculated with weighted data.

Hardness and friability

Hardness was measured using a hardness tester (YD-3) by applying pressure to the tablet until it was crushed. The test was carried out on ten tablets. Friability was measured using a friability tester (TFT 2D/C5.2). A total of 20 tablets were cleaned, weighed (W_1), and put into the tool. Then, the tool was run at 25 rpm for 4 min. The tablet was cleaned and weighed again (W_2). Friability was determined by calculating the weight loss percentage to the initial weight (Nining et al., 2020).

Disintegration time

A total of 6 tablets were placed into the disintegration tester basket (BJ-2), and a weighted disc was placed in each hole. The tool was run with water at 37° ± 2° as the medium. The basket was removed at the end of the time limit, and the tablets were observed (all tablets must be crushed entirely). If one or two tablets did not entirely disintegrate, repeat the test with an additional 12 tablets: At least 16 of the 18 tablets tested must fully disintegrate (Depkes RI, 2020).

Drug content

Drug content was determined spectrophotometrically (Agilent Cary 60) with phosphate buffer saline (PBS) pH 7.2. First, the standard solution variations were made with theophylline BPFI to determine λmax (270,0 nm) and the standard curve. Sample preparation for compressed theophylline tablets was done by grinding 20 until they became powder. A certain amount of powder (~10 mg theophylline) was weighed, dissolved in PBS pH 7.2 in a 100 mL volumetric flask, diluted, and measured for absorbance at the λmax obtained previously.

Dissolution

The test procedure utilized a dissolution tester (Hanson Research SR 8 plus) with a paddle stirrer type. PBS pH 7.2 was used as a dissolution medium with an agitation speed of 100 rpm and a temperature of 37 ± 0.5°C. The pH of PBS is adjusted to 7.2 in order to simulate the pH conditions in the proximal ileum during the fasting state (Hamed et al., 2016). The sampling process was conducted at 15, 30, 45, 60, 90, 120, 240, 300, 360, 420, and 480 min. The sample is replaced with a new dissolution medium of equal volume to maintain a constant medium volume. The sample absorbance was measured, and the dissolved drug content was determined using λmax and a standard curve previously determined (Ainurofiq et al., 2014).

Release kinetics modeling

The in-vitro studies results were entered into several kinetic model equations (8)-(11), such as zero-order, first-order, Higuchi, and Korsmayer-Peppas, to characterize kinetic release studies and determine the drug release mechanism (Kamboj et al., 2014). Each kinetic model's linear regression line equation was created using its principles.

(a) Zero-order kinetics: $Q_t = Q_0 + K_0 t$ ……(8)

where Q_t is the amount of drug dissolved at time t, Q_0 is the initial amount of drug in solution, and K_0 is the zero-order release constant. A linear graph shows the cumulative amount of drug the system releases (Q_t) and time (t).

(b) First-order kinetics: $\ln Q_t = \ln Q_0 - K$ …… (9)

where K is the first-order release constant. A linear graph shows the logarithm of the drug cumulative amount (In Q_t) and time (t).

(c) Higuchi model kinetics: $Q_t = K_H t^{½}$ …… (10)

where K_H is the Higuchi dissolution constant. A linear graph shows the drug cumulative amount (Q_t) and the root of time (t ½).

(d) Kinetics of the Korsmayer-peppas model: $M_t/M_\infty = Kt^n$ ……(11)

where M_t/M_∞ is the fraction of drug released over time t, and n is the release exponent. The exponent value (n) indicates the drug release mechanism.

A linear graph is shown between the logarithm of the drug released cumulative amount < 60% and the logarithm of time as indicated by a correlation coefficient value close to one (r^2 > 0,98). Determination of the kinetic model for drug release from tablets was determined from the r^2 value in the linear regression equation obtained by each formulation. If r^2 approaches one, the kinetics follows the release of the regression equation from that kinetic model (Nining et al., 2021).

Data Analysis

A theoretical approach was carried out on some evaluation data by comparing it with the requirements contained in compendial and other standard books. Statistical analysis was carried out on tablet evaluation data with one-way ANOVA (α=0.005), and then, the Tukey HSD test was continued to determine the significance of the differences between formulas.

RESULT AND DISCUSSION

Packing and flow properties

Granules were made using the wet granulation method. The packing and flow properties, such as bulk and tapped density, Hausner ratio, Carr index, flow rate, and angle of repose, are shown in Table 2. Some fundamental parameters that govern the efficiency of many processes include solid particle packing, density, and void proportion. Porosity is connected to the inner structure of the particle (affecting particle density), whereas vacancy is related to the gaps between the particles (affecting bulk density) (Kalman & Portnikov, 2020). The bulk and tapped density for all granules ranged from 0.51 g/mL to 0.54 g/mL, with drying losses ranging from 4.59% to 5.33%. The granules' moisture accumulates on the surface and creates water-bridging forces that reduce the bulk density. Bulk and tapped density estimate powder volume at a particular production scale. The test is one of the most straightforward approaches for determining "flowability" with the Carr index and Hausner ratio classification. These two indices represent powder packing behaviour with and without tapping (Akseli et al., 2019). The difference in bulk and tapped density values is between 0.2 and 0.3, which indicates that the volume has mostly stayed the same even though 500 tappings have been carried out. That confirms that the granule size is the same and reproducible (Singh et al., 2021). Carr index and Hausner ratio showed low values, < 10% and < 1.11, respectively, which predicted acceptable flow. Both were used to estimate powder flow since they are related to powder density and internal friction. In particular, both describe inertial forces generated by tapping (for tapped density) and interparticle friction relative to gravitational forces (for bulk density). Powders that exhibit low internal friction relative to their weight cannot withstand the force of their gravity and, therefore, will compact based on density measurements. Further rearrangement stimulated by tapping did not cause a significant reduction in volume, and the powder was characterized by a low Carr index and Hausner ratio (Akseli et al., 2019).

Table 2. Evaluation data of F1-F3 batches teophylline granule core

Parameter	F1	F2	F3
Bulk density (g/mL)	0.51 ± 0.00	0.51 ± 0.01	0.51 ± 0.00
Tapped density (g/mL)	0.54 ± 0.01	0.53 ± 0.01	0.54 ± 0.00
Carr index (%)	5.42 ± 1.16	3.75 ± 0.62	4.79 ± 0.58
Hausner ratio	1.06 ± 0.01	1.04 ± 0.01	1.05 ± 0.01
Flow rate (g/s)	13.77 ± 0.20	16.23 ± 0.22	16.44 ± 0.18
Angle of repose (°)	28.44 ± 1.63	27.44 ± 0.41	29.23 ± 1.38
Loss on drying (%)	5.33 ± 0.41	4.59 ± 0.01	4.69 ± 0.11
Granule size (πm)	553.28 ± 7.70	569.04 ± 11.04	627.28 ± 10.67

Solid particle flow is the movement of particles relative to neighbouring particles to create a sliding surface. At the same time, the angle of repose is defined as the angle of inclination of the free surface to the horizontal of the bulk solid pile. It is a criterion for the ability to flow solid particles and a fundamental parameter in bulk material storage (Kalman, 2021). The angle of repose obtained ranges from 27.44° to 29.23° with a granule size ranging from 553.28 πm to 627.28 πm, which means it is excellent to flow. Particles larger than 250 πm usually flow relatively freely in contrast to particles under 100 πm in size, which tend to become cohesive and have problems with the flow (Avbunudiogba et al., 2020).

Physicochemical properties of coating tablets

Various physicochemical properties of coating tablets, such as diameter and thickness, weight variations, hardness, friability, and tablet disintegration time, are presented in Table 3.

Table 3. Evaluation data of theophylline tablet

Parameter	F1 (1:3)	F2 (1:4)	F3 (1:5)
Size variation			
Diameter (mm)	9.24 ± 0.06	9.26 ± 0.05	9.24 ± 0.07
Thickness (mm)	5.15 ± 0.07	5.07 ± 0.07	5.07 ± 0.12
Weight variation (mg)	333.38 ± 4.40	334.99 ± 7.29	339.56 ± 11.65
Coefficient of variation (CV, %)	1.32	2.18	3.43
Acceptability value	6.53	7.70	13.58
Hardness (kgf)	11.61 ± 1.17	13.69 ± 0.01	18.86 ± 2.45
Friability (%)	0.186 ± 0.003	0.155 ± 0.003	0.103 ± 0.001
Disintegration time (min)	20.69 ± 0.38	24.25 ± 0.75	27.36 ± 1.09
Drug content (%)	98.51 ± 0.93	98.51 ± 0.08	98.55 ± 0.10

Tablets must have good dosage uniformity. Tablets with a drug content of ≥ 25 mg with an active substance ratio of ≥ 25% were tested for preparation uniformity using the weight variation method (Depkes RI, 2020). All formulas' variation coefficients are below 5%, and the acceptance value is below 15.0. Both prove that tablets have a similar amount of active substance in the dosage unit. The acceptability value was calculated by estimating the drug content in each tablet against the drug content of each dosage formula. The drug content obtained ranged from 98.51% to 98.55%. The granules' flow properties greatly influence the moulded mass's weight or dosage uniformity, including their porosity (Iswandana et al., 2018; Syukri, 2018).

Tablet hardness is a parameter of a tablet's resistance to mechanical stress, such as shock and tablet cracking during packaging, transportation, and usage (Syukri, 2018). Tablet hardness in all batches ranged from 11.61 kgf to 18.86 kgf. Increasing the coating concentration increases the tablet's hardness. This observation may be caused due to the stronger bond between the guar gum polymer and HPMC-K 15M. Another study reported something similar when tablets were formed using methacrylate polymer (Avbunudiogba et al., 2020). Tablet friability indicates the resistance of the tablet surface to impact during packaging. The value is good if the amount is below 0.8% (Syukri, 2018). The friability value decreases as the coating polymer concentration increases. This increase in concentration is thought to increase the thickness of the coating layer, thereby preventing the release of powder particles from the tablet surface. This finding is inversely proportional to the tablet's friability with a NaCMC matrix (Iswandana et al., 2018). Even though HPMC and NaCMC are hydrophilic polymers, the coating system will be more effective in reducing friability in tablets than the matrix system.

Disintegration time is required for a tablet to break completely into small particles or granules, as indicated by the hole in the tool basket passing through (Syukri, 2018); the disintegration time obtained ranged from 20.69 min to 27.36 min. Increasing the polymer concentration increases the tablet disintegration time with the exact estimation of the tablet's friability. Coated tablets must disintegrate within 60 min (Syukri, 2018). Several factors influenced the disintegration time, excipient usage, production tablet method, type and concentration of lubricant, machine compression during tabletting, as well as physicochemical properties of tablet ingredients (Nining et al., 2020).

Drug release kinetics

The purpose of sustained-release preparations is to slow the drug release rate in the digestive system and reduce the frequency of drug administration. The release rate of a dosage form regulates drug absorption from the sustained-release dosage form so that there is a constant rate to minimize

unexpected toxic peaks and subtherapeutic troughs in plasma levels, often occurring at various doses (Caldwell & Kaushal, 2017). For this purpose, it is necessary to characterize the drug release profile of the preparation using an in-vitro dissolution test (Al-Hashimi et al., 2018). Before testing, the maximum wavelength and calibration curve were determined to be used to measure dissolved drug levels spectrophotometrically. The maximum wavelength obtained is 270 nm with a calibration curve equation Y = 0.05970 µg/mL and 10.9 µg/mL. In the dissolution test, the solubility of the theophylline was measured at several time points for 8h or 480 min. A paddle-type tool was used with a speed setting of 60 rpm at 37°C with PBS pH 7.2 medium. Sampling was conducted at 15, 30, 60, 90, 120, 180, 240, 300, 360, 420, and 480 min.

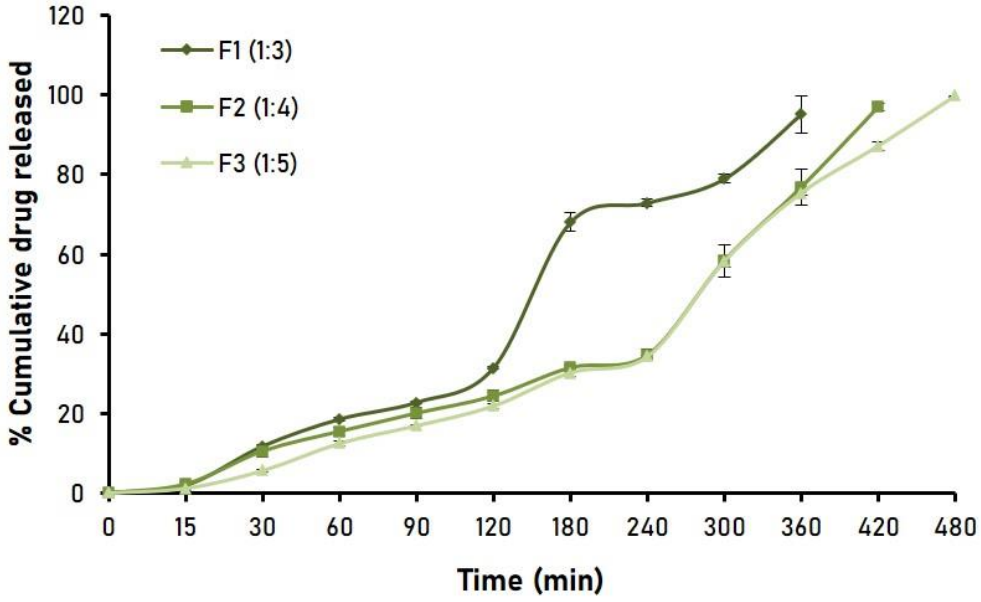

Figure 1. In-vitro dissolution profile of theophylline coated tablets in PBS 7,2

In Figure 1, the large amount of drug release in F1 began to occur significantly at 180 min (3h), which is very different from F2 and F3. Meanwhile, in F2 and F3, a significant difference in drug release occurred starting at 300 min. Regarding the shape of the curve, drug release in F2 and F3 shows almost the same shape. However, the F3 coating slightly inhibits drug release compared to F2, which is indicated by the position of the F3 curve below F2 on the graph. Theophylline is slightly soluble in water (Mohamed et al., 2013). Water-soluble drugs exhibit rapid release rates, usually through diffusion, whereas insoluble drugs are primarily released through gel erosion. In addition, water-soluble drugs tend to experience increased osmotic pressure, resulting in rapid diffusion—osmotic pressure applied to the sponge gel core causes polymer swelling (Mohamed et al., 2013). The results showed that increasing the concentration ratio of HPMC K15M to guar gum resulted in a decrease in theophylline dissolution. The mechanism for drug release from the preparation occurred through the process of developing the coating polymer (Singh et al., 2021). This event results in the formation of a gel around the tablet and inhibits the slow release of the drug. In this case, HPMC K15M is a polymer with high viscosity, which absorbs water significantly to form a gel. The dissolution medium penetrates the gel layer, and the drug molecules exit the system by diffusion. That can be seen from each formula in the dissolution rate data (Majumder et al., 2016).

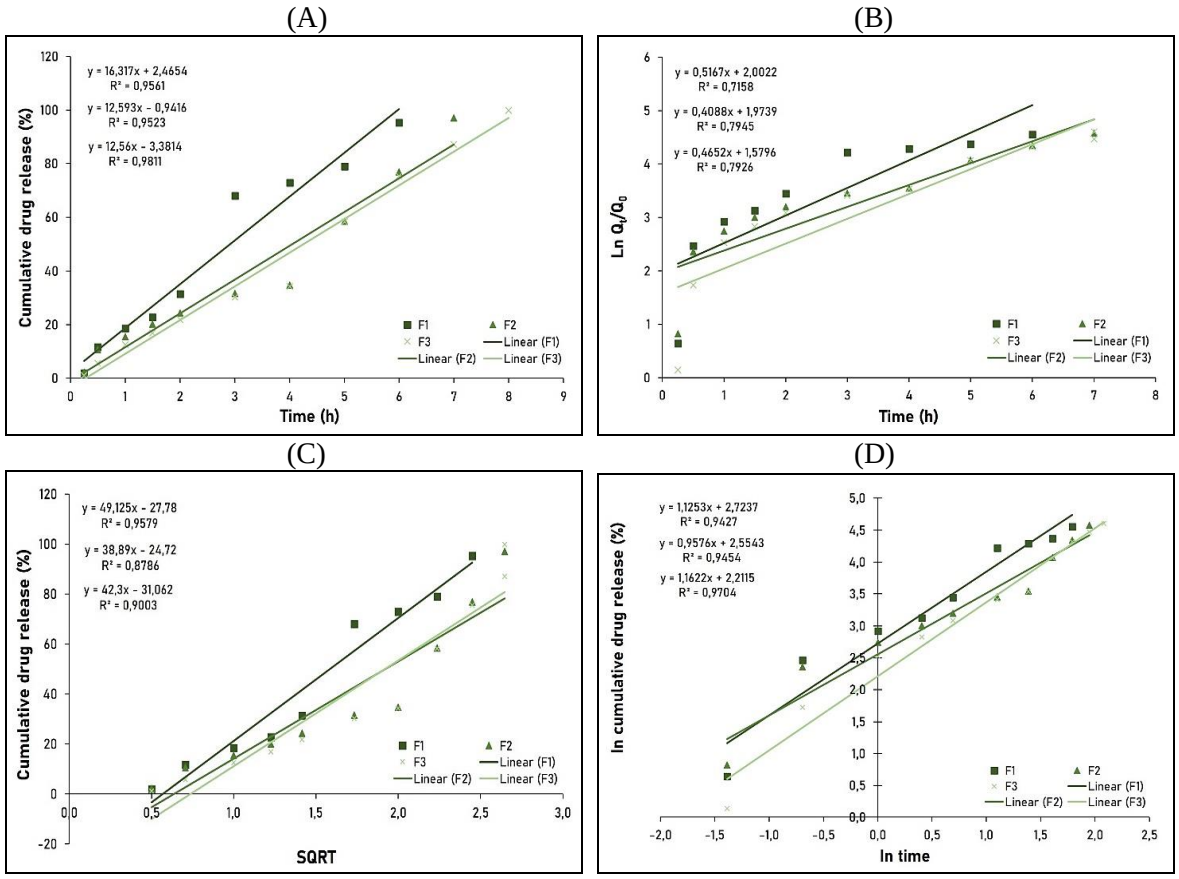

Figure 2. Comparative linear plots of (A) zero-order, (B) first-order, (C) Higuchi (SQRT), and (D) Korsmeyer-Peppas release kinetics model for F1-F3

Based on cumulative drug release data at 360 min, F3 (1:5) showed the most retarded release of up to 75.42% compared to F2 (1:4) and F1 (1:3), with drug release of 76.91% and 95.24%, respectively. These data show that increasing the HPMC K15M polymer by 1% in the preparation can hold the drug for 1.49–18.33%. That was also found in research on releasing salbutamol sulphate coated with various polymer concentrations. These differences cause the polymer thicknesslayer on the granules to vary and affect the drug release rate. Increasing the polymer's thickness will reduce the film layer's porosity, slowing drug release (Al-Hashimi et al., 2018). The physicochemical properties and the polymer amount used to coat the surface regulate the drug release rate. Moreover, it is regulated by changing the coating layer's thickness, tortuosity, and permeability (Seo et al., 2020).

Table 5. Estimated correlation coefficient and diffusion exponent values from theophylline dissolution data

Tablet	Zero-order		First-order		Higuchi		Korsmeyer-Peppas	
	r^2	K_0 (mol)	r^2	K_1 (h^{-1})	r^2	K_H	r^2	n
F1 (1:3)	0.9561	16.32	0.7158	0.52	0.9579*	49.12	0.9427	1.12
F2 (1:4)	0.9523*	12.59	0.7945	0.41	0.8786	38.89	0.9454	0.96
F3 (1:5)	0.9811*	12.56	0.7926	0.46	0.9003	42.30	0.9704	1.16

Table 5 and Figure 2A-2D show various release kinetic models to predict tablet drug release mechanisms and verify whether diffusion is Fickian or non-Fickian. The results with the highest linearity (r^2 closest to 1) show the behaviour of the zero-order kinetic model (Figure 2A) at F2 and F3 with rate constant (k) values of 12.59 and 12.56 mol, respectively. In general, these results do not show significant differences in slowdown rate. From the first to the 6h, the released drug concentration was almost similar between F2 and F3, but there was a significant difference at the 7h. A delivery system that follows zero-order kinetics will release the same amount of drug per unit of time and is the best release technique to achieve delayed effects (Rasul et al., 2020). F1 leads to two kinetic models with comparable correlation coefficients: the zero-order and the Higuchi models. That may imply that the viscosity of hydrated coatings may be the same despite differences in viscosity levels (Hirun, 2022). In the Kosrmayer-Peppas kinetic model (Table 5), relatively good linearity was also demonstrated in all three tablet formulas, and the release exponent (n) values were found to be in the range of 0.96–1.16, indicating a super-case II transport mechanism. It refers to the drug transport mechanism related to pressure and transition in hydrophilic glass polymers swelling in water or biological fluids (Solanki & Motiwale, 2020). The conclusive findings indicated that the tablet coating with the lowest concentration of film coating, F1 (1:3), adhered to the zero-order model, but the other two, F2 (1:4) and F3 (1:5), adhered to the Higuchi models.

CONCLUSION

Suitable quality theophylline tablets with HPMC K15M and guar gum coating have been successfully produced. Increasing the concentration ratio of HPMC K15M to the coating solution resulted in a decrease in the drug release rate. The maximum release is provided at F3 with a ratio of 1:5, which releases the drug for up to 480 min or 8h. The drug release kinetics formulations followed the Higuchi (F1) and zero-order kinetic model (F2 and F3).

ACKNOWLEDGEMENT

The authors thank Lemlitbang UHAMKA for grant support (298/F.03.07/2023) and the Faculty of Pharmacy and Science UHAMKA for the facilities provided until this research was completed.

REFERENCES

Agustin, R., & Ratih, H. (2015). Profil disolusi tablet sustained release natrium diklofenak dengan menggunakan matriks metolose 90 SH 4000. *Jurnal Sains Farmasi & Klinis*, *01*(02), 176–183. https://doi.org/https://doi.org/10.29208/jsfk.2015.1.2.33

Ainurofiq, A., Nurcahyo, I. F., & Yulianto, R. (2014). Preparation, characterization and formulation of nanocomposite matrix na-montmorillonite intercalated medium molecular weight chitosan for theophylline sustained release tablet. *International Journal of Pharmacy and Pharmaceutical Sciences*, *6*(11), 131–137.

Akseli, I., Hilden, J., Katz, J. M., Kelly, R. C., Kramer, T. T., Mao, C., Osei-Yeboah, F., & Strong, J. C. (2019). Reproducibility of the measurement of bulk/tapped density of pharmaceutical powders between pharmaceutical laboratories. *Journal of Pharmaceutical Sciences*, *108*, 1081–1084. https://doi.org/10.1016/j.xphs.2018.10.009

Al-Hashimi, N., Begg, N., Alany, R. G., Hassanin, H., & Elshaer, A. (2018). Oral modified release multiple-unit particulate systems: compressed pellets, microparticles and nanoparticles. *Pharmaceutics*, *10*(176), 1–23. https://doi.org/10.3390/pharmaceutics10040176

Avbunudiogba, J. A., Alalor, C. A., & Okolocha, Q. D. (2020). A controlled release theophylline delivery system based on a bilayer floating system. *Turkish Journal of Pharmaceutical Sciences*, *17*(6), 645–652. https://doi.org/10.4274/tjps.galenos.2019.53325

Caldwell, W. B., & Kaushal, A. M. (2017). Multiparticulate technologies for fixed-dose combinations. In A. R. Rajabi-Siahboomi (Ed.), *Multiparticulate drug delivery: formulation, processing and manufacturing* (pp. 155–168). Springer. https://doi.org/10.1007/978-1-4939-7012-4_7

Depkes RI. (2020). Farmakope Indonesia edisi VI. In *Departemen Kesehatan Republik Indonesia*.

George, A., Shah, P. A., & Shrivastav, P. S. (2018). Guar gum: Versatile natural polymer for drug delivery applications. *European Polymer Journal*, *112*(October), 722–735. https://doi.org/10.1016/j.eurpolymj.2018.10.042

Hamed, R., Awadallah, A., Sunoqrot, S., Tarawneh, O., Nazzal, S., AlBaraghthi, T., Al Sayyad, J., & Abbas, A. (2016). pH-Dependent Solubility and Dissolution Behavior of Carvedilol—Case Example of a Weakly Basic BCS Class II Drug. *AAPS PharmSciTech*, *17*(2), 418–426. https://doi.org/10.1208/s12249-015-0365-2

Hirun, N. (2022). Drug-polymers composite matrix tablets: effect of hydroxypropyl methylcellulose (HPMC) K-series on porosity, compatibility, and release behavior of the tablet containing a BCS class I drug. *Polymers*, *14*(3406), 1–14. https://doi.org/doi.org/10.3390/polym14163406

Iswandana, R., Lestari, D. A. T., & Sutriyo, S. (2018). Combination of HPMC and PEG 400 as a taste masking agent of film-coated tablets containing Momordica charantia Linn. extract. *International Journal of Applied Pharmaceutics*, *10*(3), 5–9. https://doi.org/10.22159/ijap.2018v10i3.24025

Jana, S., Maiti, S., Jana, S., Sen, K. K., & Nayak, A. K. (2019). Chapter 7: Guar gum in drug delivery applications. In *Natural Polysaccharides in Drug Delivery and Biomedical Applications*. Elsevier Inc. https://doi.org/10.1016/B978-0-12-817055-7.00007-8

Kalman, H. (2021). Quantification of mechanisms governing the angle of repose, angle of tilting, and Hausner ratio to estimate the flowability of particulate materials. *Powder Technology*, *382*, 573–593. https://doi.org/10.1016/j.powtec.2021.01.012

Kalman, H., & Portnikov, D. (2020). Analyzing bulk density and void fraction: B. Effect of moisture content and compression pressure. *Powder Technology*, *381*, 285–297. https://doi.org/10.1016/j.powtec.2020.12.019

Kamboj, S., Saini, V., & Bala, S. (2014). Formulation and characterization of drug loaded nonionic surfactant vesicles (Niosomes) for oral bioavailability enhancement. *The Scientific World Journal*, *2014*. https://doi.org/10.1155/2014/959741

Kapoor, D., Maheshwari, R., Verma, K., Sharma, S., Ghode, P., & Tekade, R. K. (2019). Coating technologies in pharmaceutical product development. In *Drug Delivery Systems*. Elsevier Inc. https://doi.org/10.1016/B978-0-12-814487-9.00014-4

Lee, S. H., Bajracharya, R., Min, J. Y., Han, J., Park, B. J., & Han, H. (2020). Strategic approaches for colon targeted drug delivery: an overview of recent advancements. *Pharmaceutics*, *12*(68), 1–20. https://doi.org/10.3390/pharmaceutics12010068

Majumder, T., Biswas, G. R., & Majee, S. B. (2016). Hydroxy propyl methyl cellulose: different aspects in drug delivery. *Journal of Pharmacy and Pharmacology*, *4*(August), 381–385. https://doi.org/10.17265/2328-2150/2016.08.003

Mohamed, F. A., Robert, M., Seton, L., Ford, J. L., Levina, M., & Rajabi-siahboomi, A. R. (2013). The influence of HPMC concentration on release of theophylline or hydrocortisone from extended release mini-tablets. *Drug Development and Industrial Pharmacy*, *39*(March 2012), 1167–1174. https://doi.org/10.3109/03639045.2012.681053

Nining, N., Lestari, P. M., & Indah, P. M. (2020). Efek disintegrasi pati biji cempedak (Artocarpus champeden Lour) terpragelatinasi pada tablet ibuprofen. *Majalah Farmasi Dan Farmakologi*, *24*(3), 77–82. https://doi.org/10.20956/mff.v24i3.10776

Nining, N., Srifiana, Y., & Fadlianty, E. M. (2021). Preparation and characterization of enteric-coated delayed-release microsphere of phytosome loading allicin-rich extract. *International Journal of Applied Pharmaceutics*, *13*(Special Issue 3), 71–75. https://doi.org/10.22159/IJAP.2021.V13S3.15

Palai, S., Chandra, S., Pandey, N., & Singh, R. (2023). Theophylline: A bioactive dimethylxanthine alkaloid. In D. K. Semwal (Ed.), *The Essential Guide to Alkaloids* (Issue January, pp. 205–217). Nova Science Publishers. https://doi.org/10.52305/KXUM3530

Prusty, A., & Patra, A. (2022). Formulation and evaluation of ciprofloxacin colon targeted tablets by compression coating technique using guar gum and hydroxypropyl methylcellulose. *Journal of Research in Pharmacy*, *26*(6), 1593–1607. https://doi.org/10.29228/jrp.251

Rahmawati, D., Rositama, M. R., Permana, M. I., & Masyitah, N. (2018). *Penentuan kadar teofilin dalam sediaan tablet Bronsolvan® dengan metode standar adisi menggunakan spektrofotometer UV-visible*.

Rasul, A., Khan, M. I., Rehman, M. U., Abbas, G., Aslam, N., Ahmad, S., Abbas, K., Shah, P. A., Iqbal, M., Subari, A. M. A. Al, Shaheer, T., & Shah, S. (2020). In vitro characterization and release studies of combined nonionic surfactant-based vesicles for the prolonged delivery of an immunosuppressant model drug. *International Journal of Nanomedicine*, *15*, 7937–7949. https://doi.org/10.2147/IJN.S268846

Seo, K., Bajracharya, R., Lee, S. H., & Han, H. (2020). Pharmaceutical application of tablet film coating. *Pharmaceutics*, *12*(853), 1–20. https://doi.org/10.3390/pharmaceutics12090853

Sharma, A., & Kansal, A. (2023). Brief overview on sustained release theophylline (SRT): an older drug for COPD. In *Novel Aspects on Pharmaceutical Research Vol. 3* (pp. 109–112). BP International. https://doi.org/10.9734/bpi/napr/v3/3726E

Shukla, A. K., Bishnoi, R. S., Kumar, M., & Jain, C. (2019). Development of natural and modified gum based sustained-release film-coated table ts containing poorly water-soluble drug. *Asian Journal of Pharmaceutical and Clinical Research*, *12*(3), 266–271. https://doi.org/10.22159/ajpcr.2019.v12i3.30296

Singh, P., Shrivastava, A. K., Kumar, S., & Dwivedi, M. D. (2021). Formulation and evaluation of sustained release matrix tablets of aceclofenac. *Borneo Journal of Pharmacy*, *4*(2), 99–109. https://doi.org/10.33084/bjop.v4i2.1854

Solanki, D., & Motiwale, M. (2020). Studies on drug release kinetics and mechanism from sustained release matrix tablets of isoniazid using natural polymer obtained from Dioscorea alata. *International Journal of ChemTech Research*, *13*(03), 166–173. https://doi.org/10.20902/IJCTR.2019.130313

Syukri, Y. (2018). *Buku Ajar: Teknologi Sediaan Obat dalam Bentuk Solid*. Universitas Islam Indonesia.

Yi, S., Wang, J., Lu, Y., Ma, R., Gao, Q., Liu, S., & Xiong, S. (2019). Novel hot melt extruded matrices of hydroxypropyl cellulose and amorphous felodipine–plasticized hydroxypropyl methylcellulose as controlled release systems. *AAPS PharmSciTech*, *20*(219), 1–14. https://doi.org/10.1208/s12249-019-1435-7

Zaid, A. N. (2020). A comprehensive review on pharmaceutical film coating: past, present, and future. *Drug Design, Development and Therapy*, *14*, 4613–4623. https://doi.org/10.2147/DDDT.S277439

Pharmaciana
Vol.14, No.3, Nov 2024, Page. 408-422
ISSN: 2088 4559; e-ISSN: 2477 0256
DOI: 10.12928/pharmaciana.v14i3.30281

Application of vegetable oils as pharmaceutical ingredient: the impact of liquid lipid type on the characteristics of nanostructured lipid carrier

Annas Binarjo, Ernidawati, Khusnul Khotimah, Iis Wahyuningsih, Nuri Ari Efiana*
Department of Pharmaceutics and Pharmaceutical Technology, Universitas Ahmad Dahlan Yogyakarta
Jl. Prof. Dr. Soepomo, S.H., Warungboto, Umbulharjo, Yogyakarta,Indonesia

Submitted: 30-10-2024 ***Reviewed: 09-11-2024*** ***Accepted: 24-11-2024***

ABSTRACT

Recently, drug encapsulation using a Nanostructured Lipid Carrier (NLC) has gained attention in formulation studies due to its high loading capacity and prevent drug expulsion during storage. Drug loading capacity is mainly affected by lipid type and composition, especially liquid lipids. Therefore, this research aimed to evaluate the potential of avocado oil as a liquid lipid of NLC replacing pure oleic acid. All components including oil, glyceryl monostearate, Tween 20®, and Span 60® were processed to NLC by solvent injection method. The colloidal characteristics of NLC dispersion in water and 20 mM PBS pH 7 were determined, including transmittance, particle size, size distribution, zeta potential, loading capacity (LC), and loading efficiency (LE) of capsanthin in NLC. The results showed that NLC containing oleic acid (F_{ola}) and avocado oil (F_{avo}) dispersion in PBS exhibited a similar transmittance and zeta potential of 69-74% and -51 to -58 mV, respectively, whereas the particle size and size distribution of F_{avo} were significantly higher than F_{ola}. Moreover, the 1.3-fold higher LC and LE of F_{avo} compared to F_{ola} was insignificant ($p>0.05$). Additionally, the Tween 20® and Span 60® ratio of F_{avo} should be improved to obtain an ideal particle size and size distribution as in F_{ola}. In conclusion, avocado oil indicated the potential to be utilized as a liquid lipid of NLC formulation regarding zeta potential and drug loading. However, the surfactant composition should be adjusted to reduce the particle size of the NLC, leading to permeability enhancement in delivery, particularly oral administration.

Keywords: nanostructured lipid carrier, nanocarrier, avocado oil, vegetable oil application

Corresponding author:
Nuri Ari Efiana
Department of Pharmaceutics and Pharmaceutical Technology, Universitas Ahmad Dahlan
Jl. Prof. Dr. Soepomo, S.H., Warungboto, Umbulharjo, Yogyakarta, Indonesia
Email: nuri.efiana@pharm.uad.ac.id

INTRODUCTION

Recently, drug discovery has been moving toward two categories, small-molecule drugs and macromolecule biological products. The first category is dominated by lipophilic substances exhibiting low water solubility properties thereby categorized in Class II or IV of the Biopharmaceutics Classification System (BCS) leading to low oral bioavailability (Leeson, 2016; Lobo, 2020; Walters et al., 2011). Meanwhile, the second category meets a stability problem against the harsh environment of the gastrointestinal tract due to enzymatic activities and extreme pH. Moreover, biological product macromolecules also show low permeability across high-viscosity intestinal mucus and lipophilic-nature gastrointestinal membranes (Fuhrmann & Fuhrmann, 2017). One of the efforts to address such problems is the development of a nanocarrier system, including nanostructured lipid carrier (NLC), which has been proven to increase drug- dissolution and stability in gastrointestinal medium, and drug permeability across gastrointestinal barrier (Elmowafy et al., 2017; Mahor et al., 2023; Shahzadi et al., 2021).

NLC was developed to ameliorate the properties of solid lipid nanoparticles (SLN) by introducing liquid lipid, a key component that is not available in SLN formulation. This differentiating component modifies the characteristic of the lipid core leading to the enhancement of the capability of the nanocarrier to load the intended drug (Khan et al., 2022). The solubility of drugs in the core of SLN is affected by the crystal structure of the composing lipid. Therefore, the similar lipid composition of SLN might produce a different drug loading capacity due to lipid crystal polymorphism phenomena. A dense triglyceride polymorph, namely β-form, serves fewer crystal voids and spaces leading to decreased drug solubility, thereby loading capacity (Zhong & Zhang, 2019). Additionally, the drug can occupy the crystal defect (imperfection) in which much space is available due to crystal disorder (Mukherjee et al., 2009). Therefore, increasing the part of crystal defect of lipid or selecting an unstable solid form, including an amorphous state is proven to augment the solubility of the drug in the lipid core, leading to drug loading enhancement. However, during storage, the lipid molecules in the part of the crystal defect or amorphous self-arranges bringing the solid into perfect crystal leading to drug expulsion (Mukherjee et al., 2009). In NLC, alongside utilizing surfactants as in SLN, the liquid lipid is added producing a core consisting of a mixture of liquid and solid lipid. The introduction of liquid lipids in the lipid nanocarrier holds the imperfect condition of the lipid mixture, thereby enhancing the drug loading at a lower risk of drug expulsion (Chauhan et al., 2020; Ghasemiyeh & Mohammadi-Samani, 2018). Several types of liquid lipids could be used to formulate NLC, such as triglyceride, fatty acid, fatty alcohol, and vegetable or animal oil (Qushawy, 2021; Saedi et al., 2018; Soeratri et al., 2019; Veider et al., 2022).

The inhibition of lipid crystallization as well as directing the crystallization to a specific polymorphic form by liquid lipid producing a more accommodating crystal are determined by the type of liquid lipid (Bertoni et al., 2021; Yang et al., 2024). In the same liquid lipid type, for instance, free fatty acid, the carbon-chain length also determines the crystal packing of the lipid mixture (Beddoes et al., 2021). The similar aforementioned situations are likely to appear in NLC preparation, explaining the effect of liquid lipids on drug loading in NLC. Moreover, since emulsification is one of the steps in NLC preparation, the conformity between surfactant HLB and lipid mixture RHLB determines the diameter of NLC. Changing the liquid lipid type of the emulsion means shifting the RHLB resulting in an alteration of the internal phase (the pre-NLC) characteristics (Griffin, 1949). In previous study implemented various types of lipid fatty acid ester, namely triglyceride, ester propylene glycol, ester long chain alcohol, and polyethylene glycol in NLC formulation, concluded that the type of fatty acid ester affected the particle size and drug loading (Houacine et al., 2020).

The role of liquid lipid type in determining the characteristics of NLC underlies the needs of this research. Avocado oil was employed as a liquid lipid in NLC formulation to increase vegetable oil utilization. Avocado oil contained in NLC not only acts as an oil but also as an active ingredient since it shows various biological activities (Lin & Li, 2024). Therefore, as a first stage, this study aimed to identify the effect of lipid types, namely avocado oil and oleic acid on the characteristics of NLC. Avocado oil is a crude vegetable oil containing mostly triglyceride showing an esterified oleic acid substructure (Liu et al., 2023). Therefore, an NLC formulation containing oleic acid as a free fatty acid form was developed as a comparator formulation. Several characteristics of NLC formulations were

determined including transmittance of NLC dispersion, particle size, polydispersity index, and zeta potential. Moreover, capsanthin derived from paprika extract was used as a model drug to calculate loading efficiency (LE) and loading capacity (LC). The pharmacological activities of capsanthin and avocado oil are expected to support each other in delaying degenerative diseases, for instance, cardiovascular disease and diabetes (Jo et al., 2017; Kim et al., 2022).

MATERIALS AND METHOD

Materials

Avocado oil used as the liquid lipid of the first formulation of NLC was a cold-press product of PT Tamba Sanji Wani, Bali, Indonesia, whereas oleic acid was purchased from Alfa Kimia, Yogyakarta. Other materials used in both NLC formulations were glyceryl monostearate (GMS, Multi Jaya Kimia, Indonesia), Tween 20®, and Span 60® were purchased from (Nitrakimia, Yogyakarta). Standard capsanthin is of analytical grade purchased from BOC Sciences (USA). Capsanthin was purchased from the Qin Health Industry (Xi'an, China) as a paprika extract. The capsanthin concentration in the extract determined by spectrophotometric method is 37%. All components of the phosphate buffer saline (PBS), namely potassium phosphate mono- and dibasic and sodium chloride, were analytical grade of Sigma Aldrich (Singapore). Purified water and 95% ethanol were purchased from General Labora, Yogyakarta.

Methods

Preparation of NLC

NLC was prepared by solvent injection method (Duong et al., 2020) with slight modification according to the formulation as listed in Table 1. Firstly, a paprika extract containing about 185 mg of capsanthin was dissolved in 1000 µL of ethanol 70% at room temperature assisted by a magnetic bar stirring at about 300 rpm for 30 minutes. A similar stirring method was also applied to dissolve GMS and Span 60® in 70% ethanol, each of 700 µL, and the temperature was set at 60 °C. These three solutions were mixed at room temperature by stirring at 1000 rpm for 30 minutes before transferring into a vial containing liquid lipids. Subsequently, about 2000 µL of ethanol 70% was added to the rinse and the solution containing capsanthin, GMS, and Span 60®. The solution was added to the main mixture under continuous stirring at room temperature to get a homogenous oil phase. Afterward, Tween 20® solution in 50 mL of water was added dropwise into the continuously stirred oil phase to produce NLC dispersion in water. The unstructured and coarse structured lipids were separated by centrifugation at 4000 rpm for 15 minutes. The supernatant, colloidal dispersion of NLC, was collected and freeze-dried to remove the solvent. The NLC powder was stored in the fridge until further experiment.

Table 1. Formulation of NLC containing oleic acid (F_{ola}) and avocado oil (and F_{avo})

Components	Functions	Amount (mg)	
		F_{ola}	F_{avo}
Paprika extract (containing 37% of capsanthin)	Active substance	500	500
Glyceryl monostearate	*Solid lipid*	600	600
Oleic acid	*Liquid lipid*	300	-
Avocado oil	*Liquid lipid*	-	300
Tween 20®	Hydrophilic Surfactant	600	600
Span 60®	Lipophilic Surfactant	300	300

Note: The composition is for a processing batch of 50 mL in an emulsification (dispersion) step using purified water

Measurement of transmittance, particle size, polydispersity index, and zeta potential of NLC dispersion

About 10 mg of NLC was dispersed in 5 ml water as well as in 20 mM PBS pH 7 by stirring at 300 rpm for 30 minutes at 37°C. The transmittance of dispersed NLC was measured at a wavelength of 650 nm using a Shimadzu UV1900 spectrophotometer. Moreover, the characteristics of the NLC, namely

particle size, polydispersity index, and zeta potential were determined using Zetasizer® (Malvern Panalytical).

Loading Capacity (LC) and Loading Efficiency (LE) Determination

Loading capacity reflects the concentration in percent mass of drug loaded in the carrier. In this research, LC was determined by direct method (Garms et al., 2021) by measuring the concentration of capsanthin dissolved from the NLC in ethanol. Briefly, a precise weight of about 10 mg of NLC sample containing capsanthin (Mp) was dissolved in ethanol up to 5 mL (Ve). Thereafter, the absorbance of the solution was measured at its maximum wavelength (λ_{max}) of 476 nm to calculate the capsanthin concentration (Cc) using a calibration curve. Loading capacity (LC) was calculated using Equation 1 (Garms et al., 2021).

$$LC(\%) = \frac{(Cc\ x\ Ve)}{Mp}\ x\ 100\% \quad \text{.....(1)}$$

The amount of capsanthin loaded (CcxVe) in a precise weight of NLC (Mp) in LC determination was also used to calculate loading efficiency (LE). Some additional data was needed in the LE calculation (Equation 2) (Garms et al., 2021), including the mass of total capsanthin processed in a batch as stated in Table 1 (Mc) and the mass of total NLC recovered from a process (Mt). To define Mt, we pre-weighed the mass of the plastic tube for the freeze-drying procedure and determined the mass of the plastic tube containing NLC once the freeze-drying step was finished. Mt was calculated as mass differences of such values.

$$LE(\%) = \frac{(Mt/Mp\ x\ Cc\ x\ Ve)}{Mc}\ x\ 100\% \quad \text{.....(2)}$$

Data Analysis

Independent sample t-test at a 95% confidence interval was performed using SPSS Statistics 17 (IBM, 2008) to analyze the differences between two groups regarding the effect of medium disperse (water and PBS) on NLC colloid characteristics, including transmittance, particle size, polydispersity index, and zeta potential of each formulation, as well as the effect of liquid lipid type constructing NLC on above characteristics either in water medium or PBS. Moreover, the same statistical approach was also used to determine the effect of liquid lipid type on loading capacity and loading efficiency.

RESULTS AND DISCUSSION

The development of vegetable oil extraction technology increases the variety of oils to be used as nutrients as well as pharmacological materials (Saputra et al., 2024). Avocado oil extracted by cold-pressing preserves its composition as original (Çakaloğlu et al., 2018; Wandhekar et al., 2023) showing potential as anticancer, anti-inflammatory, antidiabetic, and anti-cholesterol (Alkhalaf et al., 2019; de Oliveira Marques et al., 2022; Del Toro-Equihua et al., 2016; Ericsson et al., 2023; Ilesanmi et al., 2022). Utilization of vegetable oil, as a component of lipid nanocarrier, namely avocado oil, is expected to obtain two advantages including physical and biological characteristics. Before this application, several pre-studies should be conducted as in the present research. The NLC formulation products were subjected to characterization (Figure 1). Both NLC formulations showed a red color due to capsanthin and could not be distinguished visually.

Effect of liquid lipid on the transmittance of colloidal dispersion

Fast and cheap investigation of particle size can be performed by measuring the transmittance of colloidal dispersion of NLC using a Spectrophotometer set up at 650 nm. The type of dispersed medium did not give any significant effect (at $p<0.05$) on the transmittance of NLC dispersion. Generally, NLC dispersion showing transmittance at above 70% is accepted regarding the particle size, namely, less than 500 nm (McClements & Rao, 2011). This submicron-sized particle is still possible to be absorbed by

the gastrointestinal membrane via pinocytosis mechanism (Wang et al., 2023). Based on transmittance data available in Figure 2, both formulations were predicted to exhibit an acceptable size (McClements & Rao, 2011; Wang et al., 2023). However, since other factors alongside particle size also determine the transmittance of colloidal dispersion (Zhang & Reineccius, 2016), a confirmation from a standard instrument for particle size measurement was conducted.

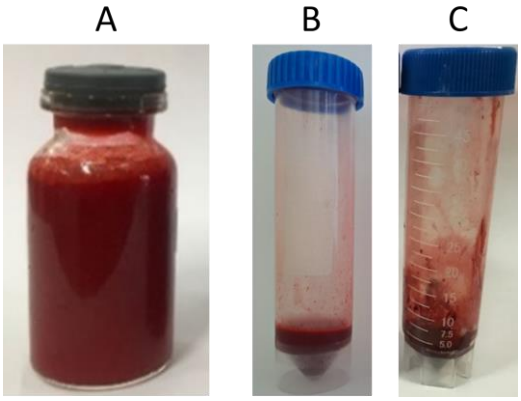

Figure 1. Photograph of NLC: emulsification step of NLC formulation (A), the supernatant of NLC formulation before freeze drying (B), The freeze-dried product of NLC (C)

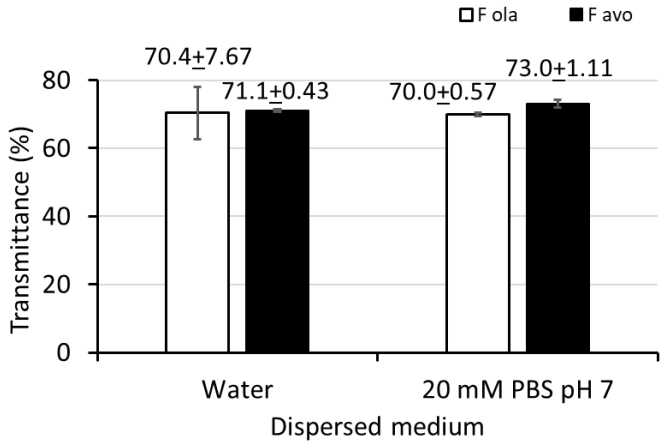

Figure 2. The transmittance of colloidal dispersion in water and PBS at a solid concentration of 2 mg/mL. The data is presented as mean ± SD of three replications

Effect of liquid lipid type on NLC characteristic

Liquid lipid type affects the particle size, size distribution, and zeta potential

In this research, two lipid types, namely, pure oleic acid and avocado oil, were utilized. In explaining the effect of liquid lipid type on NLC characteristics, the chemical information of avocado oil is provided in Figures 3 and 4. The lipid composition of avocado oil and the general molecular structure of the main lipid type are depicted in Figure 3 (Liu et al., 2023), whereas the variety of fatty acids present in avocado oil as either free or bonded to glycerol is shown in Figure 4 (Nasri et al., 2023).

As shown in Figure 5, dispersing NLC containing avocado oil, either in water or in PBS produced a significantly ($p<0.05$) higher particle size compared to that of F_{ola}. The higher particle size of NLC containing crude vegetable oil compared to oleic acid was also determined previously (Soeratri et al.,

2019). Two possibilities likely arose to argue the situation as follows. Firstly, as shown in Figure 4, the mass fraction of the polar substructure of oleic acid liquid lipid, namely COOH, is higher than that in the corresponding triglyceride, the most abundant lipid type of avocado oil (Figure 3). Exhibiting about 16% of the polar group, alongside as liquid lipid, oleic acid exhibits surfactant properties with a low HLB of about 1 (Martin & Bustamante, 1993; Sinko, 2006). This liquid lipid can assist Tween 20® and Span 60® in emulsifying the other lipid, leading to the production of small particles. The second argument is by applying the HLB-RHLB conformity theory suggesting that stable emulsion and structured lipid suspension are achieved in the nearest value between the HLB of surfactant/surfactants mixture and RHLB of lipid/lipids mixture. As a liquid lipid, oleic acid was assumed to have an RHLB of about 14-16, the value of general fatty acids (Pasquali et al., 2009), whereas the RHLB of avocado oil could be approximated from other vegetable oils by about 7 (Pham et al., 2022; Rave et al., 2020). Since the HLB of Tween 20® and Span 60® mixture at a 2:1 ratio is calculated to be about 13, it is closer to oleic acid than avocado oil. This second argument can also be used as a basis to improve the future formulation of NLC containing avocado oil, particularly in particle size issues. Once the exact value of the RHLB of avocado oil is known, the composition of the surfactant could be adjusted to reach the HLB approaching the RHLB. Moreover, the surfactant-to-lipid ratio and surfactant concentration in the dispersion system of preparation could be increased to reduce particle size in a targeted value, for instance, less than 200 nm to ensure permeability and stability during administration or delivery.

Showing a particle size of about 600 nm, the NLC applying avocado oil as liquid lipid is in the border of colloidal and coarse dispersion. Since the 600 nm value is the mean from a bulk NLC, some part of the bulk particle is in the colloidal range namely below 500 nm, and the other part is in the nanoparticle range, i.e. 500-1000 nm. In oral application, the colloidal particles below 200 nm are absorbed by nonspecific pinocytosis transport in all regions of the intestine. The larger particles are absorbed via M-cell contained in Peyer's patch and delivered to the lymphatic system where the particles are destroyed. Then, the smaller particles are delivered to the systemic circulation by-passing the liver (Cai et al., 2011; Delon et al., 2022; Trevaskis et al., 2007). In F_{ola} formulation, along with pinocytosis transport as in F_{avo}, some parts of NLC particles are below 50 nm which can be absorbed via a paracellular route in between intestinal cell (Mok, 2024).

Figure 5 likely disproves Figure 2 since Figure 5 shows that the particle size of F_{avo} was significantly ($p<0.05$) higher than F_{ola} in both mediums, while Figure 2 informs that the transmittance of colloidal dispersion predicted the equal particle size. However, they are not contradictory as explained in the following. The curve of transmittances as a function of particle size slews in a certain particle size depends on the dispersion type. For lipid/oil nano-carrier, the turning point usually lies in the range of 500-1000 nm, in which the border of the size-based dispersion type rests. Previous studies about lipid nanocarriers determined that the transmittance vs particle/droplet size curve shows a negative slope meaning the larger the particle/droplet the lower the transmittance is (Jan et al., 2022; Khan et al., 2020; Negi et al., 2014; Ziani et al., 2012). Inversely, coarse dispersion containing greater particle/droplet size, for instant emulsion, shows a greater transmittance (Linke & Drusch, 2016; Orafidiya & Oladimeji, 2002) It means that around 500 nm, for instance, 300-600 nm as in the present research, the transmittance significantly did not change.

Regarding the higher zeta potential in the negative direction of F_{ola} than F_{avo} dispersion in water medium as shown in Figure 6, it is explained by Figure 4 that the ionization ability of the hydrophilic substructure of oleic acid which is on the surface of lipid particles is higher than that of avocado oil consisting mostly of triglyceride. Consequently, it was likely that the solid surface of NLC containing oleic acid was more negative than that of avocado oil. The presence of electrolyte in dispersed medium likely donated the cation adsorbed on the particle surface of F_{ola} explaining the equal zeta potential of both NLC formulations in PBS dispersion.

The more negative zeta potential of NLC formulation containing oleic acid in comparison to that of lipid type other than free fatty acid which also evaluated in previous research (Andalib et al., 2012; Chinsriwongkul et al., 2012; Soeratri et al., 2019) indicates that oleic acid lays on the particle interphase. This strengthens the evidence that oleic acid has surfactant properties as mentioned previously. The

change in zeta potential by introducing a specific surfactant is adopted in the formulation of zeta potential changing nanocarrier. For instance, introducing a cationic surfactant in a lipid-based nanocarrier system, trimethyl tetradecyl ammonium bromide, brought the zeta potential of the nanocarrier to be positive, and *vice versa* for the addition of anionic surfactant (Efiana et al., 2022).

Zeta potential plays a crucial role regarding the stability during storage and the permeability in administration. The high zeta potential, either in a positive or negative direction hinders the flocculation of the dispersed phase of liquid formulation due to high electron repulsion, thereby hindering the increase in particle size and size distribution (Deryabin et al., 2015). Since both NLC formulations showed more than 30 mV (in a negative direction) then it is categorized as stable formulations (Malvern-Instrument, 2015). The negative value of zeta potential also provides a benefit in permeation across the mucus layer of the gastrointestinal membrane. The mucus of GI is constructed by oligosaccharides containing sialic acid sub-structure capable of ionizing. This negatively charged molecule attracts positively charged nanocarrier inhibiting nanocarrier permeation to the GI membrane (Griffin et al., 2016).

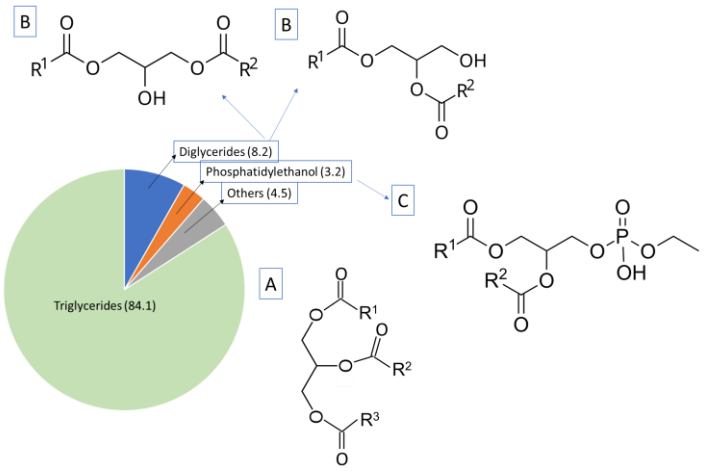

Figure 3. Lipid composition of avocado oil (Liu et al., 2023) and general molecular structure of triglyceride (A), diglyceride (B), and phosphatidylethanol (C). R^1-R^3 are carbon chains with or without double bonds which can be the same or different in carbon number

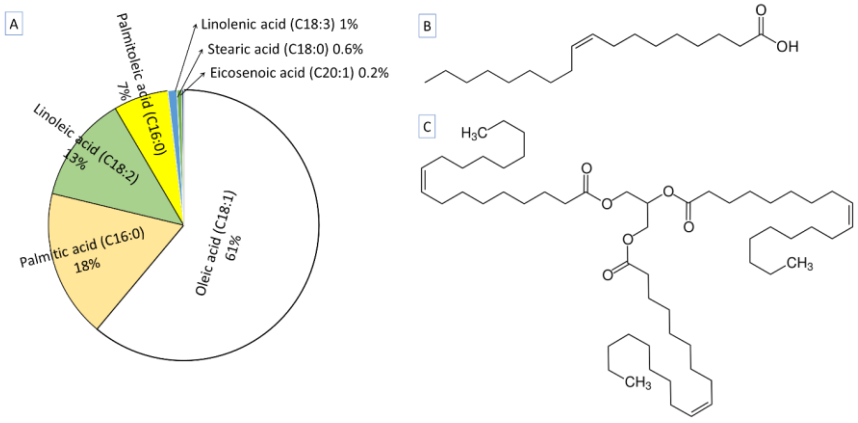

Figure 4. Average composition of fatty acid from 8 varieties of avocado oil (A) (Nasri et al., 2023), molecular structure of oleic acid (B) and glyceryl trioleate (C)

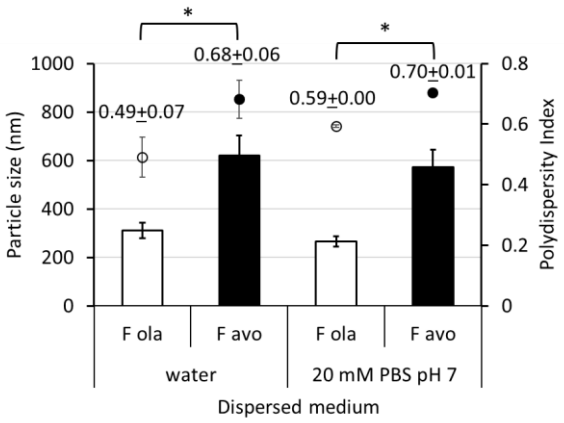

Figure 5. Particle size (bar) and polydispersity index (dot) of NLC particle dispersed in water and PBS of F_{ola} (white) and F_{avo} (black). The data is presented as mean ± SD of three replications. The star notation (*) indicates that the differences are significant at $p<0.05$, either for size or polydispersity index

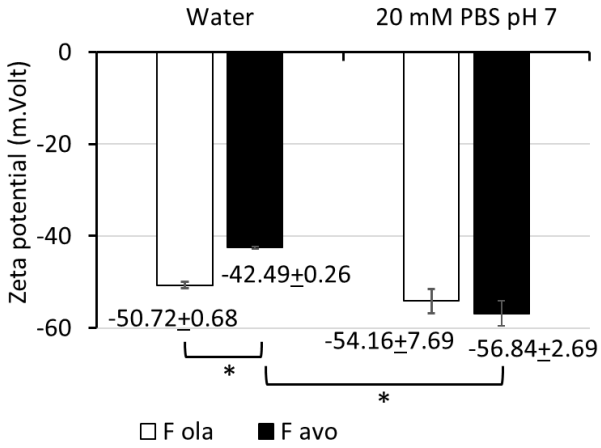

Figure 6. Zeta potential of NLC particle dispersed in water and PBS of F_{ola} (white) and F_{avo} (black). The data is presented as mean ± SD of three replications. The star notation (*) indicates that the difference is significant at $p<0.05$

Effect of liquid lipid type on NLC's drug loading

Drug loading in lipid nanoparticles (loading capacity, LC) reflects the solubility of drug molecules in the solid lipid constructing structured lipid carrier. The solubility of a drug in solid lipid is mostly determined by drug solubility in melted lipid at its melting point as an intrinsic property of drug and lipid (Alskär et al., 2016; Xu et al., 2022). Additionally, the crystallinity of solid lipids also plays a role in loading capacity in which low crystallinity solid, namely high defect lipid crystal, adopts more drug molecules leading to LC enhancement (Chauhan et al., 2020; Rosenblatt & Bunjes, 2017), thereby increasing the process efficiency. To induce and maintain lipid crystal defect, two liquid lipids were introduced in NLC formulation containing glyceryl monostearate solid lipid, namely oleic acid and vegetable oil. Capsanthin was used as a drug model to study the effect of resulted crystal defect on drug loading, and the data is shown in Figure 7.

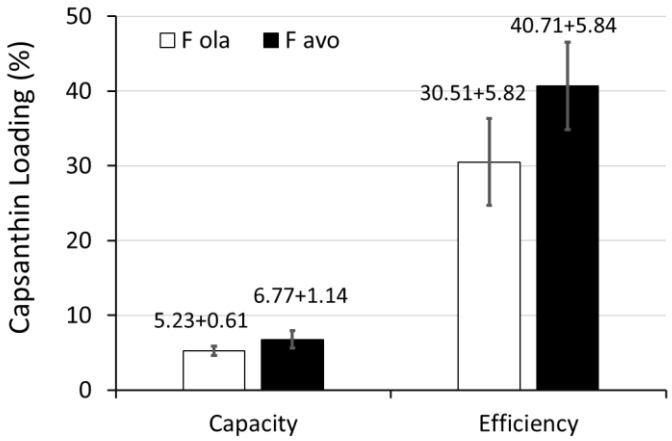

Figure 7. Loading capacity and loading efficiency of capsanthin in NLC formulation containing oleic acid (white bar) and avocado oil (black bar). The data is presented as mean ± SD of three replications

Figure 7 shows the slight differences in LC and LE of NLC due to the differences in liquid lipid components. It is predicted that a single-component liquid lipid, for instance, oleic acid, could be adopted more orderly during the crystallization of monoglyceride compared to a random molar ratio of multi-component liquid lipid as in vegetable oil. Therefore, the incorporation of avocado oil liquid lipids intensively decreased the crystallinity of solid lipids, higher than that of oleic acid. However, the high coefficient variation of the replication caused the differences are not significant (in $p<0.05$). Additionally, the physical characteristics might be used to indicate such lipid crystal imperfection (Aragão & Maximo, 2024; Flakemore et al., 2014; Folayan et al., 2019).

Effect of medium disperse on NLC characteristic

In particle size analysis using the dynamic light scattering method, particle size is represented by hydrodynamic diameter. The size is not only determined by solid-state diameter but also includes the electric Stern layer, an ionic solution extending from the surface of the solid to the slip plane when the particle is moving (Gordillo-Galeano & Mora-Huertas, 2021; Maguire et al., 2018). Since the thickness of the Stern layer is affected by ionic strength determined by the salt concentration in the dispersed medium (Brown et al., 2016), measuring the particle size in different mediums might yield different results. Moreover, the electrolyte concentration in the medium also affects the electric repulsion determined by the zeta potential of particles (Hutin et al., 2023). In this research, the characteristics of colloidal dispersion of NLC in 20 mM PBS pH 7 representing the condition in the gastrointestinal medium were measured and compared to those in water.

Figure 5 indicates that the particle size of both NLC formulations was decreased by the availability of electrolytes in the dispersed medium. Since the dispersed particle was the same, the differences in particle size after dispersion are affected by at least two possibilities, namely the particle aggregation and Stern layer shrinking or extending. In this study, the second likelihood is preferred since the particle size in the electrolyte medium is lower than in water which is in line with a theory suggesting that the thickness of the Stern layer is reduced by enhancing the ionic strength of the medium (Brown et al., 2016). The decrease in particle size due to the enhancement of ionic strength up to 3% was also evaluated in emulsion (Narukulla et al., 2020). The mechanism of electric layer compression due to electrolyte addition into medium disperse was explained by Guerrero-Garcia and co-workers. Briefly, the electrolyte presented in medium disperse increases the colloidal surface charge density, thereby inducing the deswelling of the electric field (Guerrero-García et al., 2019). Nonetheless, several previous studies identified that the particle size of NLC dispersed in electrolyte solution was higher than that in water. It

is explained that electrolytes induce particle aggregation (Choi et al., 2014; Gordillo-Galeano & Mora-Huertas, 2021). It is also possible that aggregation in PBS medium increasing the particle size has occurred but in a less pronounced than Stern layer shrinking. The higher size distribution of both NLC formulations dispersed in PBS in comparison to that in water correlated to aggregation. The electrolyte induced some parts of the NLC particle to aggregate, while another part remained as separate particles. This situation produced a higher size distribution in the PBS medium (Figure 5).

Regarding the higher zeta potential of both NLC formulations when dispersed in PBS (Figure 6), it is justified as follows. Potential-determining ion, the cation in this case, adsorbed onto the solid surface, followed by anionic counterions (*gegenions*) adsorbed on the next-outer layer by the slip plane. In the water medium, the availability of potential-determining ions and *gegenions* is not enough to decrease the negatively charged surface resulting in a maintaining of the more negative of F_{ola} until the slip plane. The more negative of the solid surface of F_{ola} formulation could be countered by cation and anions available in PBS medium resulting in equal zeta potential to F_{avo}. It should be noted that the thickness of the Stern layer in the PBS medium is less than in water, explaining why the similar zeta potential is more negative in the PBS medium than in water. However, it should be considered that based on statistical analysis the effect of the dispersed medium was only significant ($p<0.05$) on the zeta potential of F_{avo} and the polydispersity index of F_{ola}.

CONCLUSION

Pre-formulation studies on the use of avocado oil in NLC formulations have been conducted to improve the utilization of this oil for pharmaceutical applications as an alternative to oleic acid. This oil has the potential to be used in NLC formulation since the zeta potential, loading capacity, and loading efficiency are in an acceptable range and close to the NLC standard applying oleic acid liquid lipid. However, the higher particle size and size distribution of NLC-containing avocado oil in comparison to NLC-containing oleic acid should be addressed. It is suggested to adjust the surfactant ratio in the formulation of NLC containing avocado oil to reduce particle size and size distribution. Alternatively, the nonionic surfactant type could be used in further research, including in the NLC formulation applying other vegetable oils.

ACKNOWLEDGEMENT

The authors thank Lembaga Penelitian dan Pengabdian Masyarakat (LPPM) Universitas Ahmad Dahlan for supporting this research.

REFERENCES

Akusu, O. M., Obinna-Echem, P. C., Opurum, P. C. C., & Chibor, B. S. (2021). Comparative analysis of the physicochemical characteristics, phytochemical components and fatty acid profile of Avocado Pear (Persea Americana L) pulp and seed oil. *European Journal of Agriculture and Food Sciences*, *3*(1), Article 1. https://doi.org/10.24018/ejfood.2021.3.1.212

Alkhalaf, M. I., Alansari, W. S., Ibrahim, E. A., & ELhalwagy, M. E. A. (2019). Anti-oxidant, anti-inflammatory and anti-cancer activities of avocado (*Persea americana*) fruit and seed extract. *Journal of King Saud University - Science*, *31*(4), 1358–1362. https://doi.org/10.1016/j.jksus.2018.10.010

Alskär, L. C., Porter, C. J. H., & Bergström, C. A. S. (2016). Tools for early prediction of drug loading in lipid-based formulations. *Molecular Pharmaceutics*, *13*(1), 251–261. https://doi.org/10.1021/acs.molpharmaceut.5b00704

Aragão, V. C., & Maximo, G. J. (2024). Thermophysical properties of blends composed of Amazonian fats and soybean oil. *Food Research International*, *177*, 113911. https://doi.org/10.1016/j.foodres.2023.113911

Beddoes, C. M., Rensen, D. E., Gooris, G. S., Malfois, M., & Bouwstra, J. A. (2021). The importance of free fatty chain length on the lipid organization in the long periodicity phase. *International Journal of Molecular Sciences*, *22*(7), 3679. https://doi.org/10.3390/ijms22073679

Bertoni, S., Passerini, N., & Albertini, B. (2021). Liquid lipids act as polymorphic modifiers of tristearin-based formulations produced by melting technologies. *Pharmaceutics*, *13*(7), Article 7. https://doi.org/10.3390/pharmaceutics13071089

Brown, M. A., Goel, A., & Abbas, Z. (2016). Effect of Electrolyte concentration on the stern layer thickness at a charged interface. *Angewandte Chemie*, *128*(11), 3854–3858. https://doi.org/10.1002/ange.201512025

Cai, S., Yang, Q., Bagby, T. R., & Forrest, M. L. (2011). Lymphatic drug delivery using engineered liposomes and solid lipid nanoparticles. *Advanced Drug Delivery Reviews*, *63*(10–11), 901–908. https://doi.org/10.1016/j.addr.2011.05.017

Çakaloğlu, B., Özyurt, V. H., & Ötleş, S. (2018). Cold press in oil extraction. A review. *Ukrainian Food Journal*, *7*(4), 640–654. https://doi.org/10.24263/2304- 974X-2018-7-4-9

Chauhan, I., Yasir, M., Verma, M., & Singh, A. P. (2020). Nanostructured lipid carriers: a groundbreaking approach for transdermal drug delivery. *Advanced Pharmaceutical Bulletin*, *10*(2), 150–165. https://doi.org/10.34172/apb.2020.021

Chinsriwongkul, A., Chareanputtakhun, P., Ngawhirunpat, T., Rojanarata, T., Sila-on, W., Ruktanonchai, U., & Opanasopit, P. (2012). Nanostructured lipid carriers (NLC) for parenteral delivery of an anticancer drug. *AAPS PharmSciTech*, *13*(1), 150–158. https://doi.org/10.1208/s12249-011-9733-8

Choi, K.-O., Aditya, N. P., & Ko, S. (2014). Effect of aqueous pH and electrolyte concentration on structure, stability and flow behavior of non-ionic surfactant based solid lipid nanoparticles. *Food Chemistry*, *147*, 239–244. https://doi.org/10.1016/j.foodchem.2013.09.095

de Oliveira Marques, S., Muller, A. P., Luciano, T. F., dos Santos Tramontin, N., da Silva Caetano, M., Luis da Silva Pieri, B., Amorim, T. L., de Oliveira, M. A. L., & de Souza, C. T. (2022). Effects of Avocado Oil supplementation on insulin sensitivity, cognition, and inflammatory and oxidative stress markers in different tissues of diet-induced obese mice. *Nutrients*, *14*(14), Article 14. https://doi.org/10.3390/nu14142906

Del Toro-Equihua, M., Velasco-Rodríguez, R., López-Ascencio, R., & Vásquez, C. (2016). Effect of an avocado oil-enhanced diet (*Persea americana*) on sucrose-induced insulin resistance in Wistar rats. *Journal of Food and Drug Analysis*, *24*(2), 350–357. https://doi.org/10.1016/j.jfda.2015.11.005

Delon, L., Gibson, R. J., Prestidge, C. A., & Thierry, B. (2022). Mechanisms of uptake and transport of particulate formulations in the small intestine. *Journal of Controlled Release*, *343*, 584–599. https://doi.org/10.1016/j.jconrel.2022.02.006

Deryabin, D. G., Efremova, L. V., Vasilchenko, A. S., Saidakova, E. V., Sizova, E. A., Troshin, P. A., Zhilenkov, A. V., & Khakina, E. E. (2015). A zeta potential value determines the aggregate's size of penta-substituted [60]fullerene derivatives in aqueous suspension whereas positive charge is required for toxicity against bacterial cells. *Journal of Nanobiotechnology*, *13*, 50. https://doi.org/10.1186/s12951-015-0112-6

Duong, V.-A., Nguyen, T.-T.-L., & Maeng, H.-J. (2020). Preparation of solid lipid nanoparticles and nanostructured lipid carriers for drug delivery and the effects of preparation parameters of solvent injection method. *Molecules*, *25*(20), Article 20. https://doi.org/10.3390/molecules25204781

Efiana, N. A., Fürst, A., Saleh, A., Shahzadi, I., & Bernkop-Schnürch, A. (2022). Phosphate decorated lipid-based nanocarriers providing a prolonged mucosal residence time. *International Journal of Pharmaceutics*, *625*, 122096. https://doi.org/10.1016/j.ijpharm.2022.122096

Elmowafy, M., Ibrahim, H. M., Ahmed, M. A., Shalaby, K., Salama, A., & Hefesha, H. (2017). Atorvastatin-loaded nanostructured lipid carriers (NLCs): Strategy to overcome oral delivery drawbacks. *Drug Delivery*, *24*(1), 932–941. https://doi.org/10.1080/10717544.2017.1337823

Ericsson, C. I., Pacheco, L. S., Romanos-Nanclares, A., Ecsedy, E., Giovannucci, E. L., Eliassen, A. H., Mucci, L. A., & Fu, B. C. (2023). Prospective study of avocado consumption and cancer risk in us men and women. *Cancer Prevention Research (Philadelphia, Pa.)*, *16*(4), 211. https://doi.org/10.1158/1940-6207.CAPR-22-0298

Flakemore, A. R., McEvoy, P. D., Balogun, R. O., Malau-Aduli, B. S., Nichols, P., & Malau-Aduli, A. E. O. (2014). Degummed crude canola oil supplementation affects fat depot melting points in purebred and first-cross merino sheep. *Animal and Veterinary Sciences*, *2*(3), Article 3. https://doi.org/10.11648/j.avs.20140203.14

Folayan, A. J., Anawe, P. A. L., Aladejare, A. E., & Ayeni, A. O. (2019). Experimental investigation of the effect of fatty acids configuration, chain length, branching and degree of unsaturation on biodiesel fuel properties obtained from lauric oils, high-oleic and high-linoleic vegetable oil biomass. *Energy Reports*, *5*, 793–806. https://doi.org/10.1016/j.egyr.2019.06.013

Fuhrmann, K., & Fuhrmann, G. (2017). Recent advances in oral delivery of macromolecular drugs and benefits of polymer conjugation. *Current Opinion in Colloid & Interface Science*, *31*, 67–74. https://doi.org/10.1016/j.cocis.2017.07.002

Garms, B. C., Poli, H., Baggley, D., Han, F. Y., Whittaker, A. K., A, A., & Grøndahl, L. (2021). Evaluating the effect of synthesis, isolation, and characterisation variables on reported particle size and dispersity of drug loaded PLGA nanoparticles. *Materials Advances*, *2*(17), 5657–5671. https://doi.org/10.1039/D1MA00410G

Ghasemiyeh, P., & Mohammadi-Samani, S. (2018). Solid lipid nanoparticles and nanostructured lipid carriers as novel drug delivery systems: Applications, advantages and disadvantages. *Research in Pharmaceutical Sciences*, *13*(4), 288–303. https://doi.org/10.4103/1735-5362.235156

Gordillo-Galeano, A., & Mora-Huertas, C. E. (2021). Hydrodynamic diameter and zeta potential of nanostructured lipid carriers: Emphasizing some parameters for correct measurements. *Colloids and Surfaces A: Physicochemical and Engineering Aspects*, *620*, 126610. https://doi.org/10.1016/j.colsurfa.2021.126610

Griffin, B., Guo, J., Presas, E., Donovan, M. D., Alonso, M. J., & O'Driscoll, C. M. (2016). Pharmacokinetic, pharmacodynamic and biodistribution following oral administration of nanocarriers containing peptide and protein drugs. *Advanced Drug Delivery Reviews*, *106*, 367–380. https://doi.org/10.1016/j.addr.2016.06.006

Griffin, W. C. (1949). Classification of Surface-Active Agents by "HLB." *Journal of Cosmetic Science*, *1*, 311–326

Guerrero-García, G. I., González-Tovar, E., Chávez-Páez, M., & Wei, T. (2019). Expansion and shrinkage of the electrical double layer in charge-asymmetric electrolytes: A non-linear poisson-boltzmann description. *Journal of Molecular Liquids*, *277*, 104–114. https://doi.org/10.1016/j.molliq.2018.11.163

Houacine, C., Adams, D., & Singh, Kamalinder. K. (2020). Impact of liquid lipid on development and stability of trimyristin nanostructured lipid carriers for oral delivery of resveratrol. *Journal of Molecular Liquids*, *316*, 113734. https://doi.org/10.1016/j.molliq.2020.113734

Hutin, A., Lima, N., Lopez, F., & Carvalho, M. (2023). Stability of silica nanofluids at high salinity and high temperature. *Powders*, *2*(1), Article 1. https://doi.org/10.3390/powders2010001

Ilesanmi, T. M., Oladipo, O. O., Olaleye, A. C., & Osasona, O. D. (2022). Antimicrobial activity of essential oil from Avocado (Persea americana) seed and pulp on some pathogenic organisms. *South Asian Journal of Research in Microbiology*, 61–68. https://doi.org/10.9734/sajrm/2022/v12i330276

Jan, Y., Al-Keridis, L. A., Malik, M., Haq, A., Ahmad, S., Kaur, J., Adnan, M., Alshammari, N., Ashraf, S. A., & Panda, B. P. (2022). Preparation, modelling, characterization and release profile of vitamin D3 nanoemulsion. *LWT*, *169*, 113980. https://doi.org/10.1016/j.lwt.2022.113980

Jo, S. J., Kim, J. W., Choi, H. O., Kim, J. H., Kim, H. J., Woo, S. H., & Han, B. H. (2017). Capsanthin inhibits both adipogenesis in 3T3-L1 preadipocytes and weight gain in high-fat diet-induced obese Mice. *Biomolecules & Therapeutics*, *25*(3), 329–336. https://doi.org/10.4062/biomolther.2017.048

Khan, S. A., Rehman, S., Nabi, B., Iqubal, A., Nehal, N., Fahmy, U. A., Kotta, S., Baboota, S., Md, S., & Ali, J. (2020). Boosting the brain delivery of atazanavir through nanostructured lipid carrier-based approach for mitigating NeuroAIDS. *Pharmaceutics*, *12*(11), Article 11. https://doi.org/10.3390/pharmaceutics12111059

Khan, S., Sharma, A., & Jain, V. (2022). An overview of nanostructured lipid carriers and its application in drug delivery through different routes. *Advanced Pharmaceutical Bulletin*, *13*(3), 446. https://doi.org/10.34172/apb.2023.056

Kim, S., Lee, Y.-R., Lee, E.-O., Jin, H., Choi, Y.-H., Joo, H.-K., & Jeon, B.-H. (2022). Capsanthin inhibits atherosclerotic plaque formation and vascular inflammation in ApoE−/− Mice. *Biomedicines*, *10*(8), Article 8. https://doi.org/10.3390/biomedicines10081780

Leeson, P. D. (2016). Molecular inflation, attrition and the rule of five. *Advanced Drug Delivery Reviews*, *101*, 22–33. https://doi.org/10.1016/j.addr.2016.01.018

Lin, X., & Li, Z. (2024). Key components and multiple health functions of avocado oil: A review. *Journal of Functional Foods*, *122*, 106494. https://doi.org/10.1016/j.jff.2024.106494

Linke, C., & Drusch, S. (2016). Turbidity in oil-in-water-emulsions—Key factors and visual perception. *Food Research International*, *89*, 202–210. https://doi.org/10.1016/j.foodres.2016.07.019

Liu, Y., Xia, Q., Qian, Y., Kuang, Y., Liu, J., & Lin, L. (2023). Effects of three extraction methods on Avocado oil lipid compounds analyzed via UPLC-TOF-MS/MS with OPLS-DA. *Foods*, *12*(6), Article 6. https://doi.org/10.3390/foods12061174

Lobo, S. (2020). Is there enough focus on lipophilicity in drug discovery? *Expert Opinion on Drug Discovery*, *15*(3), 261–263. https://doi.org/10.1080/17460441.2020.1691995

Maguire, C. M., Rösslein, M., Wick, P., & Prina-Mello, A. (2018). Characterisation of particles in solution – a perspective on light scattering and comparative technologies. *Science and Technology of Advanced Materials*, *19*(1), 732. https://doi.org/10.1080/14686996.2018.1517587

Mahor, A. K., Singh, P. P., Gupta, R., Bhardwaj, P., Rathore, P., Kishore, A., Goyal, R., Sharma, N., Verma, J., Rosenholm, J. M., & Bansal, K. K. (2023). Nanostructured lipid carriers for improved delivery of therapeutics via the oral route. *Journal of Nanotechnology*, *2023*(1), 4687959. https://doi.org/10.1155/2023/4687959

Malvern-Instrument. (2015). *ZetaPotential- an Introduction in 30 minute*. Malvern Instruments Worldwide.

Martin, A. N., & Bustamante, P. (1993). *Physical Pharmacy: Physical Chemical Principles in the Pharmaceutical Sciences*. Lea & Febiger

McClements, D. J., & Rao, J. (2011). Food-grade nanoemulsions: formulation, fabrication, properties, performance, biological fate, and potential toxicity. *Critical Reviews in Food Science and Nutrition*, *51*(4), 285–330. https://doi.org/10.1080/10408398.2011.559558

Mok, Z. H. (2024). The effect of particle size on drug bioavailability in various parts of the body. *Pharmaceutical Science Advances*, *2*, 100031. https://doi.org/10.1016/j.pscia.2023.100031

Mukherjee, S., Ray, S., & Thakur, R. S. (2009). Solid lipid nanoparticles: a modern formulation approach in drug delivery system. *Indian Journal of Pharmaceutical Sciences*, *71*(4), 349. https://doi.org/10.4103/0250-474X.57282

Narukulla, R., Ojha, U., & Sharma, T. (2020). Effect of NaCl concentration on stability of a polymer–Ag nanocomposite based pickering emulsion: validation via rheological analysis with varying temperature. *RSC Advances*, *10*(36), 21545–21560. https://doi.org/10.1039/D0RA03199B

Nasri, C., Halabi, Y., Hajib, A., Choukri, H., Harhar, H., Lee, L.-H., Mani, V., Ming, L. C., Goh, K. W., Bouyahya, A., & Tabyaoui, M. (2023). Proximate composition, lipid and elemental profiling of eight varieties of avocado (Persea americana). *Scientific Reports*, *13*(1), 22767. https://doi.org/10.1038/s41598-023-50119-y

Negi, L. M., Jaggi, M., & Talegaonkar, S. (2014). Development of protocol for screening the formulation components and the assessment of common quality problems of nano-structured lipid carriers. *International Journal of Pharmaceutics*, *461*(1), 403–410. https://doi.org/10.1016/j.ijpharm.2013.12.006

Orafidiya, L. O., & Oladimeji, F. A. (2002). Determination of the required HLB values of some essential oils. *International Journal of Pharmaceutics*, *237*(1), 241–249. https://doi.org/10.1016/S0378-5173(02)00051-0

Pasquali, R. C., Bregni, C., & Taurozzi, M. P. (2009). New values of the required hydrophilic-lipophilic balance for oil in water emulsions of solid fatty acids and alcohols obtained from solubility parameter and dielectric constant values. *Journal of Dispersion Science and Technology*, *30*(3), 328–331. https://doi.org/10.1080/01932690802540517

Pham, N. T. T., Le, Q. N., Vo, N. K., Nguyen, N.-S., Le, T. X., & Tran, T. V. (2022). Formulation of virgin coconut oil microemulsion with natural excipients. *Science and Technology Development Journal: Health Sciences*, *3*(2), Article 2. https://doi.org/10.32508/stdjhs.v3i2.521

Qushawy, M. (2021). Effect of the surfactant and liquid lipid type in the physico-chemical characteristics of beeswax-based Nanostructured Lipid Carrier (NLC) of Metformin. *Pharmaceutical Nanotechnology*, *9*(3), 200–209. https://doi.org/10.2174/2211738509666210222143716

Rave, M. C., Echeverri, J. D., & Salamanca, C. H. (2020). Improvement of the physical stability of oil-in-water nanoemulsions elaborated with *Sacha inchi* oil employing ultra-high-pressure homogenization. *Journal of Food Engineering*, *273*, 109801. https://doi.org/10.1016/j.jfoodeng.2019.109801

Rosenblatt, K. M., & Bunjes, H. (2017). Evaluation of the drug loading capacity of different lipid nanoparticle dispersions by passive drug loading. *European Journal of Pharmaceutics and Biopharmaceutics*, *117*, 49–59. https://doi.org/10.1016/j.ejpb.2017.03.010

Saedi, A., Rostamizadeh, K., Parsa, M., Dalali, N., & Ahmadi, N. (2018). Preparation and characterization of nanostructured lipid carriers as drug delivery system: influence of liquid lipid types on loading and cytotoxicity. *Chemistry and Physics of Lipids*, *216*, 65–72. https://doi.org/10.1016/j.chemphyslip.2018.09.007

Saputra, H., Azrifirwan, A., & Firdani, F. (2024). Evaluation of vegetable oil extraction methods on crude oil yields in Indonesia. Systematic Literature Review. *GreenTech*, *1*(1), Article 1

Shahzadi, I., Fürst, A., Knoll, P., & Bernkop-Schnürch, A. (2021). Nanostructured Lipid Carriers (NLCs) for oral peptide drug delivery: about the impact of surface decoration. *Pharmaceutics*, *13*(8), 1312. https://doi.org/10.3390/pharmaceutics13081312

Sinko, P. J. (2006). *Martin's Physical Pharmacy and Pharmaceutical Sciences: Physical Chemical and Biopharmaceutical Principles in the Pharmaceutical Sciences*. Lippincott Williams & Wilkins

Soeratri, W., Hidayah, R., & Rosita, N. (2019). Effect of combination soy bean oil and oleic acid to characteristic, penetration, physical stability of nanostructure lipid carrier resveratrol. *Folia Medica Indonesiana*, *55*(3), Article 3. https://doi.org/10.20473/fmi.v55i3.15505

Trevaskis, N. L., Charman, W. N., & Porter, C. J. (2007). Lipid-based delivery systems and intestinal lymphatic drug transport: A mechanistic update. *Advanced Drug Delivery Reviews*, *60*(6), 702. https://doi.org/10.1016/j.addr.2007.09.007

Veider, F., Akkuş-Dağdeviren, Z. B., Knoll, P., & Bernkop-Schnürch, A. (2022). Design of nanostructured lipid carriers and solid lipid nanoparticles for enhanced cellular uptake. *International Journal of Pharmaceutics*, *624*, 122014. https://doi.org/10.1016/j.ijpharm.2022.122014

Walters, W. P., Green, J., Weiss, J. R., & Murcko, M. A. (2011). What Do Medicinal Chemists Actually Make? A 50-Year Retrospective. *Journal of Medicinal Chemistry*, *54*(19), 6405–6416. https://doi.org/10.1021/jm200504p

Wandhekar, S., Pawar, V., Shinde, S., & Gangakhedkar, P. (2023). Extraction of oil from oilseeds by cold pressing: A review. *Indian Food Industry Mag*, *4*, 63–69

Wang, D., Jiang, Q., Dong, Z., Meng, T., Hu, F., Wang, J., & Yuan, H. (2023). Nanocarriers transport across the gastrointestinal barriers: The contribution to oral bioavailability via blood circulation and lymphatic pathway. *Advanced Drug Delivery Reviews*, *203*, 115130. https://doi.org/10.1016/j.addr.2023.115130

Xu, L., Wang, X., Liu, Y., Yang, G., Falconer, R. J., & Zhao, C.-X. (2022). Lipid nanoparticles for drug delivery. *Advanced NanoBiomed Research*, *2*(2), 2100109. https://doi.org/10.1002/anbr.202100109

Yang, D., Lee, Y.-Y., Lu, Y., Wang, Y., & Zhang, Z. (2024). Internal factors affecting the crystallization of the lipid system: triacylglycerol structure, composition, and minor components. *Molecules*, *29*(8), 1847. https://doi.org/10.3390/molecules29081847

Zhang, J., & Reineccius, G. A. (2016). Factors controlling the turbidity of submicron emulsions stabilized by food biopolymers and natural surfactant. *LWT - Food Science and Technology*, *71*, 162–168. https://doi.org/10.1016/j.lwt.2016.03.035

Zhong, Q., & Zhang, L. (2019). Nanoparticles fabricated from bulk solid lipids: Preparation, properties, and potential food applications. *Advances in Colloid and Interface Science*, *273*, 102033. https://doi.org/10.1016/j.cis.2019.102033

Ziani, K., Fang, Y., & McClements, D. J. (2012). Fabrication and stability of colloidal delivery systems for flavor oils: Effect of composition and storage conditions. *Food Research International*, *46*(1), 209–216. https://doi.org/10.1016/j.foodres.2011.12.017

Pharmaciana
Vol.14, No.3, Nov 2024, Page. 423-433
ISSN: 2088 4559; e-ISSN: 2477 0256
DOI: 10.12928/pharmaciana.v14i3.27850

DNA-based detection of Rat in the meatballs product using a real-time polymerase chain reaction method

Etin Diah Permanasari[1,4,5], Hadi Sunaryo[2,4,5], Adia Putra Wirman[3,5], Nuriza Rahmadini[2,4,5], Savira Yustinah Aggasy[3], Nurul Azmah Nikmatullah[3,4,5*],
[1]Magister Ilmu Farmasi, Sekolah Pascasarjana, Universitas Muhammadiyah Prof. DR. HAMKA
Jl Delima II, Duren Sawit, East Jakarta, DKI Jakarta, Indonesia
[2]Program Studi Sarjana Farmasi, Fakultas Farmasi dan Sains, Universitas Muhammadiyah Prof. DR. HAMKA
Jl Delima II, Duren Sawit, East Jakarta, DKI Jakarta, Indonesia
[3]Program Studi Analis Kesehatan, Fakultas Farmasi dan Sains, Universitas Muhammadiyah Prof. DR. HAMKA
Jl Delima II, Duren Sawit, East Jakarta, DKI Jakarta, Indonesia
[4]Pusat Kajian Halal, Universitas Muhammadiyah Prof. DR. HAMKA
Jl Delima II, Duren Sawit, East Jakarta, DKI Jakarta, Indonesia
[5]Pusat Laboratorium Pengujian, Universitas Muhammadiyah Prof. DR. HAMKA
Jl Delima II, Duren Sawit, East Jakarta, DKI Jakarta, Indonesia

Submitted: 10-12-2023 ***Reviewed: 28-02-2024*** ***Accepted: 22-08-2024***

ABSTRACT

The meat-based products are highly susceptible to counterfeiting, primarily due to high consumer demand of meat derivative products, such as meatballs. This demand creates opportunities for food fraud by specific industries, including adulterating meat with non-halal species, such as rats. This research aimed to detect rat meat contamination in meatball samples from the Indonesian local market using Real-time Polymerase Chain Reaction (RT-PCR). The RT-PCR amplification involved an initial denaturation step at 95°C for 3 minutes, followed by denaturation at 95°C for 15 seconds, and annealing/extension at 60°C for 1 minute. The rat-specific probe primer included in the kit produced an increasing curve in the External Positive Control (EPC) with a Ct value of 27.22, and no amplification occurred in the Negative Control (NTC). The analysis of 30 samples from meatball vendors yielded negative results, as there was no increase in the FAM (rat) curve, indicating that none of the meatballs were contaminated with rat DNA.

Keywords: food fraud, meatballs, Rat, Real-time PCR, meat-based products

Corresponding author:
Nurul Azmah Nikmatullah
Analis Kesehatan, Fakultas Farmasi dan Sains, Universitas Muhammadiyah Prof. DR. HAMKA
Pusat Kajian Halal, Universitas Muhammadiyah Prof. DR. HAMKA
Pusat Laboratorium Pengujian, Universitas Muhammadiyah Prof. DR. HAMKA
Jl Delima II, Duren Sawit, East Jakarta, DKI Jakarta, Indonesia
Email: nurulazmah@uhamka.ac.id

INTRODUCTION

Nowadays, public halal awareness in Indonesia is rising as food frauds and adulterations increase. The increasing awareness is also affected by the implementation of the Indonesian Halal Regulation on Law Number 33 of 2014 concerning Halal Product Assurance. However, food adulteration and fraud incidents have continually occurred (Nida et al., 2020). These cases also happen globally and threaten the market (Owolabi & Olayinka, 2021). In the case of meat-based products the high consumer demand for meat-based products has led several industries to commit fraud in terms of mixing meat with non-halal materials. Meatball fraud is the most common food fraud in the Indonesian market. Meatballs are one of the popular dishes in Indonesia (Purnomo & Rahardiyan, 2008). The primary ingredient is beef; however, the beef is mixed or replaced with other animals at relatively lower prices to reduce costs, such as chicken, pig, boar, or rats.

It has been reported that 7.83% of beef samples were mixed with boar meat throughout 2013-2017 in Bogor (Nida et al., 2020). A study of commercial beef meatballs reported that 22 of 36 meatballs samples in Bojonegoro, East Java, contained pork (Siswara et al., 2022). Nine cases of pork contamination in the meatball samples were reported in Yogyakarta Province (Erwanto et al., 2014). Other studies also revealed pork contamination in Indonesian meatballs (Cahyadi et al., 2020; Indriati & Yuniarsih, 2019; Siswara et al., 2021; Waluyo et al., 2023). In addition to pork contamination, dog meat was also found in the adulterated beef meatball formulation (Guntarti & Purbowati, 2019; Rohman, Pebriyanti, et al., 2020; Rohman, Rahayu, et al., 2020). Recently, the cases of rat meat contamination have also increased in meatball products (Cahyadi et al., 2020; IkaWidyasa et al., 2015; Lestari et al., 2022; Suryawan et al., 2020). In addition, other processed meat products, including sausages, are also reported to contain rat meat (Sunaryo et al., 2022).

As halal authenticity is essential, various detection techniques have been elaborared to confirm the presence of non-halal species in meat-based products, like meatballs. The most common and accurate technique was Polymerase Chain Reaction (PCR). To conduct the PCR technique, the DNA contained in the samples was extracted (Sunaryo et al., 2023). There are many studies on pork detection in meatball samples by conventional PCR (Cahyadi et al., 2020; Erwanto et al., 2014; Indriati & Yuniarsih, 2019). In those studies, several gene targets were used to detect the presence of porcine genomics, such as cytochrome-b-genes and 12S rRNA genes (Cahyadi et al., 2020, 2021). A real-time PCR was also used to test such meat contaminations since the method provides faster and more reliable detection of meat-based products (Dalsecco et al., 2018). It has been reported that RT-PCR has high sensitivity and specificity over other methods; thus, it is used as a standard halal authentication analysis and frequently employed to detect traces of pork in foods (Hibaturrahman et al., 2023; Rohman, Rahayu, et al., 2020; Deepak et al., 2007). The pork detections by Real-time PCR were also reported (Mustaqimah et al., 2021; Raharjo et al., 2017; Salamah et al., 2019; Waluyo et al., 2023). Meanwhile, several studies on rat detection were conducted by PCR using several genes target of rats, such as mitochondrial cytochrome-b-genes of *Rattus argentiventer* and the Mt-atp6 genes of *Rattus norvegicus* (IkaWidyasa et al., 2015; Masnaini et al., 2023; Sihotang et al., 2023; Sunaryo et al., 2022; Suryawan et al., 2020). Some protein markers of *Rattus norvegicus* were also used to detect rat contamination in meat-based products (Aini et al., 2022).

In this study, we used a real-time PCR technique to detect rat meat contaminations on the meatball samples from the Indonesian local market in DKI Jakarta Province. Prior to the PCR test, the DNA samples were extracted using *the Progenus EasyFast™ Extraction Kit for Meat Products*, as described in the previous study (Sunaryo et al., 2023). This study is of urgent importance as the research on rat detection in the meatball samples using a real-time PCR is yet limited. The result of this study will significantly contribute to public halal awareness of meatball products that are commercially distributed in the local Indonesian market.

MATERIALS AND METHOD

Materials

The instruments were micropippet (Bio-Rad™), mortar set, centrifuge (Thermoscientific™), heat block (My block, Benchmark), NanoDrop 2000 spectrophotometer (Thermoscientific™), Real-time PCR from CFX96 Deep Well, Bio-Rad™, and analytical balance. The materials were a 30-samples of meatballs from a local Indonesian market around DKI Jakarta Province, a *Progenus EASYFAST™ kit for Rat Detection kit, a Progenus EasyFast™ Extraction Kit for Meat Products, rat meat as a positive control, PCR tubes, and 1.5 mL microtubes.*

Sample collections

This study obtained 30 DNA sample from meatballs in Cengkareng district, DKI Jakarta Province, Indonesia. All samples were labeled, and their DNA was extracted directly. The rat meat was used as a standard. The standard DNA was also extracted and prepared for PCR amplification.

DNA extractions

The genomic DNA of meatballs and rat meat was extracted by kit, as described by Sunaryo et al. 2023. The first step began with solution A. Solution A was added to sample tubes. The solution was homogenized and heated at 95°C for 1 hour. It was then continued by adding solution B. All the solutions in the microtubes were mixed. The supernatant was transferred to the microtube. The final solution was diluted with 10X of nuclease-free water. The extracted DNA was analyzed by a NanoDrop 2000 spectrophotometer.

Measurement of test purity and DNA content

The purity of the DNA sample was analyzed using a spectrophotometer. The measurements were performed in the wavelength of 260 nm, 280 nm, and 260/280 nm (Sunaryo et al., 2023).

Amplification with the real-time PCR

The RT-PCR process was conducted using CFX96 Deep Well by Bio-Rad™, USA, as described in the previous study (Sunaryo et al., 2023). All the PCR tubes were prepared. Each reaction mixture was prepared by adding MIX reagent (18 µL) and either the samples or External Positive Control (EPC) or rat meat as standard or Nuclease-free water as negative control (2 µL), in order to give the total reaction volume as 20 µL. All the tubes were then put in the PCR instrument. The PCR was performed by setting in all the parameters: the cycle of pre-denaturation and denaturation-annealing-extension step. The pre-denaturation was conducted at 95°C - 3 minutes. The denaturation-annealing-extension was carried out at 95°C for 15 seconds (denaturation) and 60°C for 1 minute (annealing-extension). The FAM value at 494/520 nm represents *Rattus* species. The VIC value at 538/554 nm represents the gene target for vertebrates (internal control).

Analysis of real-time PCR result

The data obtained in this study was based on identifying DNA rats in the meatball samples. The primary data was analyzed descriptively and presented in the cycle threshold (Ct) value based on the fluorescence results on the Real-time PCR instruments.

RESULT AND DISCUSSION

Meat consumption in Indonesia increases yearly and is accompanied by an increasing need for protection against falsely labeled food. Even though halal labels on meat products are mandatory as an implementation of Indonesian halal regulations, there are still many incidents of food fraud and

adulterations. Therefore, public halal awareness demands a vast exploration of the detection of the non-halal material in foods.

The most common method used for detection in foods, especially meat-based products, is Polymerase Chain Reaction (PCR). Apart from the conventional PCR, the Real-time PCR is also widely used for detection. The RT-PCR method for meat-fraud detection is very accurate, sensitive, and efficient in detecting the presence of DNA content in the samples. The method was chosen as the amount of DNA amplified can be directly observed without gel electrophoresis analysis. In this study, 30 samples of meatballs were collected from the meatball sellers around Cengkareng district, DKI Jakarta Province. All samples were collected by accessible population sampling, which requires at least 30 samples as a minimum for sufficient research (Thomson, 2011).

The DNA extraction was the first step prior to the PCR amplification. In this study, we extracted DNA for all meatball products as samples and rat meat as a standard. The extracted DNA was used as a template for amplification. The parameters, which were purity and concentration of DNA, were analyzed using a Nanodrop 2000 spectrophotometer. The ratio in the absorbance of 260nm and 280nm were used to analyze the DNA quality (Glasel, 1995). It is known that the recommended protein standard range was suggested by an A260/280 ratio of 1.70-2.00 (Adriany et al., 2020). However, an A260/280 ratio above 1.0 is acceptable for the analysis to continue using real-time PCR (Priyanka et al., 2017). The results of the DNA quantitative analysis described that the extraction and isolation process involved sufficient steps, yielding in a pure DNA sample. It is known that high DNA purity can affect the validity of the PCR method. Therefore, analyzing the quality and quantity of DNA was an important and crucial step.

In this study, the ratio samples of A260/280 were in the range of 1.28-2.24, as shown in Table 1. The obtained A260 value is the DNA absorbed at the wavelength of 260 nm. Meanwhile, the A280 value at a wavelength of 280 nm indicates the presence of contaminations. Therefore, the high or low value of A260 is very critical for DNA purity. The highest value of A260 does not always mean that the purity of the DNA is high; rather, it can be influenced by the A280 value of contaminations. Table 1 shows that the purity value of the meatballs was within normal limits. However, some were less or more than the ideal value. This result is probably caused by some reagent components, such as phenol, alcohol, and chloroform at extraction time. Other factors that can affect the DNA's quality and purity are the presence of protein, RNA, and other impurities that come originally from the sample.

The concentration of the DNA is one of the critical factors during PCR. If the amount of the DNA is relatively low, the PCR yield will not be optimum. According to the previous study, the recommendation of DNA concentration required for PCR ranged from 10-100 µg/mL, whereas another study stated that the optimum concentration in PCR with 30 cycles was 50 µg/mL (Maryam et al., 2016; Nugroho et al., 2017). In this study, the DNA concentration extracted from the meatball sample was relatively low. It happened because of the added ingredients that were mixed in the samples. Ingredients such as flour, spices, and other ingredients can probably disrupt the extraction process. Certain procedures in meatball production can produce difficulties during DNA extraction. According to the previous study, those procedures might disrupt DNA extraction, such as grinding meat, heating treatment at a very high temperature, and mixing additives in the meatballs (Indriati & Yuniarsih, 2019).

It is reported that the extraction of DNA can be performed from meat that has been heating at 100°C and 120°C for 30 minutes (Matsunaga et al., 1999). The previous study successfully extracted and amplified DNA from meat-based products such as sausages, corned beef, meatballs, and beef jerky; in other words, the DNA was not destructed by heating (Nuraini, 2004). A study stated that PCR amplification was not affected by adding ingredients or cooking processes (Martín et al., 2007). Another study successfully amplified 12S rRNA in genomic samples of several animals heated at high temperatures (Kesmen et al., 2007). However, our data on the extracted DNA in this study showed good purity and concentration. To avoid the unsuccessful in amplifying the DNA of meatball samples in this study, the PCR was performed at a 40-cycles.

The obtained DNA samples were then run by real-time PCR. The analysis data of 30 samples of meatball products were shown as *Cycle Threshold* (Ct) values. The number of cycles needed to replicate the DNA content to be detected crossing a threshold is considered the Ct value. The higher Ct value indicates a smaller amount of DNA/RNA in the samples, suggesting that more cycles are needed for detection. Meanwhile, the low Ct value represents a larger amount of DNA/RNA in the sample, indicating that fewer cycles are needed for detection. However, if the gene target on the samples is absent, the value was shown as Not Applicable (N/A).

The *External Positive Control (EPC)* from the kit contains the gene target of rats and vertebrates, whereas the control negative contains *Nuclease Free Water (NFW)*. The EPC and negative control in this study showed valid results following the kit recommendations, in which the Ct value of both VIC and FAM were less than 30 for positive controls, and the Ct value of both VIC and FAM were more than 38 for negative controls, as shown in Table 2 and Figure 1.

Table 1. The parameters of DNA in standard and meatball samples by Nanodrop 2000 Spectrophotometer

Samples	Purity A260/280 (nm)	Concentration (ng/mL)
ST	1.87	3045.9
PB1	1.57	2789.6
PB2	1.91	2130.6
PB3	1.64	3027.6
PB4	1.82	1831.1
PB5	1.88	3027.5
PB6	1.95	1827.2
PB7	2.24	2684.1
PB8	1.79	2817.9
PB9	1.81	2141.8
PB10	1.28	1005.4
PB11	1.99	1627.4
PB12	1.78	1268.3
PB13	2.21	1458.4
PB14	1.76	2916.4
PB15	1.88	1629.2
PB16	1.79	3364.8
PB17	1.86	1418.2
PB18	1.77	1922.6
PB19	2.15	1404.7
PB20	2.04	2132.4
PB21	1.80	1862.4
PB22	1.53	1507.3
PB23	1.96	2086.8
PB24	1.78	2284.1
PB25	1.82	1949.3
PB26	1.80	2466.4
PB27	1.81	1418.2
PB28	1.72	2389.7
PB29	1.60	1730.3
PB30	1.79	3067.4

Notes: ST (standard contains rat meat); PB (meatballs samples)

The amplification curves of EPC and NFW was shown by Figure 1, which indicates a sigmoid increase in the curve of VIC (shown in yellow) for vertebrates and FAM (shown in blue) for rats. Meanwhile, there is no increase in the sigmoidal curve for the control negative in both VIC and FAM. This result alligns the literature that the positive control is characterized by a fluorescent signal crossing the baseline threshold. Meanwhile, the curve of negative control does not show the increase in the sigmoidal curve and does not pass the baseline threshold. The validity of this study based on the positive and negative control results is in accordance with similar studies (IkaWidyasa et al., 2015; Rohman, Rahayu, et al., 2020). Therefore, it can be concluded that the experiment in this study was in good condition, and the work process was good.

Table 2. The Ct values (VIC and FAM) for positive and negative control, rat meat, and meatball samples

Samples	Ct value	
	VIC	FAM
EPC	28.84	27.22
NFW	N/A	N/A
Standard	14.97	14.27
PB1	21.98	N/A
PB2	21.95	N/A
PB3	21.97	N/A
PB4	16.27	N/A
PB5	16.26	N/A
PB6	16.25	N/A
PB7	20.50	N/A
PB8	20.51	N/A
PB9	20.48	N/A
PB10	18.75	N/A
PB11	18.73	N/A
PB12	18.76	N/A
PB13	17.19	N/A
PB14	17.21	N/A
PB15	17.20	N/A
PB16	18.95	N/A
PB17	18.91	N/A
PB18	18.96	N/A
PB19	18.32	N/A
PB20	18.35	N/A
PB21	18.33	N/A
PB22	18.95	N/A
PB23	18.96	N/A
PB24	18.95	N/A
PB25	18.64	N/A
PB26	18.62	N/A
PB27	18.61	N/A
PB28	17.86	N/A
PB29	17.59	N/A
PB30	17.93	N/A

Notes: EPC (External Positive Control); NFW (Nuclease Free Water); PB (meatballs samples)

In addition, Figure 2 showed that the Ct values of both VIC and FAM from the pure rat meat as standard were 14.97 and 14.27, as shown in Table 2 and Figure 2, suggesting that the DNA rat in the standard is abundant. This result showed that the analysis sample of rat meat using Real-time PCR was well detected.

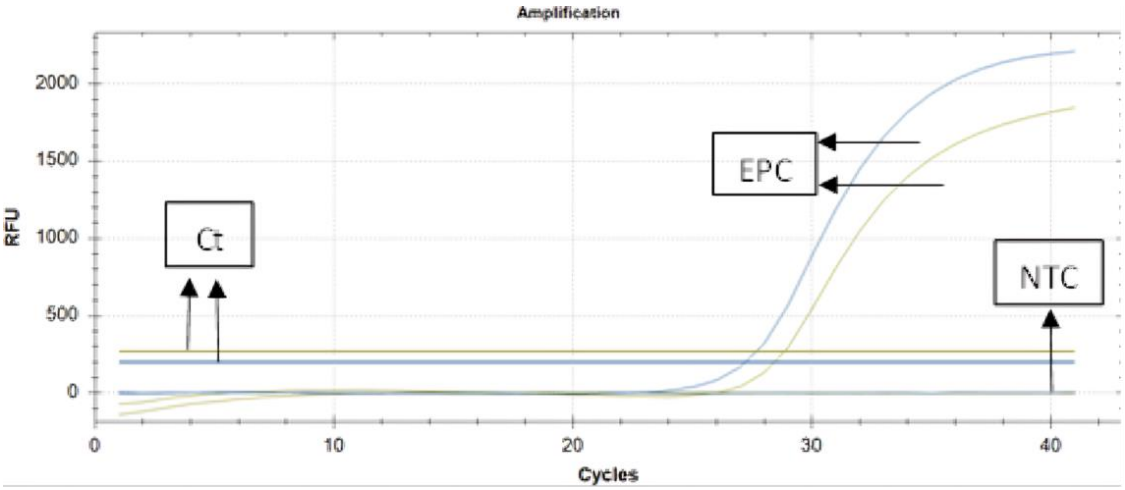

Figure 1. The amplification curves of external positive control (EPC) and nuclease free water (NFW) as negative control (NTC) from progenus easyfast™ kit. the VIC value is shown in yellow. The FAM value is shown in blue

However, according to the amplification results from the samples shown in Table 2 and Figure 3, all meatball samples from Cengkareng district, DKI Jakarta Province, did not contain the DNA of rat meat. The Ct value of all samples for VIC was less than 30, and FAM was more than 38 or as Not Applicable (N/A), suggesting that all samples contain the gene target of vertebrate, but the DNA of rat meats was not detected in all of the meatball samples.

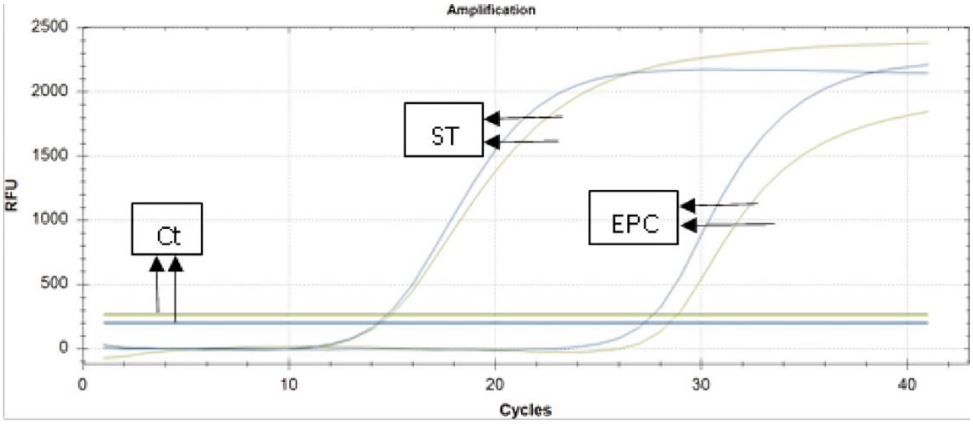

Figure 2. The amplification curves of rat meat as a standard (ST) and External Positive Control (EPC) from progenus easyfast™ kit. the VIC value is shown in yellow. The FAM value is shown in blue

Figure 3 shows the representative result of the amplification curve from the *Progenus EasyFast*TM kit control and meatball sample (PB2) with a purity value of A260/280 of 1.91. The PB2 of the

meatball sample showed a sigmoidal increase in the VIC curve (yellow) to detect vertebrates, but there was no increase in FAM (blue). This result exhibited that the meatball samples analyzed using real-time PCR were negative for rats, but there were vertebrates with a Ct value of 21.95 in the meatball samples. The VIC value of the samples indicated that the meatball samples contained vertebrates that possibly originated from beef meat. A similar study showed no positive contaminant in the samples (Indriati & Yuniarsih, 2019).

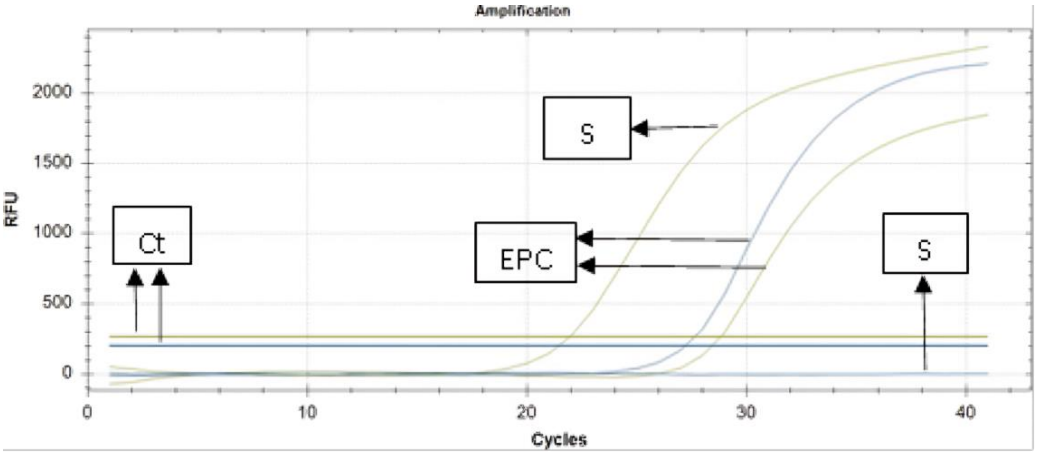

Figure 3. The amplification curves of external positive control (EPC) and PB2 samples (S) from progenus easyfast™ kit. The VIC value is shown in yellow. The FAM value is shown in blue. The VIC and FAM values of samples were shown in S yellow and blue

CONCLUSION

Based on the research conducted on the detection of rat DNA contamination in the 30 meatball samples from the Cengkareng district using the Real-time PCR method, no positive results were obtained. Therefore, we concluded that the meatball samples circulating in the area are relatively safe because they do not contain rat DNA.

ACKNOWLEDGEMENT

We thank the Pusat Kajian Halal UHAMKA team for the great discussions and Pusat Laboratorium Pengujian UHAMKA for providing the laboratory facility to conduct our research.

REFERENCES

Adriany, D. T., Bakri, A. A., & Bungalim, M. I. (2020). Comparison of DNA isolation methods on dna purity for detection of white spot syndrome virus (WSSV) on bamboo lobster (Panulirus versicolor). *Prosiding Simposium Nasional VII Kelautan Dan Perikanan 2020 Fakultas Ilmu Kelautan Dan Perikanan*

Aini, A. N., Airin, C. M., & Raharjo, T. J. (2022). Protein markers related to Non-halal slaughtering process of rat as mammal animal's model detected using mass spectrometry proteome analysis. *Indonesian Journal of Chemistry*, *22*(1), 867. https://doi.org/10.22146/ijc.73656

Cahyadi, M., Fauzıah, N. A. D., Suwarto, I. T., & Boonsupthip, W. (2021). Detection of species substitution in raw, cooked, and processed meats utilizing multiplex-PCR assay. *Indonesian Journal of Biotechnology*, *26*(3), 128. https://doi.org/10.22146/ijbiotech.63472

Cahyadi, M., Wibowo, T., Pramono, A., & Abdurrahman, Z. H. (2020). A novel multiplex-PCR assay to detect three non-halal meats contained in meatball using mitochondrial 12S rRNA gene. *Food*

Science of Animal Resources, *40*(4), 628–635. https://doi.org/10.5851/kosfa.2020.e40

Dalsecco, L. S., Palhares, R. M., Oliveira, P. C., Teixeira, L. V., Drummond, M. G., & de Oliveira, D. A. A. (2018). A fast and reliable real-time PCR method for detection of ten animal species in meat products. *Journal of Food Science*, *83*(2), 258–265. https://doi.org/10.1111/1750-3841.14001

Deepak, S.A., K.R. Kottapalli, R. Rakwal, G. Oros, K.S. Rangappa, H. Iwahashi, Y. Masuo, & G.K. Agrawal. (2007). Real-time PCR: revolutionizing detection and expression analysis of genes. *Current Genomics*, *8*(4), 234–251. https://doi.org/10.2174/138920207781386960

Erwanto, Y., Zainal Abidin, M., Muslim, E. Y. P., Sugiyono, & Rohman, A. (2014). Identification of pork contamination in meatballs of Indonesia local market using polymerase chain reaction-restriction fragment length polymorphism (PCR-RFLP) analysis. *Asian-Australasian Journal of Animal Sciences*, *27*(10), 1487–1492. https://doi.org/10.5713/ajas.2014.14014

Glasel, J. (1995). Validity of nucleic acid purities monitored by 260nm/280nm absorbance ratios. *BioTechniques*.

Guntarti, A., & Purbowati, Z. A. (2019). Analysis of dog fat in beef sausage using FTIR (Fourier Transform Infrared) combined with chemometrics. *Pharmaciana*, *9*(1), 21. https://doi.org/10.12928/pharmaciana.v9i1.10467

Hibaturrahman, S. N., Kusnandar, F., Yuliana, N. D., & Heryani, H. (2023). Sensitivitas real-time polymerase chain reaction dengan primer tanabe dalam mendeteksi gelatin Babi pada confectionery. *Jurnal Teknologi Dan Industri Pangan*, *34*(1), 119–128. https://doi.org/10.6066/jtip.2023.34.1.119

IkaWidyasa, Y., . S., & Rohman, A. (2015). Detection of Rat Meat Adulteration in Meat Ball Formulations Employing Real Time PCR. *Asian Journal of Animal Sciences*, *9*(6), 460–465. https://doi.org/10.3923/ajas.2015.460.465

Indriati, M., & Yuniarsih, E. (2019). Multiplex PCR method of detecting pork to guarantee halal status in meat processed products. *Jurnal Ilmu Produksi Dan Teknologi Hasil Peternakan*, *7*(3), 96–101. https://doi.org/10.29244/jipthp.7.3.96-101

Kesmen, Z., Sahin, F., & Yetim, H. (2007). PCR assay for the identification of animal species in cooked sausages. *Meat Science*, *77*(4), 649–653. https://doi.org/10.1016/j.meatsci.2007.05.018

Lestari, D., Rohman, A., Syofyan, S., Yuliana, N. D., Abu Bakar, N. K. B., & Hamidi, D. (2022). Analysis of beef meatballs with rat meat adulteration using Fourier Transform Infrared (FTIR) spectroscopy in combination with chemometrics. *International Journal of Food Properties*, *25*(1), 1446–1457. https://doi.org/10.1080/10942912.2022.2083637

Martín, I., García, T., Fajardo, V., López-Calleja, I., Hernández, P. E., González, I., & Martín, R. (2007). Species-specific PCR for the identification of ruminant species in feedstuffs. *Meat Science*, *75*(1), 120–127. https://doi.org/10.1016/j.meatsci.2006.06.019

Maryam, S., Sismindari, Raharjo, T. J., Sudjadi, & Rohman, A. (2016). determination of porcine contamination in laboratory prepared dendeng using Mitochondrial D-Loop686 and cyt b gene primers by real time polymerase chain reaction. *International Journal of Food Properties*, *19*(1), 187–195. https://doi.org/10.1080/10942912.2015.1020434

Masnaini, M., Achyar, A., Chatri, M., Putri, D. H., Ahda, Y., & Irdawati. (2023). *Primer design and optimization of PCR methods for detecting mixed Rat meat in food samples* (pp. 282–289). https://doi.org/10.2991/978-94-6463-166-1_37

Matsunaga, T., Chikuni, K., Tanabe, R., Muroya, S., Shibata, K., Yamada, J., & Shinmura, Y. (1999). A quick and simple method for the identification of meat species and meat products by PCR assay. *Meat Science*, *51*(2), 143–148. https://doi.org/10.1016/S0309-1740(98)00112-0

Mustaqimah, D. N., Septiani, T., & Roswiem, A. P. (2021). Deteksi DNA Babi pada produk sosis menggunakan real time-polymerase chain reaction (RT-PCR). *Indonesian Journal of Halal*, *3*(2), 106–111. https://doi.org/10.14710/halal.v3i2.10130

Nida, L., Pisestyani, H., & Basri, C. (2020). Studi kasus: pemalsuan daging Sapi dengan daging Babi hutan di kota Bogor. *Jurnal Kajian Veteriner*, *8*(2), 121–130. https://doi.org/10.35508/jkv.v8i2.2326

Nugroho, K., Terryana, R. T., & Lestari, P. (2017). Metode ekstraksi DNA cabai (Capsicum annuum L.) menggunakan modifikasi buffer CTAB (Cethyl trimethyl ammonium bromide) tanpa nitrogen cair. *Scripta Biologica*, *4*(2), 91. https://doi.org/10.20884/1.sb.2017.4.2.423

Nuraini, H. (2004). *Pengembangan sekuen porcine repetitive element-1 (PRE-1) sebagai penanda molekuler untuk mendeteksi material babi pada produk daging olahan. (Diseratation)*. Institut Pertanian Bogor.

Owolabi, I. O., & Olayinka, J. A. (2021). Incidence of fraud and adulterations in ASEAN food/feed exports: A 20-year analysis of RASFF's notifications. *PLOS ONE*, *16*(11), e0259298. https://doi.org/10.1371/journal.pone.0259298

Priyanka, V. A., Ristiarini, S., & Yuda, P. (2017). The Detection of Pork Contamination in the Beef Sausage Products in Yogyakarta City with polymerase chain reaction method. *Jurnal Atma Jaya Yogyakarta*, *2017*, 1–17.

Purnomo, H., & Rahardiyan, D. (2008). Review Paper Indonesian Traditional Meatball. *International Food Research Journal*, *15*(2), 101–108. https://www.researchgate.net/publication/279548228_Indonesian_traditional_meatball

Raharjo, T. J., Alfiraza, E. N., Enjelina, E., & Pranowo, D. (2017). Validation of a non-specific dye real-time PCR assay for porcine adulteration in meatball using ND5 primer. *Indonesian Journal of Chemistry*, *17*(2), 167. https://doi.org/10.22146/ijc.22646

Rohman, A., Pebriyanti, N. W., Sismindari, Windarsih, A., Ramadhani, D., Larasati, R., & Yulisa, H. (2020). Real-time polymerase chain reaction for identification of dog meat in adulterated beef meatball using specific primer targeting on cytochrome-b for halal authentication. *International Journal of Food Properties*, *23*(1), 2231–2241. https://doi.org/10.1080/10942912.2020.1844748

Rohman, A., Rahayu, W. S., Sudjadi, S., & Martono, S. (2020). The use of real-time polymerase chain reaction combined with specific-species primer for analysis of dog meat DNA in meatball. *Indonesian Journal of Chemistry*, *21*(1), 225. https://doi.org/10.22146/ijc.48930

Salamah, N., Erwanto, Y., Martono, S., & Rohman, A. (2019). Real-time PCR-based detection of bovine DNA by specific targeting on cytochrome-B. *Pharmaciana*, *9*(2), 201. https://doi.org/10.12928/pharmaciana.v9i2.14070

Sihotang, M., Sophian, A., Purba, M., & Wilasti, Y. (2023). Development of rat meat detection using Mt-atp6 Rattus norvegicus gene genetic marker. *Current Applied Science and Technology*, *23*(1). https://doi.org/10.55003/cast.2022.01.23.006

Siswara, H. N., Erwanto, Y., & Suryanto, E. (2021). *Deteksi unsur Babi dan Ayam pada bakso Sapi dengan metode Polymerase chain reaction di kabupaten Bojonegoro dan Boyolali. (Thesis)*. Universitas Gadjah Mada.

Siswara, H. N., Erwanto, Y., & Suryanto, E. (2022). Study of meat species adulteration in Indonesian commercial beef meatballs related to halal law implementation. *Frontiers in Sustainable Food Systems*, *6*. https://doi.org/10.3389/fsufs.2022.882031

Sunaryo, H., Nikmatullah, N. A., & Mufidah, S. (2022). Detection of rat contamination in sausage samples with real time PCR. *Farmasains*, *9*(2), 57–64.

Sunaryo, H., Wirman, A. P., Permanasari, E. D., Nikmatullah, N. A., Lestari, D., & Nurjanah, D. (2023). Optimization of DNA extraction methods in fresh meat (Rat and Chicken Meat) based on incubation time. *Indonesian Journal of Halal Research*, *5*(2), 99–108. https://doi.org/10.15575/ijhar.v5i2.21325

Suryawan, G. Y., Suardana, I. W., & Wandia, I. N. (2020). Sensitivity of polymerase chain reaction in the detection of rat meat adulteration of beef meatballs in Indonesia. *Veterinary World*, *13*(5), 905–908. https://doi.org/10.14202/vetworld.2020.905-908

Thomson, S. B. (2011). Sample Size and Grounded Theory. *Journal of Administration and Governance*, *5*(5).

Waluyo, S., Malau, J., Raekiansyah, M., Yulian, E., & Hardiman, I. (2023). Detection and quantification of porcine contamination on precessed meat using real-time PCR. *Al-Kauniyah:*

Jurnal Biologi, *16*(1), 46–52. https://doi.org/10.15408/kauniyah.v16i1.20203

Pharmaciana
Vol.14, No.3, Nov 2024, Page. 434-442
ISSN: 2088 4559; e-ISSN: 2477 0256
DOI: 10.12928/pharmaciana.v14i3.29919

Phytochemical constituent, α-amylase and α-glucosidase inhibitory activities of Black Soybean (*Glycine soja* (L.) Merr.) ethanol extract

Afifah Bambang Sutjiatmo[1], Suci Narvikasari[1], Ananda Khairunisa Solihat[1], Wahyu Widowati[2]*, Hanna Sari Widya Kusuma[3], Fadhilah Haifa Zahiroh[3]

[1]Faculty of Pharmacy, Universitas Jenderal Achmad Yani,
Jl. Ters Jend Sudirman, Cibeber, Cimahi *Sel., Cimahi 40531, West Java, Indonesia*
[2]Faculty of Medicine, Maranatha Christian University,
Jl. Surya Sumantri no 65, Bandung 40164, West Java, Indonesia
[3]Biomolecular and Biomedical Research Center, Aretha Medika Utama
Jl. Babakan Jeruk II No. 9, Bandung 40163, West Java, Indonesia,

Submitted: 02-09-2024 ***Reviewed: 10-09-2024*** ***Accepted: 06-10-2024***

ABSTRACT

Diabetes is characterized as a hyperglycemic condition impacted by β-cell dysfunction and insulin deficiency. Black soybean (*Glycine soja* (L.) Merr.) is widely known as an origin of nutritious food that has shown activities in preventing cardiovascular disease and reducing hyperglycemia. This research aimed to evaluate the potential of black soybeans ethanol extract (BSEE) as an α-amylase and α-glucosidase activity inhibitor. Black soybean seeds were extracted using the Soxhlet method with 50% ethanol as a solvent. The BSEE were screened for the presence of phytochemicals content. Inhibitory activity of α-amylase and α-glucosidase enzymes was tested in vitro with acarbose as a control. The absorbance measurement was conducted at 565 nm and 400 nm, respectively. BSEE contained alkaloids, flavonoids, polyphenols, saponins, quinones, tannins, and terpenoids. The results indicated that BSEE exhibited a weak inhibitory effect of α-amylase enzyme activity, with an IC_{50} value of 360.37 ± 20.80 µg/mL, in contrast to acarbose, which showed a significantly lower IC_{50} of 4.02 ± 0.56 µg/mL. Meanwhile, BSEE was classified as an active inhibitor of α-glucosidase enzyme activity, presenting 25.67 ± 0.27 µg/mL IC_{50} value, while acarbose demonstrated 10.85 ± 0.5 µg/mL IC_{50} value. In conclusion, BSEE inhibits α-amylase and α-glucosidase.

Keywords: α-amylase, α-glucosidase, acarbose, antidiabetic, black soybean (*Glycine soja* (L.) Merr.)

Corresponding author:
Wahyu Widowati
Faculty of Medicine, Maranatha Christian University,
Jl. Surya Sumantri no 65, Bandung 40164, Indonesia
Email: wahyu_w60@yahoo.com

INTRODUCTION

Diabetes Mellitus (DM) known as condition marked by disturbances in the metabolism of fat, proteins, and carbohydrates as a consequences of inadequate insulin secretion and Hyperglycemia. Both of which can cause damage, abnormalities, and failure in tissues and organs such as the kidneys, heart, nerves, and blood vessels even cause death (Alam et al., 2014). Several varieties of diabetes exist, including gestational, type I, type II (Baynest, 2015). Type II DM is common and accounts for between 90% of people with diabetes. Type II DM is a chronic disease caused by cell dysfunction and insulin deficiency (World Health Organization, 2019).

One of the pharmacological therapies used to treat DM is the use of oral antidiabetic which has a mechanism of inhibiting α-amylase and α-glucosidase enzyme (Gondokesumo et al., 2017; Hamid et al., 2015; Widowati et al., 2022). α-amylase can hydrolyze α-(1,4)-glucosidic bonds to form glucose and maltose, while α-glucosidase releases glucose from sucrose and maltose thereby increasing the level of glucose in the blood. By blocking the activity of these two enzymes, it is possible to postpone glucose absorption into the bloodstream, thereby helping reduce the symptoms of diabetes mellitus (Hamid et al., 2015).

Chemical drugs are widely used for the treatment of DM such as miglitol and acarbose, but some of these drugs are pricey and have some complications, such as diarrhea and abdominal distention (Dipiro et al., 2020). So many studies have been carried out to find active compounds that have antidiabetic activity derived from plants as an alternative diabetes treatment with minimum side effects. It is assumed that traditional herbal therapy has hypoglycemic properties. More than 800 plant species have been found to have anti-diabetic effects (Rosemar et al., 2014).

Many plants contain phytochemical compounds with various biological activities. These biological activities use plants or herbal medicines for treatment, including diabetes mellitus. An important group of phytochemical compounds, including phenols, flavonoids, tannins, and saponins, is responsible for most plant extracts' beneficial activities. Many phytochemical compounds are also high in antioxidants because they can scavenge ROS (Si & Liu, 2014). With this, phytochemical screening in plants is an important step toward their empirical medicinal utilization.

Soybean (*Glycine soja* L) refers to legume species originating from East Asia that is commonly cultivated for its seeds. Soybeans are widely consumed as a nutrient-rich food consisting of protein, oil, carbohydrates, and dietary fiber, as well as a large number of vitamins and minerals. Soybean seed coats have a variety of colors, including brown, black, yellow, and green. The black soybean seed coat improves insulin sensitivity and reduces hyperglycemia (Kurimoto et al., 2013). Black soybeans are also beneficial in improving blood vessel function and preventing cardiovascular disease (Yamashita et al., 2020). This study investigates the black soybean (*G. soja* (L.) Merr.)'s extract anti-diabetic activities, namely inhibitor of α-amylase and α-glucosidase, that are carried out in vitro.

MATERIALS AND METHOD

Materials

Materials used are ethanol (Merck KGaA, 10.099.831.000), Magnesium powder (Mg) powder (Merck, 1.05815.1000), HCl, Mayer's reagent, Dragendroff's reagent, Stiasny reagent, Liebermann Burchard reagent, NaOH, $FeCl_3$ reagent, α-amylase enzyme (Sigma Aldrich, A75955-50ML), ddH_2O, Lugol, DMSO, phosphate buffer (pH 7.4), p-nitrophenyl-α-D-glucopyranoside (PNPG) (N1377, Sigma Aldrich, St. Louis, USA), α-glucosidase enzyme, Na_2CO_3 (Merck, 1.063.921.000).
Equipments employed in this study are microplate reader (Thermo Fisher Logical, Multiskan GO Microplate Spectrophotometer).

Preparation of black soybean extract

The production of black soybean extract (BSEE) was carried out using the Soxhlet method of extraction. Black soybean seeds are obtained from PT Lingkar Organik, Sleman Regency, Special Region of Yogyakarta, Indonesia. Plant identification was performed at Jatinangor Herbarium, Plant Taxonomy Laboratory, Department of Biology, Padjadjaran University. The dried black soybean seeds were ground and then weighed as much as 200 g, wrapped in a filter paper sleeve, and then put into a Soxhlet tube, then as much as 2000 mL of 50% ethanol was put into a round bottom flask and

extracted until the solvent liquid dripping on the material became clear. The filtrate was concentrated utilizing a rotary vacuum evaporator set to 20 Psi and 70°C. After that, a freeze-drying process was carried out to obtain a solid extract. The dried black soybean extract was then immersed in 50% distilled ethanol, the filtrate then filtered for every 24 hours until it became colorless. Black soybean ethanol extract (BSEE) was obtained after the filtrate was evaporated, subsequently stored at 20°C (Widowati et al., 2022).

Phytochemical screening of Soybean ethanol extract

Phytochemical screening of BSEE included examination of flavonoid compounds, alkaloids, tannins, saponins, steroids/triterpenoids, quinones, and polyphenols.

Flavonoids identification

BSEE 1 g was diluted in aquadest, then heated in a water bath, and then filtered. Fill a test tube with 2 mL of filtrate, 1 mL Magnesium powder (Mg) powder, and 1 mL 2N HCl, then heat for 5 minutes and filter. To the filtrate, up to amyl alcohol 5 mL was added, shaken, and allowed to separate. The formation of a reddish-orange to purplish-red color indicates a positive reaction for the flavonoid compounds (Safrina et al., 2022).

Alkaloids identification

Alkaloids identification was initiated with subjecting 0.5 g of BSEE into a mortar and crushing it. Then 5 mL of dilute ammonia and chloroform 5 mL were added and crushed. Then the solution was filtered, and 5 mL of 2N HCl was subjected to the filtrate. The mixture then shaken and left for some time to form two layers. The top layer is splited into two test tubes. To the first tube, Mayer's reagent 3 drops were added. If a white or yellow precipitate forms, the reaction is positive for alkaloids. Add 3 drops of Dragendorff's reagent to the second tube. If an orange precipitate forms, there is a positive reaction for alkaloids (Prahastuti et al., 2019).

Tannins identification

BSEE, as much as 1 g, was dissolved in distilled water, heated in water bath, then filtered. After that, five drops Stiasny reagent were added to the filtrate. The positive reaction of tannin compounds is indicated by the formation of a pink precipitate (Benzidia et al., 2019).

Saponins identification

The test tube contained SSE 10 mg was filled with a small amount of water, and it was then brought to a boil for five minutes. The presence of foam on the surface after shaking indicates a positive reaction to the presence of saponins (Prahastuti et al., 2019).

Steroids/triterpenoids identification

BSEE was subjected as much as 10 mg to dropping plate, subsequently added with acetic acid. Sulfuric acid (H_2SO_4) (Merck, 109073) after 10-15 minutes. Green or blue color demonstrated the steroid presence. Meanwhile, red/orange sediment formation demonstrated the triterpenoid presence (Pavani & Shasthree, 2022).

Quinones identification

One gram of BSEE was dissolved in aquadest, then filtered above on an air bath. The filtrate was added with 3 drops of 1N NaOH. The positive reaction of quinone compounds is indicated by the yellow-to-red color formation (Prahastuti et al., 2019).

Polyphenols identification

One gram of BSEE was dissolved in distilled water, then heated in a water bath, and then filtered. Added 2 drops of $FeCl_3$ reagent (Merck 1.03861.0250). Green, purple, blue, red, and black are indications of positive polyphenol reactions (Rao, 2016).

α-amylase inhibitory activity assay

A modified method was utilized to evaluate the activity of α-amylase inhibition (Gondokesumo et al., 2017; Widowati et al., 2018). Subsequently, 25 µL of starch added to positive control well and sample well, then 25 µL of ddH_2O added to negative and blank control well. The 50 µL samples were added to the wells of smple and the blank wells. Each positive control well and sample received 50 µL of the α-amylase enzyme. Ten minutes at 37°C were spent incubating the plate. Each well was filled with 50 µL of HCl and 25 µL of Lugol to halt the enzymatic reaction. The microplate reader was utilized to measure the absorbance at λ = 565 nm. Mapping of the assay is shown in Table 1. Equation 1 was utilized to calculate the α-glucosidase inhibition percentage.

Table 1. Mapping of the α-amylase inhibitory assay

	Positive control well	Negative control well	Sample well	Blank well
Starch	25 µL	-	25 µL	-
ddH_2O		25 µL	-	25 µL
Sample	-	-	50 µL	50 µL
α-amylase enzyme	50 µL		50 µL	
HCl	50 µL	50 µL	50 µL	50 µL
Lugol	25 µL	25 µL	25 µL	25 µL

$$Inhibition\ (\%) = \frac{(C-S)\times 100}{C} \quad \text{.....(1)}$$

C: control absorbance
S: sample absorbance

α-glucosidase inhibitory activity assay

A modified procedure was utilized to evaluate α-glucosidase inhibitory activity (Gondokesumo et al., 2017; Widowati et al., 2021). Samples and comparisons were inserted into the wells, DMSO in the control wells, and blanks. Then, phosphate buffer (pH 7.4) and p-nitrophenyl-α-D-glucopyranoside (PNPG) (N1377, Sigma Aldrich, St. Louis, USA) were added to all wells. The α-glucosidase enzyme added to control well, sample, and comparison, incubated 30 minutes in 37°C, then sodium carbonate (Na_2CO_3) was added. The microplate reader was utilized to measure the absorbance at λ = 400 nm. Equation 1 was utilized to calculate the α-glucosidase inhibition percentage.

Statistical analysis

Statistical analysis was conducted in SPSS ver 20.0. while the GraphPad Prism 9 was utilized to analyze research data. Differences in the mean between the sample and analysis were analyzed utilizing ANOVA followed Tukey HSD post hoc test ($P < 0.05$). α-amylase and α-glucosidase inhibition activity was ascertained using linear regression based on the mean inhibition (IC_{50}).

RESULT AND DISCUSSION

Black soybean (*Glycine soja* (L.) Merr.) seed extract contains various chemical compounds. In this study, alkaloids, flavonoids, polyphenols, saponins, quinones, tannins, and terpenoids were found as secondary metabolites in BSEE. The results of which were strongly influenced by cultivars (Table 2). BSEE in other research contains tannins, saponins, alkaloids, and steroids/triterpenoids (Prahastuti et al., 2019). These polyphenols and flavonoids have been shown to contribute to treating DM by increasing cellular antioxidant activity, increasing ROS scavengers, reducing glucotoxicity, decreasing α-glucosidase activity, and increasing cellular viability (Li et al., 2017). The phytochemical content in black soybean seeds has been widely studied for use as an anti-inflammatory, anti-obesity, anti-apoptotic, and anti-dyslipidemia (Hidayat et al., 2015; Prahastuti et al., 2016; Widowati et al., 2018).

Table 2. Phytochemical screening of black seed soy extract

Phytochemical Test	Results (+/-)
Alkaloid	+
Flavonoid	+
Polyphenol	+
Saponin	+
Quinone	+
Tannin	+
Steroid Triterpenoid	+
Monoterpenoid-Sesquiterpenoid	+

+ = detected, - = not detected

α-amylase is an enzyme that contributes to the starch degradation process by hydrolyzing starch glycosidic bonds of starch. The α-amylase inhibitory activity causes inhibition of starch hydrolysis, which reduces the speed of carbohydrate digestion and absorption, resulting in less post-prandial hyperglycemia (Soeng et al., 2015). In this research, BSEE inhibited the α-amylase activity (Figure 1, Table 3). α-amylase inhibition increased when the concentration of BSEE increased. The most effective inhibitory activity of BSEE was the highest concentration (750 µg/mL) which could inhibit α-amylase activity with a percentage of BSEE inhibition of 63.88% with an IC_{50} of 360.37 ± 20.80 µg/mL, even though BSEE has less inhibitory activity than acarbose which had an 4.02 ± 0.56 µg/mL IC_{50}. Inhibition of α-amylase is caused by the presence of flavonoids in BSEE which inhibit α-amylase in two ways, specifically by directly interacting with amino acid residues on the enzyme active site and displacing the binding substrate, so that glucose cannot hydrolyze starch into maltose compounds (Zhu et al., 2020). (Jia et al. 2024) reported that genistein, one of predominant black soybean compound, binds to α-amylase and α-glucosidase through hydrophobic interactions and hydrogen bonds, forming complexes that inhibit both enzymes.

The presence of α-glucosidase inhibitory activity in Figure 2 and Table 3 indicates that BSEE can act as an antidiabetic. α-glucosidase is an important enzyme in carbohydrate metabolism because it has an impact on the breakdown of carbohydrates into glucose (Chen & Guo, 2017). According to research, inhibition of α-glucosidase can help reduce DM symptoms by delaying glucose absorption into the bloodstream (Hamid et al., 2015). α-glucosidase inhibition increased significantly with increasing BSEE concentration ($p<0.05$) (Figure 2). The most effective BSEE inhibitory activity was the highest concentration (23.81 µg/mL) which might inhibit α-glucosidase activity at IC_{50} of 25.67 ± 0.27 µg/mL (Table 4). Based on the results, the IC_{50} value is in the IC_{50} range = 25–50 g/mL which means the inhibitor is active, while the inhibition of Acarbose is in the IC_{50} range = <10 g/mL which is classified as very active (Marjoni & Zulfisa, 2017). Acarbose is an inhibitor that works competitively with the p-nitrophenyl-D-glucopyranoside substrate to bind to the active enzyme site, preventing the breakdown of the substrate into p-nitrophenol and glucose. This leads to high inhitory activity.

BSEE has inhibitory activity due to its secondary metabolite content on black soybeans. Flavonoid compounds in BSEE can competitively inhibit α-glucosidase enzyme activity by binding to the active enzyme site (Yang et al., 2021). The potential of flavonoids to inhibit α-glucosidase activity is influenced by the structure of the flavonoid, its position, and several OH groups (Proença et al., 2017). The anthocyanins contained in BSEE are also thought to provide α-glucosidase enzyme inhibitory activity. Moreover, the addition of hydroxyl groups at positions C3' and C4' on ring b can increase the strength of anthocyanins in inhibiting α-glucosidase enzyme activity (Promyos et al., 2020). Therefore, BSEE has the potential as the treatment of DM by inhibit α-glucosidase and α-amylase.

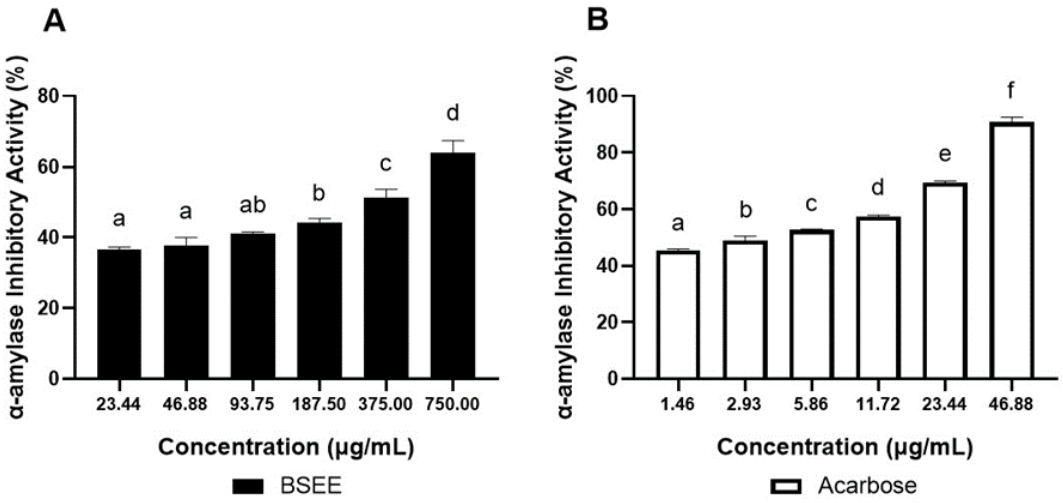

Figure 1. Histogram of black soybeans etanol extract (A) and acarbose (B) on alfa amylase inhibition

**The data is showed as mean ± SD. A: BSEE; B: Acarbose. Based on Tukey HSD post hoc test, the various superscript marks (a, b, ab, c, d) in Figure 1A and (a, b, c, d, e, f) in Figure 1B revealed significant differences between concentrations ($p < 0.05$)

Table 3. The IC_{50} (µg/mL) values of α-amylase inhibition by BSEE Acarbose

Sample	Equation	R^2	IC_{50}
BSEE	y = 0.037x + 36.722	0.992	360.37 ± 20.80
Acarbose	y = 0.968x + 45.922	0.996	4.02 ± 0.56

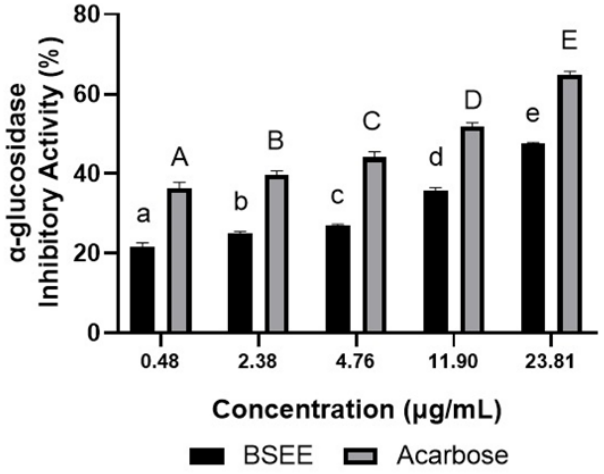

Figure 2. Histogram of black soybeans ethanol extract (A) and acarbose (B) on alfa glucosidase inhibition

**The data is presented as mean ± SD. According to Tukey HSD post hoc test, various superscript marks (a, b, c, d, e and A, B, C, D, E) revealed significant differences between concentrations ($p < 0.05$)

Table 4. The IC_{50} of α-glucosidase inhibitio by BSEE and acarbose

Sample	Equation	R^2	IC_{50} (µg/mL)
BSEE	y = 1.0939x + 21.916	0.996	25.67 ± 0.27
Acarbose	y = 1.1919x + 37.068	0.991	10.85 ± 0.5

CONCLUSION

Based on phytochemical identification, it was revealed that BSEE comprises alkaloid, flavonoid, polyphenol, saponin, quinone, tannin, steroid triterpenoid, and monoterpenoid-sesquiterpenoid. BSEE exhibited weak α-amylase inhibition activity and strong α-glucosidase inhibition activity with IC_{50} of 360.37 ± 20.80 µg/mL and 25.67 ± 0.27 µg/mL, respectively. Further research on the antidiabetic activity of BSEE in animal models of DM is recommended.

ACKNOWLEDGEMENT

The authors gratefully acknowledge financial support by research grant 2019 from the Research and Community Service Center-University of Jenderal Achmad Yani, Cimahi, Indonesia. The research methodology along with laboratory facilities were provided by Aretha Medika Utama, Bandung, West Java, Indonesia. We gratefully acknowledge the contributions of Adilah Hafizha Nur Sabrina, Fadhilah Haifa Zahiroh, Annisa Firdaus Sutendi, Vini Ayuni, Dwi Nur Triharsiwi, and Faradhina Salfa Nindya from Aretha Medika Utama, Bandung, West Java, Indonesia.

REFERENCES

Alam, U., Asghar, O., Azmi, S., & Malik, R. A. (2014). *General aspects of diabetes mellitus* (pp. 211–222). https://doi.org/10.1016/B978-0-444-53480-4.00015-1

Baynest, H. W. (2015). Classification, pathophysiology, diagnosis and management of Diabetes Mellitus. *Journal of Diabetes & Metabolism*, *06*(05). https://doi.org/10.4172/2155-6156.1000541

Benzidia, B., Barbouchi, M., Hammouch, H., Belahbib, N., Zouarhi, M., Erramli, H., Ait Daoud, N., Badrane, N., & Hajjaji, N. (2019). Chemical composition and antioxidant activity of tannins extract from green rind of Aloe vera (L.) Burm. F. *Journal of King Saud University - Science*, *31*(4), 1175–1181. https://doi.org/10.1016/j.jksus.2018.05.022

Chen, G., & Guo, M. (2017). Rapid screening for α-glucosidase inhibitors from gymnema sylvestre by affinity ultrafiltration–HPLC-MS. *Frontiers in Pharmacology*, *8*. https://doi.org/10.3389/fphar.2017.00228

Dipiro, J. T., Posey, L. M., Yee, G. C., Haines, S. T., Nolin, T. D., & Ellingrod, V. (2020). *Pharmacotherapy: a pathophysiologic approach* (Eleventh E). McGraw-Hill Companies

Gondokesumo, M. E., Kusuma, H. S. W., & Widowati, W. (2017). α-/β-Glucosidase and α-Amylase Inhibitory activities of Roselle (Hibiscus sabdariffa L.) ethanol extract. *Molecular and Cellular Biomedical Sciences*, *1*(1), 34. https://doi.org/10.21705/mcbs.v1i1.3

Hamid, H. A., Yusoff, M. M., Liu, M., & Karim, M. R. (2015). α-Glucosidase and α-amylase inhibitory constituents of Tinospora crispa: Isolation and chemical profile confirmation by ultra-high performance liquid chromatography-quadrupole time-of-flight/mass spectrometry. *Journal of Functional Foods*, *16*, 74–80. https://doi.org/10.1016/j.jff.2015.04.011

Hidayat, M., Soeng, S., Prahastuti, S., Erawijantari, P. P., & Widowati, W. (2015). Inhibitory potential of ethanol extract of Detam 1 soybean (Glycine max) seed and Jati belanda (Guazuma ulmifolia) leaves on adipogenesis and obesity models in 3T3-L1 cell line. *Journal of Scientific Research & Reports*, *6*(4), 304–312. https://doi.org/10.9734/JSRR/2015/16273

Jia, J., Dou, B., Gao, M., Zhang, C., Liu, Y., & Zhang, N. (2024). Effect of genistein on starch digestion in vitro and its mechanism of action. *Foods*, *13*(17), 2809. https://doi.org/10.3390/foods13172809

Kurimoto, Y., Shibayama, Y., Inoue, S., Soga, M., Takikawa, M., Ito, C., Nanba, F., Yoshida, T., Yamashita, Y., Ashida, H., & Tsuda, T. (2013). Black soybean seed coat extract ameliorates hyperglycemia and insulin sensitivity via the activation of AMP-Activated protein kinase in diabetic mice. *Journal of Agricultural and Food Chemistry*, *61*(23), 5558–5564. https://doi.org/10.1021/jf401190y

Li, F., Zhang, B., Chen, G., & Fu, X. (2017). The novel contributors of anti-diabetic potential in mulberry polyphenols revealed by UHPLC-HR-ESI-TOF-MS/MS. *Food Research International*, *100*, 873-884. https://doi.org/10.1016/j.foodres.2017.06.052

Marjoni, & Zulfisa. (2017). Antioxidant activity of methanol extract/fractions of Senggani leaves

(Melastoma candidum D. Don). *Pharmaceutica Analytica Acta*, *08*(08), 1–6. https://doi.org/10.4172/2153-2435.1000557

Pavani, C., & Shasthree, T. (2022). Qualitative screening and quantitative determination of secondary metabolites from different plant extracts of Solanum khasianum Clarke. *Research Journal of Chemistry and Environment*, *26*(12), 113–123. https://doi.org/10.25303/2612rjce1130123

Prahastuti, S, Hidayat, M., Hasianna, S. T., Widowati, W., Amalia, A., Yusepany, D. T., Rizal, R., & Kusuma, H. S. W. (2019). Antioxidant potential ethanolic extract of Glycine max (l.) Merr. Var. Detam and daidzein. *Journal of Physics: Conference Series*, *1374*(1), 012020. https://doi.org/10.1088/1742-6596/1374/1/012020

Prahastuti, Sijani, Hidayat, M., Kurniadi, M. W., & Christiany, S. (2016). Potency of Black Soybean (Glycine max L. Merr) and Jati Belanda Leaves (Guazuma ulmifolia Lamk) for Dyslipidemia Treatment In Vivo. *Journal Of Medicine & Health*, *1*(3). https://doi.org/10.28932/jmh.v1i3.515

Proença, C., Freitas, M., Ribeiro, D., Oliveira, E. F. T., Sousa, J. L. C., Tomé, S. M., Ramos, M. J., Silva, A. M. S., Fernandes, P. A., & Fernandes, E. (2017). α-Glucosidase inhibition by flavonoids: an in vitro and in silico structure–activity relationship study. *Journal of Enzyme Inhibition and Medicinal Chemistry*, *32*(1), 1216–1228. https://doi.org/10.1080/14756366.2017.1368503

Promyos, N., Temviriyanukul, P., & Suttisansanee, U. (2020). Investigation of anthocyanidins and anthocyanins for targeting α-glucosidase in Diabetes Mellitus. *Preventive Nutrition and Food Science*, *25*(3), 263–271. https://doi.org/10.3746/pnf.2020.25.3.263

Rao, U. M. (2016). Phytochemical screening, total flavonoid and phenolic content assays of various solvent extracts of tepal of Musa paradisiaca. *Malaysian Journal of Analytical Science*, *20*(5), 1181–1190. https://doi.org/10.17576/mjas-2016-2005-25

Rosemar, Rosidah, & Haro, G. (2014). Antidiabetic effect of roselle calyces extracts (Hibiscus sabdariffa L.) in streptozotocin-induced mice. *International Journal of PharmTech Research*, *6*(5), 1703–1711

Safrina, U., Wardiyah, W., & Cartika, H. (2022). Evaluation of total flavonoid, total phenolic, and antioxidant activity of etlingera elatior (Jack) R.M.Sm Flower, Fruit, and Leaf. *Majalah Obat Tradisional*, *27*(1), 50. https://doi.org/10.22146/mot.72210

Si, H., & Liu, D. (2014). Dietary antiaging phytochemicals and mechanisms associated with prolonged survival. *The Journal of Nutritional Biochemistry*, *25*(6), 581–591. https://doi.org/10.1016/j.jnutbio.2014.02.001

Soeng, S., Evacuasiany, E., Widowati, W., & Fauziah, N. (2015). Antioxidant and hypoglycemic activities of extract and fractions of Rambutan seeds (Nephelium lappaceum L.). *Biomedical Enginering*, *1*(1), 13–18

Widowati, W., Prahastuti, S., Hidayat, M., Hasianna, S. T., Wahyudianingsih, R., Eltania, T. F., Azizah, A. M., Aviani, J. K., Subangkit, M., Handayani, R. A. S., & Kusuma, H. S. W. (2022). Detam 1 black soybean against cisplatin-induced acute ren failure on rat model via antioxidant, antiinflammatory and antiapoptosis potential. *Journal of Traditional and Complementary Medicine*, *12*(4), 426–435. https://doi.org/10.1016/j.jtcme.2022.01.004

Widowati, W., Tjokropranoto, R., Wahyudianingsih, R., Tih, F., Sadeli, L., Kusuma, H. S. W., Fuad, N. A., Girsang, E., & Agatha, F. A. (2021). Antidiabetic potential Yacon (Smallanthus sonchifolius (Poepp.) H. Rob.) leaf extract via antioxidant activities, inhibition of α-glucosidase, α-amylase, G-6-Pase by in vitro assay. *Journal of Reports in Pharmaceutical Sciences*, *10*(2), 247–255. https://doi.org/10.4103/jrptps.JRPTPS_3_21

Widowati, W., Wargasetia, T. L., Afifah, E., Mozef, T., Kusuma, H. S. W., Nufus, H., Arumwardana, S., Amalia, A., & Rizal, R. (2018). Antioxidant and antidiabetic potential of Curcuma longa and its compounds. *Asian Journal of Agriculture and Biology*, *6*(2), 149–161

World Health Organization. (2019). *Classification of diabetes mellitus*

Yamashita, Y., Nakamura, A., Nanba, F., Saito, S., Toda, T., Nakagawa, J., & Ashida, H. (2020). Black soybean improves vascular function and blood pressure: a randomized, placebo controlled, crossover trial in humans. *Nutrients*, *12*(9), 2755. https://doi.org/10.3390/nu12092755

Yang, J., Wang, X., Zhang, C., Ma, L., Wei, T., Zhao, Y., & Peng, X. (2021). Comparative study of inhibition mechanisms of structurally different flavonoid compounds on α-glucosidase and

synergistic effect with acarbose. *Food Chemistry*, *347*, 129056. https://doi.org/10.1016/j.foodchem.2021.129056

Zhu, J., Chen, C., Zhang, B., & Huang, Q. (2020). The inhibitory effects of flavonoids on α-amylase and α-glucosidase. *Critical Reviews in Food Science and Nutrition*, *60*(4), 695–708. https://doi.org/10.1080/10408398.2018.1548428

Pharmaciana
Vol.14, No.3, Nov 2024, Page. 443-456
ISSN: 2088 4559; e-ISSN: 2477 0256
DOI: 10.12928/pharmaciana.v14i3.26643

In silico study of Sambiloto (*Andrographis paniculata)* compounds from GC-MS and LC-MS/MS as alpha-glucosidase and DPP-4 enzyme inhibitor

Herni Kusriani*, Purwaniati, Muhamad Ilham Bintang
Faculty of Pharmacy, Bhakti Kencana University,
Jl. Soekarno Hatta 754, Bandung, Indonesia

Submitted: 14-07-2023 ***Reviewed: 14-12-2023*** ***Accepted: 11-09-2024***

ABSTRACT

Diabetes mellitus is a group of metabolic diseases characterized by hyperglycemia, impaired insulin secretion, and insulin action. To overcome this disease, some people treat it with natural ingredients. Sambiloto (*Andrographis paniculata*) is reported to have a wide range of pharmacological activities, one of which is anti-diabetic. Sambiloto showed activity in lowering blood glucose which has the potential as an antidiabetic. Computational methods, such as molecular docking, can increase the effectiveness and reduce the cost of searching for new active compounds. The purpose of this study was to determine the component compounds contained in the ethanol extract of Sambiloto and obtain the potential compounds to inhibit the alpha-glucosidase and DPP-4 enzymes as anti-diabetics with molecular docking method. Sambiloto leaves were macerated for 3 x 24 hours using ethanol 96% as a solvent and concentrated with an evaporator. Sambiloto extract was analyzed using LC-MS, and GC-MS. In-silico analysis includes geometry optimization and molecular docking methods. Preparation of the test ligands was carried out by the ChemBioDraw Ultra and ChemBio3D applications, then optimization by Gaussian 09 application. The crystal structures of the target proteins used were those with PDB ID 5NN8 for alpha-glucosidase and 2QOE for DPP-4. Molecular docking was performed using Autodock 4.2.3 application. From analysis with LC- MS/MS and GC-MS methods, 18 compounds were identified. Molecular docking was performed on the identified compounds. The results of molecular docking showed that the compound S17 (*11-(P- Bromoanilino)-5H-Dibenzo [B,E] [1,4] Diazepine*), S1 (*andrographolide*) and S2 (*andrographanin*) have the potential to inhibit the activity of alpha-glucosidase enzyme; on the other hand S17 (*11-(P-Bromoanilino)-5H-Dibenzo [B,E][1,4]Diazepine*) and *S5* (*andrographolactone*) have the potential to inhibit the activity of DPP-4 enzyme. These compounds have the potential to inhibit alpha- glucosidase and DPP-4 enzymes which act as antidiabetics.

Keywords: alfa-glucosidase, diabetes mellitus, DPP-4, *molecular docking*, Sambiloto (A*ndrographis paniculata*)

Corresponding author:
Herni Kusriani
Bhakti Kencana University
Jl. Soekarno Hatta 754, Bandung 40614, Indonesia
Email: herni.kusriani@bku.ac.id

INTRODUCTION

Metabolic disorder is one of the main health problems that occur among Indonesians. Diabetes mellitus is a disease caused by a disorder in the secretion of insulin, glucagon, and other hormones resulting in impaired carbohydrate and fat metabolism. When glucose from food is not metabolized normally by the body, the accumulation of glucose increases in the blood, called hyperglycemia (Dipiro 2020). According to the International Diabetes Federation (IDF), Indonesia is ranked 7th among 10 countries with a total of 10.7 million sufferers (Kementrian Kesehatan Republik Indonesia, 2020). The WHO organization estimates that the number of people with type 2 diabetes will increase significantly over the next few years (Perkeni, 2019).

The main pathophysiology of type 2 diabetes mellitus is genetic insulin resistance and pancreatic beta cell dysfunction. In individuals under normal conditions, the pancreas can function properly and can adjust insulin secretion to maintain plasma glucose levels. If insulin release is no longer sufficient to normalize plasma glucose, dysglycemia, including prediabetes and diabetes, may occur. Pancreatic beta cells cannot maintain adequate insulin secretion and release less insulin as glucose levels increase (Dipiro 2020).

Diabetes Mellitus is influenced by several proteins, one of which is the alpha-glucosidase enzyme. An alpha-glucosidase enzyme is a key enzyme in the absorption of sugar in the intestine, and its activity is closely related to blood glucose levels (Perkeni, 2019). The mechanism of alpha-glucosidase enzyme can inhibit the breakdown of sucrose and complex carbohydrates in the small intestine. Diabetes drugs with this mechanism work competitively by inhibiting maltase, isomaltase, sucrose, and glucoamylase enzymes in the small intestine (Dipiro 2020).

Another hormone that plays a role in regulating glucose in the blood is the hormone incretin. Incretin is a peptide secreted in the small intestine in response to food in the intestine. Two types of incretin peptides affect glucose metabolism, namely GLP-1 (Glucagon Like Peptide-1) and GIP (Glucose Dependent Insulinotropic Peptide). Some people who have type 2 diabetes also have GLP-1 deficiency which is resistant to GIP hormone. GLP-1 plays a role in increasing insulin secretion, especially in phase 1 insulin secretion, by stimulating glucose in beta cells and also by inhibiting glucagon secretion. Both lead to a decrease in blood glucose levels. GLP-1 enters the bloodstream and actively works, but GLP-1 does not last long in the blood, which is only about 1-2 minutes because it is immediately destroyed by the enzyme DPP-4 (dipeptidyl peptidase- 4). One of the efforts to keep GLP-1 in the blood longer is to inhibit the DPP-4 enzyme (Dipiro, 2020).

One of the efforts to overcome diabetes mellitus is by utilizing herbs that work to help reduce blood sugar levels that have been used in traditional medicine for generations by the people of Indonesia (Safitri et al. 2015). One of the medicinal plants that have a lot of secondary metabolite content and are widely used in the community to overcome diabetes mellitus is the leaves of Sambiloto (*Andrographis paniculata*). Sambiloto is proven to show anti-hyperglycemic activity and inhibit tissue damage through oxidative stress in diabetic rat models induced by streptozotocin. Sambiloto ethanol extract showed activity to reduce blood glucose (Sivakumar and Rajeshkumar 2016). The content of chemical compounds in the sambiloto plant are diterpenoid and flavonoid compounds, including andrographolide, isoandrographolide, neoandrographolide, andrographolidegraphosterin, 14-deoxy-11, 14-deoxyandrographolide- 19- β-D-glucoside, 12-didehydroandrographolide,14-deoxyandrographolide, homoandrographolide, andrographolidegraphan, and stigmasterol (Chao and Lin 2010; Dai et al. 2019). Andrographolide is the main compound that can reduce glucose levels by inhibiting the alpha-glucosidase enzyme (Dai et al., 2019; Jarukamjorn & Nemoto, 2008; Nugroho et al., 2012). In this study, analysis compound was also carried out with GC-MS and LC-MS/MS methods and compared with previous research, to further determine in silico mechanism of action in inhibiting 2 enzymes, alpha-glucosidase and DPP4 enzyme which play a role in lowering blood sugar.

In the development of new drugs, especially in finding active compounds from herbs, the use of several computational methods has been developed, one of which is molecular docking (Knoll et al.,

2006). Drug design development can be done with Computer-Assisted Drug Design (CADD). Molecular docking is one of the most frequently used methods in Structure-Based Drug Design (SBDD). It can predict the approximate position of the ligand in the target receptor with a high degree of accuracy. Molecular docking is a computational method to predict the interaction between a receptor such as a protein or nucleic acid molecule (DNA or RNA) and its ligand, as well as to assess the binding affinity and positioning of the ligand within receptor (Morris et al. 2008). The complex interaction of the ligand with protein is identified using a docking program to predict the interaction of two molecules. The interaction can be seen from the binding site of the macromolecular target (Kalyaanamoorthy & Chen, 2011; Meng et al., 2011). Molecular docking has advantages such as shorter time and lower cost compared to in vitro tests (Cosconati et al., 2010).

In this study, we focused on herbal plant sambiloto ((*Andrographis paniculata*) and conducted in silico study with its phytoconstituents analyzed by LC-MS/MS and GC-MS. The interactions of its phytoconstituents with enzyme alpha-glucosidase protein (PBD ID 5NN8) and enzyme DPP-4 (PBB ID 2QOE) were reported by molecular docking studies. Alpha-glucosidase and DPP-4 enzymes were chosen as targets in this study. The alpha-glucosidase enzyme is an enzyme that is responsible for the process of breaking down complex carbohydrates into glucose and absorbing glucose into the circulation. Inhibition of this enzyme will prevent excess glucose intake from food. Meanwhile, the DPP-4 enzyme is staged. Our results from the present study have established the strong candidate of phytoconstituents of sambiloto to be used as a drug-like molecule for preventing diabetes mellitus.

MATERIALS AND METHODS

Materials

Sambiloto plants were obtained from the Installation of Research and Assessment of Agricultural Technology (IP2TP) Cicurug Sukabumi - West Java. The results of the determination carried out at the Jatinangor Herbarium, Faculty of Mathematics and Natural Sciences Padjadjaran University showed that the sambiloto plant used in the study is a species of *Andrographis paniculata* which belongs to the Acanthaceae family (No. 38/HB/12/2021). This plant in Indonesia is known by the common name sambiloto.

The hardware used was an Asus M509BA laptop, AMD A4-9125 Radeon R3 processor, 4 compute cores 2C+2G, 2300, Mhz, 2 Core(s). Storage SSD (Solid State Drive) 1TB, RAM 8.00 gigabytes. The software used was Masslynx V4.1, ChemBioOffice 2014 (ChemBioDraw Ultra and ChemBio3D Ultra), Discovery Studio Visualizer 2016, GaussianView 5.0, and AutoDock 1.5.6.

Methods

Extraction

80 grams of sambiloto leaves were macerated with 96% ethanol solvent for 3x24 hours, then the extract was concentrated with a rotary evaporator.

Compound analysis

Analysis of compounds in the extract was carried out by LC-MS/MS, and GC-MS. Analysis using a Liquid Chromatography-Mass Spectrometer (LC-MS/MS) instrument was conducted at Bogor Forensic Laboratory Center with UPLC (Ultra Performance Liquid Chromatography), UPLC Column HSS (High strength silica), and Two-Generation Quadrupole time-of-flight mass spectrometry. The results obtained are chromatograms and mass spectra that will be checked using Masslynx software. The mass spectrum pattern will be matched with external literature such as journals, mass bank databases, PubChem, and ChemSpider. The results of the mass spectra that have been matched with the literature will be taken for the preparation of test ligands.

For GC-MS analysis using Shimadzu-GC 2010 with the mass selective detector, carrier gas using helium. The optimization process was carried out by programming the interface temperature of 250°C, injector 150°C, and initial column temperature programmed 50°C increased to 100°C with a temperature increase set at 10°C/minute (held for 3 minutes). Then increased back to 200°C, increased

back to 250°C. Components were identified by comparing the mass spectra of the samples with the internal Willey Library7 (Rohloff, 2015).

In silico testing

The in-silico process includes ligand preparation, protein preparation, validation of molecular docking method, simulation of molecular docking of test ligand with protein, and interpretation of results.

Test ligand preparation

The test ligand used was the result of determining components of the sambiloto extract which were analyzed using LC-MS/MS and GC-MS instruments. The compounds obtained were checked with the PubChem database and made 2D and 3D compound re-structures using the ChemBioDraw Ultra and ChemBio3D applications. Then geometry optimization was carried out using the Gaussian application.

Protein target and natural ligand preparation

The proteins used are alpha-glucosidase enzyme and DPP-4 enzyme, downloaded on the Protein Data Bank website https://www.rcsb.org/structure/ (PDB ID 5NN8 for alpha-glucosidase enzyme) and (PDB ID 2QOE for DPP-4 enzyme). Preparation of the target protein and natural ligand was done by separating the protein structure and natural ligand and removing water molecules. Using the Visual Discovery Studio application.

Validation of molecular docking method

Validation of molecular docking was carried out using the AutoDock version 4.2.3 application (Morris et al., 2008). The proteins used were the alpha-glucosidase enzyme and the DPP- 4 enzyme that had been prepared. The natural ligands that had been separated from the proteins using the Discovery Studio application were then reattached to the target proteins. The grid center was placed approximately to the center of the ligand, covering all binding site residues. Determination of the Gridbox is done by setting the central region of the natural ligand and docking calculation with the number of GA runs as many as 100 maximum numbers of evals and the algorithm method used is Lamarckian Genetic Algorithm (LGA). Validation is declared valid if the Root Mean Square Deviation (RMSD) value ≤ 2Å (López-Camacho et al. 2016).

Molecular docking simulation

Simulation of molecular docking of test compounds to alpha-glucosidase and DPP-4 target proteins using the AutoDock application version 4.2.3. Gridbox settings according to the size and area that have been obtained from the validation results. Furthermore, the interpretation of molecular docking results is carried out by looking at the value of ΔG (binding free energy), and inhibition constant. Visualization using the Discovery Studio Visualizer 2016 application to explore the bond interaction formed between the test ligand with alpha-glucosidase and DPP-4 enzyme (López-Camacho et al. 2016). Visualization of docking results draws the interaction of ligands with proteins that form intermolecular bonds with amino acid residues enzyme (López-Camacho et al. 2016).

RESULT AND DISCUSSION

Analysis of compounds from Sambiloto extract by LC-MS/MS

Analysis of compounds in the extract with LC-MS/MS instrument identified some chromatographic peaks (Figure 1).

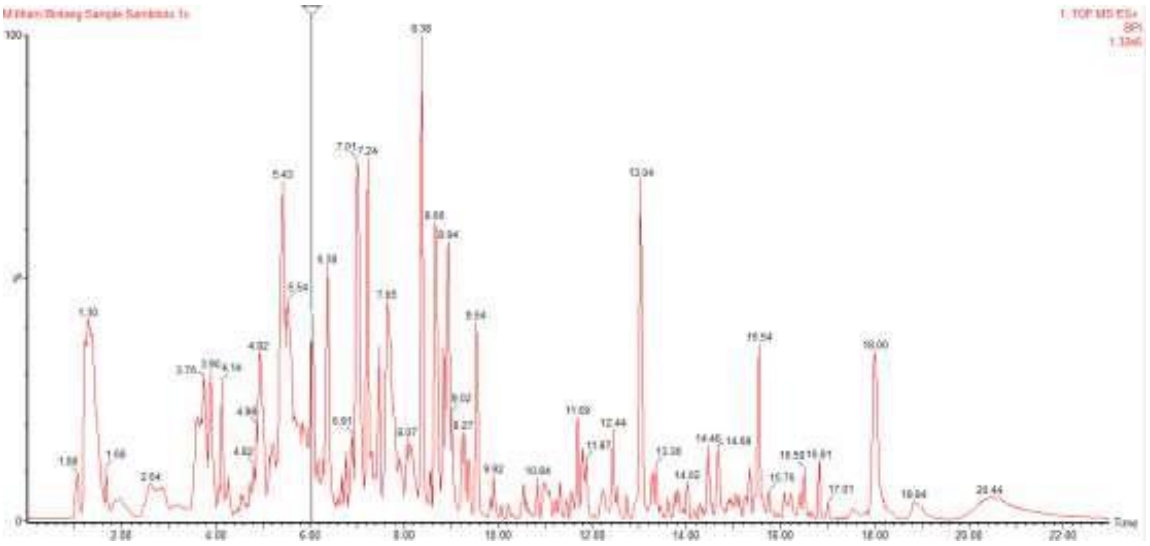

Figure 1. Chromatogram profile of LC-MS/MS analysis results of sambiloto ethanol extracts

Characterization of the structure of chromatogram peaks is based based on accurate mass, fragmentation patterns, literature data, molecular weights, and chemical formulas, matched with external literature from the form of mass spectra of compounds compared with mass bank databases, PubChemm, ChemSpider, and journals. Analysis using LC-MS/MS showed the presence of 22 peaks (Table 1), but only 16 compounds had their chemical structures identified. Other peaks whose structures cannot be carried out in silico studies. Of the 16 peaks, as listed in Table 1 were identified from the alkaloid, diterpenoid, and flavonoid compound classes including Andrographolide, Andrographanin, Bisandrographolide, 14-Deoxyandrographolide, Andrographolactone, 14-Deoxy-11,12-didehydroandrographolide, Lambertianic acid, Cevadine, Caffeoylquinic acid and 5,7-dihydroxy-3-(4-hydroxyphenyl)-66-methoxy-4H-chrome-4-one4',55,7-Trihydroxy-6-methoxy isoflavone. Several diterpenoids including 14-deoxy-11, 12-di- dehydroandrographide, andrographolide, neoandrographolide and isoandrographolide have been reported previously from *A. paniculata* (Chao & Lin, 2010).

Alkaloid compounds were detected in this extract which confirmed the presence of aromatic and oxidized nitrogen functional groups. Previous studies have confirmed the presence of hydroxyl, aromatics, alkanes, esters, amines, ethers, nitro aromatics, phenolics, and phosphine groups present in the extract of sambiloto leaf plants (Dwivedi et al. 2021). Alkaloids were detected at retention time 7.65 with m/z value 592.3492, mass number 591.7, and molecular formula $C_{32}H_{49}NO_9$. The compound detected was Cevadine, the results of the fragmentation pattern were compared with external literature contained in the mass bank database. Cevadine was detected at m/z 592 with product ions 389 and 289.

Analysis of compounds from Sambiloto extract by GC-MS

The results of GC-MS analysis identified compounds successfully extracted from ethanol solvents and derivatized by adding Trimethylsilyl in methanol. Derivatization is intended to improve the volatility of a compound so that it can be analyzed by gas chromatography. Analysis of sambiloto ethanol extract with derivatization showed more peaks (Mushtaq et al. 2014).

Further identification of each peak was carried out using mass spectra based on the database Similarity Index (SSI). Analysis of the extract using the GC-MS method identified the presence of 8 compounds. The identified metabolites will be bound to TMS which has functional groups such as amino acids (-COOH, -NH2, -OH) and monosaccharides. The results of the 8 main peaks consisted of

peak number 1 in the Willey7 internal library so the compounds were identified as 1-(3-hydroxycyclopent-2-en-1-yl)propane-2-one, furan-2,5-dicarboxylic acid, 2,4-Di-Tert-Butyl-6-Cyanoaniline, 3-hydroxy-3-(4-hydroxyphenyl)propanoic acid, 1-(2-hydroxyphenyl)ethan-1-one, propyl 4-hydroxybenzoate, 11-(P-Bromoanilino)-5H- Dibenzo[B, E][1,4]Diazepine, and 3-butyl-3,5,5-trimethyl cyclo hex- 1-en-1-ol.

Table 1. LC-MS/MS analysis of sambiloto ethanol extracts

Peak	Rt (min)	MW (g/mol)	(m/z)	Molecular formula	Compound classes
1.	1.08	167	167.013	$C_6H_3N_2O_4$	Nitrobenzenes
2.	1.30	117.15	118.146	$C_5H_{11}NO_2$	Amino acid
3.	1.68	268.10	268.104	$C_{10}H_{14}N_5O_4$	Nucleotides
4.	2.64	165.19	166.086	$C_9H_{11}NO_2$	Amino acid
5.	3.76	205.0	205.097	$C_{11}H_{12}N_2O_2$	Alkaloids
6.	3.90	355.1	355.105	$C_{16}H_{18}O_9$ (Caffeoyl quinic acid)	Phenolic acid
7.	4.14	595.5	595.167	$C_{27}H_{31}O_{15}$	Flavonoids
8.	4.92	334.4	335.220	$C_{20}H_{28}O_4$ (14-Deoxyandrographolide)	Diterpenoids
9.	5.43	332.4	333.203	$C_{20}H_{28}O_4$ (Andrographolactone)	Diterpenoids
10.	6.03	333.4	333.205	$C_{20}H_{28}O_4$ (14-Deoxy-11,12-didehydroandrographolide)	Diterpenoids
11.	6.38	350.4	351.219	$C_{20}H_{30}O_5$ (Andrographolide)	Diterpenoids
12.	7.01	350.4	701.431	$C_{20}H_{30}O_5$ (Andrographolide)	Diterpenoids
13.	7.24	318.4	319.219	$C_{20}H_{30}O_3$ (Andrograpanin)	Diterpenoids
14.	7.47	318.4	319.228	$C_{20}H_{30}O_3$ (Andrograpanin)	Diterpenoids
15.	7.65	591.7	592.349	$C_{32}H_{49}NO_9$ (Cevadine)	Alkaloids
16.	8.07	332.4	333.208	$C_{20}H_{28}O_4$ (14-Deoxy-11,12-didehydroandrographolide)	Diterpenoids
17.	8.38	318.4	319.226	$C_{20}H_{30}O_3$ (Andrograpanin)	Diterpenoids
18.	8.66	318.4	319.226	$C_{20}H_{30}O_3$ (Andrograpanin)	Diterpenoids
19.	8.94	316.4	317.210	$C_{20}H_{28}O_3$ (lambertianic acid)	Diterpenoids
20.	9.27	300.26	301.216	$C_{16}H_{12}O_6$ (5,7-dihydroxy-3-(4-hydroxyphenyl)-6-methoxy-4H- chromen-4-one 4',5,7- trihydroxy-6-methoxyisoflavone)	Flavonoids
21.	9.54	316.4	317.204	$C_{20}H_{28}O_3$ (lambertianic acid)	Diterpenoids
22.	9.92	664	665.406	$C_{40}H_{56}O_8$ (Bisoandrographolde)	Diterpenoids

LC MS/MS analysis of 3 out of 7 compounds of the diterpenoid group whose fragmentation patterns have been studied in previous studies. The fragmentation pathway and diagnostic product ions are andrographolide, 14-deoxy-11, 12- didehydroandrographolide, and bis andrographolide. One of the compounds detected was the main compound of andrographolide with the molecular formula $C_{20}H_{30}O_5$, showing fragmentation patterns at m/z 351 and 702. While other diterpenoid compounds are 14-deoxy-11, 12-didehydroandrographolide ($[M+ Ion H]^+$ with at m/z 333, bisandrographolide A on MS/MS at m/z 665 (Dwivedi et al., 2021; Solomon Jeeva, 2014).

From the results of GC-MS and LC-MS/MS analysis, the chemical structure of 18 compounds was successfully determined, while the chemical structure of several other compounds could not be determined so they could not proceed to in silico studies. The identified compounds were then

analyzed for physicochemical properties based on the Lipinski rule of five with parameters of Molecular Weight < 500 g/mol, LogP < 5, number of hydrogen bond acceptors < 10, and number of hydrogen bond donors < 5 (Lipinski, 2004). The results of the physicochemical properties analysis parameters can be seen in Table 2.

Physicochemical parameters are one of the requirements that must be met, especially for peroral drug preparations (Lipinski, 2004). The molecular weight of a drug is related to the process of the drug in penetrating biological membranes. Peroral drug requirements based on Lipinski's rules are < 500 g/mol. The results of the molecular weight determination showed that 16 test ligands had BM 500 values of less than g/mol, indicating that the test ligands could pass through the cell membrane (Table 2 marked with a).

The physicochemical property parameter that determines the hydrophobic or hydrophilic nature of a ligand is the Log P value. The requirements for drugs by the peroral route based on Lipinski's rule must have a LogP value ≤ 5 (Lipinski, 2004). 16 test ligands have a LogP value ≤ 5, indicating that the test ligand has lipophilic properties and can pass through the cell membrane so that it can reach the target. as shown in Table 2, marked with b). Bond acceptors and donors are influential in the process of membrane permeability. The requirement for the number of acceptor bond donors is < 10 and the number of hydrogen donor bonds is < 5 (Lipinski, 2004). From the determination of physicochemical parameters, fourteen test ligands have met the rules as good antidiabetic candidates (Table 2 marked with c).

Preparation of test ligands

The test ligands used in this study are ligands from the ethanol extract of sambiloto that have met the requirements of the physicochemical properties parameters that are used as test ligands based on Lipinski's rules. All ligands were made two- and three-dimensional structures using ChemDraw 2D and 3D applications using Discovery Studio Visualizer (Figure 2). Furthermore, geometry optimization was carried out using the Gaussian09 application with the Semi-Empirical (AM1) method (Julaiha et al. 2019).

Protein target and natural ligand preparation

The working targets used are the Alpha-Glucosidase enzyme and the DPP-4 enzyme which were downloaded from the Protein Data Bank (PDB) site https://www.rcsb.org/ which is managed by the Research Collaboratory for Structural Biology (RCSB). The downloaded enzymes have PDB ID codes, namely 5NN8 and 2QOE. The following visualization of the work targets and natural ligands (Figure 3):

The natural ligand on the alpha-glucosidase enzyme is acarbose which is proven to have an activity to inhibit the enzyme (Julaiha et al. 2019). The natural ligand on the DPP-4 enzyme is triazolopiperazine (Kowalchick et al. 2007) which also has activity as an inhibitor (Figure 3).

The selection of the two working targets is an enzyme that affects the increase in blood glucose in type 2 DM disease and also because these enzymes can be inhibited by the test compound so that it forms a complex between the working target and the ligand in the form of an inhibitor. The organism used in modeling is the human organism (Homo sapiens). Apart from that, the modeling method used is X-ray diffraction (XRD), this method only has one post at rest and a resolution of ≤ 2 Å. Natural ligands that form complexes with action targets are medicinal compounds that have been used and proven have a mechanism of action as inhibitor (Kowalchick et al., 2007; Roig-Zamboni et al., 2017).

Table 2. Parameters of physicochemical properties

Ligand code	Ligand name	MW (g/mol)	LogP	H-bond acceptor	H-bond donor
S1	Andrographolide [abc]	350.00	1.96260	5	3
S2	Andrographanin [abc]	318.00	4.0209	3	1
S3	Bisandrographolide	664.00	5.36789	8	4
S4	14-Deoxyandrographolide [abc]	334.00	2.99179	4	2
.00					
S5	Andrographolactone[abc]	296.00	4.22613	2	0
S6	14-Deoxy-11,12-didehydroandrographolide [abc]	332.00	2.76779	4	2
S7	Lambertianic acid[a]	316.00	5.07570	3	1
S8	5,7-dihydroxy-3-(4-hydroxyphenyl)-6-methoxy-4H-chromen-4-one 4',5,7- Trihydroxy-6-methoxyisoflavone[abc]	300.00	1.93897	6	3
S9	Cevadine [b]	591.00	0.99457	10	6
S10	Caffeoyl quinic acid [ab]	354.00	-0.6459	9	6
S11	1-(3-hydroxycyclopent-2-en-1- yl) propane-2-one [abc]	140.00	1.81740	2	1
S12	furan-2,5-dicarboxylic acid [abc]	156.00	0.67600	5	2
S13	2,4-di-tert-Butyl-6-Cyanoaniline[abc]	230.00	3.73547	2	2
S14	3-hydroxy-3-(4-hydroxyphenyl)propanoic acid[abc]	182.00	0.90030	4	3
S15	1-(2-hydroxyphenyl)ethan-1-one [abc]	136.00	1.59480	2	1
S16	propyl 4-hydroxybenzoate [abc]	180.00	1.95900	3	1
S17	11-(P-Bromoanilino)-5H-Dibenzo[B,E][1,4]Diazepine [abc]	363.00	4.70999	3	2
S18	3-butyl-3,5,5-trimethyl cyclo hex- 1-en-1-ol [abc]	196.00	4.44479	1	1

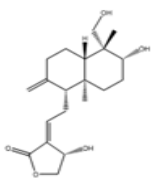

Andrographolide (S1)

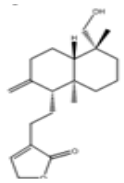

Andrographanin (S2)

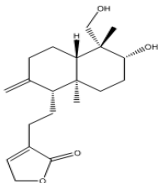

14-deoxyandrographolide(S4)

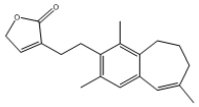

Andrographolactone (S5)

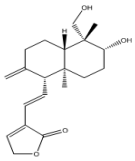

14-Deoxy-11,12-didehydroandrographolide (S6)

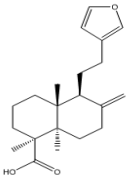

Lambertianic acid (S7)

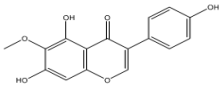

5,7-dihydroxy-3-(4-hydroxyphenyl)-6-methoxy-4H- chromen-4-one 4',5,7-Trihydroxy-6-methoxyisoflavone (S8)

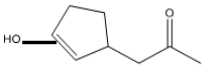

1-(3-hydroxycyclopent-2-en-1-yl)propan-2-one (S11)

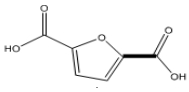

furan-2,5-dicarboxylic acid (S12)

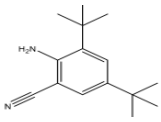

2,4-Di-Tert-Butyl-6-Cyanoaniline (S13)

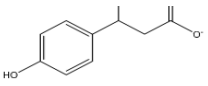

3-hydroxy-3-(4-hydroxyphenyl)propanoic acid (S14)

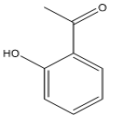

1--(2-hydroxyphenyl)ethan-1-one (S15)

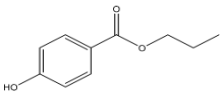

propyl 4-hydroxybenzoate (S16)

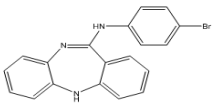

11-(P-Bromoanilino)-5H-Dibenzo[B,E][1,4]Diazepine (S17)

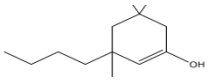

3-butyl-3,5,5-trimethylcyclohex-1-en-1-ol (S18)

Figure 2. Ligand structure modelling

A B C D

Figure 3. Target protein and natural ligands

(A) Crystallographic Structure of Alpha-Glucosidase Enzyme (B) Natural ligand Acarbose
(C) Crystallographic Structure of DPP-4 Enzyme (D) Natural ligand Triazolopiperazine
(Source: RSCB Protein Data Bank)

Besides that the enzyme can be inhibited by the test compound therefore it forms a complex with a resolution of ≤ 2 Å. Crystallographic resolution categories are divided into four categories, small (<3.00 Å), medium (2.70-2.00 Å), high (2.00-1.50 Å), and very high (<1.5 Å). The smaller the crystallographic value, the more specific the visualization of the resulting image (Riverson & Rizarullah, 2020).

Docking validation

Molecular docking was performed using Autodock version 4.2.3 (Morris et al. 2008). Validation of molecular docking is done by natural ligands docking to the test enzyme and then comparing the pose of the natural ligand before and after, known as redocking which is expressed in the form of RMSD (Root Mean Square Deviation). The purpose of redocking is to determine the validated ligand docking location in the form of the size and position of the grid box. The validation of molecular docking is declared valid if the RMSD value is ≤ 2 Å, which means that the molecular docking method provides a deviation that is not large and can be used further for the simulation of molecular docking of test ligands enzyme (López-Camacho et al. 2016).

Docking validation of alpha-glucosidase enzyme

Redocking natural ligand against alpha-glucosidase enzyme is valid with grid box (40,76,40), grid spacing 0,775A^{o,} and grid center (-14,425; -37,292; 95,129). This redocking gives an acceptable RMSD value, which is 1,705A^{o} with a ΔG value of -9,65 Kcal/mol. or equivalent to the inhibition constant of 84,93nM.

The interaction of the natural ligand redocking results is in accordance with the interaction in its crystal structure. The interaction occurs through the formation of 18 hydrogen bonds, 2 hydrophobic interactions, and several Van der Walls interactions. Visualization of the interactions can be seen in Figure 4.

Docking validation of DPP-4 (*Dipeptidyl Peptidase IV*) enzyme

Redocking natural ligand against DPP-4 enzyme is valid with grid box (46,44,44), grid spacing 0,375A^{o,} and grid center (-7,646; 66,207; 39,187). This redocking gives an acceptable RMSD value at 1,878A^{o} with an ΔG value of -8,26 Kcal/mol. or equivalent to the inhibition constant of 874,76 nM.

The interaction of the natural ligand redocking results following the interaction in its crystal structure. The interaction occurs through the formation of 6 hydrogen bonds, 3 hydrophobic interactions, and several Van der Walls interactions. Visualization of the interactions can be seen in Figure 4.

Interactions between enzymes and natural ligands can be in the form of hydrogen bonds, hydrophobic bonds, and Van der Waals interactions, which are intermolecular bonds. Intermolecular bonds are important bonds that occur between drug interactions and their targets. The conformation with the lowest binding energy shows the best interaction pose. The conformational suitability of the test ligand is compared with the native ligand to confirm the free energy value because the active ligand must bind to specific amino acid residues. The important amino acid residues responsible for activity are ALA 284, ASP 404, MET 519, ASP 616, HIS 674, ARG 600, and TRP 376 in Alpha-glucosidase enzyme while Glu 205, Glu 206 in DPP-4 enzyme (Kowalchick et al., 2007; Roig-Zamboni et al., 2017). The results of re-bonding natural ligands have interactions with amino acid residues by forming hydrogen bonds, proving the validation of molecular docking has been valid (Julaiha et al. 2019).

Molecular docking on alpha-glucosidase enzyme

Molecular docking is a computational technique used to predict the interaction between a small molecule, such as a drug candidate, and a target protein, usually an enzyme. It helps in understanding the binding affinity and the orientation of the ligand within the enzyme's active site, which is crucial

for designing effective inhibitors. A molecular docking simulation for the test ligand was carried out to obtain the interaction and affinity of the test ligand to the active side of the Alpha-glucosidase enzyme, according to the previously validated docking parameters. This simulation allows for the identification of key interactions between the ligand and the enzyme, providing insights into the potential efficacy of the ligand as an enzyme inhibitor. (Julaiha et al. 2019)

The ΔG value of the test ligands compared to the natural ligand is -9.65 kcal/mol (Table 3), where ligands S1, S1, S4, S5, S17, and S18 are predicted to have a better affinity to the enzyme. Meanwhile, the inhibition constant value of the test ligands compared to the natural ligand is 84.93 nM (Table 3), where ligands S1, S2, S4, S5, S4, S6, S17, and S18 showed less than 100 uM and are predicted as strong inhibitors (Zheng and Polli 2010). Interaction of the test ligand with the alpha-glucosidase enzyme, S1 showed the best interaction because it interacts with important amino acid residues which are responsible for the activity of ALA 284 and ASP 404 (Julaiha et al. 2019), and based on ΔG value, inhibition constant, and interaction with Alpha- glucosidase enzyme showed that ligand S17 (11-(P-Bromoanilino)-5H-Dibenzo [B,E][1,4] Diazepine), S1(andrographolide) and S2 (andrographanin) have potential as inhibitors on alpha-glucosidase enzyme (Morris et al. 2008).

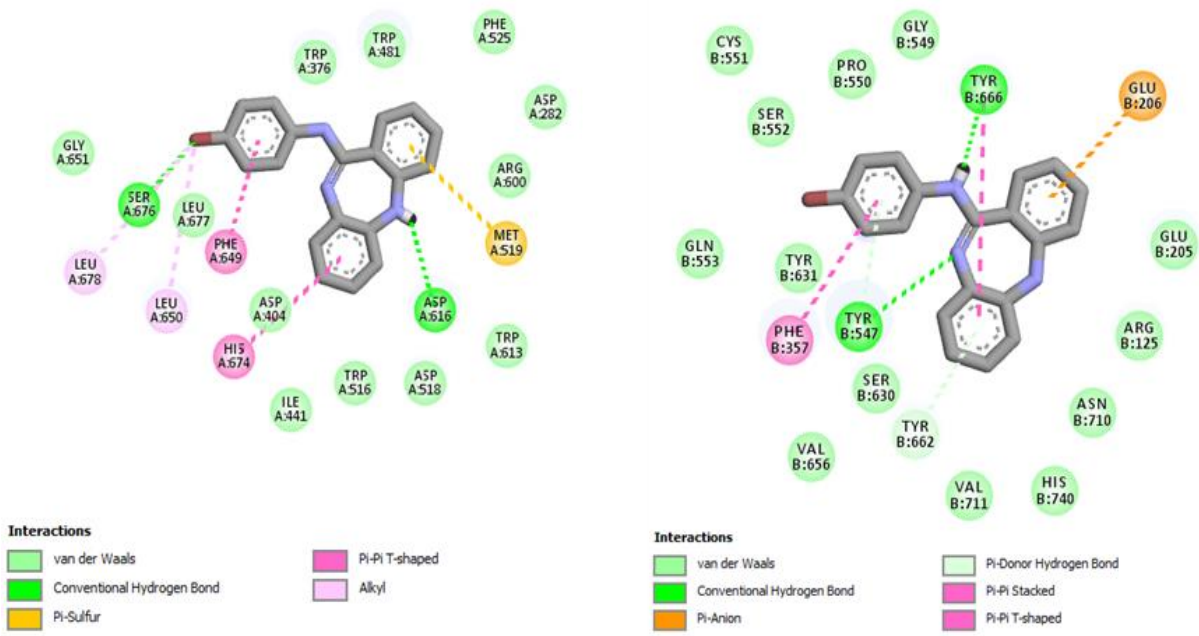

Figure 4. Visualization of alpha-glucosidase enzyme-natural ligand acarbose interaction (A) DPP-4 enzyme interaction with triazolopiperazine natural ligand(B)

Molecular docking on DPP4 enzyme

A molecular docking simulation for the test ligands was conducted to obtain the interaction and affinity of the test ligands towards the active side on the DPP-4 enzyme, under the previously validated docking parameters. This approach allows for the assessment of how well the ligands fit within the enzyme's active site, providing valuable insights into their potential to inhibit enzyme activity. By evaluating the binding energy and key interactions, the simulation helps identify the most promising candidates for further in vitro and in vivo studies, ultimately contributing to the development of more effective therapeutic agents.

The ΔG values of the test ligands (Table 4) were compared with the ΔG value of the natural ligand of -8.26 kcal/mol, where ligands S17 and S5 had more negative ΔG values than the natural ligand, so

they were predicted to have better affinity to the DPP-4 enzyme. While ligands S17 and S5 showed lower inhibition constant values compared to the natural ligand (Table 4). Value less than 100 uM are considered strong inhibitors (Zheng and Polli 2010). From the interaction of the test ligand with the DPP-4 enzyme, S17 has the best interaction because it interacts with amino acid residues GLU 205 and GLU 206 which is responsible for the activity. The best molecular docking results based on ΔG, Ki values and interactions with the DPP-4 enzyme are the S17 ligand (11-(P-Bromoanilino)-5H-Dibenzo [B,E][1,4]Diazepine) and S5 (andrographolactone), which have potential to act as an inhibitor of the DPP-4 enzyme and predicted that these ligand will have a better affinity in interacting with the enzyme (Morris et al. 2008).

Table 3. Molecular docking on alpha-glucosidase enzyme

Ligand code	ΔG (kcal/mol)	Inhibition Constant
Acarbose	-9.65	84.93 nM
S1	-7.47	3.34 uM
S2	-7.72	2.18 uM
S4	-7.05	6.84 uM
S5	-6.99	7.55 uM
S6	-7.09	6.40 uM
S7	-5.67	70.12 uM
S8	-6.05	36.50 uM
S11	-5.23	146.78 uM
S12	-0.88	227.88 mM
S13	-6.64	13.67 uM
S14	-2.75	9.66 mM
S15	-5.21	151.86 uM
S16	-5.59	80.11 uM
S17	-8.18	1.02 uM
S18	-6.92	8.43 uM

Table 4. Molecular docking on DPP-4 enzyme

Ligand code	ΔG (kcal/mol)	Inhibition constant
Triazolopiperazine	-8.26	874.76 nM
S1	-7.70	2.28 uM
S2	-8.15	1.06 uM
S4	-7.87	1.70 uM
S5	-8.28	851.87 nM
S6	-7.99	1.40 uM
S7	-6.81	10.22 uM
S8	-7.08	6.41 uM
S11	-5.33	123.74 uM
S12	-1.47	84.28 mM
S13	-6.51	16.90 uM
S14	-4.21	821.99 uM
S15	-5.53	88.91 uM
S16	-5.31	127.56 uM
S17	-9.35	140.32 nM
S18	-7.16	5.64 uM

CONCLUSION

Based on LC-MS / MS and GC-MS analysis obtained 18 identified compounds. These compounds come from alkaloids, flavonoids, and terpenoids. The results of molecular docking showed that the compound S17 (*11-(P- Bromoanilino)- 5H-Dibenzo[B,E][1,4]Diazepine*), S1 (*andrographolide*) and

S2 (*andrographanin*) have the potential to inhibit the activity of alpha-glucosidase enzyme; on the other hand, S17 (*11-(P- Bromoanilino)-5H-Dibenzo[B,E][1,4]Diazepine*) and *S5* (*andrographolactone*) have the potential to inhibit the activity of DPP-4 enzyme. These compounds have the potential to inhibit alpha- glucosidase and DPP-4 enzymes which act as antidiabetics.

ACKNOWLEDGEMENT

Thanks to Bhakti Kencana University for its support and research facilities.

REFERENCES

Chao, W. W., & Lin, B. F. (2010). Isolation and identification of bioactive compounds in Andrographis paniculata (Chuanxinlian). *Chinese Medicine*, *5*, 1–15. https://doi.org/10.1186/1749-8546-5-17

Cosconati, S., Forli, S., Perryman, A. L., Harris, R., Goodsell, D. S., & Olson, A. J. (2010). *Cosconati2010.Pdf*. 597–607.

Dai, Y., Chen, S. R., Chai, L., Zhao, J., Wang, Y., & Wang, Y. (2019). Overview of pharmacological activities of andrographis paniculata and its major compound andrographolide. *Critical Reviews in Food Science and Nutrition*, *59*(0), S17–S29. https://doi.org/10.1080/10408398.2018.1501657

DiPiro, Joseph T., Gary C. Yee, L. Posey Michael, Stuart T. Haines, Thomas D. Nolin, and Ellingrod Vicky. 2020. *Pharmacotherapy A Pathophysiologic Approach*.

Dwivedi, M. K., Mishra, S., Sonter, S., & Singh, P. K. (2021). Diterpenoids as potential anti-malarial compounds from Andrographis paniculata. *Beni-Suef University Journal of Basic and Applied Sciences*, *10*(1). https://doi.org/10.1186/s43088-021-00098-8

Jarukamjorn, K., & Nemoto, N. (2008). Pharmacological aspects of Andrographis paniculata on health and its major diterpenoid constituent andrographolide. *Journal of Health Science*, *54*(4), 370–381. https://doi.org/10.1248/jhs.54.370

Julaiha, Widodo, G. P., & Herowati, R. (2019). Predicting ADME and molecular docking analysis of Andrographis paniculata and Strobilanthes crispus chemical constituents againts antidiabetic molecular targets. *Journal of the Indonesian Chemical Society*, *2*(2), 106. https://doi.org/10.34311/jics.2019.02.2.106

Kalyaanamoorthy, S., & Chen, Y. P. (2011). Structure-based drug design to augment hit discovery. *Drug Discovery Today*, *16*(17–18), 831–839. https://doi.org/10.1016/j.drudis.2011.07.006

Kementrian Kesehatan Republik Indonesia. 2020. Tetap produktif, cegah dan atasi Diabetes Mellitus. *Pusat Data Dan Informasi Kementrian Kesehatan RI*.

Knoll, E. H., Rao, Æ. S. N., Shaw, Æ. D. E., & Friesner, R. A. (2006). *PHASE : a new engine for pharmacophore perception , 3D QSAR model development , and 3D database screening : 1 . Methodology and preliminary results*. 647–671. https://doi.org/10.1007/s10822-006-9087-6

Kowalchick, J. E., Leiting, B., Pryor, K. A. D., Marsilio, F., Wu, J. K., He, H., Lyons, K. A., Eiermann, G. J., Petrov, A., Scapin, G., Patel, R. A., Thornberry, N. A., Weber, A. E., & Kim, D. (2007). Design, synthesis, and biological evaluation of triazolopiperazine-based β-amino amides as potent, orally active dipeptidyl peptidase IV (DPP-4) inhibitors. *Bioorganic and Medicinal Chemistry Letters*, *17*(21), 5934–5939. https://doi.org/10.1016/j.bmcl.2007.07.100

Lipinski, C. A. (2004). Lead- and drug-like compounds: The rule-of-five revolution. *Drug Discovery Today: Technologies*, *1*(4), 337–341. https://doi.org/10.1016/j.ddtec.2004.11.007

López-Camacho, E., García-Godoy, M. J., García-Nieto, J., Nebro, A. J., & Aldana-Montes, J. F. (2016). A new multi-objective approach for molecular docking based on rmsd and binding energy. *Lecture Notes in Computer Science (Including Subseries Lecture Notes in Artificial Intelligence and Lecture Notes in Bioinformatics)*, *9702*, 65–77. https://doi.org/10.1007/978-3-319-38827-4_6

Meng, X., Zhang, H., Mezei, M., & Cui, M. (2011). *Molecular docking : a powerful approach for structure-based drug discovery*. 146–157.

Morris, G. M., Huey, R., & Olson, A. J. (2008). *Using AutoDock for ligand-receptor docking* (Issue

December). https://doi.org/10.1002/0471250953.bi0814s24

Mushtaq, M. Y., Choi, Y. H., Verpoorte, R., & Wilson, E. G. (2014). Extraction for metabolomics: access to the metabolome. *Phytochemical Analysis*, *25*(4), 291–306. https://doi.org/10.1002/pca.2505

Nugroho, A. E., Andrie, M., Warditiani, N. K., Siswanto, E., Pramono, S., & Lukitaningsih, E. (2012). Antidiabetic and antihiperlipidemic effect of Andrographis paniculata (Burm. f.) Nees and andrographolide in high-fructose-fat-fed rats. *Indian Journal of Pharmacology*, *44*(3), 377–381. https://doi.org/10.4103/0253-7613.96343

Perkeni. (2019). Pedoman pengelolaan dan pencegahaan DM Tipe 2 dewasa Indonesia. *Perkumpulan Endokrinologi Indonesia*, 113.

Riverson, M., & Rizarullah, R. (2020). Potensi antidiabetes benzyl beta d glucopyranoside dari daun Yacon sebagai inhibitor enzim DPP-4: metode in silico. *Prosiding Seminar Nasional Biotik 2020*, 299–305.

Rohloff, J. (2015). Analysis of phenolic and cyclic compounds in plants using derivatization techniques in combination with GC-MS-based metabolite profiling. *Molecules*, *20*(2), 3431–3462. https://doi.org/10.3390/molecules20023431

Roig-Zamboni, V., Cobucci-Ponzano, B., Iacono, R., Ferrara, M. C., Germany, S., Bourne, Y., Parenti, G., Moracci, M., & Sulzenbacher, G. (2017). Structure of human lysosomal acid α-glucosidase-A guide for the treatment of Pompe disease. *Nature Communications*, *8*(1). https://doi.org/10.1038/s41467-017-01263-3

Safitri, S., Yolanda, R., Brahmana, E. M., Studi, P., Biologi, P., & Pengaraian, U. P. (2015). Di kecamatan Rambah Samo Kabupaten Rokan Hulu. *Ejournal*, *13*(November 2014), 1–4.

Sivakumar, V., & Rajeshkumar, S. (2016). Protective effect of Andrographis paniculata on hyperglycemic mediated oxidative damage in renal tissues of diabetic rats. *The Journal of Phytopharmacology*, *4*(6), 287–294. https://doi.org/10.31254/phyto.2015.4603

Solomon Jeeva, J. J. (2014). Andrographis paniculata: a review of its traditional uses, Phytochemistry and Pharmacology. *Medicinal & Aromatic Plants*, *03*(04). https://doi.org/10.4172/2167-0412.1000169

Zheng, X., & Polli, J. (2010). Identification of inhibitor concentrations to efficiently screen and measure inhibition Ki values against solute carrier transporters. *European Journal of Pharmaceutical Sciences*, *41*(1), 43–52. https://doi.org/10.1016/j.ejps.2010.05.013